Forest change mapping using remote sensing and Google Earth Engine

A thesis

submitted in fulfilment

of the requirements for the degree

of

Doctor of Philosophy in Geography

at

The University of Waikato

by

Walawe Durage Kalpanie Vimarshana Nandasena

THE UNIVERSITY OF
WAIKATO
Te Whare Wānanga o Waikato

2023

Abstract

With advancements in data sources, software, and image analysis techniques, remote sensing has become an efficient method for forest classification. However, access to this technology has been limited for developing countries due to the high cost of high resolution images and analysis software. A potential solution is that NASA and the European Space Agency provide free access to mid-low resolution satellite images. In addition, Google Earth Engine (GEE), a free cloud-based geospatial analysis platform, has allowed researchers from developing countries to conduct research without relying on costly remote sensing software. This study evaluates the suitability of the freely available images and the GEE platform for different forest management applications in Sri Lanka. The research focused on three different scenarios in vegetation mapping: identifying home gardens, monitoring invasive pines, and forest cover mapping in a tropical montane region.

Home garden is an agroforestry class seen in tropical countries often overshadowed by global land cover classifications. This study used a random forest classification algorithm to classify the home garden, utilizing terrain data and Sentinel-2A images as the dataset. The results confirmed that the red band of Sentinel-2 and textural metrics derived from grey-level co-occurrence matrix analysis are effective in identifying home gardens from other forestry classes.

Monitoring the spread of invasive pines is important for forest management in Sri Lanka. This study used Landsat satellite images for the years 2000 and 2021 to detect the exotic Pinus caribaea species invasion of native habitats. By using an image difference technique, this research identified that the extent of these invasive pines had an overall decline over the past 21 years. Further, results showed that broadleaved forests and grasslands located within 100m of the pine plantations' borders were susceptible to invasion.

In tropical regions, analysing forests can be difficult due to cloud cover. This research also focused on methods to enhance classification accuracy using multiple data sources: Sentinel-1, Sentinel-2, PALSAR-2, and elevation. Six different methods were tested. It was found that combining radar data with optical and topographical data improved vegetation classification accuracy. In addition, feature importance analysis using the random forest algorithm indicated that radar data plays a significant role in tropical land use classification.

The three case studies used in this research demonstrate that GEE and the freely available mid-low resolution satellite images make the application of remote sensing in Sri Lanka a viable solution for the monitoring and mapping of landcover.

Acknowledgment

A PhD is a challenging journey that requires a great deal of perseverance. I am fortunate to have a strong support system that has kept me positive and motivated toward completing the PhD thesis.

I would like to express my gratitude to the supervisory panel, particularly my chief supervisor, Dr. Lars Brabyn, for providing me with the opportunity to study remote sensing and be comfortable with a subject I have never studied before. Your guidance, support, and patience throughout my Ph.D. journey have been invaluable. I also extend my heartfelt appreciation to my co-supervisor, Associate Professor Silvia Serrao-Neumann, for being a great listener, offering encouragement, and assisting me in fine-tuning all the chapters.

I also offer my gratitude to the AHEAD scholarship programme for providing me with financial assistance, and the Sabaragamuwa University of Sri Lanka for granting me the necessary leave to do my studies with ease of mind.

I would like to express my sincere gratitude to Charisse Hanson, an incredible soul who helped me with coding issues and brainstorming. I really missed you during the latter stages of Phd journey.

I would like to deeply thank Andrea Haines, a senior tutor in the Student Learning Center, for helping me improve my academic English writing. She has been a critical friend, and a valuable support system from my proposal to the final thesis.

To all my friends at the School of Social Sciences who have already graduated – Dr, Brent Commerer, Dr. Estelle Townshend, and Sumedha Amarasena – I offer my thanks for being there throughout my PhD journey. Their support and guidance helped me navigate through the different phases of my research and achieve my goals.

I am grateful for the constant support and guidance provided by my mother, Jayanie Samarakoon and father, Palitha Nandasena. They have helped me overcome stress and tension over the years and have always been there for me when I needed them the most. Their unwavering support has played a significant role in shaping me into the person I am today.

This journey in New Zealand would never have been started without the support of Nikesha Palihawadhana. Special thanks to Pham Thi Thin for providing me with accommodation and

mental support while I was alone in New Zealand and to Shaminda Kuruppu for providing me with transportation without hesitation when I first landed in New Zealand.

Finally, I am forever grateful to my biggest supporter, my husband, Pasindu Peiris, who has always given me the freedom to study, helped me relieve mental stress, and provided financial support throughout all these years. A special acknowledgment to my son Yasen Peiris, my little troublemaker and my happy pill; thank you for your presence in my life throughout these years.

Table of contents

List of Tables

List of Figures

List of acronyms & abbreviations

DEM	Digital Elevation Model
ETM+	Enhanced Thematic Mapper Plus
EVI	Enhanced Vegetation Index
GCI	Green Chlorophyll Index
GEDI	Global Ecosystem Dynamics Investigation
GEE	Google Earth Engine
GLCM	Grey-Level Co-Occurrence Matrix
HH	Horizontal Transmit And Horizontal Receive
HV	Horizontal Transmit And Vertical Receive
LiDAR	Light Detection and Ranging
MODIS	Moderate Resolution Imaging Spectroradiometer
MSS	Multispectral Scanning
NIR	Near-Infrared
NDVI	Normalised Difference Vegetation Index
NBR	Normalised Burn Ratio
NDMI	Normalised Difference Moisture Index
OLI	Operational Land Manager
PA	Producer Accuracy
PCA	Principal Component Analysis
RVI	Radar Vegetation Index
RF	Random Forest
RGCI	Red-Green Chlorophyll Index

SWIR	Shortwave Infrared
SRTM	Shuttle Radar Topographic Mission
SAR	Synthetic Aperture Radar
TCB	Tasselled Cap Brightness
TCG	Tasselled Cap Greenness
TCA	Tasselled Cap Transformation
TCW	Tasselled Cap Wetness
UA	User Accuracy
VI	Vegetation Indices
VH	Vertical Transmit and Horizontal Receive
VV	Vertical Transmit and Vertical Receive

Chapter 1
Introduction

This introductory chapter provides an overview of the significance of the research topic, how forests have changed in the Sri Lankan context, and the role of remote sensing in mapping vegetation change. The chapter also presents the aim and scope of the thesis, along with information about the thesis structure and chapter outlines.

Forests can change rapidly due to natural and anthropogenic disturbances, which affect their environment directly and indirectly. Forests are one of the most important ecosystems on Earth, as they protect water quality through watershed protection, maintain biodiversity by providing specific habitats for flora and fauna, and many help reduce climate change by sequestering carbon dioxide (Perry, 1994). Forest change occurs at different intensities and scales, from a death of single tree to a disastrous forest fire. Further, anthropogenic as well as natural threats to vegetation contribute to landscape changes and the instability of ecosystems. Deforestation in tropical forest regions is one of the main forest disturbances (Palo & Mery, 1996). This activity results in land degradation, loss of habitats, soil erosion and release of carbon into the atmosphere. Carbon emissions from deforestation and forest degradation result in the second largest anthropogenic source of carbon dioxide to the atmosphere, after the burning of fossil fuels (Zheng et al., 2021). Given that forests have significant ecological values, it is important that they are monitored. This includes mapping the extent and condition of forests and establishing forest reference emission levels to standardize national forest statistics, so that both foresters and policymakers are alerted of changes (Mensah et al., 2019; Perry, 1994).

This research investigated the use of remote sensing for mapping forest change in Sri Lanka, and focused on applications specific to this region. In particular, vegetation classes, such as “home garden”, are important to Sri Lanka, yet this vegetation class is overshadowed by the broad categories of global classifications. Additionally, invasive pines in the montane region of Sri Lanka are an issue, as these pines escape from plantation areas to natural habitats. As an island in a tropical region, Sri Lanka’s frequent cloud cover is a significant issue for the production of maps based on satellite images. Moreover, being a developing country, Sri Lanka also lacks resources to obtain high-quality satellite images and perform high-level computer processing.

1.1 Using Remote Sensing for Mapping Vegetation Change

Remote sensing is a proven method for monitoring the spatial extent and condition of a given vegetation type (Broich et al., 2011; Shimizu et al., 2019). However, change detection through remote sensing over time has many complications which need careful consideration, as revealed by Coppin and Bauer (1996) and Mishra et al. (2017). Many advances in remote sensing include new satellite data sources such as Sentinel and radar (Bouvet, Mermoz, Le Toan, et al., 2018; Poortinga et al., 2019) and new analytical techniques such as machine learning classifiers and functions (Lien, 2018). The remote sensing process and techniques are described further in Chapter 2.

The following section focuses on four aspects of remote sensing that offer opportunities for mapping vegetation change and were used by this research. These are combining different satellite images, using Google Earth Engine in a developing country, machine learning classification techniques, and different vegetation applications.

1.1.1 Combining Different Satellite Images

Most forest studies based on remote sensing use just one data source, which is easy to analyse but has limitations in accuracy. As Shimizu et al. (2019) emphasised, if using Landsat data alone, forest monitoring in cloudy tropical regions might have insufficient temporal observations in the rainy season due to cloud cover, causing delayed or omitted detections of disturbance events. However, Synthetic Aperture Radar (SAR) is particularly promising in terms of dealing with data continuity issues, as the radar signal is not affected by clouds (Carrasco et al., 2019). While this technology can be used to map deforestation and forest degradation (De Souza Mendes et al., 2019; Shimizu et al., 2019), its original high cost limited its used by less resourced countries. With the release of SAR observations from Sentinel-1 however, opportunities are now available to utilise these data more widely, especially in developing countries with limited budgets. Sentinel-1 offers dense observations in many tropical regions and there are a number of deforestation studies that use these data (Bouvet, Mermoz, Ballère, et al., 2018; Shimizu et al., 2019). However, few studies (Agapiou, 2020; Carrasco et al., 2019) combined optical and radar satellites such as Sentinel-1 to detect land-use change. Poortinga et al. (2019) have shown that a combination of Sentinel-2, Landsat-8 and Sentinel-1 provide a sufficiently dense spatial-temporal data series, even in regions with persistent cloud cover, including the ability to identify the difference between land cover and

plantation types. In particular, the combination of Sentinel-1 and PALSAR with Sentinel-2 appears to be under-researched – an issue addressed in Chapter 4 of this thesis.

1.1.2 Using Google Earth Engine

Most developing countries are not able to purchase commercial remote sensing software, nor afford the computer hardware required to run this software, as these programmes are licensed and generally cost the users. Therefore, freely available cloud-based remote sensing platforms, such as Google Earth Engine (GEE), are more accessible to developing countries. GEE is a cloud-based platform launched in 2010 for geospatial analysis that can perform massive computations (Wu et al., 2018). In particular, one of the best advantages of GEE is that it removed the need for computers with fast processing speeds and large storage capacities.

Studies that have used GEE for vegetation and forest monitoring and land cover/use change mapping include global mapping initiatives and studies in developed countries (Carrasco et al., 2019; Gorelick et al., 2017). The use of GEE for vegetation mapping in developing countries appears to be under researched (Kumar & Mutanga, 2018) and will be another focus of this thesis. All the research analysis has been done using GEE and, for the first time, this platform was used to map home gardens and detect invasive pines.

1.1.3 Using Machine Learning Classification Techniques

With a large amount of image data now available and the ability to combine data sources, machine learning techniques are proving to provide more accurate mapping results. Though machine learning classifiers may require larger amounts of training data, higher mapping accuracy can be achieved compared with conventional classifiers (Tsai et al., 2018). Johansen et al. (2015) concluded that the CART and Random Forest classifiers produced the highest user's and producer's accuracy for mapping woody vegetation in Australia using Landsat 5 and 7 images. Shimizu et al. (2019) mentioned that there is limited knowledge on the use of machine learning algorithms to detect forest disturbances through hybrid approaches that combine different data sources. This thesis used machine learning techniques to further test their suitability for enhancing forest mapping accuracy. Further, all three research papers (Chapters 3,4 and 5) used random forest algorithms for map classification and hyperparameter tuning and cross-validation in the analysis.

1.1.4 Different Vegetation Applications

Another aspect of remote sensing research is its use for developing different applications of vegetation studies. As this thesis focused on vegetation mapping, remote sensing was used for two main applications: agroforestry and forestry classification.

Home garden is an agroforestry class widely used in tropical countries' land use classification, but is neglected in global scale classification. Classifying a home garden is difficult, as it shows both cultivation and forestry characteristics and adjoins a house. Therefore, all the research on home gardens focused on diversity and structure but not the spatial element. This gap has been addressed in Chapter 3, using spectral and textural features.

Most forest applications focus on classification, including forest degradation or deforestation. Only a few studies have been conducted to investigate pines invasion, especially using remote sensing. Further, these studies (Bjerreskov et al., 2021; Kaplan, 2021) have mostly focused on commercial plantations in the temperate regions. Chapter 4 of this thesis investigates the use of remote sensing for mapping invasive pines in Sri Lanka where the forest classes are mixed, including tropical pine plantations that are maintained for soil conservation.

1.2 Aim of this research

The main intention of this thesis was to derive robust and accurate information through satellite images, using solutions that are affordable to Sri Lanka where resources are limited. This involved identifying the best combination of data sources, image analysis techniques, and also ensuring the application was relevant to Sri Lanka. For this, vegetation mapping included the identification of home gardens, and the monitoring invasive pines in the country’s tropical montane region.

1.3 Scope of this research

This research examined how openly available free remote sensing data sources and Google Earth Engine cloud platform perform to identify the vegetation cover in a tropical environment in three different scenarios. The first scenario mapped the home garden class, an agroforestry class that shares crops and perennial trees on the same landscape and mainly appears as a small forest patch, due to its stratification. Secondly, this thesis investigated how pine species escaped from the forest plantations maintained for conservation purposes and invaded the natural habitat using openly available remote sensing data. Lastly, the research explored how

well the classification accuracy increased when integrating multisource data such as radar, optical, and topography data to classify the tropical montane land cover.

A mountainous forest site in Sri Lanka was the main focus of this thesis; namely: Belihuloya in the Sabaragamuwa province – an area with a huge variation in elevation and slope, and wet and dry climatic characteristics. The area is located within an intermediate climatic zone with an elevation between 600 and 2000m, and shares different types of vegetation throughout the area. Due to the steep slopes, many pine plantations are maintained for soil conversation.

No vegetation study has been done in the intermediate zone of Sri Lanka using GEE; therefore, this research provides an opportunity to promote the use of this technology for countries in need of free cloud-based remote sensing access.

1.3.1 Specific research questions

1. Is the GEE platform suitable for mapping vegetation in developing countries?
2. What features are required to distinguish the home garden class from the other classes?
3. Can invasive pines be monitored in a complex landscape used for conservation?
4. Does the combination of radar and spectral data from different satellites improve the accuracy of vegetation mapping in cloudy tropical regions?

1.4 The thesis structure and chapter outlines

This thesis consists of six chapters: this general introductory chapter (Chapter 1), a literature review published as a book chapter (Chapter 2), three chapters comprising peer-reviewed publications (Chapters 3, 4, and 5), and a concluding chapter (Chapter 6) that provides discussions and a conclusion. Because chapters 2, 3, 4, and 5 were submitted to different publication outlets, they follow different specific formatting and referencing styles appropriate to each publisher.

Chapter 2 – "Using Remote Sensing for Sustainable Forest Management in Developing Countries"

This chapter is published as a book chapter as Nandasena, W. D. K. V., Brabyn, L., & Serrao-Neumann, S. (2020). Using Remote Sensing for Sustainable Forest Management in

Developing Countries. In *The Palgrave Handbook of Global Sustainability* (pp. 1-22). Springer International Publishing. https://doi.org/10.1007/978-3-030-38948-2_35-1

This chapter describes the remote sensing approach for sustainable forests in a developing country. Further, it elaborates on the Sustainable Development Goal 15; sustainable forest management. Moreover, it focuses on how developing countries can use open and freely available remote sensing data and platforms to conduct forest-related studies. More extensive literature can be found in each peer-reviewed paper (Chapters 3-5), as they explore three different remote sensing approaches in three different scenarios.

Chapter 3 - "Using Google Earth Engine to classify unique forest and agroforest classes using a mix of Sentinel 2a spectral data and topographical features: a Sri Lanka case study"

Chapter 3 is a peer-reviewed paper published as "W. D. K. V. Nandasenaa, Lars Brabyn and Silvia Serrao-Neumann 2022. Using Google Earth Engine to classify unique forest and agroforest classes using a mix of Sentinel 2a spectral data and topographical features: a Sri Lanka case study. *Geocarto International Journal* 37, NO. 25, 9544–9559". https://doi.org/10.1080/10106049.2021.2022010

This chapter investigates the importance of remote sensing in classifying a unique agroforestry class, a home garden. A single date Sentinel-2 image was used to extract the features to classify the home garden class. It used textural and spectral classification and showed the importance of texture features in identifying home gardens in Sri Lanka.

Chapter 4 - "Monitoring invasive pines using remote sensing: a case study from Sri Lanka"

Chapter 4: is a peer-reviewed paper published as Nandasena, W., Brabyn, L. & Serrao-Neumann, S. Monitoring invasive pines using remote sensing: a case study from Sri Lanka. *Environmental Monitoring Assessment* **195**, 347 (2023). https://doi.org/10.1007/s10661-023-10919-1

This chapter looks into the expansion of exotic pines into the natural environment using change analysis and images from two different years (2000 and 2021). Landsat-8 and Landsat-7 were used to extract the features and identify the grassland and broadleaved forest that are vulnerable to pine invasion.

Chapter 5- "Evaluating the Addition of Radar with Optical Data for Vegetation Mapping in a Tropical Montane Region: a Case Study in Sri Lanka"

Chapter 5: this paper was submitted to the " Journal of Mountain Science."

This chapter investigates the usefulness of radar data combined with optical data to map vegetation in tropical montane regions with frequent cloud cover. It evaluates six different scenarios of using spectral, backscattering, and elevation data on mapping vegetation. The chapter concludes that radar or optical data alone cannot obtain satisfactory results. However, when combining radar with optical data, the vegetation mapping accuracy is increased.

Chapter 6 – "Discussion and Conclusion"

This final chapter synthesizes previous chapters' results and summarises the research questions' answers. This chapter recaps the contribution of this research in the remote sensing of vegetation. Limitations of this research are discussed, including suggestions for future research that address these limitations.

1.5 Reference

Agapiou, A. (2020). Estimating Proportion of Vegetation Cover at the Vicinity of Archaeological Sites Using Sentinel-1 and -2 Data, Supplemented by Crowdsourced OpenStreetMap Geodata. *Applied Sciences*, *10*(14), 4764. https://www.mdpi.com/2076-3417/10/14/4764

Bjerreskov, K. S., Nord-Larsen, T., & Fensholt, R. (2021). Classification of Nemoral Forests with Fusion of Multi-Temporal Sentinel-1 and 2 Data. *Remote Sensing*, *13*(5). https://doi.org/10.3390/rs13050950

Bouvet, A., Mermoz, S., Ballère, M., Koleck, T., & Le Toan, T. (2018). Use of the SAR Shadowing Effect for Deforestation Detection with Sentinel-1 Time Series. *Remote Sensing*, *10*(8).

Bouvet, A., Mermoz, S., Le Toan, T., Villard, L., Mathieu, R., Naidoo, L., & Asner, G. P. (2018). An above-ground biomass map of African savannahs and woodlands at 25m resolution derived from ALOS PALSAR. *Remote Sensing of Environment*, *206*, 156-173. https://doi.org/https://doi.org/10.1016/j.rse.2017.12.030

Broich, M., Hansen, M. C., Potapov, P., Adusei, B., Lindquist, E., & Stehman, S. V. (2011). Time-series analysis of multi-resolution optical imagery for quantifying forest cover loss in Sumatra and Kalimantan, Indonesia. *International Journal of Applied Earth Observation and Geoinformation*, *13*(2), 277-291. https://doi.org/https://doi.org/10.1016/j.jag.2010.11.004

Carrasco, L., O'Neil, A. W., Morton, R. D., & Rowland, C. S. (2019). Evaluating Combinations of Temporally Aggregated Sentinel-1, Sentinel-2 and Landsat 8 for Land Cover Mapping with Google Earth Engine. *Remote Sensing*, *11*(3), 288. https://www.mdpi.com/2072-4292/11/3/288

Coppin, P. R., & Bauer, M. E. (1996). Digital change detection in forest ecosystems with remote sensing imagery. *Remote Sensing Reviews*, *13*(3-4), 207-234. https://doi.org/10.1080/02757259609532305

De Souza Mendes, F., Baron, D., Gerold, G., Liesenberg, V., & Erasmi, S. (2019). Optical and SAR Remote Sensing Synergism for Mapping Vegetation Types in the Endangered Cerrado/Amazon Ecotone of Nova Mutum—Mato Grosso. *Remote Sensing*, *11*(10). https://mdpi-res.com/d_attachment/remotesensing/remotesensing-11-01161/article_deploy/remotesensing-11-01161.pdf?version=1557913881

Gorelick, N., Hancher, M., Dixon, M., Ilyushchenko, S., Thau, D., & Moore, R. (2017). Google Earth Engine: Planetary-scale geospatial analysis for everyone. *Remote Sensing of Environment*, *202*, 18-27. https://doi.org/https://doi.org/10.1016/j.rse.2017.06.031

Johansen, K., Phinn, S., & Taylor, M. F. J. (2015). Mapping woody vegetation clearing in Queensland, Australia from Landsat imagery using the Google Earth Engine. *Remote Sensing Applications: Society and Environment*, *1*, 36-49.

Kaplan, G. (2021). Broad-Leaved and Coniferous Forest Classification in Google Earth Engine Using Sentinel Imagery. *Environmental Sciences Proceedings*, *3*(1), 64. https://www.mdpi.com/2673-4931/3/1/64

Kumar, L., & Mutanga, O. (2018). Google Earth Engine Applications Since Inception: Usage, Trends, and Potential. *Remote Sensing*, *10*(10), 1509. https://www.mdpi.com/2072-4292/10/10/1509

Lien, P. T. H. (2018). *Mapping Vegetation With Remote Sensing And Gis Data Using Object-Based Analysis And Machine Learning Algorithms*. University of Waikato.

Mensah, A. A., Akoto Sarfo, D., & Partey, S. T. (2019). Assessment of vegetation dynamics using remote sensing and GIS: A case of Bosomtwe Range Forest Reserve, Ghana. *The Egyptian Journal of Remote Sensing and Space Science*, *22*(2), 145-154. https://doi.org/https://doi.org/10.1016/j.ejrs.2018.04.004

Mishra, S., Shrivastava, P., & Dhurvey, P. (2017). Change detection techniques in remote sensing: A review. *International Journal of Wireless and Mobile communication for Industrial systems*, *4*(1), 1-8.

Palo, M., & Mery, G. (1996). Transition from deforestation to sustainable forestry -a distant dream? In M. Palo & G. Mery (Eds.), *Sustainable Forestry Challenges for Developing Countries* (Vol. 10, pp. 1-13). Kluwer Academic Publishers.

Perry, D. A. (1994). *Forest Ecosystems*. Johns Hopkins University Press.

Poortinga, A., Tenneson, K., Shapiro, A., Nquyen, Q., San Aung, K., Chishtie, F., & Saah, D. (2019). Mapping Plantations in Myanmar by Fusing Landsat-8, Sentinel-2 and Sentinel-1 Data along with Systematic Error Quantification. *Remote Sensing*, *11*(7), 831. https://www.mdpi.com/2072-4292/11/7/831

Shimizu, K., Ota, T., & Mizoue, N. (2019). Detecting Forest Changes Using Dense Landsat 8 and Sentinel-1 Time Series Data in Tropical Seasonal Forests. *Remote Sensing*, *11*(16). https://doi.org/10.3390/rs11161899

Tsai, Y. H., Stow, D., Chen, H. L., Lewison, R., An, L., & Shi, L. (2018). Mapping Vegetation and Land Use Types in Fanjingshan National Nature Reserve Using Google Earth Engine. *Remote Sensing*, *10*(6), 927. https://www.mdpi.com/2072-4292/10/6/927

Wu, W. J., Zhao, X. J., Gong, C., Li, X. W., & Ieee. (2018). Obtain The Patterns Of Global Forest Npp And Its Influence Factors With Google Earth Engine. In *Igarss 2018 - 2018 Ieee International Geoscience and Remote Sensing Symposium* (pp. 2898-2901). Ieee. <Go to ISI>://WOS:000451039802244

Zheng, B., Ciais, P., Chevallier, F., Chuvieco, E., Chen, Y., & Yang, H. (2021). Increasing forest fire emissions despite the decline in global burned area. *Science Advances*, *7*, eabh2646. https://doi.org/10.1126/sciadv.abh2646

Chapter 2
Using remote sensing for sustainable forest management in developing countries

This chapter is published as a book chapter as Nandasena, W. D. K. V., Brabyn, L., & Serrao-Neumann, S. (2020). Using Remote Sensing for Sustainable Forest Management in Developing Countries. In The Palgrave Handbook of Global Sustainability (pp. 1-22). Springer International Publishing. https://doi.org/10.1007/978-3-030-38948-2_35-1

Abstract

Sustainable forests are productive, multi-functional, and evolving renewable resources that can meet ever-changing needs. Investing in sustainable forests represents a global investment in social-ecological resilience because forests are capable of soil and water conservation, carbon sequestration, providing habitats, and supporting livelihoods. While the Sustainable Development Goal 15 promotes the sustainable management of all types of forests, including the restoration of degraded ecosystems to substantially increase reforestation globally, deforestation rates continue to increase worldwide. In particular, within developing countries there is often significant pressure on forests to accommodate intense population growth and support local livelihoods dependent on forest products. Hence, improved forest management initiatives are paramount. Remote sensing is recognised as an effective monitoring tool for forest sustainability. This technology is used for mapping vegetation cover and detecting deforestation and degradation from local to global scales. This chapter discusses remote sensing technology, its applications to forest studies, and how significant advances in open data policy and cloud computing over the last decade provide opportunities for developing countries to use remote sensing to map and monitor forest extent and structure, and thereby assist sustainable forest management goals.

Key Words: Open Source, Cloud Computing, Reforestation, Sustainable Development Goal 15, Google Earth Engine

2.1 Introduction

Forests play an important role in reducing water runoff and soil erosion, and in conserving and protecting biodiversity. However, rapid population growth coupled with commercial agricultural development contribute to increased deforestation, degradation, and adverse environmental impacts (Mitchell, Rosenqvist, and Mora 2017; Palo and Mery 1996). Most countries establish forest plantations to reduce encroachment on natural forests and to provide timber requirements. Nevertheless, continued pressure on forest resources raises the debate on managing forests sustainably for future generations. This has increased attention to afforestation, reforestation, and agroforestry practices such as taungya and home gardens (Cannell 1988).

Advancing the United Nations (U.N.) Millennium Development Goals, the 17 Sustainable Development Goals (SDGs) were established in 2015 to focus on global sustainability (United Nations 2015). In particular, SDG 15 (Life on Land) promotes the sustainable management of all types of forests that halts deforestation, restores degraded forests, and substantially increases afforestation and reforestation globally. To fulfil SDG 15, we need accurate information about what happened, and is happening, within the forest extent and the changes occurring over time. Remote sensing plays an important role in this by providing information on different scales (global, regional and national) which can be used for forecasting based on past land use cover changes. Furthermore, this technology is a proven method for mapping and monitoring the forest's condition (Broich et al. 2011; Shimizu, Ota, and Mizoue 2019).

Although most of the world's significant tropical forests are found in developing nations, other forest types (e.g. temperate, Mediterranean, boreal, and conifer) have drawn more interest among remote sensing scientists over the past decades (Franklin 2001). Additionally, researchers from developing countries face challenges imposed by limitations in technical expertise and significant financial investments required by high-performance computing infrastructure necessary for tropical forest research (Lechner, Foody, and Boyd 2020). Furthermore, tropical forest research is also challenged by how the near-permanent cloud cover limits optical image availability (Mitchell, Rosenqvist, and Mora 2017; Boyd and Danson 2005), as well as the remote sensing pre-processing requirements that are demanding and time-consuming. However, the availability of open-source Earth Observation (E.O.) data is ameliorating these difficulties in this research domain (Mitchell, Rosenqvist, and Mora 2017). For example, Sentinel satellites have higher temporal frequency and constellation boost

capability that functions well against cloud-dominated tropical areas (Mitchell, Rosenqvist, and Mora 2017; Bhunia, Shit, and Sengupta 2021); Sentinel's Synthetic Aperture Radar (SAR) sensor has demonstrated reliable detection of cloud-free images (Boyd and Danson 2005).

Remote sensing, machine learning approaches and time series analysis have been used to create datasets for global forest mapping, including forest change and drivers of change datasets that are freely available for subsequent analyses (see Table 2.1).

Table 2.1 Global land cover Data Sets

Data set	**Time period**	**Satellite**	**Resolution**	**Source**
University of Maryland Global Land Cover Classification	2009	AVHRR*	1km	Defries and Hansen (2010)
Global Land Cover Characterization	1992-1993	AVHRR	1km	Earth Resources Observation And Science (EROS) Center (2017)
Global Land Service	2019	Copernicus	100m	Marcel et al. (2020)
Land Cover Type (MCD12Q1) Version 6	2001-2019	MODIS**	500m	Friedl and Sulla-Menashe (2019)
Global forest change	2000-2020	Landsat	30m	Hansen et al. (2013)
Global Forest Canopy height	2019	GEDI and Landsat	30m	Potapov et al. (2021)

*Atmospheric Administration Advanced very high-resolution radiometer,** Moderate Resolution Imaging Spectroradiometer, *** Global Ecosystem Dynamics Investigation

Most global-scale land cover products consist of classes defined at the biome level (Gong et al. 2016). Land cover types that are significant but not prevalent in major biomes, however, are often neglected. Thus, global land cover datasets can experience loss of information and errors at the local scale, hiding the heterogeneity among regions (Erasmi et al. 2007). In particular, the home garden, a predominant agroforestry class in tropical developing countries, comprises a knowledge gap in current literature because it has not been included in available global land cover products (Pérez-Hoyos et al. 2017). This is because home gardens require products at a much higher resolution, such as 10m grid (Mathieu, Freeman, and Aryal 2007), when most available products are between 500m to 1km spatial resolution (see Table 2.1). Hence, details of land cover types unique to a region or a local area are hard to identify and may compromise a country's ability to manage their forests more sustainably.

This chapter advances the discussion on the use of remote sensing technology and its applications to forest studies. In particular, it explores how significant advances in open data

policy and cloud computing over the last decade provide opportunities for developing countries to manage forests more sustainably. The chapter is structured as follows. Section 2.2 describes remote sensing technologies and processes, including open-source data and cloud-based platforms. Section 2.3 analyses the applications of remote sensing in forest management, while future research opportunities are explored in Section 2.4 Lastly, the summary is presented in Section 2.5.

2.2 Remote Sensing Technology

Remote sensing is evolving rapidly, particularly because it acts as a technological interface between engineering, computer science, geography and various other disciplines (Lechner, Foody, and Boyd 2020). Hence, this technology has been used widely to detect, quantify and map forest types of rough or challenging terrain areas because it provides reliable and updated information more efficiently (Biswas et al. 2020; Liu et al. 2018). In addition, in recent years, remote sensing has been used in integrated analysis, combining optical and radar data with Geographical Information System (GIS) data, topographical data, and climate data. Remote sensing often follows a process from image capture to classification and accuracy assessment as shown in Figure 2.1. Within each step in this process, significant advances are being made. The following sections describe the different steps in this process in more detail. This process is executed using specialised remote sensing software platforms, and these are reviewed first.

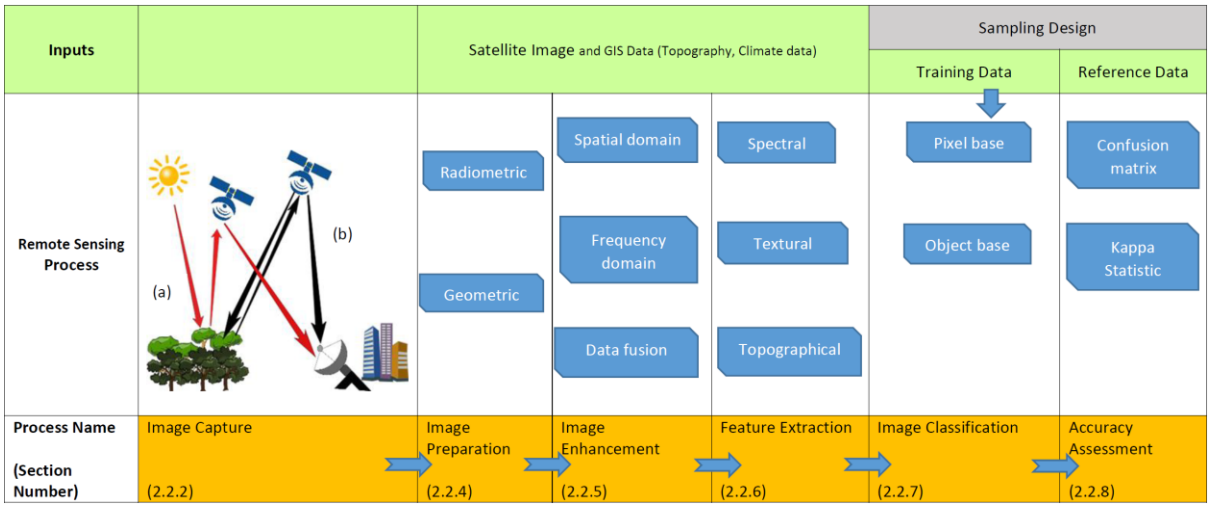

Figure 2.1 The remote sensing process

2.2.1 Remote sensing software platforms

In past years, a number of commercial remote sensing software has been developed capable of efficiently processing massive amounts of remote sensing data using various computer operating systems. These include:

1) ENVI - a commercial remote sensing software designed by L3Harris Geospatial to process large multispectral and hyperspectral remote sensing data (https://www.l3harrisgeospatial.com/Software-Technology/ENVI). This software offers a wide range of traditional and non-traditional image classifiers since 1974 and requires US$8370 for a subscription.
2) ERDAS IMAGINE - one of the oldest Geoinformatics software developed in 1978 by Hexagon Geospatial (https://www.hexagongeospatial.com/products/power-portfolio/erdas-imagine). It contains comprehensive and sophisticated tools for image analysis with $3500 expense for an annual licence.
3) PCI Geomatica - a leading remote sensing, photogrammetry, and cartographic software developed in 1982 by PCI Geomatics Corporate (https://www.pcigeomatics.com/index.php). It offers a high degree of automation and customised workflow, costing $2229 for a subscription.

In contrast, freely available remote sensing platforms have been emerging and gaining popularity, thanks to the contributions of many software developers in open source geospatial analysis (Bhunia, Shit, and Sengupta 2021). The four most common platforms currently in use are the following:

1) Geographic Resources Analysis Support System (GRASS) - an open-source software operating since 1984 for geospatial analysis, image processing, and spatial modelling. This can couple with the statistic software R and be available as a standalone package with grass scripting.
2) System for Automated Geoscientific Analyses (SAGA) specialist package - released in 2004, it offers diverse functions, including raster analysis and object-oriented classification (Rocchini et al. 2017).
3) Quantum GIS (QGIS) - released in 2002, it is more user-friendly software, and currently has one of the largest GIS user communities in the world (Steiniger and Hay 2009).
4) Google Earth Engine (GEE) – is a freely available (but not open-source) cloud-based platform for non–commercial geospatial analysis launched by Google in 2010. It

enables users to process data and create products without significant investment in computing infrastructure (Gorelick et al. 2017).

Despite the free and open-source desktop software platforms and their advancement of image processing functions, retrieving and downloading satellite images on large scales remain challenging in the abovementioned platforms. Google has addressed this issue by introducing an online geospatial analysis platform: GEE with well-trained algorithms and time-series images through the Google Earth Timelapse. GEE has focused primarily on global forest monitoring and measurement in order to support Reducing Emissions from Deforestation and Degradation Plus (REDD+) activities in the developing world. Therefore, this platform was initially built by publishing a complete archive of more than 25 years of historical Landsat imagery of tropical regions freely to developing countries (Kumar and Mutanga 2018) because these countries need to establish national baselines for deforestation as required under the REDD mechanism that would pay tropical countries to protect forests.

Currently, the GEE platform includes a massive multi-petabyte data catalogue encompassing over 40 years of E.O. datasets retrieved from different satellites, such as Landsat, MODIS, National Oceanographic and Atmospheric Administration Advanced very high-resolution radiometer (NOAA AVHRR), Sentinal-1, 2 and 3, and Advanced Land Observing Satellite (ALOS) (Kumar and Mutanga 2018). This product enables planetary wide visualisation and provides free access for the research sector, education sector, and non-profit purposes to the data processing algorithms and cloud computing facilities (Lee, Cardille, and Coe 2018). Moreover, the GEE data catalogue includes many pre-processed datasets to streamline spatial analysis and enhance the analysis with minimal cost, time, and equipment. For example, Landsat Surface Reflectance has been atmospherically corrected while Sentinel-1 SAR pre-processed for thermal noise removal, radiometric calibration, and terrain correction.

Cloud computing delivers different computer services, including networks, servers, data storage, databases, software, and analytics, over the internet without direct active management by the user. It further enables users to save storage space on desktop computers, collaborate effectively, and reduce the dependency and cost of expensive computer hardware. As a cloud computing platform, GEE enables the processing of petabytes of image data (Gorelick et al. 2017), combined with other vector data, within the cloud environment and removes the need to store, process, and analyse the large volumes of satellite data on a desk computer (Kumar and Mutanga 2018). Further, this reduces the users' dependency on specialist remote sensing software and removes the need for software license subscriptions and expensive computer

hardware that benefited developing countries the most. Furthermore, researchers can upload their vector and raster data to the platform and share the repositories with other users to view older versions of the scripts.

Therefore, understanding and monitoring forest resources can be more easily implemented in developing countries where computing resources are limited. Jahromi et al. (2020) identified Asian and African countries had employed the GEE platform more often to conduct forest-related problems. Similarly, Kumar and Mutanga (2018) recognised that GEE eliminates geospatial analysis barriers, especially for developing countries. Moreover, GEE benefits researchers worldwide, demonstrating the power of using large-scale computing to address global environmental problems and assists users to create real-time data sets. For example, global forest watch (GFW), launched in 2014, was solely developed using GEE. Table 2.2 shows recent research that uses GEE from the global to the local scale, to detect forest changes. In addition to providing a facility to monitor forests, GEE has teamed up with the Global Partnership on Sustainable Development Data of the U.N. for accelerating the progress of SDGs by providing satellites data and advanced cloud computing technologies (UNBigData 2019).

Table 2.2 Summary of recent forest studies of GEE in different scales.

Author	**Focus**	**Period**	**Area/scale**	**Satellite/ Data Source**
Hansen et al. (2013)	Forest change	2000-2012	Global Scale	Landsat
Johansen, Phinn, and Taylor (2015)	Woody vegetation change	2004-2010	Queensland, Australia	Landsat 5&7
Tsai et al. (2018)	vegetation and land use types	2011 and 2016	Fanjingshan National Nature Reserve, China	Landsat 5&8
Wu et al. (2018)	Global forest NPP	2004-2013	Global Scale	MODIS and ESA Landcover
Zurqani et al. (2018)	Land use change	1999, 2005, 2009, and 2015	Savannah River basin, U.S.	Landsat 7
Zhang et al. (2019)	mapping bamboo distribution	2013-2018	Hainan Island, China	Landsat 8
Deng et al. (2020)	Eucalyptus plantations	2013-2018	Guangxi province of China	Landsat 8, Sentinel 2, and MODIS
Srinet et al. (2020)	Mapping plant functional types	2008-2018	Northwest Himalayan foothills of India	MODIS-Terra and SRTM
Biswas et al. (2020)	Forest type mapping	2018	Myanmar	Landsat, Sentine 1&2
Ranagalage et al. (2020)	Forest cover dynamics and drivers	2019 1992 and1999	Dry zone of Sri Lanka	Landsat 8 and Forest cover maps

2.2.2 Image capture

Remote sensing technology acquires information from a distance by recording electromagnetic energy reflected or emitted from the earth surface, typically including satellite-borne or airborne sensors. Two types of sensors are used to capture an image: passive and active remote sensing. Passive remote sensing (see Figure 2.1-a) measures reflected electromagnetic radiation from a surface. Examples of passive remote sensing types are Multispectral Scanning (MSS) (Landsat) and Push Broom Scanners such as SPOT. In contrast, active remote sensing (see Figure 2.1-b) system emits radiation on the study object and measures the reflected radiation. The most common types are radar, which operates within the microwave region in the electromagnetic spectrum, and LiDAR (Light Detection and Ranging).

Most vegetation applications use optical data sources in the visible and near-visible regions of the spectrum (Shimizu, Ota, and Mizoue 2019). Forest applications have widely used the near-infrared (NIR) region because of its sensitivity to determine vegetation evapotranspiration, plant health and distinguish forest types (Verbyla 1995; Rees 2013). Radar in remote sensing is beneficial in areas with a thick cloud cover due to the advantage of low atmospheric absorption, which can penetrate through clouds. Radar falls into the microwave region where the larger than 1cm electromagnetic radiation is categorised (Rees 2013). LiDAR is an active optical sensor and airborne remote sensing with similar principles to a radar system. Since this system can determine three-dimensional space for the target location, it is beneficial for identifying biophysical information on the forest.

2.2.3 Data sources

2.2.3.1 Commercial data

Higher-resolution optical data is available commercially through missions by private companies and governments in North America and Europe, such as the following. The SPOT missions by the French National Centre for Space Studies (CNES) offer high-resolution optical imagery since 1986 and have a resolution of 5-20m. The latest satellites, SPOT 6 and SPOT 7, are identical satellites that detect ground cover changes and remain operational until 2024. The Pleiades mission was also launched by CNES in 2009 as a constellation of two spacecraft with 2.8m spatial resolution. The GeoEye mission, operated by Digital Globe of the United States with a high spatial resolution of 1.64m, was launched in 2008.

2.2.3.2 Open-source data

Free and open access data policy leads and supports the expansion of remote sensing applications, which use large amounts of data that vary spatially and temporally. Further, this leads to local, regional, and global mapping of annual forest change, global surface water extent, human settlements, and land cover. This policy maximises the societal benefit and supports remote sensing scientists from developing countries with limited resources to purchase expensive satellite images. For example, the United States Geological Survey (USGS) Landsat programme made Landsat available for free via the internet since 2008 (Zhu et al. 2019), which spurred the adoption of similar policies globally, including the European Space Agency's Sentinel images in 2014 (Carrasco et al. 2019). The emergence of free and open access data policies coincided with the expansion of cloud-based platforms, such as GEE, that have dramatically assisted the establishment of long-term forest monitoring programmes (Mitchell, Rosenqvist, and Mora 2017) and increased research using satellite data (Crowley and Cardille 2020). The Landsat and Sentinel missions are further explored in terms of how they contribute towards achieving SDG 15 and how they benefit scientific research for developing countries.

Landsat. As shown in Table 2.3, Landsat is the longest-running terrestrial satellite since 1972, started by NASA and the U.S. Geological Survey (USGS). Landsat products have been widely used for regional-scale vegetation mapping with various sensors (Xie, Sha, and Yu 2008). The Multispectral Scanner (MSS) was carried on Landsat 1, 2, and 3 with a spatial resolution of about 79 meters and Thematic Mapper sensor with a spatial resolution of 30m and collected data in seven spectral bands on Landsat 4 and 5. Currently, Landsat 7 and 8 are operational in space. The Enhanced Thematic Mapper Plus (ETM+) sensor of Landsat 7 has been designed to seasonally monitor vegetation growth cycles, deforestation and agricultural land use on a global scale . The Landsat 8 has launched in 2013 and has two sensors; the Thermal Infrared Sensor (TIRS) and the Operational Land Manager (OLI).

Table 2.3 Summary of freely available Open-source data

Satellite name	Data source	Missions	Spatial resolution	Launched in
Landsat	USGS Earth Explorer	Landsat1-8	30m	1972
Sentinel	European Space Agency	Sentinel 1-6	10m-60m	2014
MODIS	NASA	Terra and Aqua	250m	1999
NOAA-AVHRR	USGS	NOAA 6-14	1.1km	1979
GEDI	International Space Station	GEDI	1km	2019
BIOMASS P-band SAR satellite	European Space Agency	Biomass	60m	2023
SRTM	NASA	SRTM GL1	30m	2000

Sentinel. Sentinel is a family of Earth Observation missions developed by the European Space Agency under the Copernicus Programme, carrying a range of technologies, such as radar and multispectral imaging instruments for land, oceanic, and atmospheric monitoring. The Sentinel-1 mission comprises two polar-orbiting satellites: Sentinel-1A launched in 2014 and Sentinel-1B in 2016. These satellites are capable of day and night radar imaging for land and ocean services using the Synthetic Aperture Radar (SAR) sensor, with a 10m spatial resolution, that has the ability to acquire imagery in all weather conditions (European Space Agency). The Sentinel-2 mission also comprises two polar-orbiting satellites, Sentinel 2A launched in 2015 and Sentinel 2B in 2017, with a multispectral high spatial resolution image sensor. The spatial resolution of Sentinel-2 (Table 2.3) varies with the bands. The blue, green, red, and NIR bands have a resolution of 10m, the red–edge and short wave infrared (SWIR) bands 20m, and all others 60m (Poortinga et al. 2019). Sentinel-2 constellation improves the capture of canopy gaps and clearing in tropical forests (Mitchell, Rosenqvist, and Mora 2017). These satellite data have benefits for tropical forest cover studies because they acquire images with a higher spatial resolution (20m) of spectral bands in near-infrared (band5, band 6, band 7, and band 8a) (Addabbo et al. 2016). Further, Sentinel 1 radar data add more information on vegetation structure (Biswas et al. 2020).

The following sections from 2.2.4-2.2.8 explore remote sensing classification. The process of image classification through remote sensing extracts meaningful units of information from satellite imagery into different classes and involves the following main steps: image

preparation, image enhancement, feature extraction, image classification and accuracy assessment (see Figure 2.1).

2.2.4 Image preparation

Image preparation, or pre-processing, involves ensuring that the images are accurate and have minimal distortion from the atmosphere. Radiometric pre-processing affects the brightness values of an image to correct for sensor malfunctions, and geometric correction is the process of changing spatial coordinates of the image to the corresponding spatial coordinates on the Earth's surface (Rees 2013). Moreover, correction of the atmospheric propagation effect is necessary if more than one scene is to be treated in the same study because atmospheric errors are possible causes for inconstancy (Verbyla 1995). This can be done using several methods such as the histogram minimum method, dark object subtraction, and more advanced atmospheric correction models such as MODTRAN (MODerate resolution atmospheric TRANsmission) and ATCOR (Atmospheric and Topographic Correction). Different platforms have their own set of atmospheric algorithms for specific satellite images (e.g. simpleCloudScore, FMask).

2.2.5 Image Enhancement

Image enhancement aims to produce better images than the original satellite images (Lillesand, Kiefer, and Chipman 2008). Therefore, image enhancement techniques emphasise satellite image features such as edges, boundaries, or contrasts to improve the image quality and detail. As shown in Figure 2.1, there are two types of image enhancement techniques: 1) spatial domain, or spatial filtering, deals with pixel manipulation; and 2) frequency domain, or contrast modification, decomposes the image into signal via Fourier transforms (Rees 2013). Spatial filtering includes two types; low pass filter- smooths the image and reduces noise, and high pass filter- sharpens the appearance of an image and is used for edge detection. Contrast modification has several types. The linear contrast stretch is the simplest type of enhancement in this category that involves identifying maximum and minimum brightness values and applying a transformation to stretch this range to fill the entire range (Bajpai and Soni 2017). Histogram Equalisation is the most common and conventional contrast modification method used to enhance the contrast within an image because it assigns more brightness values to the frequently occurring portions of the histogram.

2.2.5.1. Data fusion

The process of combining images or data from different sources with varying extents in time and space is known as data fusion. This process brings images of varied resolution into a single image (Campbell and Wynne. 2011). Because of the broad range of characteristics of images collected by varied sensors and the routine availability of digital data, there has been an increasing incentive to bring data from varied systems together into a single image (Campbell and Wynne. 2011). Traditionally, data fusion involves merging multispectral images of coarse spatial resolution with a finer spatial resolution of the same region. Image fusion can be applied to varied forms of remotely sensed data, such as merging multispectral images with radar or digital elevation data. There are several techniques used for image fusion. The High Pass Filter (HPF) and ARSIS are methods used as spatial domain procedures; these methods extract the high-frequency variation of a fine resolution image and then insert it into the multispectral framework of a corresponding coarse resolution image.

2.2.6 Feature extraction

Feature extraction involves extracting useful information from images. This information is then used for classification. Feature extraction can involve combining data to produce higher-level information that produces more accurate classifications.

2.2.6.1 Spectral feature extraction

Spectral bands and vegetation indices that can be used for classifications are known as spectral features. Usually, spectral bands such as red-edge bands, NIR, Shortwave infrared (SWIR) and visual bands are suitable for forest analysis (Wessel, Brandmeier, and Tiede 2018; Addabbo et al. 2016). Vegetation indices (VI) are developed by combining several spectral values that are added, divided, or multiplied in a manner designed to measure biomass or vegetative vigour (Campbell and Wynne. 2011). Most vegetation indices combine the red spectral region (0.6-0.7 µm) and NIR (0.7-0.11 µm) to enhance the vegetation signal while minimising non-vegetation influences (Chuvieco 2016). These indices provide information about vegetation greenness or the presence of vegetation in the selected image, such as the normalised difference vegetation index (NDVI) use NIR and red band.

2.2.6.2 Textural feature extraction

Texture feature extraction uses statistical measures based on the spatial distribution of grey levels of an image (Kuplich, Curran, and Atkinson 2005). The common textural feature extraction methods include spatial co-occurrence and the grey-level co-occurrence matrix (GLCM). The GLCM, proposed by Haralick, Shanmugam, and Dinstein (1973), has been extensively used for forest classification (Cheng and Wang 2019; Kuplich, Curran, and Atkinson 2005), where shadow patterns caused by different tree structures give rise to a distinctive texture (Hall-Beyer 2017).

2.2.6.3 Topographical analysis

Topographical features derived from remote sensing play a significant role in forest classification and help to differentiate the spatial distribution of forest types. Further, topography improves classification accuracy for areas with significant elevation or slope differences (Deng et al. 2020). Digital Elevation Model (DEM) is used to derive topographical features such as slope, hill shade, aspect, and elevation.

2.2.7 Image classification

Forest classification can be perform using a pixel-based or object-based classification approach (Camarretta et al. 2020). Pixel-based classification uses the spectral pattern of each pixel as the numerical basis for categorisation (Vick 2008). Many researchers identified that a "salt and pepper" effect was produced in a pixel-based classification of a high spatial resolution image (Weih and Riggan, n.d.). In contrast, object-based classification groups pixels into objects and classifies those objects based on their shape, size, colour, spatial variation, and context (neighbouring information) (Crowley and Cardille 2020). According to Vick (2008), object-based classification outperformed pixel-based classification methods because spectral and contextual information usage leads to higher accuracy.

2.2.7.1 Collecting reference data

Reference data are used to interpret and analyse what is being sensed and to validate the classification. This can be collected at a different time from training data used to classify, such as field data collection or forest inventory, or to collect the reference data at the time as training data. In this case, data can be randomly split into two sets; training and reference data (Green

2017). This is an effective approach when going to the field is expensive and time-consuming. Another valid and practical option is to use high-resolution images such as Google Earth with prior knowledge of the study area to validate classification. This is when search and travel costs are prohibitive and when the extent of the study area is extensive (Biswas et al. 2020). There is also another possible way to collect the reference data at the time as training data.

2.2.7.2 Training and testing data sampling

Training data refers to a sample of observation, typically consisting of points or polygons, that relate image pixels or objects to interpret classes plays a vital role in supervised classification (Elmes et al. 2020). Five different sampling strategies have been commonly applied to build the training and testing datasets in forest research (Campbell and Wynne. 2011): 1) Simple random sampling- the elements to be verified are chosen so that all of them have the same probability of being selected; 2) Stratified random sampling is selected by dividing the population into regions or strata, according to a variable used in the classification (e.g. elevation); 3) Systematic random sampling- sample units are selected from a randomly selected starting point at regular intervals; 4) Systematic unaligned sampling - this modified systematic sampling by including the randomness into the sampling procedure reduces the regularity bias and completes the coverage of the territory; 5) Cluster sampling- a group of observations is selected as a sampling unit instead of using single pixels.

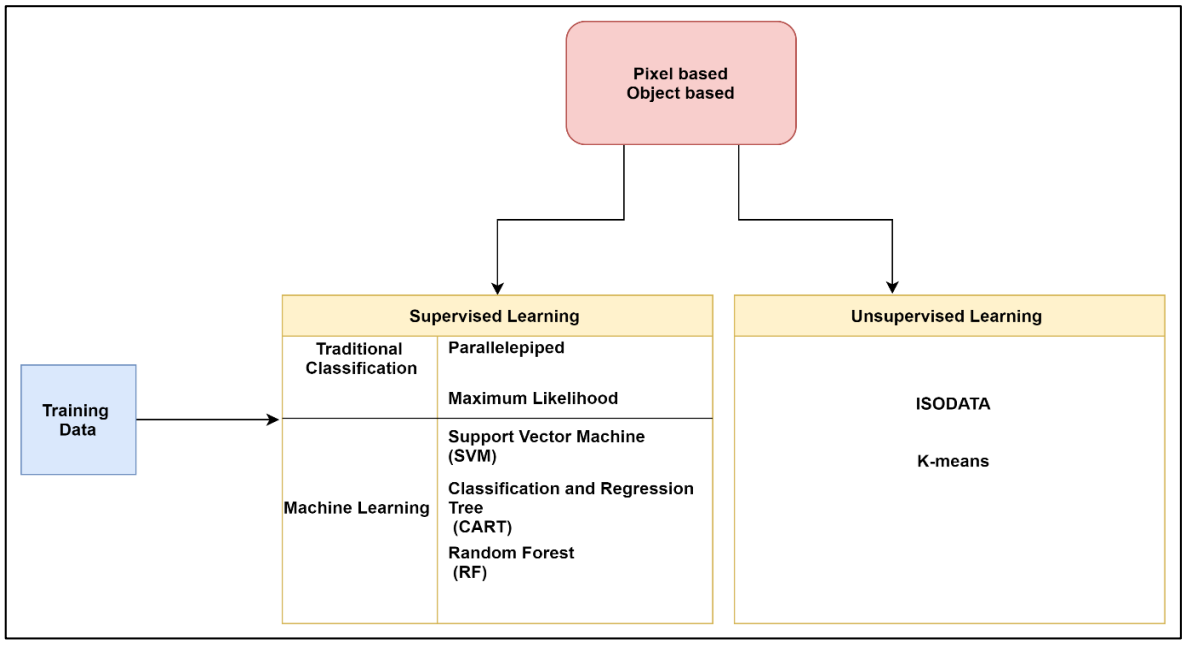

Figure 2.2 Image classification

2.2.7.3 Traditional classifications

Unsupervised classification is the process of grouping pixels' spectral properties into clusters and assigning a class to each cluster (Jensen 2016). The major problem of this approach is that the classes produced from an automated system do not closely relate to the land cover class available on the ground. The K-means algorithm tries to cluster data based on their similarity, whereas the ISODATA conventional method allows for a different number of clusters.

In contrast to unsupervised classification, supervised classification begins with the user identifying the land cover for a sample of pixels (training sets) in the image. The parallelepiped classification uses dimensional boxes, which are determined according to the number of bands in the image and then enclose the training data for each class. If a pixel exists within a particular box, then it is assigned to the corresponding class. Maximum likelihood classification shows the probability distributions for each class, using the training data, in which a given pixel with maximum likelihood is classified into a corresponding class (Rees 2013).

2.2.7.4 Machine learning classifiers

Supervised classification through the machine learning technique is a rapidly developing area in remote sensing. Researchers use various machine learning algorithms (see Figure 2.2) to map forests, monitor degradation and examine carbon sequestration. Vapnik developed SVM method in 1995 (Lien 2018), works efficiently with small training data sets. This method focuses on the optimal separation of hyperplanes between classes using training samples (Jensen 2016). CART is a multi-stage binary decision tree classifier introduced by Leo Breiman in 1984. Out of these, random forest is recognised as the most outperformed machine learning for forest classification (Johansen, Phinn, and Taylor 2015; Carrasco et al. 2019). Breiman (2001) proposed the RF classifier, which runs efficiently on large datasets, and it is an integrated learning method based on the decision tree, combined with many ensemble methods of supervised learning (Wessel, Brandmeier, and Tiede 2018). One of the main advantages of this method is that it estimates what variables are most important in the classification (Johansen, Phinn, and Taylor 2015). Although GEE provides various traditional computational algorithms for supervised and unsupervised classifications, increasingly machine learning algorithms are now being used.

2.2.8 Accuracy assessment

Accuracy assessment is a crucial step in remote sensing of forests as it determines whether the resulting classification will be useful for effective decision-making and forest analysis. Remote sensing is often an iterative process that experiments with different processes and algorithms to determine the most accurate classification. This trial and error approach relies on having robust methods for accuracy assessment.

There are a number of ways to investigate the error in image classification: An error matrix, alternatively called a confusion matrix, evaluates the classification performance and characterises the errors. In addition to these errors, a confusion matrix can be used to compute overall classification: accuracy designates the accuracy reported in the error matrix, producer accuracy is interested in how well a specific category is classified, and user accuracy indicates the probability of the selected sample classified on the image representing the selected category on the ground (Congalton 2001). Further, kappa statistic helps to estimate classification accuracy compared to the randomly assigned reference data of class to each image pixel. Kappa analysis generally comes with professional imagery analysis software as well as cloud-based platforms.

2.3 Application of remote sensing for forest monitoring and management

Recent advances in computer vision, machine learning, and remote sensing technologies offer new tools for detecting, monitoring, estimating, and mapping forests globally, regionally and locally. This section discusses the use of remote sensing applications for sustainable forest management under three categories: forest cover classification, forest structure estimation, and forest change detection.

2.3.1 Forest classification

Increasingly, information on the spatial extent and arrangement of forest cover types, forest ecosystems, and forest stands are required for effective management. Forest mapping is generally carried out within spatial, temporal, or taxonomic hierarchies and on a geographic phenomenon (Franklin 2001). Even though remote sensing is recognised as an effective tool for global-scale forest cover mapping, it may lead to the loss of regional variations in forest cover classes, including those related to sustainable forestry systems such as agroforestry practices (Carrasco et al. 2019). For example, a home garden is an agroforestry system generally regarded as a sustainable forest system (Kehlenbeck and Maass 2004), which

primarily reside in the humid tropics. This agroforestry system comprises a piece of land with a dwelling house and some form of vegetation cover (Mattsson et al. 2013). The small size and fragmented distribution may lead to the loss of this sustainable forest class from several global land cover datasets that have been developed using satellite imagery such as AVHRR, MODIS and Copernicus (Carrasco et al. 2019). This may limit the ability of tropical developing countries to effectively manage forest environments that are important to their region.

Recent developments in remote sensing techniques, including new analytical methods (Lien 2018) and satellite data sources such as sentinel, radar, and LiDAR (Bouvet et al. 2018; Poortinga et al. 2019), provide a promising alternative to accomplish and support the sustainable management of forest environments in resource-constrained countries. Therefore, feature extraction, including spectral, spatial, and textural features derived from remote sensing, play a significant role in forest classification. Biswas et al. (2020) used this combination in heterogeneous landscapes when a single pixel can cover several forest types, while Sothe et al. (2017) and Addabbo et al. (2016) used a combination of features to distinguish between species with similar spectral and temporal signatures.

2.3.2 Forest structure

Structural features of forests are helpful indicators of forest conditions. These features include tree height and species composition, such as forest crown closure, diameter at the breast height, volume, height, stem density, age, and stage of development (Franklin 2001). Traditional methods used to measure forest structure are time-consuming and costly (Camarretta et al. 2020). With technological advancements in sensors and platforms, remote sensing helps determine these indicators in order to improve ecological restoration and forest restoration projects.

Identification of canopy height is important to understand aboveground biomass and the basal area (Lim et al. 2003; Ingram, Dawson, and Whittaker 2005) used to measure ecosystem productivity and health and to assess carbon sequestration. Vegetation indices have been used widely in the estimation of biomass (Foody 2003). LiDAR technology has been used to measure tree heights and detect canopy volume by retrieving horizontal and vertical information at a high spatial resolution (Camarretta et al. 2020; Mitchell, Rosenqvist, and Mora 2017).

Another importance of recognising structural indicators is for monitoring forest restoration to measure the effectiveness of the restoration project. In this scenario, indicators such as tree dimension and aboveground biomass are helpful indicators that can be estimated through remote sensing. There is an abundance of proposed automated methods to segment crowns and measure tree heights (Camarretta et al. 2020). While several studies used optical data, LiDAR, or their fusion to measure above ground biomass, Jucker et al. (2017) developed global diameter and biomass allometries that can be used for biomass estimation using relatively simple remote sensing metrics.

2.3.3 Forest change detection

Remote sensing helps detect and monitor forest changes across an area, supporting sustainable forest management. Forest change can happen in landscape patterns, function, and all spatial and temporal scales due to natural and human disturbances and ecological succession. Many instances show remote sensing can identify changes caused by natural disturbances such as floods, wildfire, wind, insects, and diseases (Franklin 2001).

Forest fires are predominant factors of forest disturbance globally, and fires broadly impact long-term forest dynamics and biodiversity at both local and regional scales (Lafortezza et al. 2008). Detection of active fires and impact of fires have been a significant application of remote sensing. Daily global observations of fire occurrences are available through AVHRR, SPOT VEGETATION, or MODIS sensors (Franklin 2001). After a forest fire, predominate causes of forest disturbance are insect outbreaks and wind (Lafortezza et al. 2008), which are investigated chiefly through field-based activities where remote sensing influence is minimal. Several studies looked into the stressed and healthy trees while others focused on early detection, defoliation, and forest damage assessment (Muchoney and Haack 1994). However, there is a clear need for continued forest health monitoring by remote sensing.

Consequently, in an incident of canopy removal or when there is a change in the canopy cover reflectance, there is an increase in visible reflectance while a decrease in near-infrared reflectance (Franklin 2001), and at the same time, cleared areas are displaying brighter than forested areas in the spectral response of SAR images. Therefore, forest change detection helps identify ongoing deforestation and degradation around a particular area (Reusing 2000). Since forest structure change can manifest in different ways regionally, locally, and at the ecosystem level, asserting a particular method remains challenging due to the specific nature of the degradation. Thus, improved metrics for capturing forest cover change spatially and temporally

ensure sustainability among the forests. Mondal, McDermid, and Qadir (2020) have used a multi-scale, satellite-based approach to identify the forest degradation from 2000-2016 in South Asia and specified the importance of utilising the higher resolution satellite data to assess the forest cover at the national level. Further, they emphasise the disadvantages of moderate scale satellite studies towards detecting long-term negative changes affecting forest structure, composition, and functions.

2.4 Future research

The remote sensing process consist of many steps as reviewed in this chapter. There are many research opportunities to develop improvements in these steps. This section highlights a few of these research opportunities, especially with regards to the needs of developing countries.

Over the past years, there has been significant research on accuracy assessment techniques because of their importance in the practical and theoretical aspects (Foody 2002; Janssen and van der Wel 1994). Although kappa has been widely used in remote sensing research, this has also been extensively criticised because the degree of chance agreement may be overestimated (Wang and Weng 2013). Foody (2020) argued that the kappa coefficient is a chance agreement that is not an index of accuracy, and therefore, accuracy assessment should finally be heeded with confusion matrix and per-class accuracy. Wang and Weng (2013) also specify that kappa analysis is suitable when all the errors in the matrix are considered of equal importance. There is more research opportunity to develop new accuracy estimation or test the validity of kappa statistics towards forest mapping in this scenario.

The near-permanent cloud cover often challenges tropical forest researchers. In recent years, radar data from Sentinel 1 helps overcome the cloud cover limitations in the tropics (Poortinga et al. 2019), but for higher accuracy, data fusion is preferable because it combines different data sources with varying extents in time and space. Although tropical forest research focuses on spatial radar and optical data fusion, more research needs to address temporal aggregation (Biswas et al. 2020). Furthermore, South Asian regions, which are highly dynamic areas for deforestation and degradation, remain understudied compared to research carried over Europe, China and North American continent to detect temporal changes to manage the forest sustainably (Mondal, McDermid, and Qadir 2020; Miettinen, Stibig, and Achard 2014).

Advances in machine learning algorithms and open access data facilitated massive computations in cloud platforms that lead to temporal analysis on a global scale. In contrast,

smaller agroforestry classes, important for countries and cultures, are often neglected from global data sets. In order to minimise this effect, more remote sensing studies need to identify features important to sustainable forest practice in developing countries, such as home gardens. (Kehlenbeck and Maass 2004; Abebe et al. 2013).

Exploring the potential of open-source data to estimate forest variables over a large area are needed when LiDAR products are not cost-effective. In that scenario, recently launched missions such as GEDI (Potapov et al. 2021) helps estimate the forest heights, and those launching soon, such as the BIOMASS mission, carry a p-band synthetic aperture radar, hold enormous potential on forest carbon calculations (Dupuis et al. 2020). Further, Mission Algorithm and Analysis (MAAP) is a cloud-based platform developed for generating forest biomass products by NASA and ESA, fully operational from 2021. MAAP comprises tools and algorithms specifically developed to map ecosystem structures from space-born datasets such as Biomass NISAR (NASA-ISRO SAR Mission) and GEDI (Albinet et al. 2019). These opportunities will lead developing nations in monitoring and managing forest degradation before it turns into deforestation, therefore, paving the way for SDG 15.

2.5 Summary

Sustainable Development Goals were established to focus on global sustainability with broad 17 goals to be achieved by 2030. Special attention has been given to forest protection and management under the SDGs goal 15 due to its importance towards livelihood and poverty eradication. Consequently, accurate information of forest structure and spatial and temporal change detection is crucial for sustainable forest management. In that scenario, remote sensing is a proven method to monitor forest degradation, deforestation and to measure forest variables.

In recent decades, advances in remote sensing, machine learning, and GIS have created new ways to conduct forest research. The most significant advancement in remote sensing occurred with the availability of open-source data, followed by the improvement of open source or freely available software and cloud-based platforms. These factors enhance the capability of the developing countries to conduct research and monitor forests in a very effective and efficient way.

2.6 Reference

Addabbo, Pia, Mariano Focareta, Salvo Marcuccio, Claudio Votto, and Silvia Ullo. 2016. "Contribution of Sentinel-2 data for applications in vegetation monitoring." *ACTA IMEKO* 5:44. doi: 10.21014/acta_imeko.v5i2.352.

Albinet, Clément, Amanda S. Whitehurst, Laura Alisic Jewell, Kaylin Bugbee, Henri Laur, Kevin J. Murphy, Bjorn Frommknecht, et al. 2019. "A Joint ESA-NASA Multi-mission Algorithm and Analysis Platform (MAAP) for Biomass, NISAR, and GEDI." *Surveys in Geophysics* 40 (4):1017-27. doi: 10.1007/s10712-019-09541-z.

Bajpai, Kriti, and Rishi Soni. 2017. "Analysis of Image Enhancement Techniques Used in Remote Sensing Satellite Imagery." *International Journal of Computer Applications* 169 (10).

Bhunia, Gouri Sankar, Pravat Kumar Shit, and Debashish Sengupta. 2021. "Free-Open Access Geospatial Data and Tools for Forest Resources Management." In *Spatial Modeling in Forest Resources Management : Rural Livelihood and Sustainable Development*, edited by Pravat Kumar Shit, Hamid Reza Pourghasemi, Pulakesh Das and Gouri Sankar Bhunia, 651-75. Cham: Springer International Publishing.

Biswas, Sumalika, Qiongyu Huang, Anupam Anand, Myat Su Mon, Franz-Eugen Arnold, and Peter Leimgruber. 2020. "A Multi Sensor Approach to Forest Type Mapping for Advancing Monitoring of Sustainable Development Goals (SDG) in Myanmar." *Remote Sensing* 12 (19):3220.

Boyd, D. S., and F. M. Danson. 2005. "Satellite remote sensing of forest resources: three decades of research development." *Progress in Physical Geography: Earth and Environment* 29 (1):1-26. doi: 10.1191/0309133305pp432ra.

Broich, Mark, Matthew C. Hansen, Peter Potapov, Bernard Adusei, Erik Lindquist, and Stephen V. Stehman. 2011. "Time-series analysis of multi-resolution optical imagery for quantifying forest cover loss in Sumatra and Kalimantan, Indonesia." *International Journal of Applied Earth Observation and Geoinformation* 13 (2):277-91. doi: https://doi.org/10.1016/j.jag.2010.11.004.

Camarretta, Nicolò, Peter A. Harrison, Tanya Bailey, Brad Potts, Arko Lucieer, Neil Davidson, and Mark Hunt. 2020. "Monitoring forest structure to guide adaptive management of forest restoration: a review of remote sensing approaches." *New Forests* 51 (4):573-96. doi: 10.1007/s11056-019-09754-5

Campbell, James B, and Randolph H Wynne. 2011. *Introduction to Remote Sensing*. 5th Edition ed. New York: The Guilford Press.

Cannell, M. G. R. 1988. "Agroforestry - A Decade of Development. Edited by H. A. Steppler and P. K. R. Nair. Nairobi: International Council for Research in Agroforestry (1987)." *Experimental Agriculture* 24 (3):393-. doi: 10.1017/S0014479700016252.

Carrasco, Luis, Aneurin W. O'Neil, R. Daniel Morton, and Clare S. Rowland. 2019. "Evaluating Combinations of Temporally Aggregated Sentinel-1, Sentinel-2 and Landsat 8 for Land Cover Mapping with Google Earth Engine." *Remote Sensing* 11 (3):288.

Cheng, Kai, and Juanle Wang. 2019. "Forest Type Classification Based on Integrated Spectral-Spatial-Temporal Features and Random Forest Algorithm—A Case Study in the Qinling Mountains." *Forests* 10 (7):559.

Chuvieco, Emilio. 2016. *Fundamentals of Satellite Remote Sensing: An Environmental Approach*. Boca Raton: Taylor & Francis Group.

Congalton, Russell G. 2001. "Accuracy assessment and validation of remotely sensed and other spatial information." *International Journal of Wildland Fire* 10 (4):321-8.

Crowley, Morgan A., and Jeffrey A. Cardille. 2020. "Remote Sensing's Recent and Future Contributions to Landscape Ecology." *Current Landscape Ecology Reports* 5 (3):45-57. doi: 10.1007/s40823-020-00054-9.

Defries, R. S., and M. C. Hansen. 2010. "ISLSCP II University of Maryland Global Land Cover Classifications, 1992-1993." In.: ORNL Distributed Active Archive Center.

Deng, X. P., S. X. Guo, L. Y. Sun, and J. S. Chen. 2020. "Identification of Short-Rotation Eucalyptus Plantation at Large Scale Using Multi-Satellite Imageries and Cloud Computing Platform." *Remote Sensing* 12 (13):18. doi: 10.3390/rs12132153.

Dupuis, Chloé, Philippe Lejeune, Adrien Michez, and Adeline Fayolle. 2020. "How Can Remote Sensing Help Monitor Tropical Moist Forest Degradation?—A Systematic Review." *Remote Sensing* 12 (7). doi: 10.3390/rs12071087.

Earth Resources Observation And Science (EROS) Center. 2017. "Global Land Cover Characterization (GLCC)." In.: U.S. Geological Survey.

Elmes, Arthur, Hamed Alemohammad, Ryan Avery, Kelly Caylor, J. Ronald Eastman, Lewis Fishgold, Mark A. Friedl, et al. 2020. "Accounting for Training Data Error in Machine Learning Applied to Earth Observations." *Remote Sensing* 12 (6):1034.

Erasmi, Stefan, Martin Kappas, André Twele, and Muhammad Ardiansyah. 2007. "From global to regional scale: Remote sensing-based concepts and methods for mapping land-cover and land-cover change in tropical regions." In *Stability of Tropical Rainforest Margins: Linking Ecological, Economic and Social Constraints of Land Use and Conservation*, edited by Teja Tscharntke, Christoph Leuschner, Manfred Zeller, Edi Guhardja and Arifuddin Bidin, 435-60. Berlin, Heidelberg: Springer Berlin Heidelberg.

European Space Agency. 2019. "Overview." Accessed November 6. http://www.esa.int/Applications/Observing_the_Earth/Copernicus/Overview4.

Foody, G. M. 2003. "Remote sensing of tropical forest environments: Towards the monitoring of environmental resources for sustainable development." *International Journal of Remote Sensing* 24 (20):4035-46. doi: 10.1080/0143116031000103853.

Foody, Giles M. 2002. "Status of land cover classification accuracy assessment." *Remote Sensing of Environment* 80 (1):185-201. doi: https://doi.org/10.1016/S0034-4257(01)00295-4.

Foody, Giles. M. 2020. "Explaining the unsuitability of the kappa coefficient in the assessment and comparison of the accuracy of thematic maps obtained by image classification." *Remote Sensing of Environment* 239:111630. doi: https://doi.org/10.1016/j.rse.2019.111630.

Franklin, Steven E. 2001. *Remote Sensing for Sustainable Forest Management*. 1st ed. Boca Raton: Lewis Publishers.

Friedl, M, and D Sulla-Menashe. "MCD12Q1 MODIS/Terra+Aqua Land Cover Type Yearly L3 Global 500m SIN Grid V006." https://doi.org/10.5067/MODIS/MCD12Q1.006.

Gong, Peng, Le Yu, Congcong Li, Jie Wang, Lu Liang, Xuecao Li, Luyan Ji, Yuqi Bai, Yuqi Cheng, and Zhiliang Zhu. 2016. "A new research paradigm for global land cover mapping." *Annals of GIS* 22 (2):87-102. doi: 10.1080/19475683.2016.1164247.

Gorelick, Noel, Matt Hancher, Mike Dixon, Simon Ilyushchenko, David Thau, and Rebecca Moore. 2017. "Google Earth Engine: Planetary-scale geospatial analysis for everyone." *Remote Sensing of Environment* 202:18-27. doi: https://doi.org/10.1016/j.rse.2017.06.031.

Green, Kass. 2017. *Imagery and GIS : best practices for extracting information from imagery*. Redlands, California: Esri Press.

Hall-Beyer, Mryka. 2017. "Practical guidelines for choosing GLCM textures to use in landscape classification tasks over a range of moderate spatial scales." *International Journal of Remote Sensing* 38 (5):1312-38. doi: 10.1080/01431161.2016.1278314.

Hansen, M. C., P. V. Potapov, R. Moore, M. Hancher, S. A. Turubanova, A. Tyukavina, D. Thau, et al. 2013. "High-Resolution Global Maps of 21st-Century Forest Cover Change." *Science* 342 (6160):850. doi: 10.1126/science.1244693.

Haralick, R. M., K. Shanmugam, and I. Dinstein. 1973. "Textural Features for Image Classification." *IEEE Transactions on Systems, Man, and Cybernetics* SMC-3 (6):610-21. doi: 10.1109/TSMC.1973.4309314.

Ingram, J. Carter, Terence P. Dawson, and Robert J. Whittaker. 2005. "Mapping tropical forest structure in southeastern Madagascar using remote sensing and artificial neural networks." *Remote Sensing of Environment* 94 (4):491-507. doi: https://doi.org/10.1016/j.rse.2004.12.001.

Jahromi, Mojtaba Naghdyzadegan, Maryam Naghdizadegan Jahromi, Babak Zolghadr-Asli, Hamid Reza Pourghasemi, and Seyed Kazem Alavipanah. 2020. "Google Earth Engine and Its Application in Forest Sciences." In, 629-49. Cham: Springer International Publishing.

Janssen, L. L. F., and Frans van der Wel. 1994. "Accuracy assessment of satellite derived land-cover data: A review." *Photogramm. Eng. Remote Sensing 60 (1994) 419-426.* 60.

Jensen, John R. 2016. *Introductory digital image processing: a remote sensing perspective*. Illinois: Pearson education.

Johansen, K., S. Phinn, and Martin F. J. Taylor. 2015. "Mapping woody vegetation clearing in Queensland, Australia from Landsat imagery using the Google Earth Engine." *Remote Sensing Applications: Society and Environment* 1:36-49.

Jucker, Tommaso, John Caspersen, Jérôme Chave, Cécile Antin, Nicolas Barbier, Frans Bongers, Michele Dalponte, et al. 2017. "Allometric equations for integrating remote sensing imagery into forest monitoring programmes." *Global Change Biology* 23 (1):177-90. doi: https://doi.org/10.1111/gcb.13388.

Kehlenbeck, K., and B. L. Maass. 2004. "Crop diversity and classification of homegardens in Central Sulawesi, Indonesia." *Agroforestry systems* 63 (1):53-62. doi: 10.1023/B:AGFO.0000049433.95038.25.

Kumar, Lalit, and Onisimo Mutanga. 2018. "Google Earth Engine Applications Since Inception: Usage, Trends, and Potential." *Remote Sensing* 10 (10):1509.

Kuplich, T. M., P. J. Curran, and P. M. Atkinson. 2005. "Relating SAR image texture to the biomass of regenerating tropical forests." *International Journal of Remote Sensing* 26 (21):4829-54. doi: 10.1080/01431160500239107.

Lafortezza, Raffaele, Jiquan Chen, Thomas R. Crow, and Giovanni Sanesi. 2008. *Patterns and Processes in Forest Landscapes: Multiple Use and Sustainable Management*. 1. Aufl. ed. Dordrecht: Springer Netherlands.

Lechner, Alex, Giles Foody, and Doreen Boyd. 2020. "Applications in Remote Sensing to Forest Ecology and Management." *One Earth* 2:405-12. doi: 10.1016/j.oneear.2020.05.001.

Lee, Jacky, Jeffrey A. Cardille, and Michael T. Coe. 2018. "BULC-U: Sharpening Resolution and Improving Accuracy of Land-Use/Land-Cover Classifications in Google Earth Engine." *Remote Sensing* 10 (9). doi: 10.3390/rs10091455.

Lien, Pham Thi Hong. "Mapping Vegetation With Remote Sensing And Gis Data Using Object-Based Analysis And Machine Learning Algorithms." University of Waikato.

Lim, Kevin, Paul Treitz, Michael Wulder, Benoît St-Onge, and Martin Flood. 2003. "LiDAR remote sensing of forest structure." *Progress in Physical Geography: Earth and Environment* 27 (1):88-106. doi: 10.1191/0309133303pp360ra.

Liu, Yanan, Weishu Gong, Xiangyun Hu, and Jianya Gong. 2018. "Forest Type Identification with Random Forest Using Sentinel-1A, Sentinel-2A, Multi-Temporal Landsat-8 and DEM Data." *Remote Sensing* 10 (6):946.

Marcel, Buchhorn., Smets. Bruno, Bertels. Luc, De Roo Bert, Lesiv Myroslava, Tsendbazar Nandin-Erdene, Herold Martin, and Fritz Steffen. "Copernicus Global Land Service: Land Cover 100m: collection 3: epoch 2019: Globe." https://doi.org/10.5281/zenodo.3939050.

Mathieu, Renaud, Claire Freeman, and Jagannath Aryal. 2007. "Mapping private gardens in urban areas using object-oriented techniques and very high-resolution satellite imagery." *Landscape and Urban Planning* 81 (3):179-92. doi: https://doi.org/10.1016/j.landurbplan.2006.11.009.

Mattsson, Eskil, Madelene. Ostwald, S. P. Nissanka, and Buddhi. Marambe. 2013. "Homegardens as a Multi-functional Land-Use Strategy in Sri Lanka with Focus on Carbon Sequestration." *Ambio* 42 (7):892-902. doi: 10.1007/s13280-013-0390-x.

Miettinen, Jukka, Hans-Jürgen Stibig, and Frédéric Achard. 2014. "Remote sensing of forest degradation in Southeast Asia—Aiming for a regional view through 5–30 m satellite data." *Global Ecology and Conservation* 2:24-36. doi: https://doi.org/10.1016/j.gecco.2014.07.007.

Mitchell, Anthea L., Ake Rosenqvist, and Brice Mora. 2017. "Current remote sensing approaches to monitoring forest degradation in support of countries measurement,

reporting and verification (MRV) systems for REDD+." *Carbon Balance and Management* 12 (1):9. doi: 10.1186/s13021-017-0078-9.

Mondal, Pinki, Sonali Shukla McDermid, and Abdul Qadir. 2020. "A reporting framework for Sustainable Development Goal 15: Multi-scale monitoring of forest degradation using MODIS, Landsat and Sentinel data." *Remote Sensing of Environment* 237:111592. doi: https://doi.org/10.1016/j.rse.2019.111592.

Muchoney, Douglas M, and Barry N Haack. 1994. "Change detection for monitoring forest defoliation." *Photogrammetric engineering and remote sensing* 60 (10):1243-52.

Palo, Matti, and Gerardo Mery. 1996. "Transition from deforestation to sustainable forestry -a distant dream?" In *Sustainable Forestry Challenges for Developing Countries* edited by Matti Palo and Gerardo Mery, 1-13. Dordrecht Kluwer Academic Publishers.

Pérez-Hoyos, Ana, Felix Rembold, Hervé Kerdiles, and Javier Gallego. 2017. "Comparison of Global Land Cover Datasets for Cropland Monitoring." *Remote Sensing* 9 (11). doi: 10.3390/rs9111118.

Poortinga, Ate, Karis Tenneson, Aurélie Shapiro, Quyen Nquyen, Khun San Aung, Farrukh Chishtie, and David Saah. 2019. "Mapping Plantations in Myanmar by Fusing Landsat-8, Sentinel-2 and Sentinel-1 Data along with Systematic Error Quantification." *Remote Sensing* 11 (7):831.

Potapov, Peter, Xinyuan Li, Andres Hernandez-Serna, Alexandra Tyukavina, Matthew C. Hansen, Anil Kommareddy, Amy Pickens, et al. 2021. "Mapping global forest canopy height through integration of GEDI and Landsat data." *Remote Sensing of Environment* 253:112165. doi: https://doi.org/10.1016/j.rse.2020.112165.

Ranagalage, Manjula, M. H. J. P. Gunarathna, Thilina D. Surasinghe, Dmslb Dissanayake, Matamyo Simwanda, Yuji Murayama, Takehiro Morimoto, et al. 2020. "Multi-Decadal Forest-Cover Dynamics in the Tropical Realm: Past Trends and Policy Insights for Forest Conservation in Dry Zone of Sri Lanka." *Forests* 11 (8):836.

Rees, W G. 2013. *Physical Principles of Remote Sensing*. Cambridge: Cambridge University Press.

Reusing, M. 2000. Change detection of natural high forests in ethiopia using remote sensing and gis techniques.

Rocchini, Duccio, Vaclav Petras, Anna Petrasova, Ned Horning, Ludmila Furtkevicova, Markus Neteler, Benjamin Leutner, and Martin Wegmann. 2017. "Open data and open source for remote sensing training in ecology." *Ecological Informatics* 40:57-61. doi: https://doi.org/10.1016/j.ecoinf.2017.05.004.

Shimizu, Katsuto, Tetsuji Ota, and Nobuya Mizoue. 2019. "Detecting Forest Changes Using Dense Landsat 8 and Sentinel-1 Time Series Data in Tropical Seasonal Forests." *Remote Sensing* 11 (16). doi: 10.3390/rs11161899.

Sothe, Camile, Cláudia Maria de Almeida, Veraldo Liesenberg, and Marcos Benedito Schimalski. 2017. "Evaluating Sentinel-2 and Landsat-8 Data to Map Sucessional Forest Stages in a Subtropical Forest in Southern Brazil." *Remote Sensing* 9 (8):838.

Srinet, Ritika, Subrata Nandy, Hitendra Padalia, Surajit Ghosh, Taibanganba Watham, Patel R, and Prakash Chauhan. 2020. "Mapping plant functional types in Northwest Himalayan

foothills of India using random forest algorithm in Google Earth Engine." *International Journal of Remote Sensing* 41:1-14. doi: 10.1080/01431161.2020.1766147.

Steiniger, Stefan, and Geoffrey J. Hay. 2009. "Free and open source geographic information tools for landscape ecology." *Ecological Informatics* 4 (4):183-95. doi: https://doi.org/10.1016/j.ecoinf.2009.07.004.

Tsai, Yu Hsin, Douglas Stow, Hsiang Ling Chen, Rebecca Lewison, Li An, and Lei Shi. 2018. "Mapping Vegetation and Land Use Types in Fanjingshan National Nature Reserve Using Google Earth Engine." *Remote Sensing* 10 (6):927.

UNBigData. 2021. "Planet and Google are ready to help the United Nations in the data work behind the 2030 Agenda for Sustainable Development." Accessed 1st of August. https://unstats.un.org/bigdata/blog/2019/planet-google.cshtml

United Nations. "Transforming our world : the 2030 Agenda for Sustainable Development." https://sustainabledevelopment.un.org/content/documents/21252030%20Agenda%20for%20Sustainable%20Development%20web.pdf.

Verbyla, David L. 1995. *Satellite Remote Sensing of Natural Resources*. Boca Raton: Lewis Publishers.

Vick, Tyler. 2008. "Comparing Pixel- and Object-Based Classification Methods for Determining Land-Cover in the Gee Creek Watershed, Washington." *Geography Masters Research Papers.* 22. doi: 10.15760/geogmaster.22.

Wang, Guangxing, and Qihao Weng. 2013. *Remote Sensing of Natural Resources*. Baton Rouge: Taylor & Francis Group.

Wessel, Mathias, Melanie Brandmeier, and Dirk Tiede. 2018. "Evaluation of Different Machine Learning Algorithms for Scalable Classification of Tree Types and Tree Species Based on Sentinel-2 Data." *Remote Sensing* 10 (9):1419.

Wu, W. J., X. J. Zhao, C. Gong, X. W. Li, and Ieee. 2018. "Obtain the patterns of global forest npp and its influence factors with google earth engine." In *Igarss 2018 - 2018 Ieee International Geoscience and Remote Sensing Symposium*, 2898-901. New York: Ieee.

Xie, Yichun, Zongyao Sha, and Mei Yu. 2008. "Remote sensing imagery in vegetation mapping: a review." *Journal of Plant Ecology* 1 (1):9-23. doi: 10.1093/jpe/rtm005.

Zhang, M. N., P. Gong, S. H. Qi, C. Liu, and T. W. Xiong. 2019. "Mapping bamboo with regional phenological characteristics derived from dense Landsat time series using Google Earth Engine." *International Journal of Remote Sensing* 40 (24):9541-55. doi: 10.1080/01431161.2019.1633702.

Zhu, Zhe, Michael A. Wulder, David P. Roy, Curtis E. Woodcock, Matthew C. Hansen, Volker C. Radeloff, Sean P. Healey, et al. 2019. "Benefits of the free and open Landsat data policy." *Remote Sensing of Environment* 224:382-5. doi: https://doi.org/10.1016/j.rse.2019.02.016.

Zurqani, Hamdi A., Christopher J. Post, Elena A. Mikhailova, Mark A. Schlautman, and Julia L. Sharp. 2018. "Geospatial analysis of land use change in the Savannah River Basin using Google Earth Engine." *International Journal of Applied Earth Observation and Geoinformation* 69:175-85. doi: https://doi.org/10.1016/j.jag.2017.12.006.

Chapter 3
Using Google Earth Engine to classify unique forest and agroforest classes using a mix of Sentinel 2a spectral data and topographical features: a Sri Lanka case study

This chapter was published as "W. D. K. V. Nandasenaa, Lars Brabyn and Silvia Serrao-Neumann 2022. Using Google Earth Engine to classify unique forest and agroforest classes using a mix of Sentinel 2a spectral data and topographical features: a Sri Lanka case study. Geocarto International Journal 37, NO. 25, 9544–9559". https://doi.org/10.1080/10106049.2021.2022010

Abstract

Global land cover classifications may lead to the loss of important local and national nuances such as forest and agroforestry classes. These classes are important to local contexts because they contribute to sustainable land management systems. This paper demonstrates the application of Sentinel-2A satellite images, elevation data, and the Google Earth Engine platform to generate more detailed, specialist land cover classification for forestry classes important in Sri Lanka deriving ten spectral, 16 textural, and three topographical features from the input datasets. The random forest classification model discriminates vegetation types as forest, forest plantations, shrub, grassland, home garden, and cultivation with an overall accuracy of 94% and kappa value of 0.91. Results indicate the elevation feature contributes the most to discriminate forest and agroforestry classes, and red band (664.6 nm) textural metrics derived from grey-level co-occurrence matrix analysis are more useful for separating the home garden from other land cover classes.

Keywords: home garden, random forest, grey-level co-occurrence matrix

3.1 Introduction

Forests are the largest land-based carbon pool (Liu et al. 2018) and play an important role in reducing water runoff and soil erosion and conserving and protecting biodiversity. However, rapid population growth coupled with agricultural development contributes to increased

deforestation. Agroforestry systems that cultivate trees and crops together in agricultural lands can offset the deforestation effects because they can reduce the stress on forests (Mattsson et al. 2013). While cultivating trees and crops together is a traditional practice in many tropical regions around the world, attention to this land management strategy has grown more recently because of its potential contribution to achieving sustainability goals (Kumar and Nair 2006).

Nonetheless, global initiatives that classify environments inadvertently change the way environments are being conceptualised (Cheng and Wang 2019). In particular, global satellite image archives and massive shared image processing servers, such as Google Earth Engine (GEE), may lead to the loss of regional variations in land cover classes, including those related to agroforestry systems. This may limit the ability of some countries to more effectively manage forest environments important to their region. Hence, information regarding the spatial distribution of both forest and agroforest types must continue to be generated to support sustainable land cover management (Cheng and Wang 2019). Recent developments in remote sensing techniques are a promising alternative to support land management in resource-constrained countries. Specifically, the refinement of both the spatial and spectral features of sensors and increasing improvement in classification algorithms have strengthened remote sensing usability as a source for detecting forestry and agroforestry related land cover types, tree species, and tree species groups mapping. Building on this, the paper uses Sri Lanka as an example to demonstrate the application of freely available Sentinel-2A satellite images, elevation data, and the GEE platform to generate more detailed, specialist land cover classification for forestry classes. While many researchers have identified forest cover changes in Sri Lanka (Lindström et al. 2012; Perera K. et al. 2012), some studies classified the country's land cover (Premakantha et al. 2009; Rathnayake et al. 2020), while others prioritised unique land cover classes such as home garden (Perera Kithsiri and Tsuchiya 2009; Mattsson et al. 2013). Very few studies have differentiated and categorised agroforestry classes using remote sensing. In particular the mapping of the "home garden' class using remote sensing has not been researched. This paper will address this knowledge gap as this is an important land use in Sri Lanka.

3.1.1 The Use of Remote Sensing and Image Analysis for Forest Classification

During the last decade, there has been a development in the availability of medium and high-resolution satellite data and the functionality and power of remote sensing platforms (Carrasco et al. 2019). While high-resolution data help provide more accurate information on tree species

identification by gathering data on different tree spacing and tree crown sizes, they are too expensive for many developing countries like Sri Lanka. With the emergence of the GEE platform in the last decade (Zurqani et al. 2018), many scientists have successfully conducted research globally, including those in developing countries that originally could not do so because of the costs involved. This has been enabled because the GEE platform allows users to store images in the cloud and provides greater computing power for image processing and analysing (Carrasco et al. 2019).

Remote sensing is an effective tool for global-scale land cover mapping, and several global land cover datasets have been developed using satellite imagery such as AVHRR, MODIS and Copernicus (Carrasco et al. 2019). Global-scale land cover datasets consist of land cover types defined at the biome level (Gong et al. 2016), but the major classes not prevalent in the tropics are often neglected (Erasmi et al. 2007). Thus, global land cover classification datasets inevitably experience loss of information and errors because detail at local scales may be missing, thus hiding heterogeneities among regions (Erasmi et al. 2007). Nevertheless, various researchers (Stibig et al. 2007; Gong et al. 2016) have highlighted the low-level accuracy of these datasets, especially among human settlements and croplands. As Mertes et al. (2015) stated, human settlements in rural areas are easy to confuse with fallow land or bare land. Simultaneously, croplands in the tropical region are often underestimated because cropland could be mixed with natural vegetation or bare lands (Yu et al., 2013). In contrast, Stibig et al. (2007) identified the overestimation of cropland in South Asia, where infrastructure, populated areas, forest fragments, and bare lands are hard to separate from cropland and are thus incorporated. Furthermore, these products restrict the minimum detectable area of change and lead to mixed land cover types resulting in a significant information loss (Erasmi et al. 2007), especially in small-scaled heterogeneous landscapes such as annual and perennial crops, grasslands, and agroforestry systems common in the South and Southeast Asia.

Localised, national land cover classification systems vary worldwide. In the Sri Lankan context, the land cover classification system has many differences compared with global land cover datasets (Table 3.1). A key distinction is the addition of extra classes such as 'home garden'. A similar nuanced classification also applies to the forest class. In the Sri Lankan land cover classification system, the forest class is divided into four broad categories: dense forests, open forests, forest plantation and reservation. In contrast, global land cover datasets identify

forest cover according to the climate and leaf variability, such as evergreen, broadleaf, deciduous, or as a single biome.

Although many studies (Erasmi et al. 2007; Stibig et al. 2007; Rathnayake et al. 2020) have used remote sensing techniques to map land cover classes in South and Southeast Asia, very few studies focus on classifying agroforestry systems. Home gardens are an agroforestry system that requires high spatial resolution satellite data because of their small size and fragmented distribution. This agroforestry type is generally regarded as a sustainable production system (Kehlenbeck and Maass 2004), primarily in humid tropics. Home gardens have been identified as the oldest land use activity, only to shifting cultivation in the tropics (Pushpakumara et al. 2012). From the prehistoric era, home gardens have gradually spread to many humid regions in the south and southeast Asia, including Indonesia, the Philippines, Thailand, Sri Lanka, India and Bangladesh. At present, this land use is widespread throughout East and West Africa, and Mesoamerica and the Pacific Islands and also found outside the tropics, such as in Europe (Kumar and Nair 2006). Though home gardens are common in many regions, components and composition may vary between regions (Kehlenbeck and Maass 2004). In Sri Lanka, the home garden comprises a primary land use class (Das and Das 2014; Sangakkara and Frossard 2016), totalling about 18.2% of total land cover (Land Use Policy Planning Department 2020). The home garden, also known as a homestead (Rathnayake, Jones, and Soto-Berelov 2020), comprises a land with a dwelling house and some form of vegetation cover, with an average size ranging from 0.05 to 2.5 ha (Mattsson et al. 2013). This land use system is important for Sri Lanka in relation to the percentage of land area occupied and its use for timber and fuelwood production and, food and nutritional security for the household (Pushpakumara et al. 2012). Therefore, remote sensing techniques are required to identify this essential land use class.

Table 3.1 Comparison of Sri Lankan and Global Land Cover classification classes

Classification Name	University of Maryland Global Land Cover Classification GLC[1]	Global Land Cover Characterization[2]	Global Land Service[3]	Land Cover Type (MCD12Q1) Version 6 [4]	National Land use Classifiaction[5]
Extent	Global	Global	Global	Global	Sri Lanka
Water Classes	Water	Water	Seasonal water Permanent water	Water bodies	Water bodies
Forest Classes	Evergreen need leaf forest Evergreen broadleaf forest Deciduous Needleleaf forest Deciduous broadleaf forest Mixed forest	Evergreen Needleelaf forest Evergreen broadleaf forest Deciduous Needleaf forest Deciduous broadleaf forest Mixed forests	Forest	Forest	Dense forest Open forest Forest plantation Reservation
Grassland classes	Woodland Grassland Wooded grassland/scrubland	Grasslands Woody savannas Savannas	Herbaceous vegetation	Grasslands Savannas	Grasslands
Shrub Classes	Closed shrub land Open shrub land	Closed scrublands Open scrublands	Shrub land	Shrub lands	Shrub
Cropland Classes	Cropland	Croplands	Cropland	Croplands	Agricultural land
Barren land Classes	Barren	Barren or sparsely vegetated	Bare/sparse vegetation	Barren	Bare land Abandoned agricultural land
Urban area Classes	Urban and built	Urban and build-up	Build-up	Urban and built up	Built up land
Other Classes		Permanent wetlands Permanent snow and ice	Snow Moss and lichen	Wetland	Wetland Rocks Homesteads/ home garden Sandy areas

Source: Defries and Hansen (2010)[1], Earth Resources Observation and Science (EROS) Center (2017)[2], Marcel et al. (2020)[3], Friedl and Sulla-Menashe (2019)[4], Land Use Policy Planning Department (2018)[5]

3.2 Material and Methods

3.2.1 Study area

The study area covers an area of 25,517ha and is located in the Belihuloya region in the Sabaragamuwa province of Sri Lanka (Figure 3.1). The terrain is a combination of flat, rugged, and mountainous areas with the dominant soil group of Reddish Brown Earths and Low Humic Gley soils. The Hawagala mountain range, which has an altitude ranging from 530m to 1414m, is in the north of the study area, and in the south corner, there is a large reservoir known as the Samanala reservoir spreads along 897ha with an altitude of 400m. According to the Sri Lankan elevation classification, this region lies in the mid-country, where the elevation ranges between 600m to 900m. The region belongs to the intermediate climate zone and has both wet and dry characteristics as it receives 2500mm, and 1750 mm mean rainfall during the Northeast monsoon and Southwest monsoons, respectively, with a short and less prominent dry season. The mean annual temperature is about 27 ^{0}C. Vegetation in the study area presents a less marked climatic and phenological response to seasonality and consists of patches of montane forests, grasslands, shrubs and pine plantations.

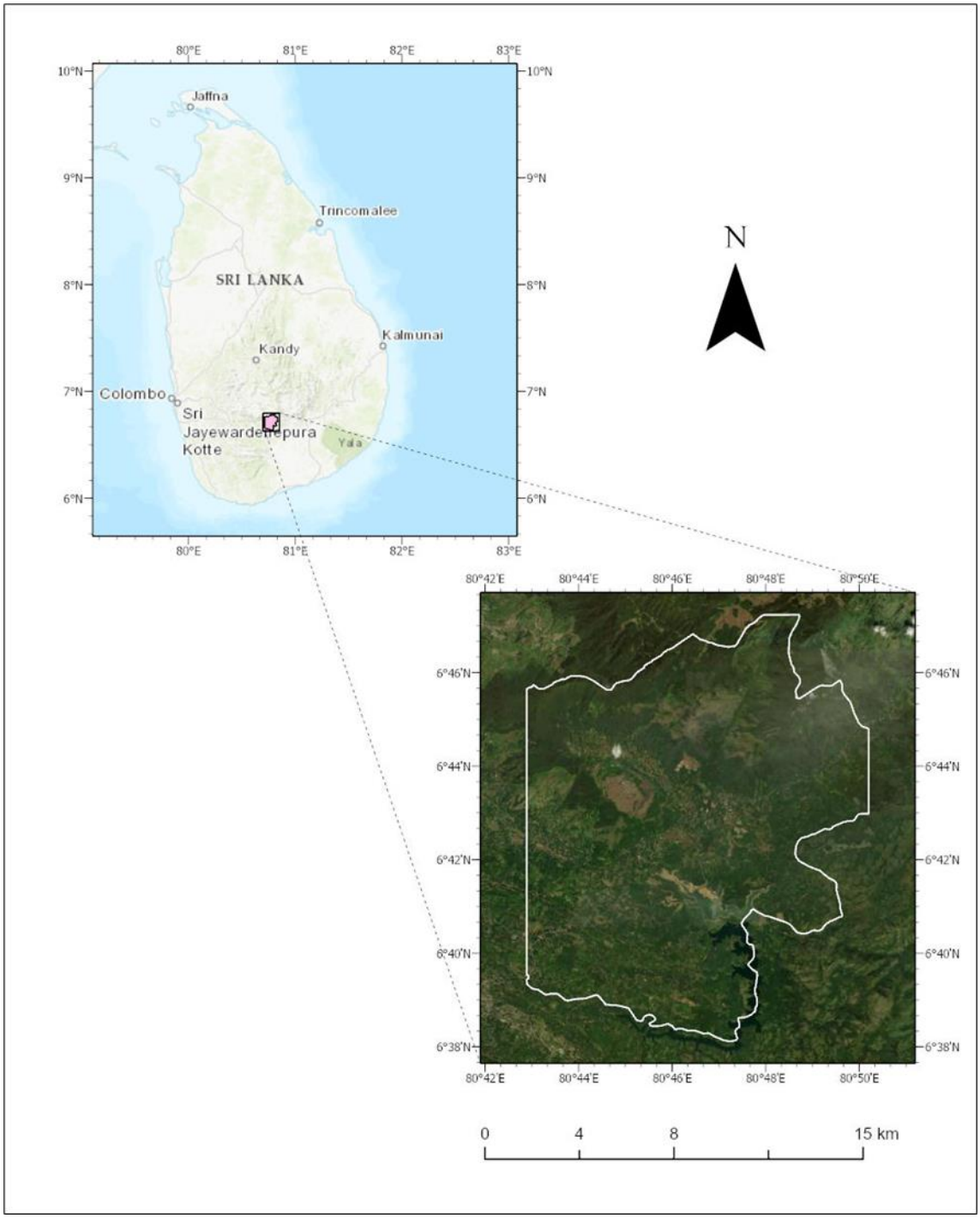

Figure 3.1 Study area

3.2.2 Inputs

Following section describes the framework (Figure 3.2) developed for this research.

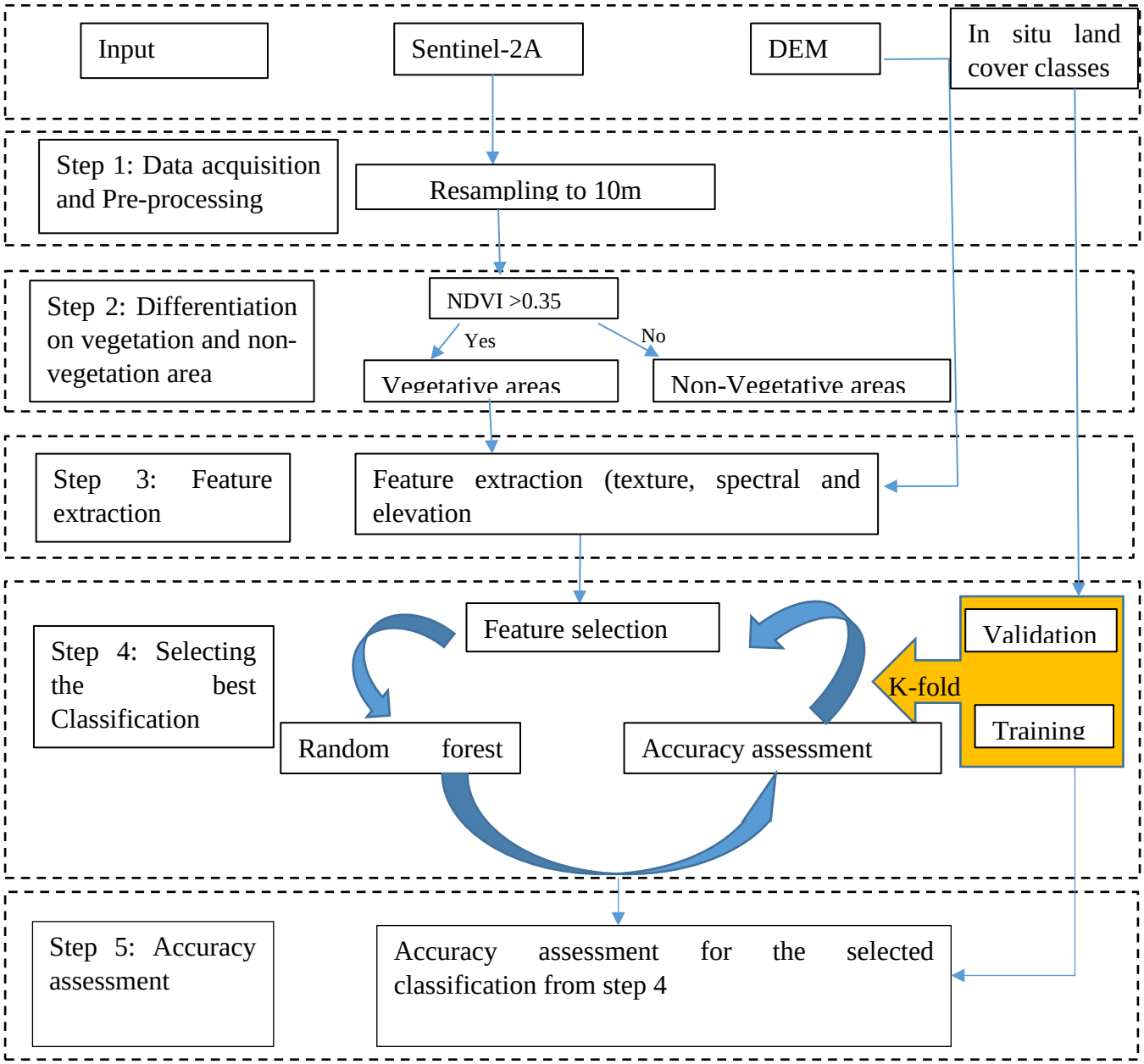

Figure 3.2 Overview of the five steps used to carry out the analyis

3.2.2.1 Multispectral Sentinel 2A Image

The Sentinel-2 constellation includes two identical satellites: Sentinel 2A was launched in 2015 and Sentinel 2B in 2017. The temporal resolution of Sentinel-2 is ten days, but it decreases to five days when both the satellites are operational, in the equator (Bhattacharjee et al. 2021) and

has a spectral resolution from 443-2190nm. The spatial resolution of both Sentinel-2 is different in 13 spectral bands. These are blue (490nm), green (560nm), red (665nm), and Near-infrared (NIR) (842nm) bands at 10m resolution, red–edge (705-783nm) and shortwave-infrared bands (SWIR) (1610-2190nm) at 20m resolution, and three atmospheric correction bands at 60m resolution, including cirrus-cloud screening (Band 10) (Forkuor et al. 2018).

Studies that use Sentinel-2 found that it outperformed Landsat 8 because of improved spatial and spectral capabilities (Forkuor et al. 2018; Biswas et al. 2020) and a practical option for forest monitoring and mapping (Addabbo et al. 2016). Moreover, this satellite has a high potential for forest species classification and the differentiation of vegetation types in a complex landscape involving small land parcels (Wessel et al. 2018; Mngadi et al. 2021). The Sentinel-2A cloud-free image acquired on 02.04.2020 used in this study was extracted from GEE. The data derived from Sentinel-2 level-2A image have been orthorectified and atmospherically corrected to obtain surface reflectance. Only the 20m spatial resolution bands were resampled to a 10m scale based on bicubic interpolation in this study. Finally, the clipping operation was executed.

3.2.2.2 Elevation Data

The Shuttle Radar Topographic Mission (SRTM) provides digital elevation data (DEM) on a near-global scale. The SRTM Plus version with a spatial resolution of 30m and vertical resolution of 10m (Bourgine and Baghdadi 2005) was acquired from GEE, and topographic features such as elevation, aspect, and slope were extracted.

3.2.2.3 Training and Validation

Mixed sampling was selected for the research: point and polygon sampling. However, point sampling does not work well in the home garden context because households and trees need to be represented. Therefore, polygonal sampling was used to get a clear picture of the home garden. The adopted classes in the study area and their respective number of points and polygons used for training were: forest (191), pine plantation (212), grassland (156), shrub (106), home garden (115), and cultivation (51).

This research used WorldView-3 images dated on 26.03.2020 and 17.04.2020 in Google Earth with prior knowledge of the study area to validate forest classes. WorldView-3 satellite

provides 1.24m multispectral resolution at the nadir and 1.38m resolution at the 20^0 off-nadir. This method is a valid and practical option when search, and travel costs are prohibitive and when the study area is extensive (Biswas et al. 2020). Google Earth imagery was used by Zhang et al. (2019), Deng et al. (2020), and Senanayake et al. (2020) to collect field sample points, where Das and Das (2014) and (Perera Kithsiri and Tsuchiya 2009) used it to validate home garden in India and forest cover in Sri Lanka, respectively.

Table 3.2 Validation points use for decide NDVI threshold

Date		Nov 13th 2020
Number of points	Vegetation area	200
	Non-vegetation area	200

3.2.3 Feature extraction

3.2.3.1 Spectral Feature Extraction

Normalised Difference Vegetation Index (NDVI – Equation 3.1) was used to select the vegetative area by filtering non-vegetative areas, including water and urban. According to USGS (2018), moderate NDVI values (from 0.2 to 0.5) correspond to sparse vegetation, and higher NDVI values (from 0.6 to 0.9) correspond to the dense vegetation. Taufik et al. (2016) selected NDVI values more than 0.35 (moderate and high NDVI values) to extract the vegetation class. Correspondingly, in this research, the mean NDVI value (0.35) of the ground sampling pixels (Table 3.2) was selected to differentiate non-vegetation and vegetation.

$$\mathrm{NDVI} = \frac{(NIR - RED)}{(NIR + RED)} \quad (3.1)$$

In forest studies, red-edge bands, NIR, SWIR and visual bands are suitable for the analysis (Addabbo et al. 2016; Wessel et al. 2018); therefore, all these bands in the Sentinel-2 image were selected to train the classifier. Furthermore, the Red-Green Chlorophyll Index (Equation 3.2) vegetation index was also used as a spectral feature.

$$\mathrm{RGCI} = \frac{Red\ edge3}{Red\ edge1} - 1 \quad (3.2)$$

3.2.3.2 Data reduction

PCA- Principal Component Analysis (PCA) is a data-dependent analysis that employed to reduce the extracted features' dimensions from data and isolate variation types in individual components (Liu et al. 2018), ultimately improving the results (Wessel et al. 2018; Nordin et al. 2019). PCA was applied to the original image to extract the principal components (Wang et al. 2016) from the data. After a visual examination, the second principal component was selected, and the other seven PC bands were eliminated.

3.2.3.3 Texture Feature Extraction

Texture, such as roughness or linear patterns, are just as useful as colour (spectral) information for differentiating land use classes (Kuplich et al. 2005). This study used the grey-level co-occurrence matrix (GLCM) for texture feature extraction, proposed by Haralick et al. (1973), which has been extensively used for land cover classification and forestry (Kuplich et al. 2005; Feng et al. 2015; Cheng and Wang 2019). This analysis often requires setting four parameters: window size, spectral bands, quantization level (defined as the range of reflectance values in a particular spectral band), and spatial component (the distance between pixels and the angle or direction) (Puetz and Olsen 2006; Sothe et al. 2017). However, GEE only allows two parameters to be set: spectral bands and window size. In this research, the textural metrics were mainly calculated for the second PC band derived from PCA classification. GLCM was applied to all nine spectral bands and but only the most important 16 textural bands were used for the classification. Out of these parameters, window size affects the performance of the textural metrics for classifying land use. Small windows may amplify differences and increase noise content in the texture of the image. However, large windows cannot effectively extract texture information due to the smoothing that results (Sothe et al. 2017). Therefore, a proper window size helps extract the particular landscape feature by matching the patch size. Three different moving windows were chosen and applied for the second PC band to analyse how classification accuracy changes with texture window size: 5×5 size (5), 10×10 size (10), and 15×15 size (15). Texture features derived at the most accurate window size (5×5) was added as a band to the selected image for further classification. Once the selection of window size was completed, the statistical measures were designed to extract the characteristics of the matrix (Ouma et al. 2008).

3.2.4 Classification using Random Forest

Random Forest (RF) was used for image classification in this study because of its robustness and efficiency (Feng et al. 2015). It is an integrated learning method based on the decision tree, combined with many ensemble methods of supervised learning (Wessel et al. 2018). Breiman (2001) proposed this method, and it has been increasingly used for image classification in remote sensing due to its flexible, nonparametric nature and ability to limit overfitting (Feng et al. 2015; Cheng and Wang 2019) and achieve higher accuracy than other machine learning methods (Sothe et al. 2017; Liu et al. 2018). In order to run the classifier, the number of trees (ntree) and the number of features in each split (mtry) need to be set up (Biswas et al. 2020). The maximum number of trees used for this research was 350, with variables per split set to the default of the random forest algorithm, which uses the square root of the number of variables concerned.

One of the main advantages of random forest method is that it can provide information on each input variable's contribution to classification accuracy (Feng et al. 2015). The mean decrease Gini (mdg) variable measured internally by the RF algorithm in GEE was used to determine the importance measure of each feature used (Forkuor et al. 2018) in partitioning the training data into the defined vegetation classes during the model building process. Higher Gini scores correspond to consistently found features and are more important to the model. Therefore, the most significant variables were selected (Table 3.3). The important variable (feature) assessment was re-run separately on the home garden to identify the significant variables. All the importance values were normalized using the mean and the standard deviation to put the variables on the same scale for a better representation.

Table 3.3 Variables used for the Main classification

Selected features		Variables
Spectral		
	Bands	B3, B4 ,B5, B6, B7 ,B8, B8A, B11,B12
	Vegetation index	RGCI
*Textural		B2_diss, B3_contrast, B3_savg, B4_diss, B4_dvar, B4_inertia, B4_savg, B4_var, B5_savg, B8A_savg ,B8_savg, B11_savg B12_savg, PC2, pc2_corr, pc2_savg
Topography		Elevation
		Slope
		Aspect

Note: * Diss- Dissimilarity, contrast- Contrast, Savg- Sum of Average dvar- Difference of variances, inertia- Inertia, Var- Variance, Corr- Correlation

3.3 Results

The final map of the forest and agroforestry classification shown in Figure 3.3 corresponds to vegetation distribution. The dense forest is the most dominant land cover class with an extent of 5347.79 ha, followed by the home garden (3448.01 ha) cultivations (2699.48 ha) and pine plantations (1455.4 ha); grassland (444.39 ha) is the least dominant vegetation type. The dense forest can be seen on the gentle slopes and the flat regions in the southern corner of the study area. In contrast, *Pinus* plantations are located on ridges and steep areas where the slope is higher than 18% (Figure 3.4). Home gardens are spread around the study area, whereas grassland is concentrated north of the study area.

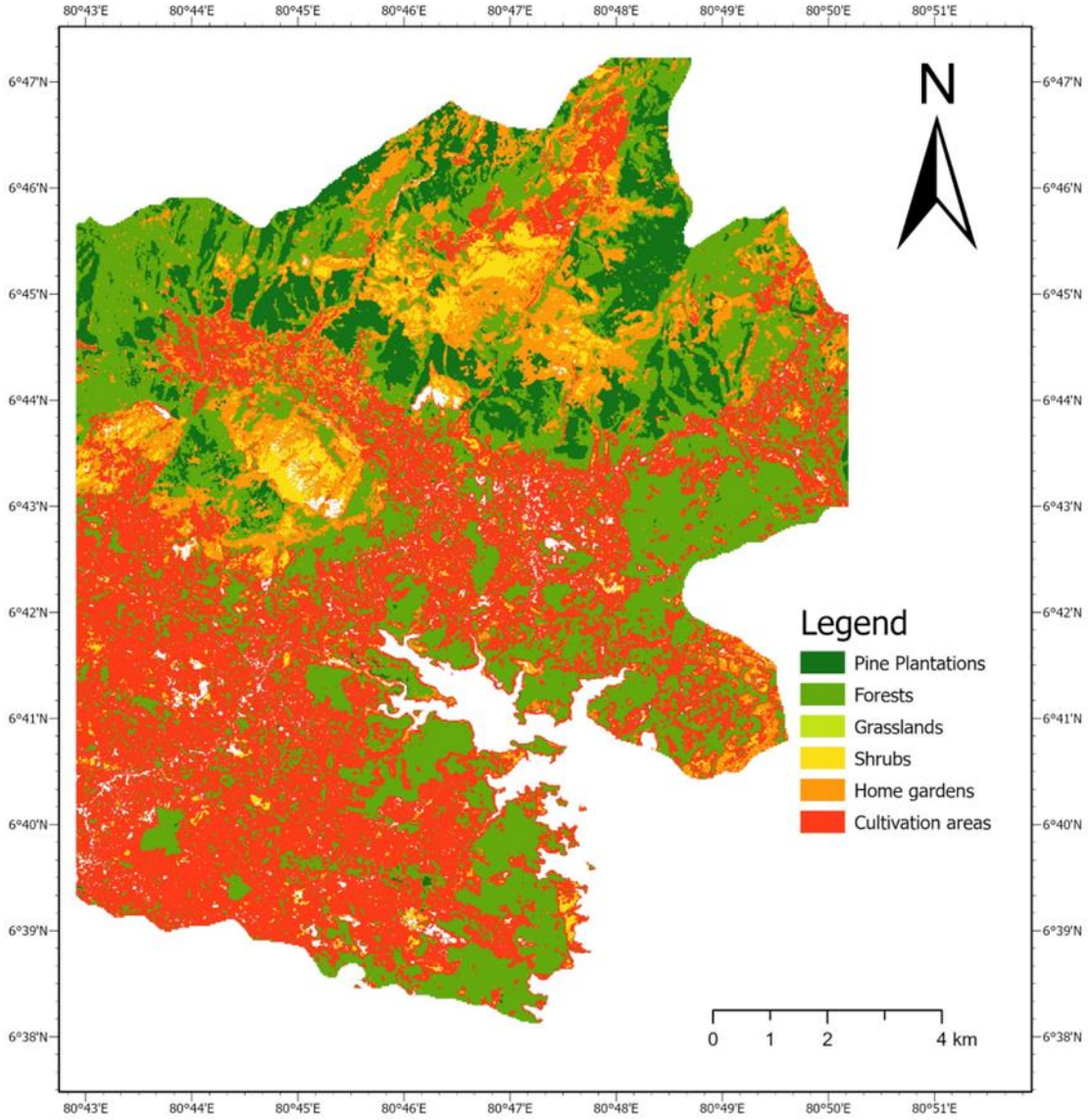

Figure 3.3 Study areas's forest and agroforestry classification

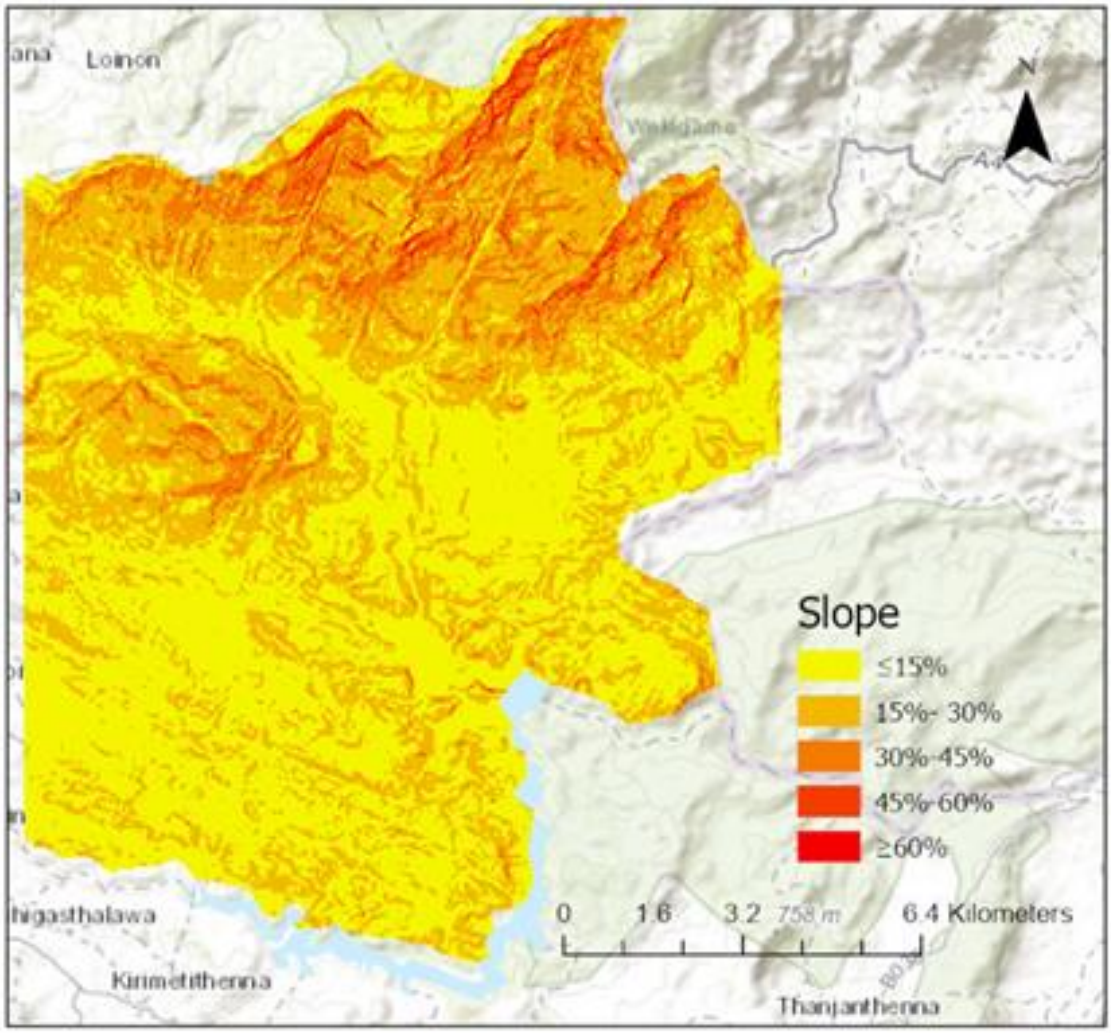

Figure 3.4 Slope map of the study area

K-fold cross-validation procedure was used to estimate the accuracy of the random forest classifier. This study adopted fivefold cross-validation by dividing the data into five randomly stratified folds. In each experiment, one of the data folds was left for validation (30%), and the remaining used to train the classifier (70%). The performance quality of the trained classifier was tested on the validation fold, and overall performance was measured (Table 3.4). Then averaged over the five experiments (k-folds). The overall accuracy (OA) and kappa coefficients are 94.26% and 0.91, respectively, indicating a successful classification result; this was possible due to the combination of spectral, textural and elevation data. All the classes reveal a well-balanced user's accuracy (UA) and the producer's accuracy (PA). The most accurately classified classes were pine plantations, forest, and home garden, with PA and UA higher than 90%, followed by shrubs and grasslands (more than 80%). The most problematic class was

cultivation, which only achieved a PA of 69.54%. Tea and annual plant cultivations practice around the homestead generated confusion in the cultivation group.

Table 3.4 Confusion matrix

Land cover	Forestry classes				Agroforestry Classes		Total
	Pine	Natural	Grassland	Shrub	HG	Cultivation	
Pine	74	1	0	0	0	0	75
Natural	0	76	0	0	0	7	83
Grassland	0	0	36	7	0	3	46
Shrub	1	1	12	41	0	0	55
HG	0	0	1	1	293	2	297
Cultivation	0	1	0	1	8	25	35
Total	75	79	49	50	301	37	591
UA (%)	98	90.38	84.83	86.87	98.6	74.97	
PA (%)	98.82	96.55	90.51	83.15	97.5	69.54	
OA (%)				94.26			
Kappa				0.91			

The results of spectral only classification presented in Figure 3.5 (a) retained the 'salt and pepper' like pixel appearance. When the GLCM is introduced in the classification process Figure 3.5 (b), the previously dominant 'salt and pepper' appearance is significantly reduced, especially in cultivation and home garden. This reflects the contribution of the GLCM texture measure with a corresponding window size of 5×5. However, this improvement is observed in Table 3.5, which compares the accuracy of adding texture, topography, and vegetation indices to the spectral bands.

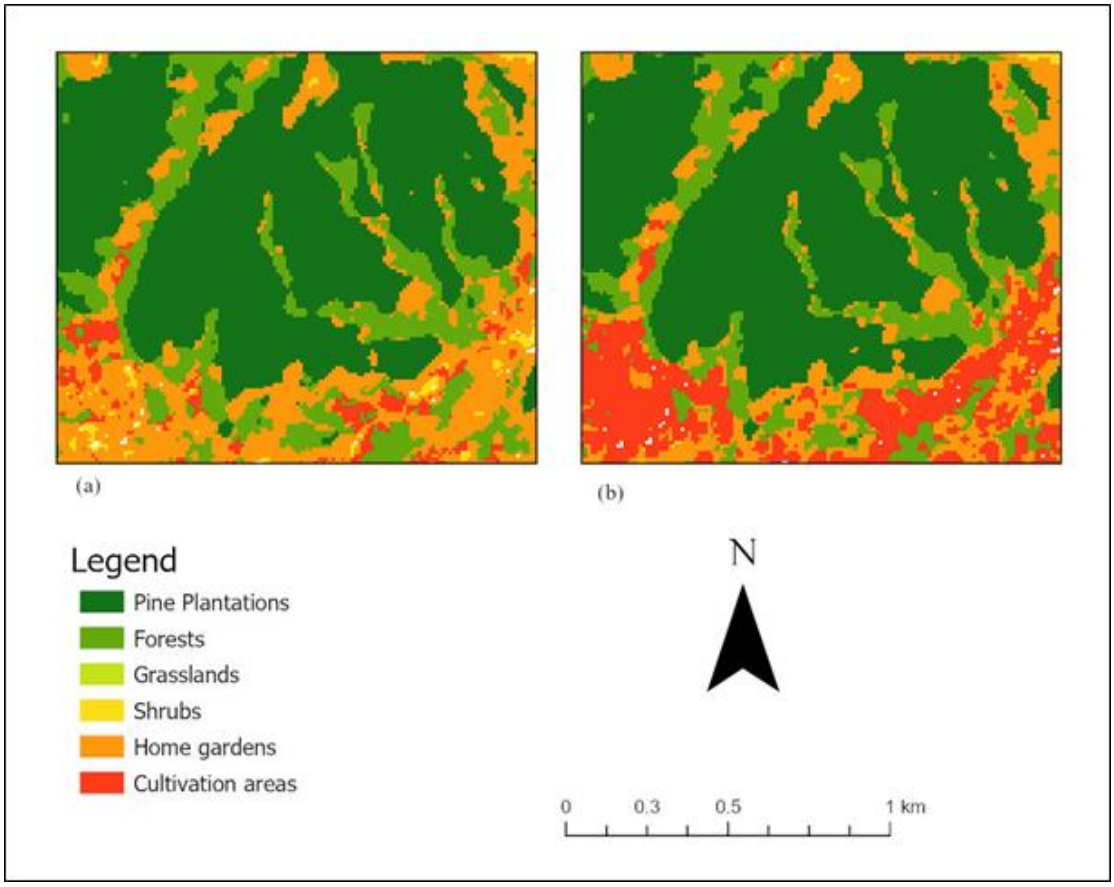

Figure 3.5 Classification results (a)Spectral only (b) Spectral and GLCM-8 Textural bands

Table 3.5 Accuracy

Variables	Overall Accuracy	Kappa
Spectral	84.70%	0.77
Spectral +Texture	92.71%	0.89
Spectral +Texture+ Topography	93.72%	0.90
Spectral+ Texture + Topography + Vegetation Index	94.26%	0.91

The feature importance can be used to extract the contribution of each selected variable towards the classification. The Gini score produced by the RF algorithm for each important variable was converted to a normalised value based on the mean and standard deviation of feature importance assessment. This feature importance assessment varied depending on the classes used in training the random forest classifier. When the classifier was trained on the complete set of the forests and agroforest classes, the importance of spatial, spectral and textural features

was different from the random forest classification run separately on the home garden. As illustrated in Figure 3.6, topographical features are the most important variables to identify forestry classes. The second vital variable group is the textural group. Finally, the third important group is spectral features: SWIR-1 (B11), NIR narrow band (B8A), SWIR-2 (B12), and this includes one vegetation index: RGCI.

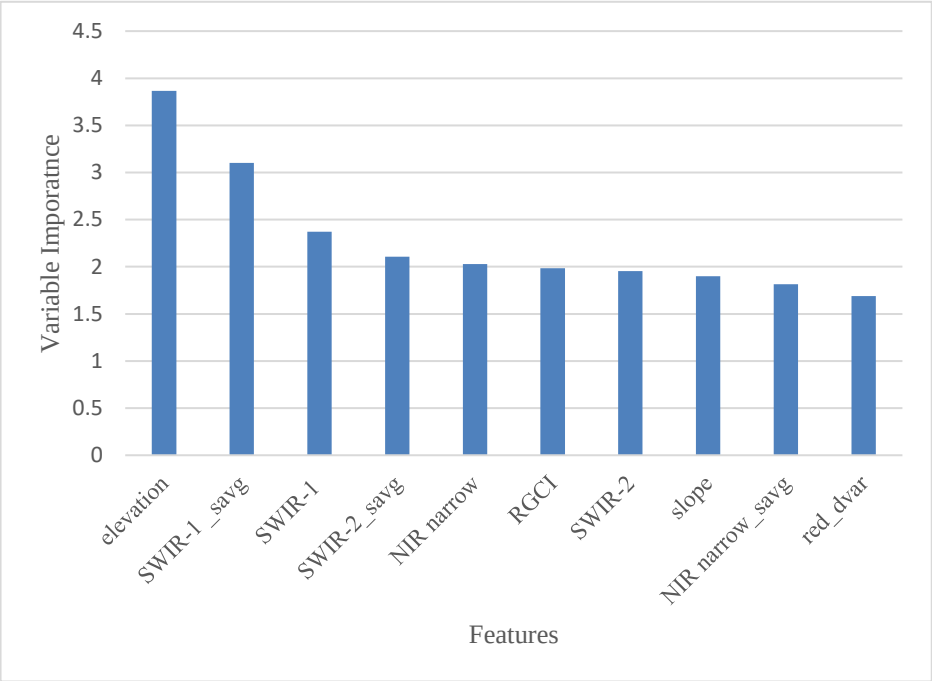

Figure 3.6 Feature importance-main classification

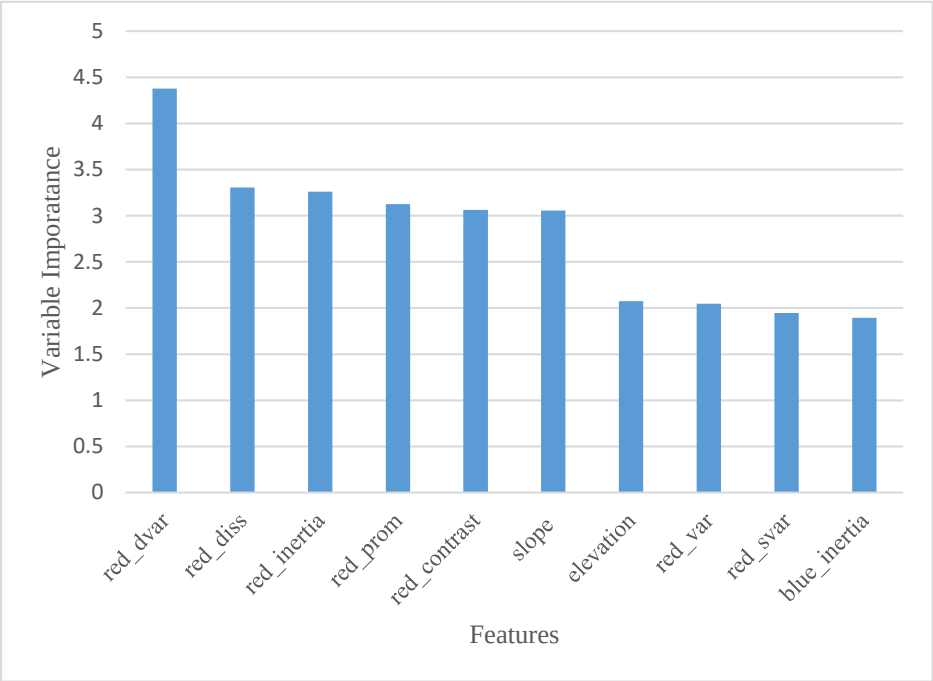

Figure 3.7 Feature importance-home garden

Figure 3.7 illustrates the feature importance of the home garden; the higher the value, the more important the feature. In contrast to the main classification, "red_dvar" is the key variable to distinguish home gardens relative to other vegetation covers, followed by "red_diss" and "red_inertia". Out of the eight textural metrics derived, metrics of the red band shows the highest relevance to distinguish the home garden from the other five vegetation covers.

3.4. Discussion

3.4.1 Combining spectral, textural, and elevation data

The present study demonstrates the importance of combining spectral and texture features, and elevation for vegetation cover classification. An OA of 94.26% was obtained by combining ten spectral, 16 textural and three elevation bands. The home garden showed 98.60% UA in the forest classification, with pine at 98%, followed by natural forest at 90.38%. In comparison, Cheng and Wang (2019) also had a good result with combining spectral, textural and elevation data with an OA of 86.88% using RF classification for forest type classification in the Qinling Mountains, China.

The influence of each type of feature set on forest and agroforestry classification was tested. Using only spectral bands produced significantly lower accuracy (OA-84.70%) than feature

sets that combined spectral, textural and topographical features (Gong et al. 2016), which achieved 93.72% accuracy. The classification accuracy is significantly improved by introducing the textural and topography features, and the increment in the OA is 9%. These results are in line with Liu et al. (2018) and Sothe et al. (2017). This differs from Immitzer et al. (2016), who argued that combining these features does not produce higher accuracy when using Sentinel-2. However, adding vegetation indices to the classification produced only a minimal improvement for the overall performance; a similar finding was made by Spracklen and Spracklen (2019), who classified old-growth forests in Europe using textural, elevation data band standard deviation and vegetation indices.

3.4.2 Extraction of forestry and agroforestry classes

Feature importance analysis demonstrated that the selected features had played an important role in discriminating various forestry and agroforestry types. Elevation, SWIR-1_Sum of Average and SWIR-1 were identified as the key features for differentiating forest types, followed by the SWIR-2_Sum of Average. The results are consistent with previous studies. For instance, Spracklen and Spracklen (2019) found elevation, SWIR bands, red edge and NIR important for differentiating forest types. Similarly, Liu et al. (2018) found the terrain contributes the most to forest type identification with multi-temporal data. The higher importance of elevation can be attributed to the study area's landform, which has a high variation in elevation and slope, whereas Deng et al. (2020) found that elevation does not act as a pivotal attribute in areas with minor elevation variation. In line with Balasubramanian (2017); Biswas et al. (2020), we identified that "savg" is the most useful texture metric for differentiating forest and agroforest types. However, the widely reported GLCM textures for vegetation related studies were not selected as important features. These include "correlation" Wang et al. (2016) and "contrast" Kuplich et al. (2005); Cheng and Wang (2019), which are demonstrated to play an important role in forest extraction. Ouma et al. (2008) have stated that vegetation's type and density can influence the texture metrics. Therefore, this rather contradictory result may be because the research focuses not only on forest extraction but also on agroforestry classes that incorporate trees and crops.

A number of researchers (Immitzer et al. 2016; Sothe et al. 2017; Biswas et al. 2020) have concluded that the reflectance of red-edge and SWIR bands are the most important for forest classification with Sentinel-2 data. The present research also confirmed the high values of both red-edge and SWIR for differentiating forest types. Though none of the red-edge bands was in

the top ten variables, the B8A band became the fifth important variable differentiating forestry and agroforestry classes.

This study further suggests that freely available remotely sensed data (Sentinel-2) have the potential for forest and agroforestry type identification and offer significant classification accuracy without the need for commercial satellite imagery and the platform.

3.4.3 Home garden

The home garden is an important land cover class in Sri Lanka and essential in South Asian rural farm households (Sangakkara and Frossard 2016). Due to plants and trees' presence, the home garden tends to be misclassified with forest (Rathnayake et al. 2020) or cultivation areas (Dong et al. 2016) which was also found in this research. This problem could arise because home gardens are mainly rain-fed (Land Use Policy Planning Department 2020), so during the dry season falls (February to April), they may show cropland characteristics.

Research studies focused on home garden primarily identified their plant species composition and abundance (Kehlenbeck and Maass 2004; Abebe et al. 2013) of home garden distribution over a region (Premakantha et al. 2009; Das and Das 2014; Sangakkara and Frossard 2016), or the change over time (Pushpakumara et al. 2012). Moreover, some researchers (Martin et al. 2019) have considered the socioeconomic characteristics of this land cover class, including the ownership and structure of home gardens (Perera AH and Rajapakse 1991). To our knowledge, this study appears to be the first to identify the important variables needed for classifying home gardening using remote sensing. Furthermore, this study depicts the feature importance of the home garden and presents similar results with other remote sensing studies concerned with forest types and crop types classification (Immitzer et al. 2016; Balasubramanian 2017). Interestingly, textural features are the main feature category that helps extract home garden class, especially metrics derived from the red band. Further, as in the main classification, elevation and slope became the second vital feature category to determine the home garden due to the topographical variability of the study area.

According to the variable importance, "red _dvar" is the most important textural feature for identifying the home garden, whereas "red _diss", "red _inertia", "red _ prom", and "red _contrast" bands were also significant textural features. Moreover, Balasubramanian (2017) found that "prom" and "diss" textural metrics are significant variables for differentiating crop types. While Cheng and Wang (2019) demonstrated that the "red_contrast" is more important

when distinguishing among evergreen forest types, which is also a significant variable in the home garden class because it is attributable to the differences in leaf structure. Further investigation is needed to identify tree species in the home garden using remote sensing to manage this agroforestry system for future sustainability.

3.5 Conclusion

The present study has demonstrated the utility of GEE and freely available satellite data sources for mapping forestry and agroforestry classes important to Sri Lanka at high spatial resolution (10m). The GEE platform was used to prepare, analyse, and produce maps using textural spectral and spatial features. This included the use of PCA and GLCM analysis methods as well as the random forest classifier. The classification produced in this research had improved accuracy resulting from the addition of textural and elevation data. The results indicate that elevation and SWIR bands are important for distinguishing forest and agroforestry classes, whereas red textural metrics and topographical features are significant for distinguishing the home garden. Thus, freely accessible remotely sensed data and platforms can effectively support developing countries, like Sri Lanka, to monitor and manage forest resources on national or local scales using unique and important classes to these countries.

3.6 References

Abebe T, Sterck FJ, Wiersum KF, Bongers F. 2013. Diversity, composition and density of trees and shrubs in agroforestry homegardens in Southern Ethiopia [Article]. Agroforestry Systems. 87(6):1283-1293. English.

Addabbo P, Focareta M, Marcuccio S, Votto C, Ullo S. 2016. Contribution of Sentinel-2 data for applications in vegetation monitoring. ACTA IMEKO. 5:44.

Balasubramanian KI. 2017. Identifying the most important spectral and textural feature features to map specific crops with very high resolution images. University of Twente.

Bhattacharjee R, Choubey A, Das N, Ohri A, Gaur S. 2021. Detecting the Carotenoid Pigmentation due to Haloarchaea Microbes in the Lonar Lake, Maharashtra, India Using Sentinel-2 Images. J Indian Soc Remote Sens. 49(2):305-316.

Biswas S, Huang Q, Anand A, Mon MS, Arnold F-E, Leimgruber P. 2020. A Multi Sensor Approach to Forest Type Mapping for Advancing Monitoring of Sustainable Development Goals (SDG) in Myanmar. Remote Sensing. 12(19):3220.

Bourgine B, Baghdadi N. 2005. Assessment of C-band SRTM DEM in a dense equatorial forest zone. Comptes Rendus Geoscience. 337(14):1225-1234.

Breiman L. 2001. Random Forests. Machine Learning. 45(1):5-32.

Carrasco L, O'Neil AW, Morton RD, Rowland CS. 2019. Evaluating Combinations of Temporally Aggregated Sentinel-1, Sentinel-2 and Landsat 8 for Land Cover Mapping with Google Earth Engine. Remote Sensing. 11(3):288.

Cheng K, Wang J. 2019. Forest Type Classification Based on Integrated Spectral-Spatial-Temporal Features and Random Forest Algorithm—A Case Study in the Qinling Mountains. Forests. 10(7):559.

Das T, Das AK. 2014. Mapping and Identification of Homegardens as a Component of the Trees Outside Forests Using Remote Sensing and Geographic Information System [Article]. J Indian Soc Remote Sens. 42(1):233-242. English.

Deng XP, Guo SX, Sun LY, Chen JS. 2020. Identification of Short-Rotation Eucalyptus Plantation at Large Scale Using Multi-Satellite Imageries and Cloud Computing Platform [Article]. Remote Sensing. 12(13):18. English.

Dong JW, Xiao XM, Menarguez MA, Zhang GL, Qin YW, Thau D, Biradar C, Moore B. 2016. Mapping paddy rice planting area in northeastern Asia with Landsat 8 images, phenology-based algorithm and Google Earth Engine [Article]. Remote Sens Environ. 185:142-154. English.

Erasmi S, Kappas M, Twele A, Ardiansyah M. 2007. From global to regional scale: Remote sensing-based concepts and methods for mapping land-cover and land-cover change in tropical regions. In: Tscharntke T, Leuschner C, Zeller M et al., editors. Stability of Tropical Rainforest Margins: Linking Ecological, Economic and Social Constraints of Land Use and Conservation. Berlin, Heidelberg: Springer p. 435-460.

Feng Q, Liu J, Gong J. 2015. UAV Remote Sensing for Urban Vegetation Mapping Using Random Forest and Texture Analysis. Remote Sensing. 7(1):1074-1094.

Forkuor G, Dimobe K, Serme I, Tondoh JE. 2018. Landsat-8 vs. Sentinel-2: examining the added value of sentinel-2's red-edge bands to land-use and land-cover mapping in Burkina Faso. GISci Remote Sens. 55(3):331-354.

Gong P, Yu L, Li C, Wang J, Liang L, Li X, Ji L, Bai Y, Cheng Y, Zhu Z. 2016. A new research paradigm for global land cover mapping. Annals of GIS. 22(2):87-102.

Haralick RM, Shanmugam K, Dinstein I. 1973. Textural Features for Image Classification. IEEE Transactions on Systems, Man, and Cybernetics. SMC-3(6):610-621.

Immitzer M, Vuolo F, Atzberger C. 2016. First Experience with Sentinel-2 Data for Crop and Tree Species Classifications in Central Europe. Remote Sensing. 8(3):166.

Kehlenbeck K, Maass BL. 2004. Crop diversity and classification of homegardens in Central Sulawesi, Indonesia. Agroforestry Systems. 63(1):53-62.

Kumar BM, Nair PKR. 2006. Introduction. In: Kumar BM, Nair PKR, editors. Tropical Homegardens: A Time-Tested Example of Sustainable Agroforestry. Dordrecht: Springer Netherlands; p. 1-10.

Kuplich TM, Curran PJ, Atkinson PM. 2005. Relating SAR image texture to the biomass of regenerating tropical forests. Int J Remote Sens. 26(21):4829-4854.

mLand Use Policy Planning Department. 2020. Data and Information of Home Gardens in ratnapura District. Ministry of Lands and Land Development.

Lindström S, Mattsson E, Nissanka SP. 2012. Forest cover change in Sri Lanka: The role of small scale farmers. Appl Geogr. 34:680-692.

Liu Y, Gong W, Hu X, Gong J. 2018. Forest Type Identification with Random Forest Using Sentinel-1A, Sentinel-2A, Multi-Temporal Landsat-8 and DEM Data. Remote Sensing. 10(6):946.

Martin M, Geiger K, Singhakumara BMP, Ashton MS. 2019. Quantitatively characterizing the floristics and structure of a traditional homegarden in a village landscape, Sri Lanka. Agroforestry Systems. 93(4):1439-1454.

Mattsson E, Ostwald M, Nissanka SP, Marambe B. 2013. Homegardens as a Multi-functional Land-Use Strategy in Sri Lanka with Focus on Carbon Sequestration. Ambio. 42(7):892-902.

Mertes CM, Schneider A, Sulla-Menashe D, Tatem AJ, Tan B. 2015. Detecting change in urban areas at continental scales with MODIS data. Remote Sens Environ. 158:331-347.

Mngadi M, Odindi J, Peerbhay K, Mutanga O. 2021. Examining the effectiveness of Sentinel-1 and 2 imagery for commercial forest species mapping. Geocarto International. 36(1):1-12.

Nordin SA, Abd Latif Z, Omar H. 2019. Individual tree crown segmentation in tropical peat swamp forest using airborne hyperspectral data. Geocarto International. 34(11):1218-1236.

Ouma YO, Tetuko J, Tateishi R. 2008. Analysis of co-occurrence and discrete wavelet transform textures for differentiation of forest and non-forest vegetation in very-high-resolution optical-sensor imagery. Int J Remote Sens. 29(12):3417-3456.

Perera AH, Rajapakse RMN. 1991. A baseline study of Kandyan Forest Gardens of Sri Lanka: Structure, composition and utilization. Forest Ecology and Management. 45(1):269-280.

Perera K, Herath S, Apan A, Tateishi R. 2012. Application of Modis Data to Assess the Latest Forest Cover Changes of Sri Lanka. ISPRS Ann Photogramm Remote Sens Spatial Inf Sci. I-7:165-170.

Perera K, Tsuchiya K. 2009. Experiment for mapping land cover and it's change in southeastern Sri Lanka utilizing 250m resolution MODIS imageries. Advances in Space Research. 43(9):1349-1355.

Premakantha KT, Puspakumara DKNG, Dayawansa N. 2009. Identification of Tree Resources Outside Forest in up country of Sri Lanka using medium resolution satellite imagery. Tropical agricultural research. 20:354-365.

Puetz A, Olsen R. 2006. Haralick texture features expanded into the spectral domain. Vol. 6233. SPIE. (Defense and Security Symposium.

Pushpakumara D, Marambe B, Gllp S, Weerahewa J, Bvr P. 2012. A review research on homegardens in Sri Lanka: the status, importance and future perspective. Tropical Agriculturist. 160:55-125.

Rathnayake CW, Jones S, Soto-Berelov M. 2020. Mapping Land Cover Change over a 25-Year Period (1993–2018) in Sri Lanka Using Landsat Time-Series. Land. 9(1):27.

Sangakkara UR, Frossard E. 2016. Characteristics of South Asian rural households and associated home gardens - A case study from Sri Lanka [Article]. Trop Ecol. 57(4):765-777. English.

Senanayake S, Pradhan B, Huete A, Brennan J. 2020. Assessing Soil Erosion Hazards Using Land-Use Change and Landslide Frequency Ratio Method: A Case Study of Sabaragamuwa Province, Sri Lanka. Remote sensing (Basel, Switzerland). 12(9):1483.

Sothe C, Almeida CMd, Liesenberg V, Schimalski MB. 2017. Evaluating Sentinel-2 and Landsat-8 Data to Map Sucessional Forest Stages in a Subtropical Forest in Southern Brazil. Remote Sensing. 9(8):838.

Stibig HJ, Belward AS, Roy PS, Rosalina-Wasrin U, Agrawal S, Joshi PK, Beuchle R, Fritz S, Mubareka S, Giri C. 2007. A land-cover map for South and Southeast Asia derived from SPOT-VEGETATION data. Journal of Biogeography. 34(4):625-637.

Taufik A, Ahmad SSS, Ahmad A. 2016. Classification of Landsat 8 Satellite Data Using NDVI Tresholds. Journal of Telecommunication, Electronic and Computer Engineering. 8:37-40.

USGS. 2018. NDVI, the Foundation for Remote Sensing Phenology. [accessed 2021 13th of November]. https://www.usgs.gov/core-science-systems/eros/phenology/science/ndvi-foundation-remote-sensing-phenology?qt-science_center_objects=0#qt-science_center_objects.

Wang T, Zhang H, Lin H, Fang C. 2016. Textural–Spectral Feature-Based Species Classification of Mangroves in Mai Po Nature Reserve from Worldview-3 Imagery. Remote Sensing. 8(1):24.

Wessel M, Brandmeier M, Tiede D. 2018. Evaluation of Different Machine Learning Algorithms for Scalable Classification of Tree Types and Tree Species Based on Sentinel-2 Data. Remote Sensing. 10(9):1419.

Zhang MN, Gong P, Qi SH, Liu C, Xiong TW. 2019. Mapping bamboo with regional phenological characteristics derived from dense Landsat time series using Google Earth Engine [Article; Proceedings Paper]. Int J Remote Sens. 40(24):9541-9555. English.

Zurqani HA, Post CJ, Mikhailova EA, Schlautman MA, Sharp JL. 2018. Geospatial analysis of land use change in the Savannah River Basin using Google Earth Engine. International Journal of Applied Earth Observation and Geoinformation. 69:175-185.

Chapter 4

Monitoring invasive pines using remote sensing: A case study from Sri Lanka

*This Chapter is a peer-reviewed paper published as Nandasena, W., Brabyn, L. & Serrao-Neumann, S. Monitoring invasive pines using remote sensing: a case study from Sri Lanka. Environmental Monitoring Assessment **195**, 347 (2023). https://doi.org/10.1007/s10661-023-10919-1*

Abstract

Production plantation forestry has many economic benefits but can also have negative environmental impacts such as the spreading of invasive pines to native forest habitats. Monitoring forest for the presence of invasive pines helps with the management of this issue. However, detection of vegetation change over a large time period is difficult due to changes in image quality and sensor types, and by the spectral similarity of evergreen species and frequent cloud cover in the study area. The costs of high-resolution images are also prohibitive for routine monitoring in resource constrained countries. This research investigated the use of remote sensing to identify the spread of *Pinus caribaea* over a 21-year period (2000 to 2021) in Belihuloya, Sri Lanka using Landsat images. It applied a range of techniques to produce cloud free images, extract vegetation features and improve vegetation classification accuracy, followed by the use of Geographical Information System to spatially analyse the spread of invasive pines. The results showed most invading pines were found within 100 m of the pine plantations' borders where broadleaved forests and grasslands are vulnerable to invasion. However, the extent of invasive pine had an overall decline of 4 ha over the 21 years. The study confirmed that remote sensing combined with spatial analysis is effective at monitoring invasive pines in countries with limited resources. This study also provides information to conservationists and forest managers to conduct strategic planning for sustainable forest management and conservation in Sri Lanka.

Keywords: Google Earth Engine, Invasive pine, Landsat, Pinus caribaea, Random forest classifier, Sri Lanka

4.1 Introduction

Forest plantations have been established worldwide to provide timber and firewood and have significantly contributed to local and global economies. However, most of these plantations were established using tree species with fast growth rates, which differ from many naturally regenerated forests in composition and structure, leading to different ecological processes and functional outcomes (Subasinghe et al., 2014). In some environments, these fast-growing exotic tree species have become invasive, replacing existing vegetation (Dash, 2020; Rejmánek & Richardson, 2013; Richardson et al., 2007).

Notably, plantations using pine species are the highest contributor to timber production globally (Burley & Barnes, 2004; McEwan et al., 2020). These species, however, can cause many adverse effects to the environment. For example, pine species native to North America and Europe have been introduced to New Zealand, South Africa, Argentina, Brazil and Chile as a foundation for exotic forestry enterprises (Pauchard, Escudero, et al., 2016; Rejmánek, 2014; Singh et al., 2018), but are now invading significant areas such as native forests, grasslands, catchments and protected areas, causing a potential transformative effect on native ecosystems (Dash, 2020; Richardson et al., 2007). Additionally, Medawatte et al. (2010) study shows that invasive pines can also contribute to an overall decrease in native biodiversity, suppress native plants, contribute to habitat loss for wildlife, decrease streamflow, cause changes in nutrient cycling, and affect groundwater supply levels.

Pinus patula and *Pinus caribaea* were introduced to Sri Lanka in 1967 to boost timber production and reduce the risk of soil erosion and landslides in the hilly regions due to their faster growth rates compared with indigenous species (Subasinghe, 2007). In particular, *Pinus caribaea* was used extensively for the reforestation of degraded areas in the country's wet and intermediate climatic zones with elevations ranging from 100 m to 2000 m above mean sea level due to its fast establishment and growth under adverse conditions (Edirisinghe, 2017; Jayawardhane & Gunaratne, 2020; Perera, 2001). However, their invasive behaviour in Sri Lanka's mountainous region has negatively affected the soil biodiversity and regeneration of native flora, and increased the occurrence of wildfires during the dry season (Nissanka et al., 2005; Wijerathna et al., 2016). In 2008, *Pinus caribaea* was identified as a potentially invasive alien species in Sri Lanka because several areas in the mid-country reported their spread (Wijesundera, 2008). As a result, the Sri Lankan government is planning to replace pine plantations with indigenous plant species (Office of the Cabinet of Ministers-Sri Lanka 2017).

Previous studies (Bjerreskov et al., 2021; Kaplan, 2021; Liu et al., 2022) have investigated the expansion of broad leaf and conifer forests maintained and managed for commercial timber production in temperate climates where the difference is very significant due to seasonal and phenological changes. Further, it is relatively easy to recognize these two types of temperate forests when coniferous species are evergreen and broad leaf trees are deciduous. Comparatively, studies conducted in tropical environments are limited in their spatial extent and are focused on the simple classification of landscapes into major land cover classes (Petersen et al., 2016). Further, Pauchard, García, et al. (2016) found that climate-induced invasion, or the latitudinal pattern of invasion, happened all around the world in both tropical and temperate locations showing a growing need to monitor the spread of exotic species, and forecast future distribution of such invasions. Most pinus invasion studies (Pauchard, Escudero, et al., 2016; Weisberg et al., 2007; Xu et al., 2018), however, have been based on temperate region and largely on grasslands and shrublands. Additionally, although there are many records of exotic pines invading the natural vegetation in tropical regions (Afrin et al., 2010; Ayala et al., 2005), few studies have been performed with the use of remote sensing techniques (Amaral et al., 2015; Goncalves et al., 2022; Petersen et al., 2016). For example, only one recent study conducted in Sri Lanka has used Geographic Information System (GIS) analysis (Medawatte et al., 2010). Mapping the expansion of invasions through field surveys is time-consuming and costly; hence, there is a need to develop remote sensing methods that are both reliable and affordable, especially in developing countries.

Remote sensing is a promising tool for mapping, detecting, and monitoring invasive non-native plants across broad geographic extents. The availability of satellite image archives permits mapping non-native invasive plants spread, retrospectively (Gavier-Pizarro et al., 2012). However, most existing studies (Amaral et al., 2015; Andrew & Ustin, 2008; Dash et al., 2019; Khare et al., 2018; Piiroinen et al., 2018) have used high-resolution hyperspectral imagery covering a relatively small area and analyses over a short period of time. From a management perspective, this limits their use for long-term assessments of invasive plant spread, particularly in developing countries where the lack of historical data further compounds management efforts. On the other hand, multispectral sensors with moderate resolutions offer an alternative for low-resourced countries because they enable both change detection and measurements of phenology over multiple years (Petersen et al., 2016; Signori & Ducati, 2019; Xu et al., 2018). Additionally, these data sets are mostly free or low-cost (Bradley, 2014). In particular, the Landsat program has been extensively used for forest monitoring, providing a rich dataset to

map the invasion of tree species at the landscape scale. The opening of the Landsat archive and its continued free and open access since 2009 has enabled the analysis of both larger areas and more extensive times series (Zhu & Woodcock, 2014).

The current study investigates the application of Landsat satellite information to map, quantify and assess spatio-temporal land cover change using a Sri Lankan study area, namely Belihuloya, over a two-decade period (2000 to 2021). The selected study area is one of the few areas that manage pines for both conservation and commercial purposes in Sri Lanka. The Belihuloya region suffers from a shortage of groundwater caused by the water uptake from pine plantations (Starkloff, 1998). This results in seasonal wildfires, so it is therefore important that pine forest expansion is monitored. This study contributes to knowledge development by analysing the spread of *Pinus caribaea* to neighbouring landscapes over a 20-year period from plantations established and operated for soil conservation in Sri Lanka. Specifically, the paper seeks to answer the following research question: to what extent is the Landsat archive for Sri Lanka suitable for mapping and tracking land cover changes associated with the historical spread and invasion of conifers? To this end, this study uses Landsat archive to distinguish unmanaged pine plantations from native forests in Sri Lanka's tropical environment.

4.2 Materials and Methods

4.2.1 Study area

This study used images from the Landsat archive for the years 2000 and 2021 to monitor the historical spread and control of invasive exotic conifers (e.g. Pinus caribaea) in Sri Lanka's intermediate climatic zone. Sri Lanka has traditionally been generalized into three climatic zones: the wet zone, dry zone, and intermediate zone, according to rainfall, soil and vegetation types. The intermediate zone separates both the wet and dry zones and receives a mean annual rainfall between 1750 and 2500mm with a short and less prominent dry season (Punyawardena, 2020). This intermediate climatic zone divides into three further zones based on altitude: low-country, mid-country, and up-country. According to the Sri Lankan climatic classification (Jayawardane & Weerasena, 2000), this study area lies in the intermediate mid-country, where the elevation ranges between 600 m to 900 m above mean sea level and contains rugged topography. The study area is located in Southeast Sri Lanka and covers an area of 6234 ha. Administratively, this area belongs to the Balangoda region in the Sabaragamuwa province of Sri Lanka (Figure 4.1). The area is densely forested, containing a mixture of forest types,

including montane broadleaf forest, pine plantations and grasslands. This area was selected because it comprises both unmanaged pineland and densely forested native broad leaf species.

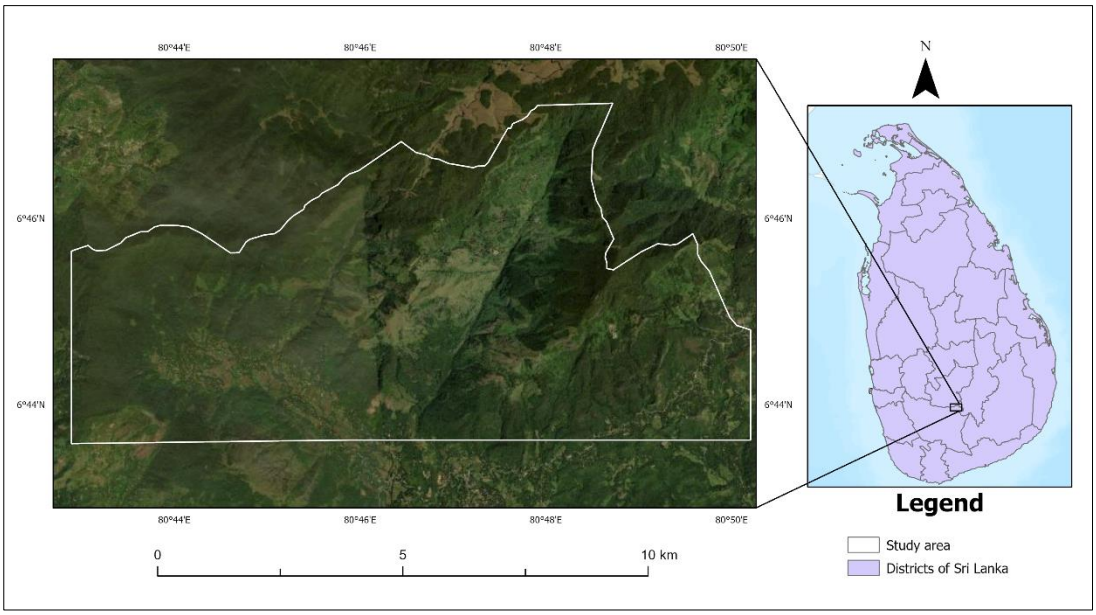

Figure 4.1 Study Area

4.2.2 Methods

The following section describes the methodology developed for this research. As shown in Figure 4.2, the study comprised five main steps: 1) Data acquisition; 2) Pre-processing; 3) Feature extraction; 4) Multitemporal Classification; and, 5) Post classification.

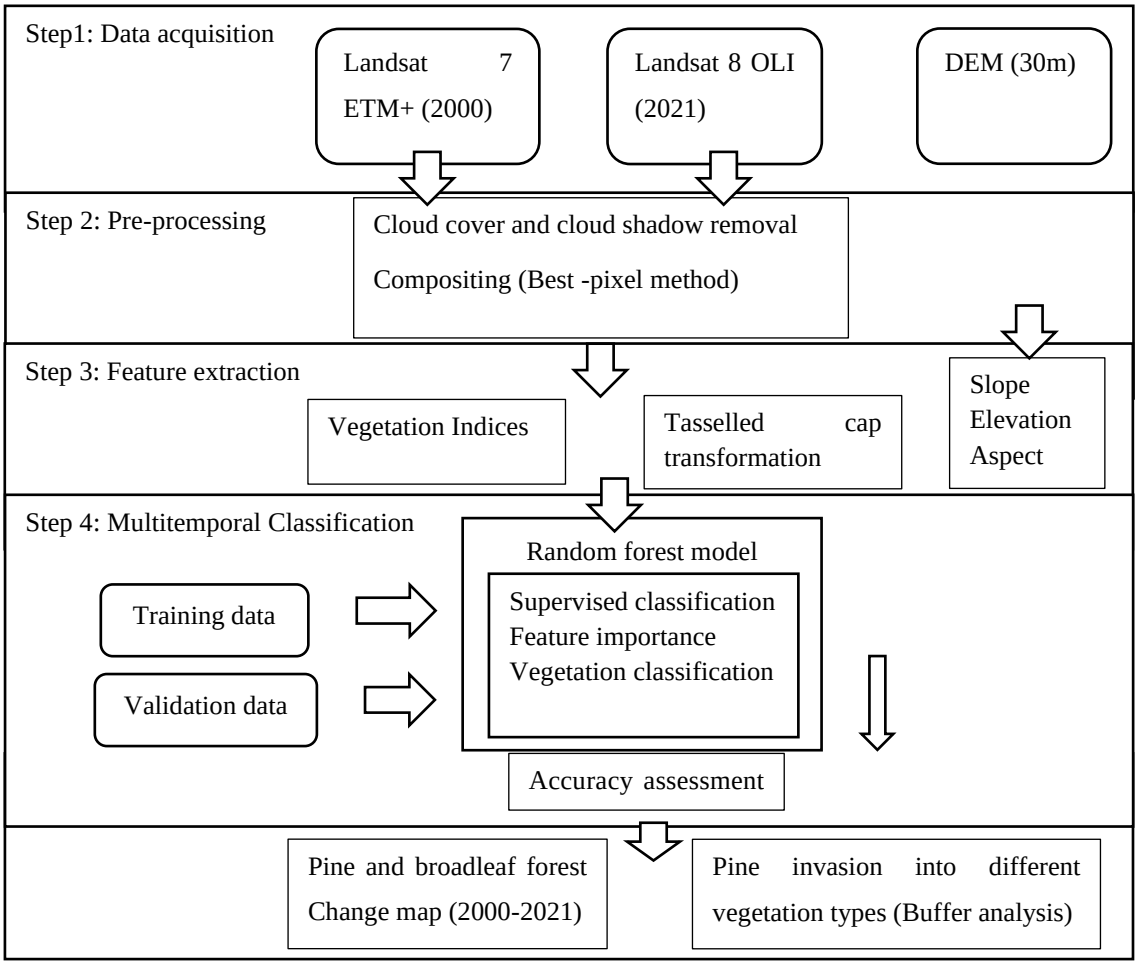

Figure 4.2 Overall methodology

Step 1: Data acquisition

Landsat 7 Enhanced Thematic Mapper Plus (ETM+) and Landsat 8 Operational Land Imager (OLI) images from the Google Earth Engine (GEE) Landsat archive (https://developers.google.com/earth-engine/datasets/catalog/landsat) for the years 2000 and 2021 were used to characterize vegetation changes. The advantage of Landsat as a moderate spatial resolution satellite collection is that the entire scene is captured at once with sun illumination, vegetative condition, and atmospheric conditions more likely to be consistent across the scene (Labonté et al., 2020). The study period 2000 and 2021 was chosen as it is

difficult to validate the classification prior to 2000 due to the absence of high-resolution images in Google Earth Pro. In 2000, only six images of Landsat 7 that covered the study area were available in the Landsat archive, and in 2021, 21 images of Landsat 8 were available. The GEE cloud-based platform was used for image pre-processing and classification (Setiani et al., 2021), while ArcGIS Pro software was used to produce maps.

The Shuttle Radar Topographic Mission (SRTM) provides digital elevation data (DEM) on a global scale. The SRTM Plus version (spatial resolution of 30m) was acquired from GEE, and topographic features such as elevation, aspect, and slope were extracted.

Step 2: Pre-processing

As the studied region is frequently cloudy it is difficult to acquire cloud-free Landsat images. Therefore, atmospheric correction, cloud/shadow masking, and image compositing were applied to construct a clean image time series. A cloud masking procedure was used to identify flagged cloud and cirrus pixels. After cloud removal, gap filling was applied using the median values of each pixel on the images. Then the median composite function in GEE was used to remove anomalous dark pixels (shadows) and bright, saturated pixels (Bjerreskov et al., 2021) in the collection and was used to create composite images for the years 2000 and 2021.

Step 3: Feature extraction

Feature extraction was carried out in GEE using Vegetation Indices derived from spectral data and Tasselled Cap Transformation, which transforms spectral data into indicators (Dash, 2020).

Vegetation indices

Throughout all wavelengths, coniferous leaves have lower transmittance than broad leaves (Lukeš et al., 2013). Though the difference between visible (VIS) and near-infrared (NIR) spectral reflectance is not hugely evident, some studies (Roberts et al., 2004; Williams, 1991) have reported that coniferous needles have slightly lower VIS reflectance and higher NIR reflectance than broadleaves. It is hard to classify land cover or identify specific species when the vegetation types are heterogeneous and often exhibit both spectral and seasonal similarities (Deng et al., 2020). Therefore, several vegetation indexes were used as shown in Table 4.1. These were: 1) Normalized difference moisture index (NDMI); 2) Normalized burn ratio (NBR); 3) Enhanced vegetation index (EVI); 4) Normalized difference vegetation index

(NDVI); and, 5) Green chlorophyll index (GCI). These indices categorized vegetation changes related to moisture stress, colorization and needle/leaf structure (Ye et al., 2021).

Table 4.1 Bands and vegetation indexes

Index	Equation	Source
NDMI	$\frac{(NIR - SWIR1)}{(NIR + SWIR1)}$	Shahfahad et al. (2022)
NBR	$\frac{(NIR - SWIR)}{(NIR + SWIR2)}$	Setiani et al. (2021)
EVI	$2.5 \times \frac{NIR - RED}{(NIR + 6 \times RED - 7.5 \times BLUE + 1)}$	Senf et al. (2013)
NDVI	$\frac{(NIR - RED)}{(NIR + RED)}$	Pu et al. (2008)
GCI	$\left(\frac{NIR}{GREEN}\right) - 1$	Kumar et al. (2018)

Tasselled cap transformation

Tasselled cap transformation (TCA) was developed by Kauth and Thomas (1976) as a function for determining a crop's life cycle. It recognizes the pattern found in the agricultural fields where there is a net increase in near-infrared and decrease in red reflectance based on soil color.

The tasselled cap transformation is a linear transformation of Landsat MSS data that projects soil and vegetation information into a single plane in a multispectral data space. TCA has been broadly engaged in forestry studies of structure, condition, successional state and change detection in various forest environments (Gómez et al., 2012). It is a special case of principal components analysis which transforms the image data into a new feature space or domain with a new set of orthogonal axes. The tasselled cap analysis reduces a multiband data set (4-6) to 3 channels as follows:

- Tasselled cap greenness (TCG) contrasts the near-infrared and visible bands, conveying information concerning the abundance and vigour of living vegetation.
- Tasselled cap brightness (TCB) is a weighted sum of all four bands. Brightness is defined in the direction of the principal variation in soil reflectance and is associated with bare areas or partially covered soil.

- Tasselled cap wetness (TCW) is related to the canopy and soil moisture which differences the sum of the visible and near-infrared bands with the longer infrared bands.

Step 4: Multitemporal classification

The supervised classification of both maps (the years 2000 and 2021) was carried out using the Random Forest (RF) classifier because of its relatively high accuracy and computational efficiency (Zhu & Woodcock, 2014). Random Forest is an integrated learning method that has become increasingly common in remote sensing applications due to its nonparametric nature and ability to limit overfitting (Cheng & Wang, 2019). The Smile Random Forest function on the GEE platform (Liu et al., 2022) was used, and the number of decision trees was set to 500. A score was calculated using the RF algorithm for each combination of parameters. The combination of parameters with the highest score was used for developing the vegetation classification maps.

Training and validation

Stratified random sampling was used to obtain a sample population that best represents each landcover class. In these samples, 20 polygons for each class were randomly identified by the visual interpretation of the Landsat images with the help of Google Earth (Mohamed & El-Raey, 2019; Zhu & Liu, 2014). Then, five hundred training samples per class were generated to train the classification for each year.

The goal of the validation was to assess the overall accuracy of the vegetation change map compared to available reference data. Validation was based on existing datasets and a combination of ancillary sources (Google earth, field plots) assembled using a human interpreter approach (Weng, 2018). High spatial resolution images from Google Earth Pro were used to manually interpret the land cover classes and also help determine land cover change at longer intervals (Kamga et al., 2020; Mohamed & El-Raey, 2019; Zhu & Woodcock, 2014). This research used high-resolution images of 2021 and 2000 in Google Earth pro as reference data. Specifically, about 120 samples were used as ground reference data for each landcover class to train the random forest classifier except for the settlement class, which was smaller in 2000. The classification accuracy was tested using the overall agreement with reference data. In addition, the user and producer agreements for the five landcover types were calculated. The producer accuracy measures the percentage of given reference data correctly classified; in

contrast, the user accuracy measures the percentage of the trained data correctly classified (April et al., 2015).

Step 5: Post classification

Following the classification of imagery for the two individual years, a post classification approach of subtracting the classification maps was applied and used to produce a detailed change detection map using the ArcGIS Pro software. This map detects more subtle classes of change and determines the invasive pine and its spread over the selected landscape. An important aspect of change detection is determining what is changing to what category of land use type (Abebe et al., 2021). Therefore, a vegetation conversion matrix was calculated to demonstrate the direction of change and the land use type that remains at the end of the study period. Quantitative data analysis of the overall land cover changes as well as gains and losses in each category between 2000 and 2021 were compiled (Haregeweyn et al., 2013; Kamga et al., 2020) and presented as a percentage of the area. In this manner, maps were created for the entire study area and provided insight into the areas affected by invasive conifer encroachment.

Buffer analysis: identification of invasive pine

In order to investigate the progressive spread of *Pinus caribaea* outside the original plantations, the distance from the perimeter of parental pine plantations were measured using six 50 m intervals between 0 and 300 m demarcated. The buffer distance was based on the previous study by Medawatte et al. (2010) in Sri Lanka. The area of invading pines was measured in relation to the distance from the plantation edge.

4.3 Results

The vegetation maps for 2000 and 2021 are shown in Figure 4.3 and Figure 4.4, respectively. These maps collectively show places with stable and changed vegetation areas appearing in the study area. Five major vegetation types were classified for 2000 and 2021: pine plantation, broadleaf forest, bare land, grassland, and invasive pines (settlements are also identified). The most prominent vegetation type found in both maps (2000 and 2021) is the broadleaf forest which is mainly distributed on the gentle slopes and the flat regions of the study area. In contrast, pine plantations and grasslands are located on ridges and steep areas with a slope higher than 18%. The vegetation classification for the year 2000 image shows that the majority of the study area was under broadleaf forest, covering about 2690 ha (43%). Grassland and bare land cover an area of 1627 ha (26%) and 969 ha (16%), respectively. Broadleaf forest

(3336 ha) still covered the largest area in 2021, which reflects the conversion of other classes to the natural forest for conservation purposes. While grassland, pine plantation, and bare land cover an area of 1284 ha,1013 ha, and 244 ha, respectively. The land areas contain pine species outside the plantation boundaries, with an absence of planting patterns, and areas smaller than 0.5 ha are identified as invasive pines.

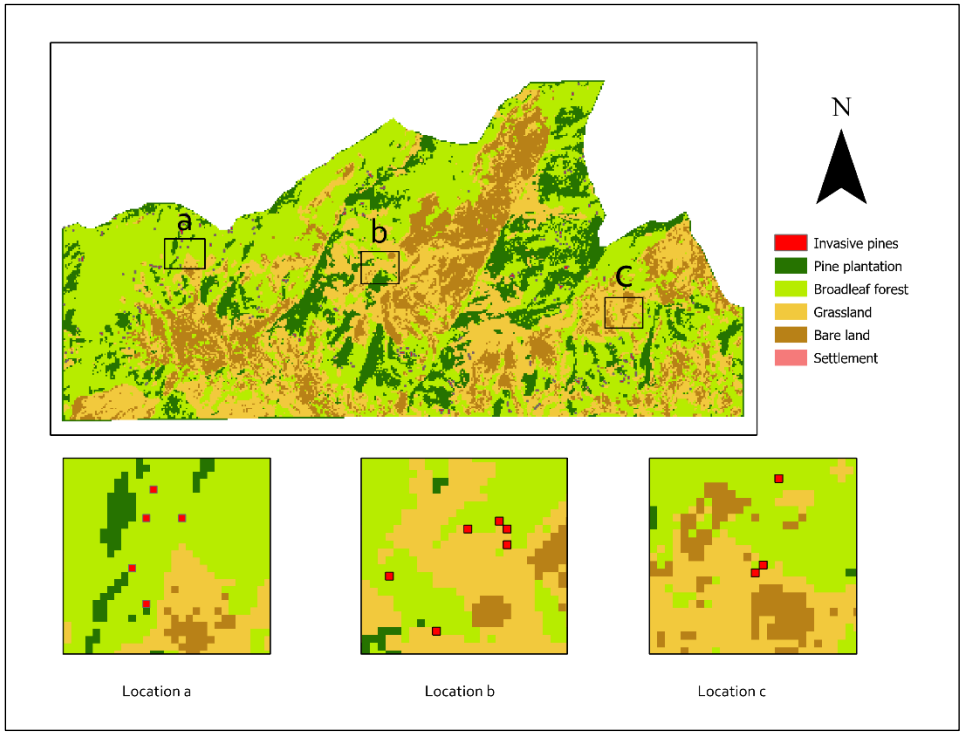

Figure 4.3 Vegetation classification for the year 2000

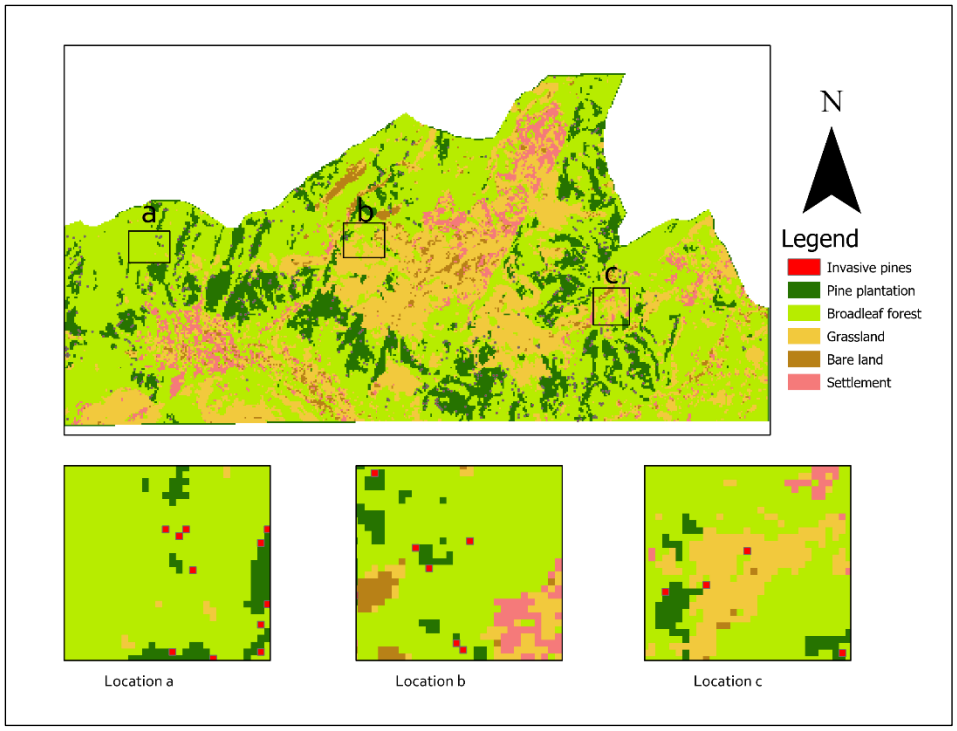

Figure 4.4 Vegetation classification for the year 2021

Overall agreement with reference data was computed for both vegetation maps. The year 2000 vegetation map produced a 72% overall accuracy, and the year 2021 vegetation map yielded an 81% overall accuracy. Vegetation groups were classified with producer accuracy ranging from 20-84 and 55-100 for the year 2000 and 2021, respectively. In the year 2000 map, the settlement had the highest user accuracy (Table 4.SM1). On the other hand, pine plantation had the highest user accuracy for the year 2021, whereas all other vegetation classes have more than 70% user accuracy except the grassland class (Table 4.SM2).

The cover and rate of changes in each vegetation type for the 21 years are summarized in Table 4.2. From 2000 to 2021, the broadleaf forest and pine plantation area increased by 24% and 19%, respectively. In contrast, bare land and grassland showed a reverse trend, reduced by 75% and 21%, respectively, during the same period. This indicates that the increasing broadleaf forest area mainly emerged in the steep slope areas, meaning some grassland and bare land areas were converted to natural forests without disturbance.

Table 4.2 Extent and rate of vegetation changes between 2000 and 2021

Vegetation type	2000		2021		Change between 2000 and 2021	
	area (ha)	%	area (ha)	%	area (ha)	%
Invasive pine	93	1	89	0	-4	-4
Pine Plantation	854	14	1013	16	159	19
Broadleaf forest	2691	43	3336	54	646	24
Grassland	1627	26	1284	21	-343	-21
Bare land	969	16	244	4	-725	-75
Settlement	0.18	0	269	4	268.82	

The vegetation conversion matrix depicts the direction of change and the land use type that remains at the end of the period. Thus, the change matrix for each period was analyzed to understand the source and destination of significant vegetation changes. Over 21 years, 3476 ha out of 6234 ha of the total area have not changed, accounting for 56% of the study area (Table 4.3). In 2021, there was a significant settlement build up activity, with an area of 269 ha or 4% of the region's total area (Table 4.2).

Significantly, from 2000 to 2020, approximately 705 ha of bare land and 663 ha of grassland have converted to other vegetated areas. The increase in settlement surfaces is coupled with the decline in these grasslands and bare land areas. Furthermore, approximately 80% of the area covered with broadleaf forest in 2000 was still the same in 2021. The remaining 20% (536 ha) was transformed to other uses in 2021. Of the total pine plantation cover in 2000, 53% remained unchanged, while the remaining portion vastly changed to grassland (100 ha) and broadleaf forest (262 ha). Overall, there was a significant increase in the broadleaf forest from 2691 ha to 3336 ha. This gradual increase is attributed to the replanting programs carried out in the western part of the study area (Kumara, 2010).

The invasive pine areas during this period showed a 4% slight decline. Concurrently, 45 ha of invasive pine areas were converted to broadleaf forest, and 15 ha were cleared. Further, 26 ha of invasive pine in 2000 were identified as pine plantations in 2021, whereas 19ha of pine plantations in 2000 was recognized as invasive pine in 2021. This misperception may be due to less aerial visibility of continuous clumps of pine cover over the area in 2000, with an identifiable canopy only appearing later.

Table 4.3 Vegetation conversion matrix between 2000 and 2021

Vegetation type in 2021 (ha)	Vegetation type in 2000 (ha)						
	Invasive Pine	Pine Plantation	Broadleaf forest	Grassland	Bare land	Settlement	Total
Invasive pine	7	19	41	16	6	0	89
Pine Plantation	26	454	383	121	29	0	1013
Broadleaf forest	45	262	2154	525	350	0	3336
Grassland	11	100	72	780	321	0	1284
Bare land	3	17	19	124	81	0	244
Settlement	1	3	22	60	183	0.2	269
Total	93	854	2691	1627	969	0.2	6234

No change | Total area 2000 | Total area 2021

As this study focuses on the dispersal of invasive pine around the study area, the following section emphasizes the extent of escaped pines from the pine plantations into the adjacent habitats. Figure 4.5 observed the conversion of pine plantations and broadleaf forests from 2000 to 2021. Moreover, an expansion of pine plantations was detected primarily around the existing plantations of 2000. Broadleaf forests in more remote valley areas tended to retain extensive forest in 2021, and broadleaf forest expansion or regeneration of the forest can be observed primarily on grassland. During the 21 years, pine plantations have increased by 159 ha, whereas invasive pine declined by 4 ha. Thus, invasive pines are more visible along with broad leaf forests managing the same borders as the pine plantations.

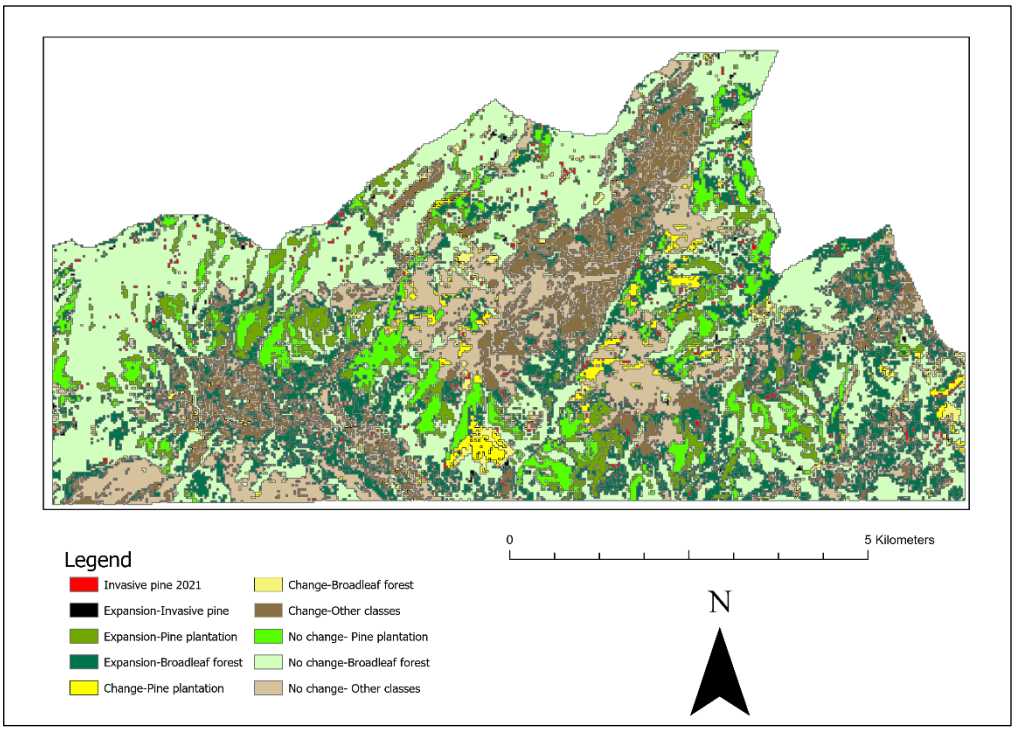

Figure 4.5 Pine and broadleaf forest change map 2000-2021

The extent of invading pines was measured with respect to the distance from the plantation edge. For the buffer analysis, three different vegetation types were selected: broadleaf forest, grassland and bare land, which are adjacent to the pine plantations. The results showed that pines invaded broadleaf forests to a greater extent than the other two habitat types (Figure 4.6). Furthermore, analysis showed that the highest scattering of pines was within 100 m buffer zone of the plantation, while encroachment of pines reduced beyond the 100 m buffer zone.

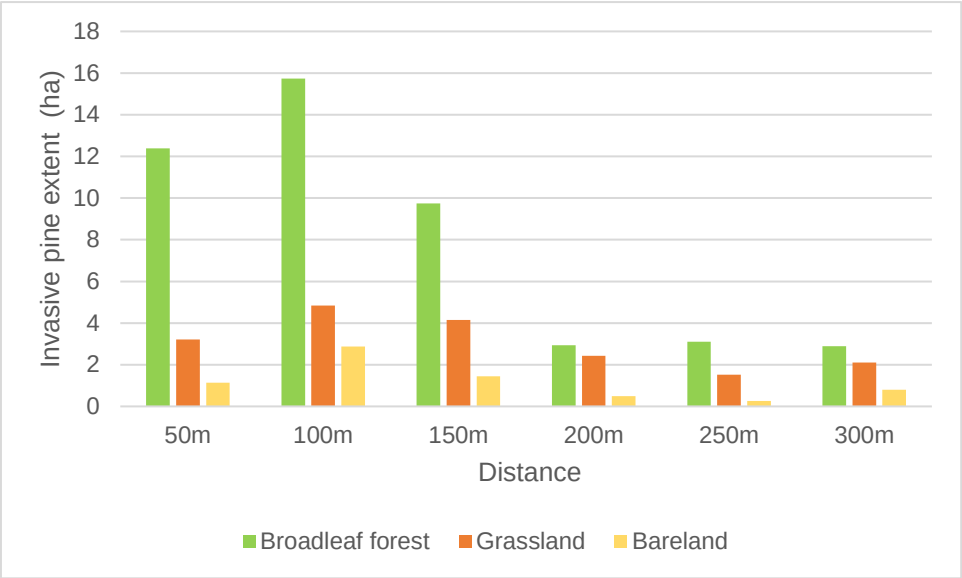

Figure 4.6 Invasive pine expansion into the different vegetation types adjacent to pine plantations

4.4 Discussion

This research demonstrated that freely available Landsat images combined with topographical data can be used for mapping vegetation change over a twenty year time period, confirming its applicability for mapping and understanding the extent of pine invasion. The results have revealed that pine invasion is at a moderate level but is decreasing, which might be attributed to anthropogenic activities.

The research has found that a combination of spectral, textural and topographical bands provides an effective solution for classifying the vegetation cover, similar to the findings of Yu et al. (2020) on forest classification in subtropical regions, and the discriminating of urban forest types in a semi-humid monsoon region in China by Zhou et al. (2019). Earlier works by Wang et al. (2006) and Zhu and Liu (2014) had specified that using topographical data with spectral data improved the discrimination between conifers and broadleaf forests. Correspondingly, studies by Peterson (2005) and April et al. (2015) had found that model accuracy was slightly better using topographical parameters. In contrast, Bjerreskov et al. (2021) found that the elevation did not improve accuracy when classifying broadleaf and conifer forest in the Danish landscape. However, it appears that elevation plays a big role in forest classification in mountain terrain or when the landscape is complex, as demonstrated by this research.

This study obtained accuracies for the vegetation cover classification similar to those obtained by other studies using multi-year Landsat images (Coyle et al., 2020; Gómez et al., 2012), and the accuracies obtained for land classification using other higher resolution satellite images (Hantson et al., 2012; Perera, 2001). The classification accuracy of forest types obtained in this study is higher that obtained studies by Akumu et al. (2021) , Senf et al. (2013), and an investigation by Sá et al. (2017), which focuses on the invasion of *Acacia longifolia* in a pine forest. However, studies by Andrew and Ustin (2008); Bjerreskov et al. (2021); Fagan et al. (2018); Hestir et al. (2008); Underwood et al. (2003) obtained higher classification accuracies than the present study by using satellite imagery with a higher resolution.

Even though better results can be obtained with higher resolution images (Goncalves et al., 2022), Landsat has been shown to provide long-term assessments of invasive plant spread (Gavier-Pizarro et al., 2012; Labonté et al., 2020; Sá et al., 2017). Furthermore, the freely available Landsat series of satellites is one of the most important data sources for developing countries that have budget constraints (Gavier-Pizarro et al., 2012; Haregeweyn et al., 2013). Liu et al. (2022) concluded that Landsat is better for detecting long-term changes in Chinese pine tree species because of its availability over a long time period. For developing countries such as Sri Lanka, we conclude that Landsat images provide a vital low-cost solution for the frequent monitoring of vegetation change.

According to this study's findings, broadleaved forests and grasslands are vulnerable to invasion. Previous researchers (Dash et al., 2019; Higgins & Richardson, 1998; Medawatte et al., 2010) found that grasslands were more prone to invasion than other areas. However, Goncalves et al. (2022), Förster et al. (2017) and Ayala et al. (2005) identified forest habitats as the most vulnerable to the pine invasion. Forest habitats become vulnerable to pine invasion when exposed to disturbances such as wildfire (Medawatte et al., 2010). Moreover, most invading pines were found within a 100 m buffer zone for all types of habitats, while encroachment declined sharply beyond the 50-100 m buffer zone. These results are in line with those of Ayala et al. (2005).

An important finding in this research was the decline in invasive pine in the Belihuloya region. Wijesundera (2008) had stated that *Pinus caribaea* had spread rapidly in several mid country areas and predicted that it could be a potential invasive alien in the near future. Due to social pressure from local communities, pine planting was stopped (Edirisinghe, 2017), and the country has identified pines an invasive species (Medawatte et al., 2010). In 2017 the Sri

Lankan government implemented a project to plant indigenous plant species to develop an under-storey in the existing pine plantations (Office of the Cabinet of Ministers-Sri Lanka 2017). This research gives insight into the invasion of pines in the intermediate zone and helps inform management strategies to maintain this downward trend.

While the study could have obtained better classification accuracy using higher spatial or spectral resolution images, these are not free and are only available for recent years. Extending the study period to before 2000 could also have reduced its limitation, but it would have been difficult to validate a classification prior to 2000 due to the absence of high-resolution images in Google Earth Pro.

Future research could seek to understand the spatial variation in vegetation change and the reasons the invasive pines spread to certain areas. For example, the relationship between pine invasion and disturbances such as forest fires could be explored. Areas impacted by forest fire could be remotely sensed using satellite images. Furthermore, mapping and monitoring invasive pines in other climatic regions would also be relevant for forest management and conservation planning.

4.5 Conclusion

This study demonstrated the extent of pine invasion in the Belihuloya region, Sri Lanka. Remote sensing has enabled the mapping of vegetation change in the study area between 2000 and 2021 using freely available Landsat data. A combination of spectral, textural and topographical bands provided an effective solution for detecting the spread of invasive *Pinus caribaea*. This study provided evidence that pines have invaded the natural habitat in the intermediate climate areas of Sri Lanka, especially native forests, and grasslands but the extent of this invasion has declined between 2000 and 2021.

It is clear that remote sensing is a valuable tool for monitoring and understanding forest dynamics, and the use of freely available satellite images, such as Landsat are particularly important for developing countries such as Sri Lanka. The availability of the Google Earth Engine platform and its extensive range of analysis functions and free processing power is also very beneficial for countries with limited financial resources.

4.6 References

Afrin, S., Sharmin, S., & Mowla, Q. A. (2010). The Environmental Impact of Alien Invasive Plant Species in Bangladesh. International Conference on Environmental Aspects of Bangladesh (ICEAB10), Japan.

Amaral, C. H., Roberts, D. A., Almeida, T. I. R., & Souza Filho, C. R. (2015). Mapping invasive species and spectral mixture relationships with neotropical woody formations in southeastern Brazil. *ISPRS Journal of Photogrammetry and Remote Sensing*, *108*, 80-93. https://doi.org/https://doi.org/10.1016/j.isprsjprs.2015.06.009

Andrew, M. E., & Ustin, S. L. (2008). The role of environmental context in mapping invasive plants with hyperspectral image data. *Remote Sensing of Environment*, *112*(12), 4301-4317. https://doi.org/https://doi.org/10.1016/j.rse.2008.07.016

April, S., E., Sarr, D. A., Van Kirk, R. W., & Jules, E. S. (2015). Quantifying habitat loss: Assessing tree encroachment into a serpentine savanna using dendroecology and remote sensing. *Forest Ecology and Management*, *340*, 9-21. https://doi.org/https://doi.org/10.1016/j.foreco.2014.12.019

Ayala, L., Perevolotsky, A., Kigel, J., & Noy-Meir, I. (2005). Invasion of Pinus halepensis from Plantations into Adjacent Natural Habitats. *Applied Vegetation Science*, *8*(1), 85-92. http://www.jstor.org/stable/4620435

Bjerreskov, K. S., Nord-Larsen, T., & Fensholt, R. (2021). Classification of Nemoral Forests with Fusion of Multi-Temporal Sentinel-1 and 2 Data. *Remote Sensing*, *13*(5). https://doi.org/10.3390/rs13050950

Bradley, B. A. (2014). Remote detection of invasive plants: a review of spectral, textural and phenological approaches. *Biological Invasions*, *16*(7), 1411-1425. https://doi.org/10.1007/s10530-013-0578-9

Burley, J., & Barnes, R. D. (2004). Tropical Ecosystems | Tropical Pine Ecosystems and Genetic Resources. In J. Burley (Ed.), *Encyclopedia of Forest Sciences* (pp. 1728-1740). Elsevier. https://doi.org/https://doi.org/10.1016/B0-12-145160-7/00089-2

Cheng, K., & Wang, J. (2019). Forest Type Classification Based on Integrated Spectral-Spatial-Temporal Features and Random Forest Algorithm—A Case Study in the Qinling Mountains. *Forests*, *10*(7), 559. https://www.mdpi.com/1999-4907/10/7/559

Dash, J. P. (2020). *On the Detection and Monitoring of Invasive Exotic Conifers in New Zealand Using Remote Sensing.* University of Canterbury. https://ir.canterbury.ac.nz/bitstream/handle/10092/101329/Dash%2C%20Jonathan_Final%20PhD%20Thesis.pdf?sequence=1&isAllowed=y

Dash, J. P., Watt, M. S., Paul, T. S. H., Morgenroth, J., & Pearse, G. D. (2019). Early Detection of Invasive Exotic Trees Using UAV and Manned Aircraft Multispectral and LiDAR Data. *Remote Sensing*, *11*(15). https://doi.org/10.3390/rs11151812

Deng, X., Guo, S., Sun, L., & Chen, J. (2020). Identification of Short-Rotation Eucalyptus Plantation at Large Scale Using Multi-Satellite Imageries and Cloud Computing Platform. *Remote Sensing*, *12*(13). https://doi.org/10.3390/rs12132153

Edirisinghe, N. (2017). *Enrichment of Pine Plantations of Sri Lanka with native species* https://www.apfnet.cn/uploads/file/20170425/1493111411376528.pdf

Förster, M., Gränzig geb. Schmidt, T., Wolf, R., Kleinschmit, B., Fassnacht, F., Cabezas Peña, J., & Kattenborn, T. (2017). *Detecting the spread of invasive species in central Chile with a Sentinel-2 time-series* 9th International Workshop on the Analysis of Multitemporal Remote Sensing Images (MultiTemp), Brugge, Belgium. https://ieeexplore.ieee.org/document/8035216

Gavier-Pizarro, G. I., Kuemmerle, T., Hoyos, L. E., Stewart, S. I., Huebner, C. D., Keuler, N. S., & Radeloff, V. C. (2012). Monitoring the invasion of an exotic tree (Ligustrum lucidum) from 1983 to 2006 with Landsat TM/ETM+ satellite data and Support Vector Machines in Córdoba, Argentina. *Remote Sensing of Environment*, *122*, 134-145. https://doi.org/https://doi.org/10.1016/j.rse.2011.09.023

Gómez, C., Wulder, M. A., White, J. C., Montes, F., & Delgado, J. A. (2012). Characterizing 25 years of change in the area, distribution, and carbon stock of Mediterranean pines in Central Spain. *International Journal of Remote Sensing*, *33*(17), 5546-5573. https://doi.org/10.1080/01431161.2012.663115

Goncalves, V. P., Ribeiro, E. A., & Imai, N. N. (2022). Mapping Areas Invaded by Pinus sp. from Geographic Object-Based Image Analysis (GEOBIA) Applied on RPAS (Drone) Color Images. *Remote Sensing*, *14*(12). https://doi.org/10.3390/rs14122805

Haregeweyn, N., Tsunekawa, A., Tsubo, M., Meshesha, D., & Melkie, A. (2013). Analysis of the invasion rate, impacts and control measures of Prosopis juliflora: a case study of Amibara District, Eastern Ethiopia. *Environmental Monitoring and Assessment*, *185*(9), 7527-7542. https://doi.org/10.1007/s10661-013-3117-3

Higgins, S. I., & Richardson, D. M. (1998). Pine Invasions in the Southern Hemisphere: Modelling Interactions between Organism, Environment and Disturbance. *Plant Ecology*, *135*(1), 79-93. http://www.jstor.org/stable/20050598

Jayawardane, S. S. B. D. G., & Weerasena, L. A. (2000). Crop Diversification in Sri Lanka. Crop Diversification in the Asia-Pacific Region., Bangkok.

Jayawardhane, J., & Gunaratne, A. (2020). Restoration Success Evaluation of a Thinned and Enriched Pine Plantation in Sri Lanka. *Journal of Tropical Forest Science*, *32*(4), 402-413. https://www.jstor.org/stable/26940730

Kamga, M. A., Nguemhe Fils, S. C., Ayodele, M. O., Olatubara, C. O., Nzali, S., Adenikinju, A., & Khalifa, M. (2020). Evaluation of land use/land cover changes due to gold mining activities from 1987 to 2017 using landsat imagery, East Cameroon. *GeoJournal*, *85*(4), 1097-1114. https://doi.org/10.1007/s10708-019-10002-8

Kaplan, G. (2021). Broad-Leaved and Coniferous Forest Classification in Google Earth Engine Using Sentinel Imagery. *Environmental Sciences Proceedings*, *3*(1), 64. https://www.mdpi.com/2673-4931/3/1/64

Kauth, R. J., & Thomas, G. S. P. (1976). The Tasselled Cap -- A Graphic Description of the Spectral-Temporal Development of Agricultural Crops as Seen by Landsat. Symposium on Machine Processing of Remotely Sensed Data, West Lafayette, Indiana.

Khare, S., Latifi, H., & Ghosh, S. K. (2018). Multi-scale assessment of invasive plant species diversity using Pléiades 1A, RapidEye and Landsat-8 data. *Geocarto International*, *33*(7), 681-698. https://doi.org/10.1080/10106049.2017.1289562

Kumar, V., Sharma, A., Bhardwaj, R., & Thukral, A. K. (2018). Comparison of different reflectance indices for vegetation analysis using Landsat-TM data. *Remote Sensing Applications: Society and Environment*, *12*, 70-77. https://doi.org/https://doi.org/10.1016/j.rsase.2018.10.013

Kumara, C. (2010). *Effectiveness of Establishing Forest Buffer Zones as a Community Forest Management Approach a Case Study from the Sripada Tropical Peak Wilderness Sanctuary in Sri Lanka.* University of Agder.

Labonté, J., Drolet, G., Sylvain, J.-D., Thiffault, N., Hébert, F., & Girard, F. (2020). Phenology-Based Mapping of an Alien Invasive Species Using Time Series of Multispectral Satellite Data: A Case-Study with Glossy Buckthorn in Québec, Canada. *Remote Sensing*, *12*(6), 922. https://www.mdpi.com/2072-4292/12/6/922

Liu, L., Guo, Y., Li, Y., Zhang, Q., Li, Z., Chen, E., Yang, L., & Mu, X. (2022). Comparison of Machine Learning Methods Applied on Multi-Source Medium-Resolution Satellite Images for Chinese Pine (Pinus tabulaeformis) Extraction on Google Earth Engine. *Forests*, *13*(5). https://doi.org/10.3390/f13050677

Lukeš, P., Stenberg, P., Rautiainen, M., Mõttus, M., & Vanhatalo, K. M. (2013). Optical properties of leaves and needles for boreal tree species in Europe. *Remote Sensing Letters*, *4*(7), 667-676. https://doi.org/10.1080/2150704X.2013.782112

McEwan, A., Marchi, E., Spinelli, R., & Brink, M. (2020). Past, present and future of industrial plantation forestry and implication on future timber harvesting technology. *Journal of Forestry Research*, *31*(2), 339-351. https://doi.org/10.1007/s11676-019-01019-3

Medawatte, W., Tennakoon, K., Hulme, P., Gunatilleke, C., & Gunatilleke, I. (2010). Is Caribbean pine invading grasslands in the Knuckles range. *Invasive alien species–strengthening capacity to control introduction and spread in Sri Lanka*, 131-140.

Mohamed, S. A., & El-Raey, M. E. (2019). Land cover classification and change detection analysis of Qaroun and Wadi El-Rayyan lakes using multi-temporal remotely sensed imagery. *Environmental Monitoring and Assessment*, *191*(4), 229. https://doi.org/10.1007/s10661-019-7339-x

Nissanka, S. P., Mohotti, K., & Wijetunga, A. (2005). Alleopathic influences of Pinus caribea on vegetation regeneration and soil biodiversity. Fourth World Congress on Allelopathy, Wagga Wagga, NSW, Australia.

Office of the Cabinet of Ministers-Sri Lanka (2017). *Conversion of the Pinus Plantation in Sri Lanka into a Plantation of indigenous plant species*. Office of the Cabinet of Ministers-Sri Lanka Retrieved from http://www.cabinetoffice.gov.lk/cab/index.php?option=com_content&view=article&id=16&Itemid=49&lang=en&dID=8386

Pauchard, A., Escudero, A., García, R. A., de la Cruz, M., Langdon, B., Cavieres, L. A., & Esquivel, J. (2016). Pine invasions in treeless environments: dispersal overruns microsite heterogeneity. *Ecology and Evolution*, *6*(2), 447-459. https://doi.org/10.1002/ece3.1877

Pauchard, A., García, R., Zalba, S., Sarasola, M., Zenni, R., Ziller, S., & Nuñez, M. A. (2016). Pine Invasions in South America: Reducing Their Ecological Impacts Through Active Management. In J. Canning-Clode (Ed.), *Biological Invasions in Changing*

Ecosystems: Vectors, Ecological Impacts, Management and Predictions (pp. 318-342). De Gruyter Open Poland. https://doi.org/10.1515/9783110438666-020

Perera, A. (2001). Perera, G.A.D. 2001. Secondary forest situation in Sri Lanka: a review. Journal of Tropical Forest Science, 13(4): 768-785. *Journal of Tropical Forest Science*, *13*, 768-785.

Petersen, R., Goldman, E. D., Harris, N. L., Sargent, S. N., Aksenov, D., Manisha, A., Esipova, E., Shevade, V. S., Loboda, T. V., Kuksina, N., & Kurakina, I. (2016). Mapping Tree Plantations with Multispectral Imagery: Preliminary Results for Seven Tropical Countries.

Peterson, E. B. (2005). Estimating cover of an invasive grass (Bromus tectorum) using tobit regression and phenology derived from two dates of Landsat ETM+ data. *International Journal of Remote Sensing*, *26*(12), 2491-2507. https://doi.org/10.1080/01431160500127815

Piiroinen, R., Fassnacht, F. E., Heiskanen, J., Maeda, E., Mack, B., & Pellikka, P. (2018). Invasive tree species detection in the Eastern Arc Mountains biodiversity hotspot using one class classification. *Remote Sensing of Environment*, *218*, 119-131. https://doi.org/https://doi.org/10.1016/j.rse.2018.09.018

Pu, R., Gong, P., Tian, Y., Miao, X., Carruthers, R. I., & Anderson, G. L. (2008). Invasive species change detection using artificial neural networks and CASI hyperspectral imagery. *Environmental Monitoring and Assessment*, *140*(1), 15-32. https://doi.org/10.1007/s10661-007-9843-7

Punyawardena, B. V. R. (2020). Climate. In R. B. Mapa (Ed.), *The Soils of Sri Lanka* (pp. 13-22). Springer International Publishing. https://doi.org/10.1007/978-3-030-44144-9_2

Rejmánek, M. (2014). Invasive trees and shrubs: where do they come from and what we should expect in the future? *Biological Invasions*, *16*(3), 483-498. https://doi.org/10.1007/s10530-013-0603-z

Rejmánek, M., & Richardson, D. M. (2013). Trees and shrubs as invasive alien species – 2013 update of the global database. *Diversity and Distributions*, *19*(8), 1093-1094. https://doi.org/https://doi.org/10.1111/ddi.12075

Richardson, D., Rundel, P., Jackson, S., Teskey, R., Aronson, J., Bytnerowicz, A., Wingfield, M., & Procheş, Ş. (2007). Human Impacts in Pine Forests: Past, Present, and Future. *Annual Review of Ecology, Evolution and Systematics*, *38*, 275-97297. https://doi.org/10.1146/annurev.ecolsys.38.091206.095650

Roberts, D. A., Ustin, S. L., Ogunjemiyo, S., Greenberg, J., Dobrowski, S. Z., Chen, J., & Hinckley, T. M. (2004). Spectral and Structural Measures of Northwest Forest Vegetation at Leaf to Landscape Scales. *Ecosystems*, *7*(5), 545-562. https://doi.org/10.1007/s10021-004-0144-5

Sá, N. C. d., Carvalho, S., Castro, P., Marchante, E., & Marchante, H. (2017). Using Landsat Time Series to Understand How Management and Disturbances Influence the Expansion of an Invasive Tree. *IEEE Journal of Selected Topics in Applied Earth Observations and Remote Sensing*, *10*(7), 3243-3253. https://doi.org/10.1109/JSTARS.2017.2673761

Senf, C., Pflugmacher, D., Van Der Linden, S., & Hostert, P. (2013). Mapping Rubber Plantations and Natural Forests in Xishuangbanna (Southwest China) Using Multi-Spectral Phenological Metrics from MODIS Time Series. *Remote Sensing*, *5*(6), 2795-2812. https://doi.org/10.3390/rs5062795

Setiani, P., Devianto, L. A., & Ramdani, F. (2021). Rapid estimation of CO2 emissions from forest fire events using cloud-based computation of google earth engine. *Environmental Monitoring and Assessment*, *193*(10), 669. https://doi.org/10.1007/s10661-021-09460-w

Shahfahad, Talukdar, S., Ali, R., Nguyen, K.-A., Naikoo, M. W., Liou, Y.-A., Islam, A. R. M. T., Mallick, J., & Rahman, A. (2022). Monitoring drought pattern for pre- and post-monsoon seasons in a semi-arid region of western part of India. *Environmental Monitoring and Assessment*, *194*(6), 396. https://doi.org/10.1007/s10661-022-10028-5

Signori, L., & Ducati, J. (2019). Spatio-Temporal Mapping of the Invasive Alien Species Pinus Sp in the Northern Area of the Lagoa Do Peixe National Park-Rs. *Revista Árvore*, *43*. https://doi.org/10.1590/1806-90882019000100007

Singh, S. P., Inderjit, Singh, J. S., Majumdar, S., Moyano, J., Nuñez, M. A., & Richardson, D. M. (2018). Insights on the persistence of pines (Pinus species) in the Late Cretaceous and their increasing dominance in the Anthropocene. *Ecology and Evolution*, *8*(20), 10345-10359. https://doi.org/10.1002/ece3.4499

Starkloff, R. (1998). *Social and environmental aspects of watershed vulnerability in the Sri Lankan hill country. Paper 135 of Session 13*.

Subasinghe, K., Sumanapala, A. P., & Weerawardhena, S. R. (2014). The impact of forest conversion on bird communities in the northern flank of the Knuckles Mountain Forest Range, Sri Lanka. *Journal of Asia-Pacific Biodiversity*, *7*(4), 367-373. https://doi.org/https://doi.org/10.1016/j.japb.2014.07.004

Subasinghe, S. (2007). *Plantation forestry in Sri Lanka challenges and constraints* Annual Sessions of the Institute of Biology, Sri Lanka.

Wang, L., Zhang, X., Luo, Y., Shi, J., & Huang, H. (2006, 31 July-4 Aug. 2006). A Study on the Changes of Pinus Massoniana Spatial Pattern by Pine Wood Nematode Invasion Based on Remote Sensing and GIS. 2006 IEEE International Symposium on Geoscience and Remote Sensing, Denver, CO, USA.

Weisberg, P. J., Lingua, E., & Pillai, R. B. (2007). Spatial Patterns of Pinyon-Juniper Woodland Expansion in Central Nevada. In (Vol. 60, pp. 115-124): Society for Range Management.

Weng, Q. (2018). *Remote sensing time series image processing*. CRC Press, Taylor & Francis Group.

Wijerathna, N., Hettiarachchi, C., & Wickramagamage, P. (2016). Effect of Pinus Caribaea Plantation on Vegetation Diversity and Distribution by Reforestation in Lower Hantana. International Conference on the Humanities and the Social Sciences (ICHSS) 2016, Peradeniya, Sri Lanka.

Wijesundera, S. (2008, 11th November). Major invasive plant species in different climatic zones of Sri Lanka. Proceedings of the National Symposium on Invasive Alien Species (IAS 2008), Sri Lanka Foundation Institute.

Williams, D. L. (1991). A comparison of spectral reflectance properties at the needle, branch, and canopy level for selected Conifer species. *Remote Sensing of Environment*, *35*(2), 79-93. https://doi.org/https://doi.org/10.1016/0034-4257(91)90002-N

Xu, D., Chen, B., Yan, Y., Sun, X., & Xin, X. (2018). Spatial-temporal dynamic monitoring of Mongolian pine (Pinus sylvestris var. mongolica) based on remote sensing data. *Remote Sensing Letters*, *9*(11), 1079-1088. https://doi.org/10.1080/2150704X.2018.1508908

Ye, S., Rogan, J., Zhu, Z., Hawbaker, T. J., Hart, S. J., Andrus, R. A., Meddens, A. J. H., Hicke, J. A., Eastman, J. R., & Kulakowski, D. (2021). Detecting subtle change from dense Landsat time series: Case studies of mountain pine beetle and spruce beetle disturbance. *Remote Sensing of Environment*, *263*, 112560. https://doi.org/https://doi.org/10.1016/j.rse.2021.112560

Yu, X., Lu, D., Jiang, X., Li, G., Chen, Y., Li, D., & Chen, E. (2020). Examining the Roles of Spectral, Spatial, and Topographic Features in Improving Land-Cover and Forest Classifications in a Subtropical Region. *Remote Sensing*, *12*(18). https://doi.org/10.3390/rs12182907

Zhou, X., Li, L., Chen, L., Liu, Y., Cui, Y., Zhang, Y., & Zhang, T. (2019). Discriminating Urban Forest Types from Sentinel-2A Image Data through Linear Spectral Mixture Analysis: A Case Study of Xuzhou, East China. *Forests*, *10*(6), 478. https://www.mdpi.com/1999-4907/10/6/478

Zhu, X., & Liu, D. (2014). Accurate mapping of forest types using dense seasonal Landsat time-series. *ISPRS Journal of Photogrammetry and Remote Sensing*, *96*, 1-11. https://doi.org/https://doi.org/10.1016/j.isprsjprs.2014.06.012

Zhu, Z., & Woodcock, C. E. (2014). Continuous change detection and classification of land cover using all available Landsat data. *Remote Sensing of Environment*, *144*, 152-171. https://doi.org/https://doi.org/10.1016/j.rse.2014.01.011

Chapter 5

Evaluating the Addition of Radar with Optical Data for Vegetation Mapping in a Montane Region in Sri Lanka

This chapter was published as Nandasena, W.D.K.V., Brabyn, L. & Serrao-Neumann, S. Evaluating the addition of radar with optical data for vegetation mapping in a montane region in Sri Lanka. *J. Mt. Sci.* **20**, 2898–2912 (2023). https://doi.org/10.1007/s11629-023-8181-8

Abstract

The use of freely available multi-source imagery for mapping vegetation in montane terrain is important for many developing countries that do not have the funding for high-resolution data capture. Radar images are also now freely available and include Sentinel-1 in dual polarisation, and PALSAR-2. These images can penetrate cloud cover and provide the advantage of acquiring data in a cloudy tropical region. This research evaluated whether the addition of radar with optical and topographic data improves classification accuracy in a montane region in Sri Lanka. Six classification experiments were designed based on different combinations of image data to test whether radar data improved land cover classification accuracy compared with optical data alone. Random forest classifier in the Google Earth Engine has been utilised to classify the tropical montane vegetation. The results indicate that radar or optical data alone cannot obtain satisfactory results. However, when combining radar with optical data the overall accuracy increased by approximately 5%, and by an additional 2% when topography data were added. The highest accuracy (92%) was achieved with multiple imagery, and adding the vegetation indices improved the model slightly by 0.3%. In addition, feature importance analysis showed that radar data makes a significant contribution to the classification. These positive outcomes demonstrate that freely accessible multi-source remotely sensed data have impressive capability for vegetation mapping and support the monitoring and managing of forest ecological resources in tropical montane regions.

Keywords: DEM, Google Earth Engine, PALSAR, Random Forest classifier, Sentinel, Tropical montane

5.1 Introduction

Land cover maps are essential for determining current land use, as well as monitoring changes over time. Land cover maps provide information for estimating carbon sinks, planning for climate and disaster mitigation, and conservation goals (Cheng & Wang, 2019). Thus, there is a great demand for up-to-date vegetation maps and records of land cover change. Map generation has changed from paper-based, manually prepared maps to computer-induced automated maps. Geographic Information System (GIS) and remote sensing techniques have dramatically improved mapping and related production of precise land cover maps. Satellite imagery has become crucial for producing land cover maps because of its broad spatial coverage and the real-time update of the ground. However, until recently, access to satellite imagery has been limited or expensive.

Free and open access data policies support applications that use large amounts of data spatially and temporally. These policies maximize societal benefits by aiding remote sensing scientists from developing countries with limited resources to generate more accurate land cover maps (Nandasena et al., 2020). There are now many coarse to medium spatial resolution satellite images available for free, such as MODIS and Landsat (Lopes et al., 2020). In 2014, the Copernicus Programme introduced satellites with high spatial resolution, dramatically increasing opportunities to detect small elements in the landscapes, thereby enhancing the classification of vegetation types (Lopes et al., 2020). The Copernicus Sentinel-2 satellite has been widely used for vegetation analysis due to the red edge bands it provides and the frequent image capture (Addabbo et al., 2016; Forkuor et al., 2018; Immitzer et al., 2019). However, being a passive optical sensor, it has some limitations; the most intrinsic drawback of optical data is its high chance of losing information due to cloud coverage in tropical areas (Pham et al., 2022).

The persistent cloud cover in tropical regions affects the availability of cloud-free images, resulting in spatial inconsistencies in classification. A solution to this problem is the use of synthetic aperture radar (SAR) images. SAR uses electromagnetic waves in the microwave regions, which is not prone to atmospheric interference compared to optical images. SAR data can be acquired in atmospheric conditions inappropriate for optical sensors (Evans & Costa, 2013). Therefore, radar images have become an important source for land-cover classification in the past decade, especially in tropical regions (Li et al., 2012). The most widely used active

satellite sensor for vegetation mapping is Sentinel-1. This sensor has the ability to capture the seasonality of land cover and to differentiate between non-vegetated and vegetated surfaces through the backscatter mechanism of the C-band (Pham et al., 2022). The PALSAR-2 is another freely available active radar satellite sensor with L-band. The PALSAR-2 backscatter provides information on thicker layers of vegetation and soil under vegetation cover, which is useful for forests, wetlands, and agriculture studies (Lapini et al., 2020). However, SAR backscatter also has high noise interference, compared to optical images (Holtgrave et al., 2020) which can reduce the mapping accuracy.

Optical remote sensing is more frequently used than SAR remote sensing because spectral data are easily accessible and have proven suitable for vegetation monitoring (Addabbo et al., 2016). Optical data will outperform SAR data by itself for vegetation mapping (Holtgrave et al., 2020), however, these data sources can be used in combination (Camargo et al., 2019). The benefits of the combined use of optical and SAR data for vegetation mapping has been confirmed by several authors (Morin et al., 2019; Spracklen & Spracklen, 2021). Several studies have evaluated the integration of both PALSAR and Sentinel-2 data for vegetation mapping accuracy (Costa et al., 2021; Vafaei et al., 2018), where some researchers evaluate the fusion of Sentinel-1 and Sentinel-2 for land cover classification (Biswas et al., 2020; Lopes et al., 2020; Zhou, 2019), and for crop classification (Jiao et al., 2022; Van Tricht et al., 2018). Several authors (Huang et al., 2018; Omar et al., 2017) also used the Sentinel-1 and PALSAR data together to classify the vegetation, as they provide comprehensive information on the forest structure. However, very few studies (Lehmler et al., 2022; Pham et al., 2020) have used both PALSAR and Sentinel-1 as SAR data sources and Sentinel-2 as the optical data source in their research. Lehmler et al. (2022) used PALSAR, Sentinel-1and 2 to calculate green volume in urban and semi-urban areas in Germany, concluding that combining both radar sensors slightly improves the modelling performance. Similarly, Pham et al. (2020) showed that the integration of PALSAR, Sentinel-1and 2 improves the prediction accuracy of mangrove biomass estimation. This highlights the potential of radar data to increase classification accuracy. Further, data are not restricted to SAR and optical images and can be extended to combine auxiliary data such as topography and textural data.

This study explores the possibility of applying radar, optical, and topographical data together with machine learning in classifying vegetation cover in a mountainous tropical landscape in Sri Lanka. In order to address this objective, six classification experiments were designed based

on different combinations of image data that tested whether the addition of radar data improved land cover classification accuracy compared with optical data alone. The following two specific research questions were considered: 1) Do combined SAR and optical sensors provide a more accurate vegetation cover map, compared to using them independently? 2) What is the contribution of each of the different data sources to the accuracy of the vegetation cover map?

5.2 Materials and Method

5.2.1 Study Area

The study area is situated within the Balangoda Divisional Secretariat Division (DSD) in the Sabaragamuwa province of Sri Lanka, precisely between 80^0 35' 5"E -80^0 51' 33"E to $6^0$38' 11"N- $6^0$48' 21" N (see Figure 5.1). The area includes flat, rough, and mountainous terrain. There are medium-range mountain peaks located in the northern and eastern parts, namely Hawagala, Papulalgala, and Paraviyangala. Based on Sri Lankan elevation classification, this area is located in the mid-country, with an elevation range of 600 to 900 meters above the mean sea level. The area falls under the intermediate climate zone and experiences both wet and dry weather. It receives an average of 2500mm and 1750mm rainfall during the Northeast and Southwest monsoons, respectively. This study area serves as the watershed area for Belihuloya, which flows from Horton Plains National Park, a world heritage site. Pine plantations tend to be planted in large blocks with trees in straight lines, whereas the montane forest lies in the valley and conservation areas, with trees sporadically distributed. Grasslands and shrubs tend to be randomly distributed and are the result of wildfires. Home gardens and cultivations such as paddy, tea, and vegetables are scattered around the area.

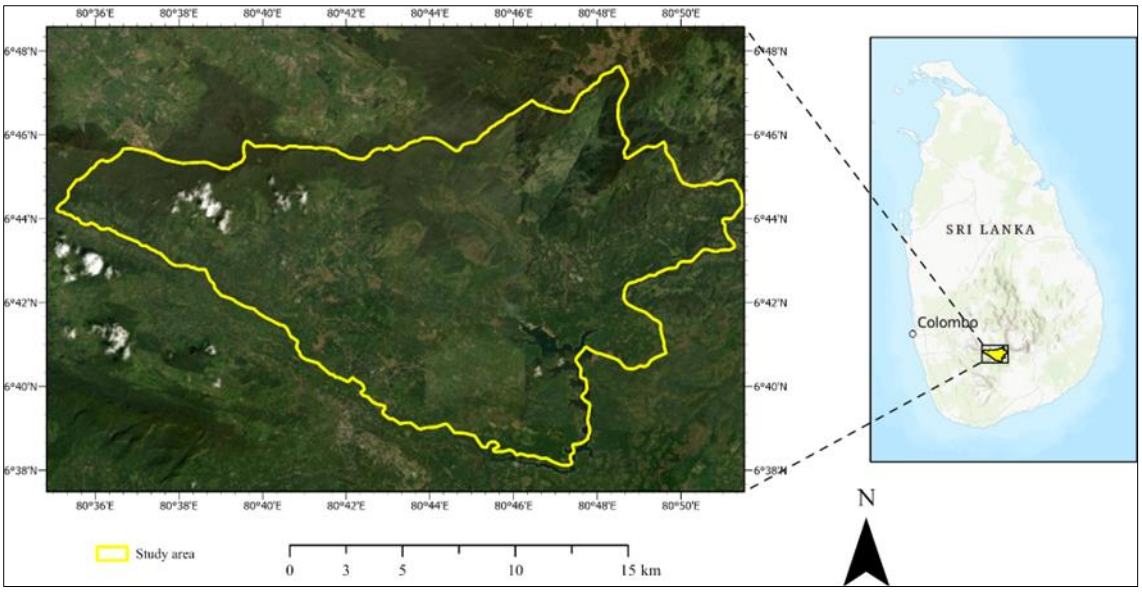

Figure 5.1 Study area in the Ibulpe gram Niladari Division (GND), Sri Lanka

5.2.2 Method

Figure 5.2 provides an overview of the remote sensing method used for this research. The method can be divided into the following three steps: 1) data acquisition and data pre-processing; 2) feature extraction; and 3) classification and accuracy assessment. Each of these stages are described separately below.

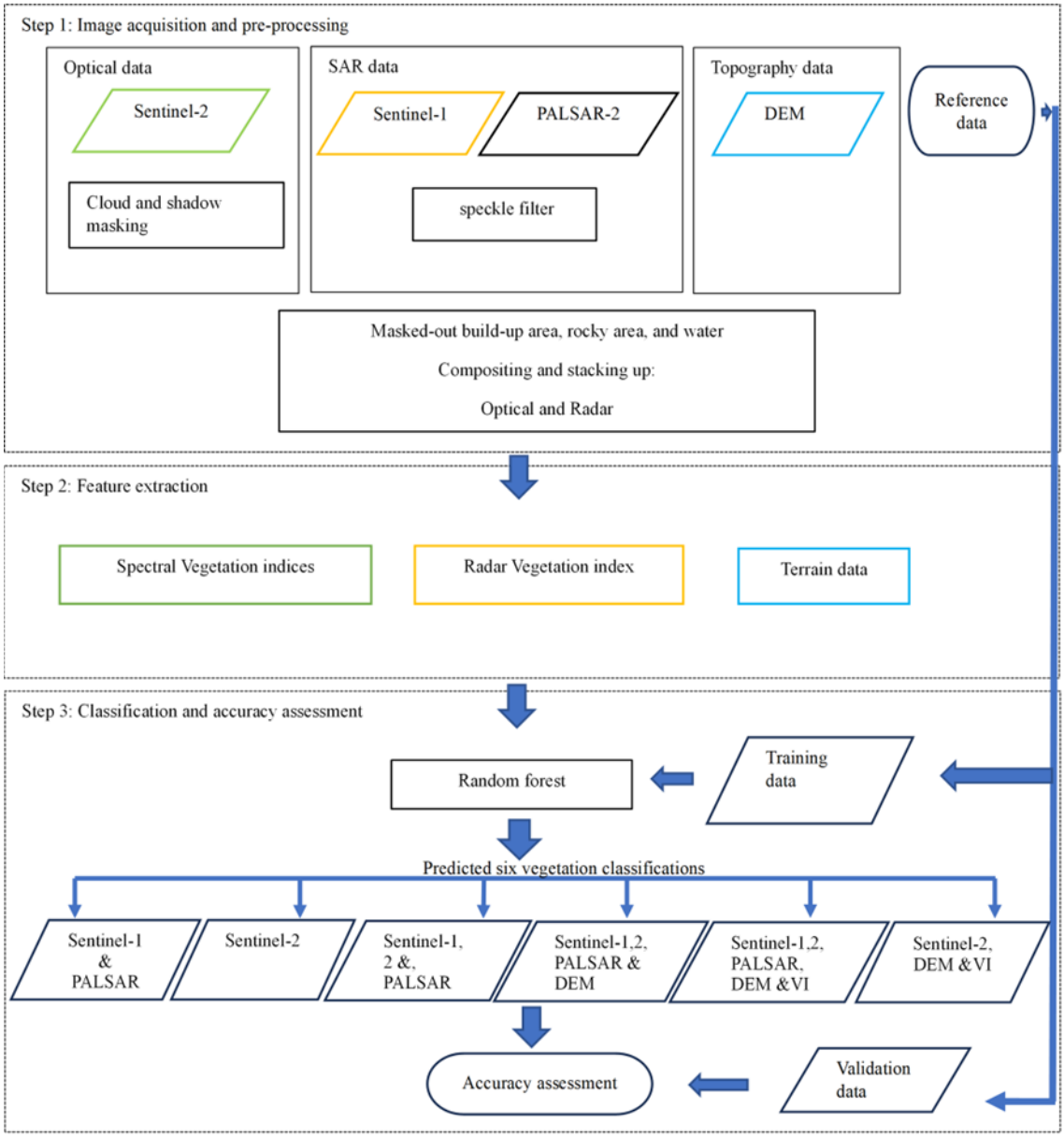

Figure 5.2 Overview of remote sensing method

Step 1: Image acquisition and pre-processing

This research uses the Sentinel-1 SAR and Sentinel-2 MSI satellite images distributed by the European Space Agency (ESA) and PALSAR images from the Japan Aerospace Exploration Agency, which are available on the Google Earth Engine (GEE) platform within the time frame of January 1st, 2020, to December 31st, 2020. GEE is a cloud-based computing platform that includes access to the archive of Sentinel and PALSAR imagery. This platform enables scientists to research spatial and temporal scales without depending on expensive software and

computer hardware (Poortinga et al. 2019). Optical imagery from Sentinel-2 and SAR images from Sentinel-1 and PALSAR were combined into a single stack of images as well as fused into combinations of different single images.

The Copernicus Sentinel-2 Mission is dedicated to monitoring variability in surface conditions and changes in vegetation during the growing season. The spatial resolution for Sentinel-2 varies for the different bands (Table 5.1). To ensure consistency and facilitate classification, the spatial resolution of the 20m bands was resampled to 10m through the implementation of bicubic interpolation. For this research, Harmonized Sentinel-2 MSI: Multispectral Instrument, Level-2A, surface reflectance provided by GEE has been used. This dataset is orthorectified and atmospherically corrected using the sen2cor algorithm by the GEE team. Less than 5% of cloud cover images were filtered, and a cloud mask was performed using the QA60 band to create a clean image stack.

The Copernicus Sentinel-1 mission provides synthetic aperture radar images using the dual-polarised C-band with a 10 m spatial resolution (Table 5.1), which is the first satellite of the Copernicus Global Monitoring Program for Environmental Monitoring (Metrikaityte et al. 2022). This research uses the level-1 ground range detected (GRD) product which is available in GEE. Two polarisation modes were used: single co-polarisation with vertical transmit and vertical receive (VV) and dual-band co-polarisation with vertical transmit and horizontal receive (VH). A four-band composite image across the year was then created by selecting the first clear observation at each pixel. A speckle filter (Refined Lee) was applied to reduce speckles in the image, which makes them functional for land cover detection.

Table 5.1 Data source information

Data Source	Band	Spectral range /polarisation	Wavelength range (nm)	Spatial resolution	Number of images
Sentinel-2	B2	Blue	496.6	10	13
	B3	Green	560	10	
	B4	Red	664.5	10	
	B5	Red edge1	703.9	20	
	B6	Red edge2	740.2	20	
	B7	Red edge3	782.5	20	
	B8	NIR	835.1	10	
	B8A	Red edge	864.8	20	
	B11	SWIR	1613.7	20	
	B12	SWIR	2202.4	20	
Sentinel-1	C	VV VH	5.6 cm	10	30
PALSAR-2	L	HH HV	23 cm	25	2

The PALSAR dataset was provided by the Earth Observation Research Centre, Japan Aerospace Exploration Agency (JAXA). This study used L-band at 25-m PALSAR orthorectified mosaic data, which is available from GEE. Two polarisation modes were used: horizontal transmission and horizontal reception (HH), and horizontal transmit and vertical receive (HV). A speckle filter was applied to reduce speckles in the image stack.

Shuttle Radar Topographic Mission (SRTM) provides digital elevation data (DEM) on a near-global scale (Farr 2007). Therefore, we obtained the elevation data by acquiring the SRTM Plus version from GEE, which has a spatial resolution of 30 m.

The reference data for the classification were acquired using the visual interpretation of high-resolution images in Google Earth using prior knowledge of the region. This approach was also adopted by (Deng et al. 2020; Pham et al. 2022; Zhang et al. 2009). The reference data comprised 240 polygons inside the vegetation mask, distributed in six classes: forest, pine plantation, grassland, shrub, home garden, and cultivation (Figure 5.3). Subsequently, the reference dataset was split randomly but in a stratified manner into training (70%) and validating (30%) subsets at the polygon level to ensure independent pixels for training and validation. In total, 3000 samples are used for training, and 1260 samples are reserved for validation. Specifically, 500 training samples were generated for each vegetation class to train the classification and 210 samples for the validation process.

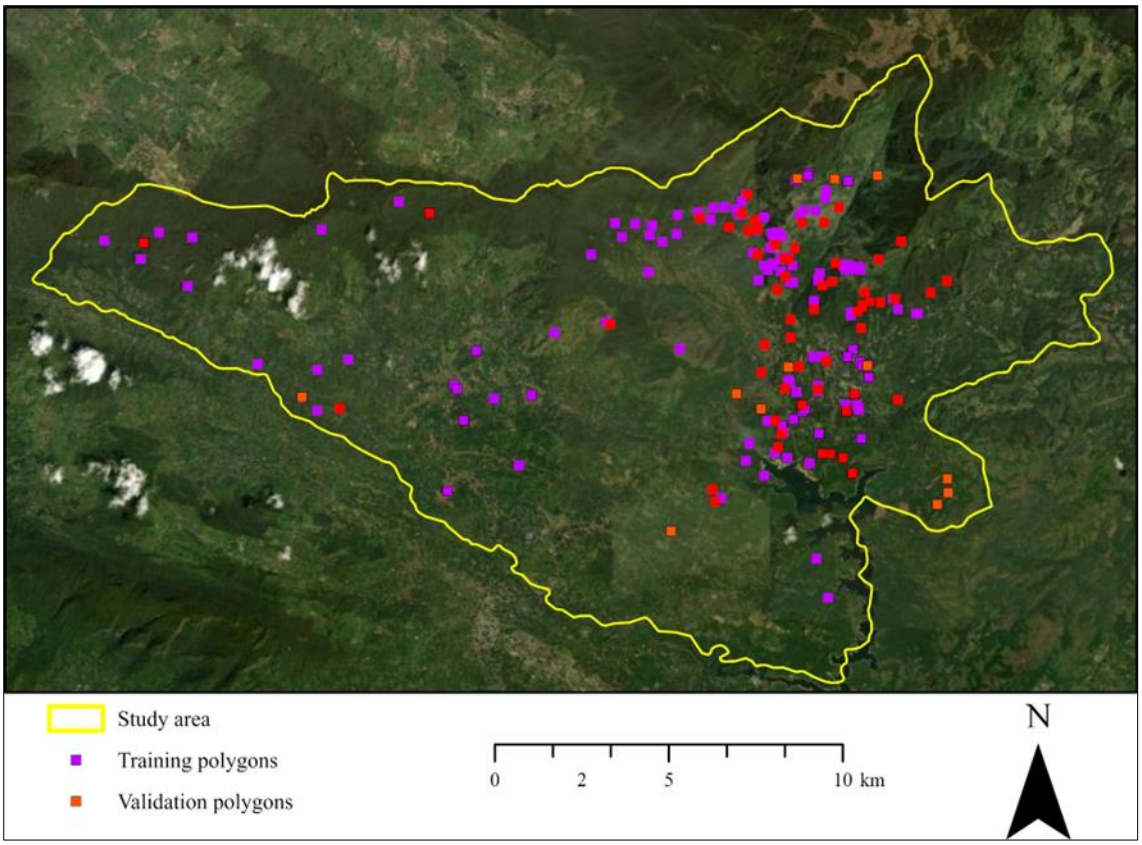

Figure 5.3 Training sites

Step 2: Feature extraction

Radar backscatter is impacted by forest type, structural orientation, and environmental conditions such as moisture and seasons. Therefore, an extra band, VV-VH, was also created, using the difference between the two polarisation modes. A radar vegetation index (RVI) was also derived using the VV and VH bands. Radar Vegetation Index (RVI) is a microwave vegetation cover metric that uses dual-polarised or quad-polarised SAR data (Holtgrave et al., 2020). This index is less sensitive to environmental conditions, such as soil moisture, than single polarization backscatter and therefore can be advantageous for vegetation monitoring (Kumar et al., 2013). The quad-pol RVI was proposed by Kim and Zyl (2009). Later, Nasirzadehdizaji et al. (2019) proposed an adaptation by modifying the index for Sentinel-1 data, which was used for this study (see Equation 5.1).

$$RVI = (4*VH)/(VV+VH) \qquad \text{Equation (5.1)}$$

Identifying land cover or specific species becomes difficult when the different vegetation types have similar spectral and seasonal characteristics (Deng et al., 2020). Vegetation indices assist in differentiating vegetation types when this is the case. Indices specified in Table 5.2 that are well-known in the literature for vegetation monitoring have been selected for the study to distinguish the five vegetation classes (Carrasco et al. 2019; Spracklen and Spracklen 2021; Xue and Su 2017). Due to the study area's surface roughness, indices such as Normalised Difference Moisture Index (NDMI), Soil Adjusted Vegetation Index (SAVI), Enhanced Vegetation Index (EVI) and Normalised Burned Ratio (NBR), which are sensitive to differences in soil and vegetation moisture content were selected. Further, Green Chlorophyll Index (GCI) and Red-Green Chlorophyll Index (RGCI) indices have been used to measure the chlorophyll differences of the vegetation classes (Addabbo et al. 2016; Nandasena et al. 2022). In addition, to distinguish vegetative areas from non-vegetative areas like water, we employed the Normalised Difference Vegetation Index (NDVI).

Table 5.2 Equations and bands used for the different vegetation indices

Index	Equation
NDMI	$\frac{(NIR\ -\ SWIR1)}{(NIR + SWIR1)}$
GCI	$\frac{NIR}{GREEN} - 1$
NBRI	$\frac{(NIR\ -\ SWIR2)}{(NIR + SWIR2)}$
SAVI	$\frac{(NIR\ -\ RED)}{(NIR +\ RED)\ +\ L\ )} \times (1 + L)$
EVI	$2.5 \times \frac{NIR - R}{NIR + R} + L$
RGCI	$\frac{Red\ edge3}{Red\ edge1} - 1$
NDVI	$\frac{(NIR\ -\ RED)}{(NIR + RED)}$

Data preparation involved compositing and stacking up the optical and radar datasets and masking out the non-vegetative areas using the NDVI threshold values. Figure 5.4 shows the

NDVI band and the mask generated using the NDVI threshold. This study utilised NDVI value less than 0.0 to differentiate areas with vegetation from non-vegetation areas. This determination was based on a thorough analysis of ground sampling pixel values. Correspondingly, this is in line with the Huang et al. (2021) and Jones and Vaughan (2010) studies, which show water bodies have negative NDVI values, while rocks, bare soil, sands, and concrete surfaces are close to zero, and vegetation including crops, shrubs, grasses, and forests have positive values. After the initial filtering for the study area, the period of interest (2020.01.01-2020.12.31) and masking of the non-vegetation area composting the datasets were conducted. Six experiments were tested, and the datasets and the variables used in each scenario are provided in Table 5.3. In order to integrate PALSAR-2 data with the Sentinel-1 and Sentinel-2 imagery at the pixel level, we resampled PALSAR-2 data to a spatial resolution of 10 m using a bicubic interpolation. Then, all the data were clipped to the study area. Finally, The PALSAR-2 and Sentinel-1 datasets were coregistered by utilising ground control points selected from Sentinel-2 imagery using ArcGIS Pro. The root-mean-square error of the ground control points was found to be less than 0.5 pixels.

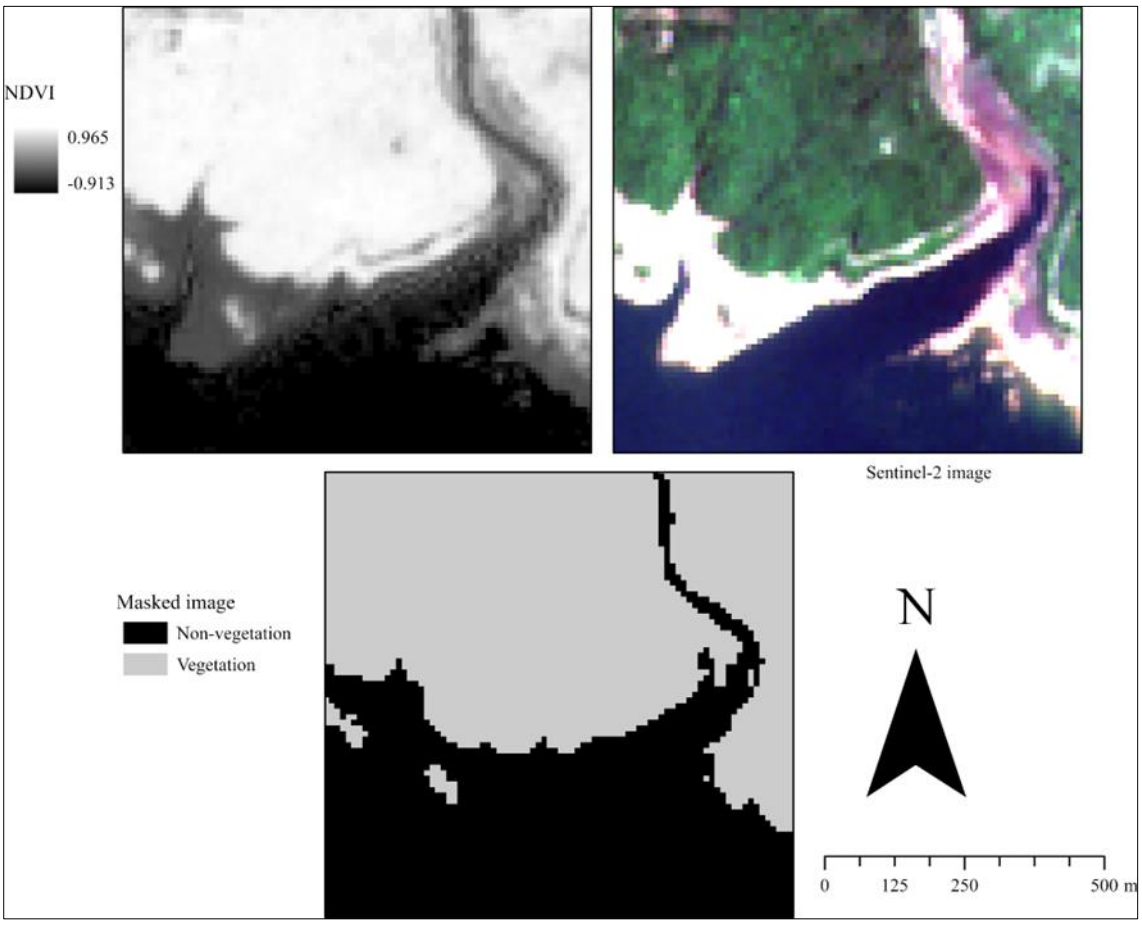

Figure 5.4 NDVI map and the masked image for vegetation

Table 5.3 Variables used in different scenarios

Experiments	Data sets	Variables
1	Radar only	VV, VH, VV-VH, RVI, HH, and HV
2	Optical only	B2, B3, B4, B5, B6, B7, B8, B8A, B11, B12
3	Radar and optical data	VV, VH, VV-VH, HH, HV and B2, B3, B4 ,B5, B6, B7, B8, B8A, B11, B12
4	Radar, optical data, and topographical data	VV, VH, VV-VH, HH, HV, B2, B3, B4, B5, B6, B7, B8, B8A, B11, B12, and slope, aspect, elevation
5	Radar, optical data, topographical and vegetation indices	VV, VH, VV-VH, HH, HV, B2, B3, B4, B5, B6, B7, B8, B8A, B11, B12, slope, aspect, elevation, NDMI, NBRI, SAVI, GLI, RGCI, GCI, EVI
6	Optical data, topographical and vegetation indices	B2, B3, B4, B5, B6, B7, B8, B8A, B11, B12, slope, aspect, elevation, NDMI, NBRI, SAVI, GLI, RGCI, GCI, EVI

Step 3: Classification and accuracy assessment

In remote sensing, RF is one of the most popular and effective supervised training algorithms introduced by Breiman (2001). In this study, RF was applied by utilising the smileRandomforest algorithm of GEE. RF is a multi-class classifier based on ensemble classification methods that perform better than a single decision tree. All the trees participate in the classification process by voting for their classes, and the final response of the random forest was calculated based on the majority vote results. RF has many benefits, such as fast computation, noise insensitivity, and reduced overfitting (Heckel et al. 2020). In order to run the classifier, the number of trees (ntree) and the number of features in each split (mtry) needed to be specified (Biswas et al. 2020). Further, this study conducted hyper-parameter tuning using a grid search, which involves assessing a classifier's performance by executing various combinations of parameters. (De Luca et al. 2022). The optimum number of trees and the best Bag fraction parameters are used for the maximum performance of the algorithm. According to Table 5.4, the highest score is 0.8648 at the parameter ' Bagfraction' = 0.8 and number of trees: 350. Therefore, the random forest model with those two parameters is used to classify vegetation. Finally, the performances of classifications were assessed based on a comparison between classified and validation reference data. For validation of the RF classification results,

30% of reference data were used. The accuracy of the produced vegetation cover maps was evaluated by computing the confusion matrix based on the validation set and extracted metrics: Overall accuracy, Kappa coefficient, User's accuracy, and Producer's accuracy.

Table 5.4 Hyperparameter tuning

Tuning parameter	Score	Best parameter
Number of trees=[100,150,200,250,300,350,400] Variables per split (sqrt), Bagfraction=[0.5]	0.856915	Number of trees=350
Number of trees=[100,150,200,250,300,350,400] Variables per split (sqrt), Bagfraction=[0.6]	0.856915	Number of trees=350
Number of trees=[100,150,200,250,300,350,400] Variables per split (sqrt), Bagfraction=[0.7]	0.860095	Number of trees=350
Number of trees=[100,150,200,250,300,350,400] Variables per split (sqrt), Bagfraction=[0.8]	0.864864	Number of trees=350
Number of trees =[100,150,200,250,300,350,400] Variables per split (sqrt), Bagfraction=[0.9]	0.860095	Number of trees=350

5.3 Results

5.3.1 Classification

Figure 5.5 and Figure 5.6 show the land use maps resulting from the six classification experiments. Figure 5.7 provides overall accuracy statistics, and Table 5.5 show user and producer accuracy, respectively. When comparing the maps generated by the six experiments there is visual evidence that the radar classification is different from the other five experiments (Figure 5.5). These radar experiments also had the lowest overall accuracy (83%) and did not show high accuracy for any particular land use cover class, according to the user and producer accuracy statistics. These results show that radar by itself is not particularly useful for land use mapping. Moreover, the misclassification of the natural forests class is visible in the northwestern corner of the study site based on optical experiments. However, as can be observed in Figure 6, the classification maps of vegetation types are smoother when combing all SAR, spectral, textural, and topographical features and improve overall and specific accuracy.

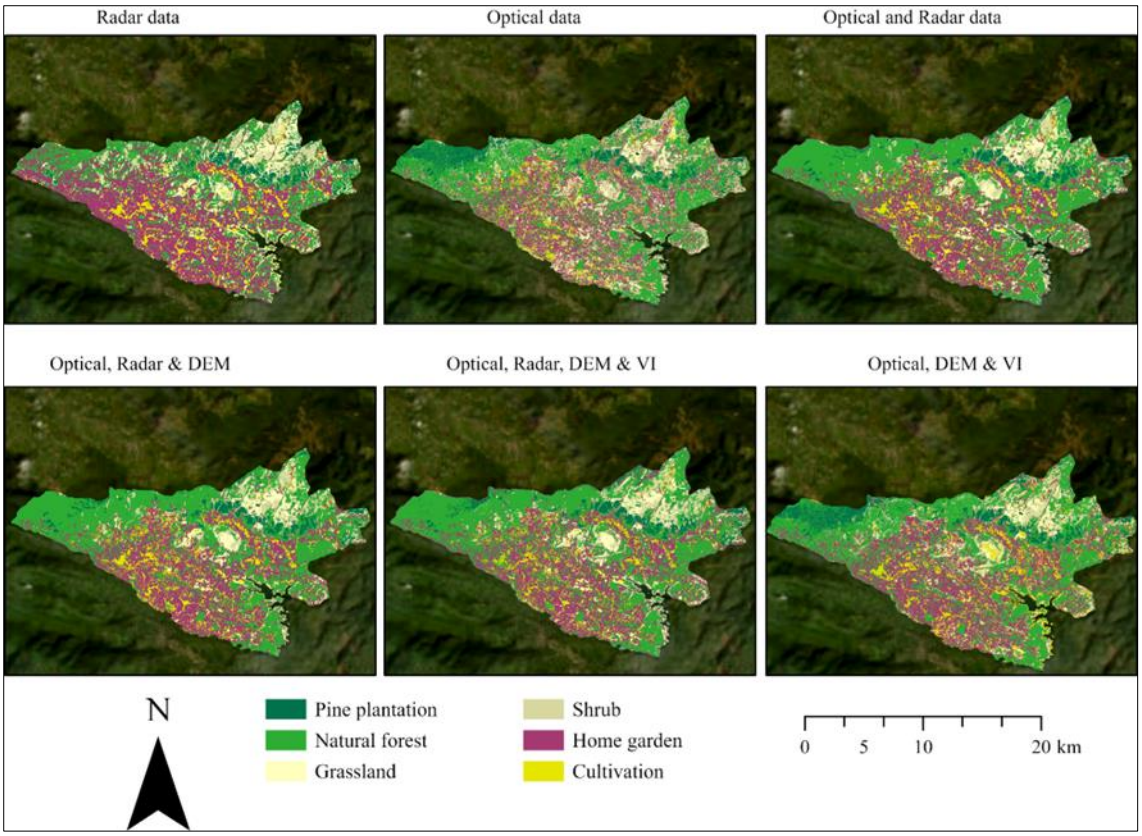

Figure 5.5 Land use maps resulting from the six classification experiments

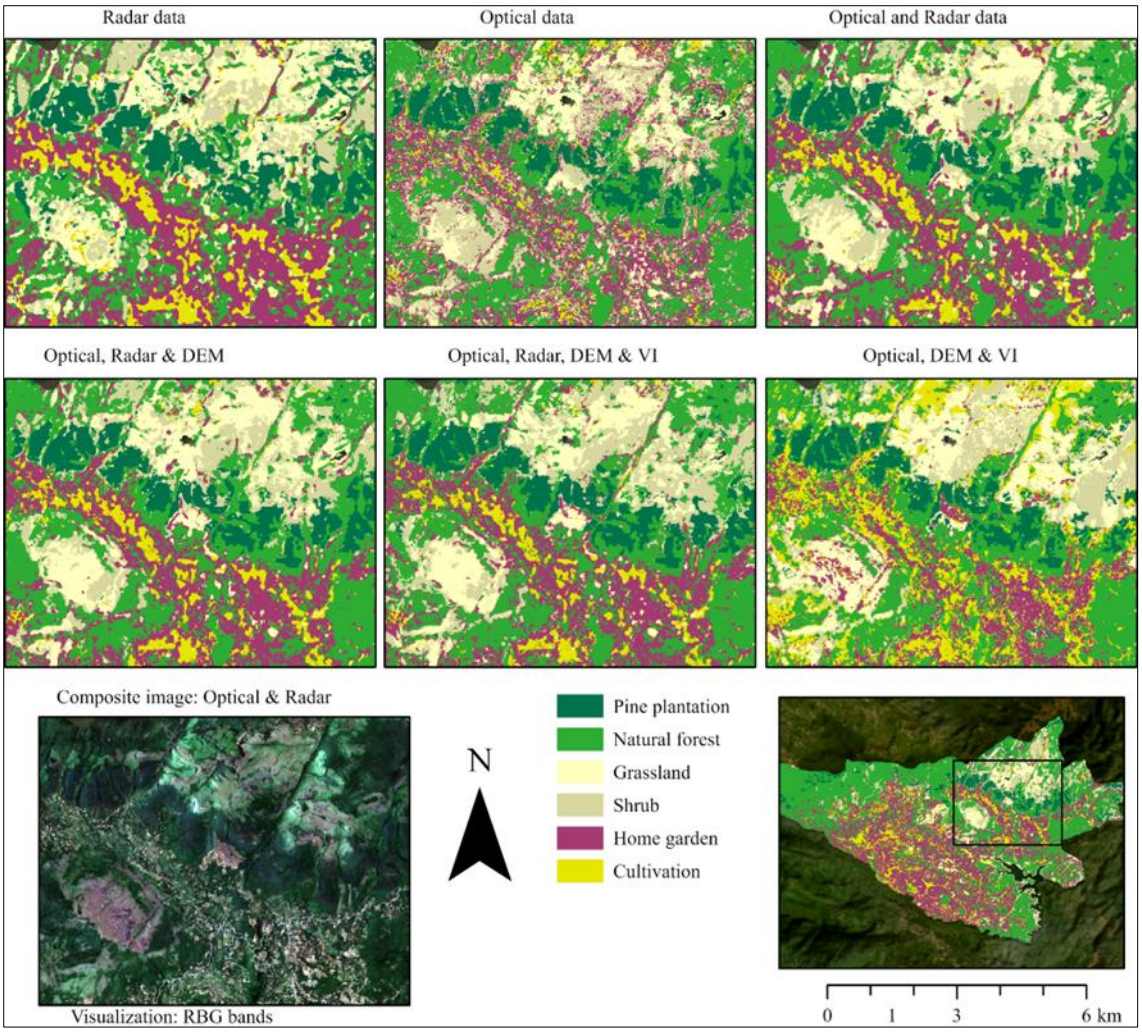

Figure 5.6 Six classification experiments and the composite image of optical and radar data

Optical images by themselves performed better than the radar images – 85% and 83%, respectively (Figure 5.7). However, the combination of optical and radar data had higher accuracy than optical by itself, both for overall accuracy (90%) and for most classes. Topographical indices, when combined with radar and optical images, improved the overall (92%) and specific class accuracy; however, surprisingly, the addition of vegetation indices only made a slight improvement by 0.3%. Comparatively, using optical data with DEM and VI did not increase the overall accuracy as much as combining all radar, optical, DEM, and VI data to the final classification. Adding radar data solely to optical data helped improve the overall accuracy by 5%, and gradually adding topography data improves the overall accuracy by 2%.

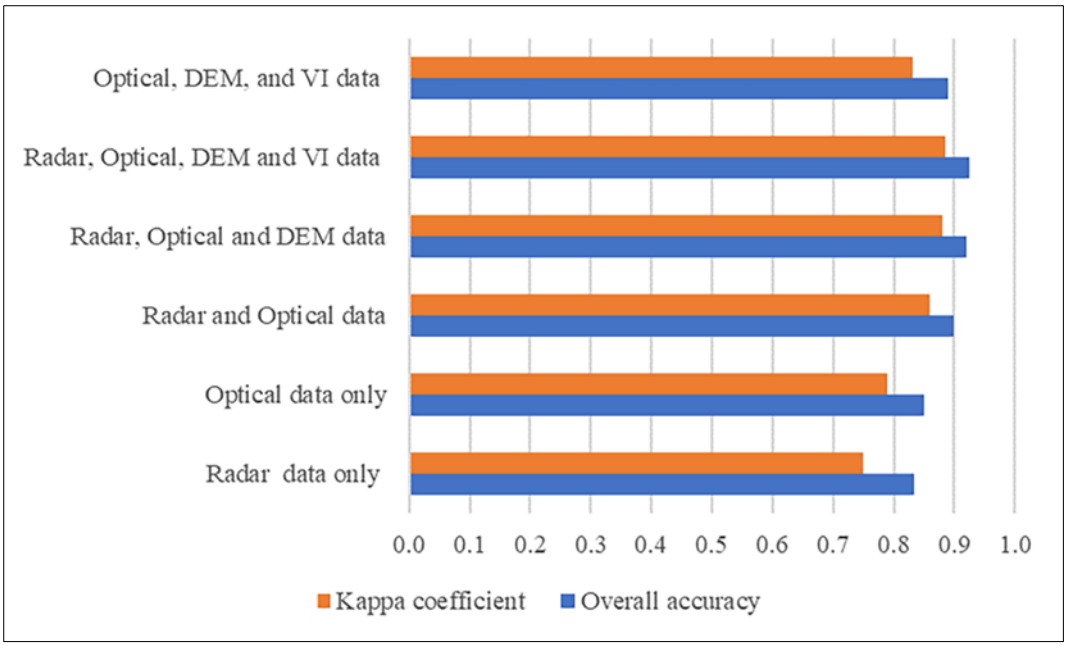

Figure 5.7 Overall accuracy and Kappa coefficient

5.3.2 Class-specific Accuracy

When considering the class-specific accuracy, pine plantations were identified accurately in this research, as they exhibit different textural and spectral reflectance compared to the other classes (see Table 5.5). Further, it is spread on steep slopes of the study area. The least accurate class was cultivation which includes paddy tea and vegetable cultivation. The mixing of these cultivation classes resulted in the spectral signature being varied potentially leading to their misclassification. The other difficult class to classify was shrubs, often misclassified with the grassland and cultivation classes. This may be because these two classes share the same landscape and act as the transitional zone between forest patches and occur mainly in the highest mountainous areas as well as at the edges of the reservoir.

Table 5.5 Land use class specific accuracy; User Accuracy (UA), Producer Accuracy (PA)

Land use type	Radar data only		Optical data only		Radar & Optical data		Radar, Optical & DEM data		Radar, Optical, DEM & VI data		Optical, DEM, & VI data	
	UA	PA	UA	PA	UA	PA	UA	PA	UA	PA	UA	PA
Pine plantation	0.93	0.84	0.99	0.96	1.00	0.95	1.00	0.97	1.00	0.95	0.99	0.99
Natural forest	0.64	0.81	0.89	0.94	0.87	0.94	0.91	0.94	0.90	0.99	0.91	0.91
Grassland	0.61	0.78	0.61	0.67	0.72	0.86	0.72	0.82	0.73	0.80	0.63	0.63
Shrub	0.68	0.38	0.58	0.52	0.75	0.54	0.94	0.68	0.83	0.70	0.89	0.64
Home garden	0.96	0.94	0.94	0.91	0.97	0.97	0.97	0.99	0.97	0.98	0.93	0.96
Cultivation	0.53	0.54	0.57	0.76	0.68	0.70	0.71	0.70	0.67	0.68	0.61	0.68

As shown in Table 5.5, for every scenario, the pine plantation class achieved the highest accuracy, ranging from 1 to 0.93, and the home garden had the second highest user accuracy (0.97 - 0.93). Considering each scenario's user accuracy, all classes showed higher accuracy when using spectral, radar, and topographical data. When considering the producer accuracy (see Table 5.5), the home garden class had the highest accuracy (0.99-0.91), followed by the pine plantation class (0.99-0.84). Again, as in the user accuracy, producer accuracy was high in all classes when using data combines except for the cultivation class, where scenario two gave the highest producer accuracy.

5.3.3 Feature Importance

This study identified the importance of 27 features selected by RF land use type identification, including three topographic features, six backscattering features, and 18 spectral features. Table 5.6 displays the top ten most important variables for the classification model. These variables were acquired using the final classification with the highest overall accuracy. The mean decrease in Gini index was used to determine the contribution of each of the 27 input variables for vegetation classification. This index determines the importance of each feature used in partitioning the training data into designated vegetation classes (Mahdianpari et al. 2020). The higher the value of mean decrease Gini score, the higher the importance of the variable in the model (Shetty 2019).

In contrast to the accuracy numbers, the results suggested that the RVI, VH-VV, VH, and VV bands from Sentinel-1 and the HV and HH bands from the PALSAR are important variables when classifying the vegetation in the tropical montane area. In addition, SWIR-1(B11),

SWIR-2 (B12), and red edge (B5) spectral bands derived from the optical data are important variables for the random forest classification when using data from Sentinel-2. The slope band derived from the DEM data also significantly impacts the classification. The slope contributed the most to vegetation type identification, especially in the mountain area with steep slopes and different elevations ranging from 200m to 3200m. Surprisingly, no vegetation indices were found in the top 10 categories, but spectral bands such as B11, B12, and B5 bands scored high importance and remained within the top ten features.

Table 5.6 Variable importance

Data Source	Variable	Importance
Sentinel-1	Radar Vegetation Index (RVI)	407.62
PALSAR	HV	403.08
Topography	Slope	402.53
Sentinel-1	VV-VH	398.09
PALSAR	HH	380.67
Sentinel-1	VV	346.47
Sentinel-1	VH	340.52
Sentinel-2	SWIR-1(B11)	317.83
Sentinel-2	SWIR-2 (B12)	283.28
Sentinel-2	Red edge band (B5)	277.14

5.4 Discussion

This study focused on evaluating the addition of radar data with optical data for mapping the tropical montane region using RF algorithm within the GEE environment. Six experiments have been conducted to find suitable remote sensing variables for tropical montane vegetation classification. This framework has been developed by radar and optical data alone and also by integrating spectral bands, SAR features, derived vegetation indices, and ancillary elevation data features into a single composite dataset. The lowest overall accuracy was observed with the radar data only experiment; this is also consistent with previous studies (Amoakoh et al. 2021; Costa et al. 2021). However, our study reported a relatively high overall accuracy of 83% for the radar dataset compared to other land cover studies that utilised SAR and RF classifiers (Camargo et al. 2019; Dobrinić et al. 2021). It may be due to the advantage of the use of radar

features from both L band and C band, which increased the accuracy of mapping vegetation due to the sensitivity to identify the various structures of the vegetation, allowing for better distinguishing the type of forest (De Souza et al. 2019; La et al. 2020). Nevertheless, optical data only showed the highest overall accuracy and kappa values than radar-only classification. This may be due to higher number of bands in the Sentinal-2, meaning that the total amount of information made available for the classifier in this scenario is much higher (Gómez 2017). Certainly, the optical data are useful to map the vegetation type in tropical montane region; however, these data are usually unavailable during the rainy season and some information is missing due to the high cloud cover. Additionally, the optical data cannot extract information from the structure of the vegetation as SAR data (Amoakoh et al. 2021; Camargo et al. 2019). Therefore, combining radar and optical data helps improve vegetation classification accuracy in tropical montane areas, as mapping these vegetation classes is challenging using single source datasets due to structural complexity and high heterogeneity.

This study supports previous findings that the addition of radar data improves vegetation mapping accuracy. This is in contrast to a study of the Amazon region (De Souza et al. 2019), which concluded that the classification accuracy was higher when using the optical data of Sentinel-2 alone rather than combining the radar and optical data. However, our study's classification accuracy increased by 5% when combining optical and radar data. Similarly, other studies (Mercier et al. 2019; Pham et al. 2022; Zhou 2019) of tropical regions and several other authors (De Luca et al. 2022; Spracklen and Spracklen 2021; Torbick et al. 2017) have recently demonstrated that combining optical and SAR data optimises classification accuracy. This is because radar data can overcome cloud cover issues, while Sentinel-2 has several red-edge bands that offer additional information about vegetation to the classifier (Zhou 2019). Further, L and C bands of PALSAR-2 and Sentinel-1 facilitate the classification of vegetation types with different structures and surface roughness (La et al. 2020). However, it is worth noting that the combination of SAR, optical and topographical data performed better than optical data and radar data alone. The reason for this is because the DEM provides topographic information that helps identify various vegetation habitat types based on their geomorphologic characteristics (Amoakoh et al. 2021; Liu et al. 2018). Although the models using solely radar, optical, and topography imagery had higher classification accuracy (~92%), to our surprise, the classification accuracy based on adding VI data slightly increased the classification accuracy by 0.3%. Likewise, Carrasco et al. (2019) obtained the lowest level of accuracy while using vegetation indices to classify land cover in the United Kingdom. It was expected that adding

vegetation indices as new variables would improve the classification results, but the increase was insignificant. This may be be attributed to the fact that vegetation indices are merely an arithmetic combination of the Sentinel-2 spectral bands. Hence, due to the existence of redundant features, the accuracy improvement was not significant, which was also proved by other studies conducted by (Amoakoh et al. 2021; Gómez 2017). Additionally, as in our study, Müller et al. (2015) demonstrated that the class-specific accuracy of croplands and grassland areas were lower than other classes, while Sano et al. (2005) reported the same problem; this is due to the spectral similarity between cropland, grassland, and shrub, which can increase the uncertainty when mapping.

The radar features have a significant impact on vegetation type discrimination. According to the feature importance analysis, backscattering data and radar vegetation index are more useful for distinguishing between different types of vegetation compared to spectral information., which other studies confirmed. This also aligns with Zhang et al. (2020) study, which found that PALSAR-2 data has higher extraction accuracy for forests and shrublands and Heckel et al. (2020) study, where Sentinel-1 data improved forest cover predictions in open savanna environments with heterogeneous regional features. Feature importance shows the RVI, VV-VH, and VV bands of Sentinel-1 and HV and HH bands from PALSAR as the most significant radar layers for RF prediction. This confirmed the findings of other studies (Garg et al. 2022; Holtgrave et al. 2020) concerning the high efficiency of the backscattering bands for vegetation mapping. Further, Mercier et al., 2019 found VV and VH polarisations were the most important SAR features for discriminating forest-agriculture mosaics land cover classes in Brazil and Spain. This can be mainly due to the radar band sensitivity to the surface roughness and the biomass, which helps distinguish different vegetation types (Fu et al. 2021).

As most researchers specified, vegetation indices are more significant in distinguishing vegetation types (Cheng and Wang 2019; Immitzer et al. 2019; Liu et al. 2018); however, none of the vegetation indices have been selected as the top ten variables. However, only the SWIR-1, SWIR-2, and Red edge band (B5) scored in eighth, ninth, and tenth place in the feature importance analysis, respectively. Comparatively, many scholars have widely demonstrated the importance of SWIR and red edge bands of Sentinel-2 for mapping vegetation, forests, and land cover classes (Heckel et al. 2020).

HV became one of the crucial variables in distinguishing selected land cover. This has been further assured in Qin et al. (2015) study, which emphasised that HV is an effective indicator

to distinguish forests from water and cropland. Further, Shimada et al. (2014) emphasised that forest and non-forest can be easily distinguished in HV polarised images. Jensen (2006) found it to be the best band for forest mapping in mountainous areas as it is less sensitive to slope variations.

Our study demonstrated the high suitability of the RVI index for the separation of land use classes based on vegetation types. This indicates that detecting the texture, pattern, and roughness of the canopy through Sentinel-1 is essential in distinguishing between plantation, agriculture, and natural forest. Several studies (Agapiou 2020; Ling et al. 2009) used this vegetation index for forest classification, land use, and vegetation analysis, showing the contribution of the RVI for the classification and the robustness of this radar vegetation analysis. In our study, the RVI outperformed the simple VH/VV ratio, which was also confirmed by Holtgrave et al. (2020). They assumed this because the RVI has an advantage over the VH/VV ratio because its formula gives more weight to the VH backscatter.

Finally, our study confirmed that topography is a key feature in classifying land use in mountainous areas. It also showed that elevation data derived from the DEM also helps to improve the classification. In particular, classification accuracy is significantly improved by introducing the topography features, resulting in an increment of 2% in the OA. Liu et al. (2018) showed that terrain contributes the most to forest type identification as the different geomorphologic characteristics reflect the habitats of different vegetation types and can help their identification. Similarly, in our study, the slope was a crucial component in the classification of mountainous regions. The higher importance of slope can be attributed to the landform in our study area, which has a high variation in elevation and slope.

5.5 Conclusion

This study demonstrated that freely accessible multi-source imagery significantly improves vegetation classification accuracy by comparatively analysing six scenario experiments. It also confirmed the need for using radar data for improving classification in vegetation analysis. In addition, feature importance analysis showed that radar data makes a significant contribution to classification; six of the ten feature analyses illustrated were radar data. However, this research showed that radar data by itself produces poor classification accuracy. In tropical mountainous regions with high levels of cloud cover combining radar data with optical data for vegetation classification improves accuracy. It is also important to use topographical variables in a complex mountainous environment. Optical, radar and topographical data sets are now

freely accessible using the GEE platform and can effectively support developing countries like Sri Lanka to monitor and manage forest resources.

5.6 Reference

Addabbo, P., Focareta, M., Marcuccio, S., Votto, C., & Ullo, S. (2016). Contribution of Sentinel-2 data for applications in vegetation monitoring. *ACTA IMEKO*, *5*, 44. https://doi.org/10.21014/acta_imeko.v5i2.352

Agapiou, A. (2020). Estimating Proportion of Vegetation Cover at the Vicinity of Archaeological Sites Using Sentinel-1 and -2 Data, Supplemented by Crowdsourced OpenStreetMap Geodata. *Applied Sciences*, *10*(14), 4764. https://www.mdpi.com/2076-3417/10/14/4764

Biswas, S., Huang, Q., Anand, A., Mon, M. S., Arnold, F.-E., & Leimgruber, P. (2020). A Multi Sensor Approach to Forest Type Mapping for Advancing Monitoring of Sustainable Development Goals (SDG) in Myanmar. *Remote Sensing*, *12*(19), 3220. https://www.mdpi.com/2072-4292/12/19/3220

Breiman, L. (2001). Random Forests. *Machine Learning*, *45*(1), 5-32. https://doi.org/10.1023/A:1010933404324

Camargo, F. F., Sano, E. E., Almeida, C. M., Mura, J. C., & Almeida, T. (2019). A Comparative Assessment of Machine-Learning Techniques for Land Use and Land Cover Classification of the Brazilian Tropical Savanna Using ALOS-2/PALSAR-2 Polarimetric Images. *Remote Sensing*, *11*(13). https://mdpi-res.com/d_attachment/remotesensing/remotesensing-11-01600/article_deploy/remotesensing-11-01600.pdf?version=1562324911

Carrasco, L., O'Neil, A. W., Morton, R. D., & Rowland, C. S. (2019). Evaluating Combinations of Temporally Aggregated Sentinel-1, Sentinel-2 and Landsat 8 for Land Cover Mapping with Google Earth Engine. *Remote Sensing*, *11*(3), 288. https://www.mdpi.com/2072-4292/11/3/288

Cheng, K., & Wang, J. (2019). Forest Type Classification Based on Integrated Spectral-Spatial-Temporal Features and Random Forest Algorithm—A Case Study in the Qinling Mountains. *Forests*, *10*(7), 559. https://www.mdpi.com/1999-4907/10/7/559

Costa, J. D., Liesenberg, V., Schimalski, M. B., Sousa, R. V., Biffi, L. J., Gomes, A. R., Neto, S. L., Mitishita, E., & Bispo, P. D. (2021). Benefits of Combining ALOS/PALSAR-2 and Sentinel-2A Data in the Classification of Land Cover Classes in the Santa Catarina Southern Plateau. *Remote Sensing*, *13*(2). https://mdpi-res.com/d_attachment/remotesensing/remotesensing-13-00229/article_deploy/remotesensing-13-00229-v3.pdf?version=1611214927

De Luca, G., M. N. Silva, J., Di Fazio, S., & Modica, G. (2022). Integrated use of Sentinel-1 and Sentinel-2 data and open-source machine learning algorithms for land cover mapping in a Mediterranean region. *European Journal of Remote Sensing*, *55*(1), 52-70. https://doi.org/10.1080/22797254.2021.2018667

De Souza Mendes, F., Baron, D., Gerold, G., Liesenberg, V., & Erasmi, S. (2019). Optical and SAR Remote Sensing Synergism for Mapping Vegetation Types in the Endangered

Cerrado/Amazon Ecotone of Nova Mutum—Mato Grosso. *Remote Sensing*, *11*(10). https://mdpi-res.com/d_attachment/remotesensing/remotesensing-11-01161/article_deploy/remotesensing-11-01161.pdf?version=1557913881

Evans, T. L., & Costa, M. (2013). Landcover classification of the Lower Nhecolândia subregion of the Brazilian Pantanal Wetlands using ALOS/PALSAR, RADARSAT-2 and ENVISAT/ASAR imagery. *Remote Sensing of Environment*, *128*, 118-137. https://doi.org/https://doi.org/10.1016/j.rse.2012.09.022

Farr, T. G., Rosen, P. A., Caro, E., Crippen, R., Duren, R., Hensley, S., Kobrick, M., Paller, M., Rodriguez, E., Roth, L., Seal, D., Shaffer, S., Shimada, J., Umland, J., Werner, M., Oskin, M., Burbank, D., & Alsdorf, D. . (2007). The Shuttle Radar Topography Mission. *Reviews of Geophysics*, *45*(2). https://doi.org/10.1029/2005rg000183

Forkuor, G., Dimobe, K., Serme, I., & Tondoh, J. E. (2018). Landsat-8 vs. Sentinel-2: examining the added value of sentinel-2's red-edge bands to land-use and land-cover mapping in Burkina Faso. *Giscience & Remote Sensing*, *55*(3), 331-354. https://doi.org/10.1080/15481603.2017.1370169

Holtgrave, A.-K., Röder, N., Ackermann, A., Erasmi, S., & Kleinschmit, B. (2020). Comparing Sentinel-1 and -2 Data and Indices for Agricultural Land Use Monitoring. *Remote Sensing*, *12*, 2919. https://doi.org/10.3390/rs12182919

Huang, X., Ziniti, B., Torbick, N., & Ducey, M. (2018). Assessment of Forest above Ground Biomass Estimation Using Multi-Temporal C-band Sentinel-1 and Polarimetric L-band PALSAR-2 Data. *Remote Sensing*, *10*, 1424. https://doi.org/10.3390/rs10091424

Immitzer, M., Neuwirth, M., Böck, S., Brenner, H., Vuolo, F., & Atzberger, C. (2019). Optimal Input Features for Tree Species Classification in Central Europe Based on Multi-Temporal Sentinel-2 Data. *Remote Sensing*, *11*(22), 2599. https://www.mdpi.com/2072-4292/11/22/2599

Jiao, X., McNairn, H., Yekkehkhany, B., Dingle Robertson, L., & Ihuoma, S. (2022). Integrating Sentinel-1 SAR and Sentinel-2 optical imagery with a crop structure dynamics model to track crop condition. *International Journal of Remote Sensing*, *43*(17), 6509-6537. https://doi.org/10.1080/01431161.2022.2142077

Kim, Y., & Zyl, J. J. v. (2009). A Time-Series Approach to Estimate Soil Moisture Using Polarimetric Radar Data. *IEEE Transactions on Geoscience and Remote Sensing*, *47*(8), 2519-2527. https://doi.org/10.1109/TGRS.2009.2014944

Kumar, S. D., Sitiraju, S., & Sharma, J. (2013). *Radar Vegetation Index as an Alternative to NDVI for Monitoring of Soyabean and Cotton* XXXIII INCA International Congress, Jodhpur.

Lapini, A., Pettinato, S., Santi, E., Paloscia, S., Fontanelli, G., & Garzelli, A. (2020). Comparison of Machine Learning Methods Applied to SAR Images for Forest Classification in Mediterranean Areas. *Remote Sensing*, *12*(3). https://mdpi-res.com/d_attachment/remotesensing/remotesensing-12-00369/article_deploy/remotesensing-12-00369-v2.pdf?version=1580641917

Lehmler, S., Förster, M., & Frick, A. (2022). *Modelling green volume using Sentinel-1, -2, PALSAR-2 satellite data and machine learning for urban and semi-urban areas in*

Germany. Research Square Platform LLC. https://dx.doi.org/10.21203/rs.3.rs-2349291/v1

Li, G., Lu, D., Moran, E., Dutra, L., & Batistella, M. (2012). A comparative analysis of ALOS PALSAR L-band and RADARSAT-2 C-band data for land-cover classification in a tropical moist region. *ISPRS Journal of Photogrammetry and Remote Sensing*, *70*, 26-38. https://doi.org/https://doi.org/10.1016/j.isprsjprs.2012.03.010

Ling, F., Li, Z., Chen, E., & Wang, Q. (2009, 26-30 Oct. 2009). Comparison of ALOS PALSAR RVI and Landsat TM NDVI for forest area mapping. 2009 2nd Asian-Pacific Conference on Synthetic Aperture Radar,

Liu, Y., Gong, W., Hu, X., & Gong, J. (2018). Forest Type Identification with Random Forest Using Sentinel-1A, Sentinel-2A, Multi-Temporal Landsat-8 and DEM Data. *Remote Sensing*, *10*(6), 946. https://www.mdpi.com/2072-4292/10/6/946

Lopes, M., Frison, P.-L., Crowson, M., Warren-Thomas, E., Hariyadi, B., Kartika, W. D., Agus, F., Hamer, K. C., Stringer, L., Hill, J. K., & Pettorelli, N. (2020). Improving the accuracy of land cover classification in cloud persistent areas using optical and radar satellite image time series [https://doi.org/10.1111/2041-210X.13359]. *Methods in Ecology and Evolution*, *11*(4), 532-541. https://doi.org/https://doi.org/10.1111/2041-210X.13359

Metrikaityte, G., Suziedelyte Visockiene, J., & Papsys, K. (2022). Digital Mapping of Land Cover Changes Using the Fusion of SAR and MSI Satellite Data. *Land*, *11*(7).

Morin, D., Planells, M., Guyon, D., Villard, L., Mermoz, S., Bouvet, A., Thevenon, H., Dejoux, J.-F., Le Toan, T., & Dedieu, G. (2019). Estimation and Mapping of Forest Structure Parameters from Open Access Satellite Images: Development of a Generic Method with a Study Case on Coniferous Plantation. *Remote Sensing*, *11*(11). https://mdpi-res.com/d_attachment/remotesensing/remotesensing-11-01275/article_deploy/remotesensing-11-01275.pdf?version=1559124264

Müller, H., Rufin, P., Griffiths, P., Barros Siqueira, A. J., & Hostert, P. (2015). Mining dense Landsat time series for separating cropland and pasture in a heterogeneous Brazilian savanna landscape. *Remote Sensing of Environment*, *156*, 490-499. https://doi.org/https://doi.org/10.1016/j.rse.2014.10.014

Nandasena, W. D. K. V., Brabyn, L., & Serrao-Neumann, S. (2020). Using Remote Sensing for Sustainable Forest Management in Developing Countries. In *The Palgrave Handbook of Global Sustainability* (pp. 1-22). Springer International Publishing. https://doi.org/10.1007/978-3-030-38948-2_35-1

Nasirzadehdizaji, R., Balik Sanli, F., Abdikan, S., Cakir, Z., Sekertekin, A., & Ustuner, M. (2019). Sensitivity Analysis of Multi-Temporal Sentinel-1 SAR Parameters to Crop Height and Canopy Coverage. *Applied Sciences*, *9*(4). https://mdpi-res.com/d_attachment/applsci/applsci-09-00655/article_deploy/applsci-09-00655.pdf?version=1550208973

Omar, H., Misman, M. A., & Kassim, A. R. (2017). Synergetic of PALSAR-2 and Sentinel-1A SAR Polarimetry for Retrieving Aboveground Biomass in Dipterocarp Forest of Malaysia. *Applied Sciences*, *7*(7). https://mdpi-res.com/d_attachment/applsci/applsci-07-00675/article_deploy/applsci-07-00675.pdf?version=1498827928

Pham, L. H., Pham, L. T. H., Dang, T. D., Tran, D. D., & Dinh, T. Q. (2022). Application of Sentinel-1 data in mapping land-use and land cover in a complex seasonal landscape: a case study in coastal area of Vietnamese Mekong Delta. *Geocarto International*, *37*(13), 3743-3760. https://doi.org/10.1080/10106049.2020.1869329

Pham, T. D., Yokoya, N., Xia, J., Ha, N. T., Le, N. N., Nguyen, T. T., Dao, T. H., Vu, T. T., Pham, T. D., & Takeuchi, W. (2020). Comparison of Machine Learning Methods for Estimating Mangrove Above-Ground Biomass Using Multiple Source Remote Sensing Data in the Red River Delta Biosphere Reserve, Vietnam. *Remote Sensing*, *12*(8). https://mdpi-res.com/d_attachment/remotesensing/remotesensing-12-01334/article_deploy/remotesensing-12-01334.pdf?version=1587650177

Poortinga, A., Tenneson, K., Shapiro, A., Nquyen, Q., San Aung, K., Chishtie, F., & Saah, D. (2019). Mapping Plantations in Myanmar by Fusing Landsat-8, Sentinel-2 and Sentinel-1 Data along with Systematic Error Quantification. *Remote Sensing*, *11*(7), 831. https://www.mdpi.com/2072-4292/11/7/831

Qin, Y., Xiao, X., Dong, J., Zhang, G., Shimada, M., Liu, J., Li, C., Kou, W., & Moore, B. (2015). Forest cover maps of China in 2010 from multiple approaches and data sources: PALSAR, Landsat, MODIS, FRA, and NFI. *ISPRS Journal of Photogrammetry and Remote Sensing*, *109*, 1-16. https://doi.org/https://doi.org/10.1016/j.isprsjprs.2015.08.010

Sano, E. E., Ferreira, L. G., & Huete, A. R. (2005). Synthetic Aperture Radar (L band) and Optical Vegetation Indices for Discriminating the Brazilian Savanna Physiognomies: A Comparative Analysis. *Earth Interactions*, *9*(15), 1-15. https://doi.org/10.1175/ei117.1

Shimada, M., Itoh, T., Motooka, T., Watanabe, M., Shiraishi, T., Thapa, R., & Lucas, R. (2014). New global forest/non-forest maps from ALOS PALSAR data (2007–2010). *Remote Sensing of Environment*, *155*, 13-31. https://doi.org/https://doi.org/10.1016/j.rse.2014.04.014

Spracklen, B., & Spracklen, D. V. (2021). Synergistic Use of Sentinel-1 and Sentinel-2 to Map Natural Forest and Acacia Plantation and Stand Ages in North-Central Vietnam. *Remote Sensing*, *13*(2). https://mdpi-res.com/d_attachment/remotesensing/remotesensing-13-00185/article_deploy/remotesensing-13-00185-v2.pdf?version=1610241527

Torbick, N., Chowdhury, D., Salas, W., & Qi, J. (2017). Monitoring Rice Agriculture across Myanmar Using Time Series Sentinel-1 Assisted by Landsat-8 and PALSAR-2. *Remote Sensing*, *9*(2). https://mdpi-res.com/d_attachment/remotesensing/remotesensing-09-00119/article_deploy/remotesensing-09-00119-v2.pdf?version=1487336211

Vafaei, S., Soosani, J., Adeli, K., Fadaei, H., Naghavi, H., Pham, T. D., & Tien Bui, D. (2018). Improving Accuracy Estimation of Forest Aboveground Biomass Based on Incorporation of ALOS-2 PALSAR-2 and Sentinel-2A Imagery and Machine Learning: A Case Study of the Hyrcanian Forest Area (Iran). *Remote Sensing*, *10*(2). https://mdpi-res.com/d_attachment/remotesensing/remotesensing-10-00172/article_deploy/remotesensing-10-00172.pdf?version=1516898085

Van Tricht, K., Gobin, A., Gilliams, S., & Piccard, I. (2018). Synergistic Use of Radar Sentinel-1 and Optical Sentinel-2 Imagery for Crop Mapping: A Case Study for Belgium. *Remote Sensing*, *10*(10).https://mdpi-res.com/d_attachment/remotesensing/remotesensing-10-01642/article_deploy/remotesensing-10-01642.pdf?version=1539685241

Xue, J., & Su, B. (2017). Significant Remote Sensing Vegetation Indices: A Review of Developments and Applications. *Journal of Sensors*, *2017*, 1353691. https://doi.org/10.1155/2017/1353691

Zhang, R., Tang, X., You, S., Duan, K., Xiang, H., & Luo, H. (2020). A Novel Feature-Level Fusion Framework Using Optical and SAR Remote Sensing Images for Land Use/Land Cover (LULC) Classification in Cloudy Mountainous Area. *Applied Sciences*, *10*(8), 2928. https://doi.org/10.3390/app10082928

Zhang, Y., Wang, C., Wu, J., Qi, J., & Salas, W. A. (2009). Mapping paddy rice with multitemporal ALOS/PALSAR imagery in southeast China. *International Journal of Remote Sensing*, *30*(23), 6301-6315. https://doi.org/10.1080/01431160902842391

Zhou, W. (2019). High-resolution Remote Sensing to Identify Tree Plantations from Natural Forests and Agriculture in Southern India [master's thesis, University of Michigan].

Chapter 6
Discussion and conclusion

6.1 Thesis integration and key questions addressed by this research

This thesis follows a sequence of increasing sophistication in land cover analysis in Sri Lanka using GEE and freely available satellite data. Chapter 3 is dedicated to the differentiation of agroforestry practices from forestry classes, with a particular focus on the home garden class, which is overshadowed by global land use classifications. Chapter 4 examines the mapping of *Pinus caribaea*, which is identified as a potentially invasive alien species in Sri Lanka, particularly in the intermediate mid-country, where the research study area is located. Chapter 5 researches the integration of radar and spectral data for addressing the difficulty of mapping the tropical montane regions due to the intricate land use patterns, topographical variations, and heavy cloud cover, which is common in tropical regions. Figure 6.1 shows how the aforementioned chapters perform an integrated piece of work to classify the tropical montane vegetation in Sri Lanka. Overall, this thesis provides a comprehensive analysis of the challenges and solutions involved in mapping land cover in tropical montane region in Sri Lanka. The demonstrated methodology and techniques have significantly improved the classification accuracy and sophistication of land cover mapping in Sri Lanka.

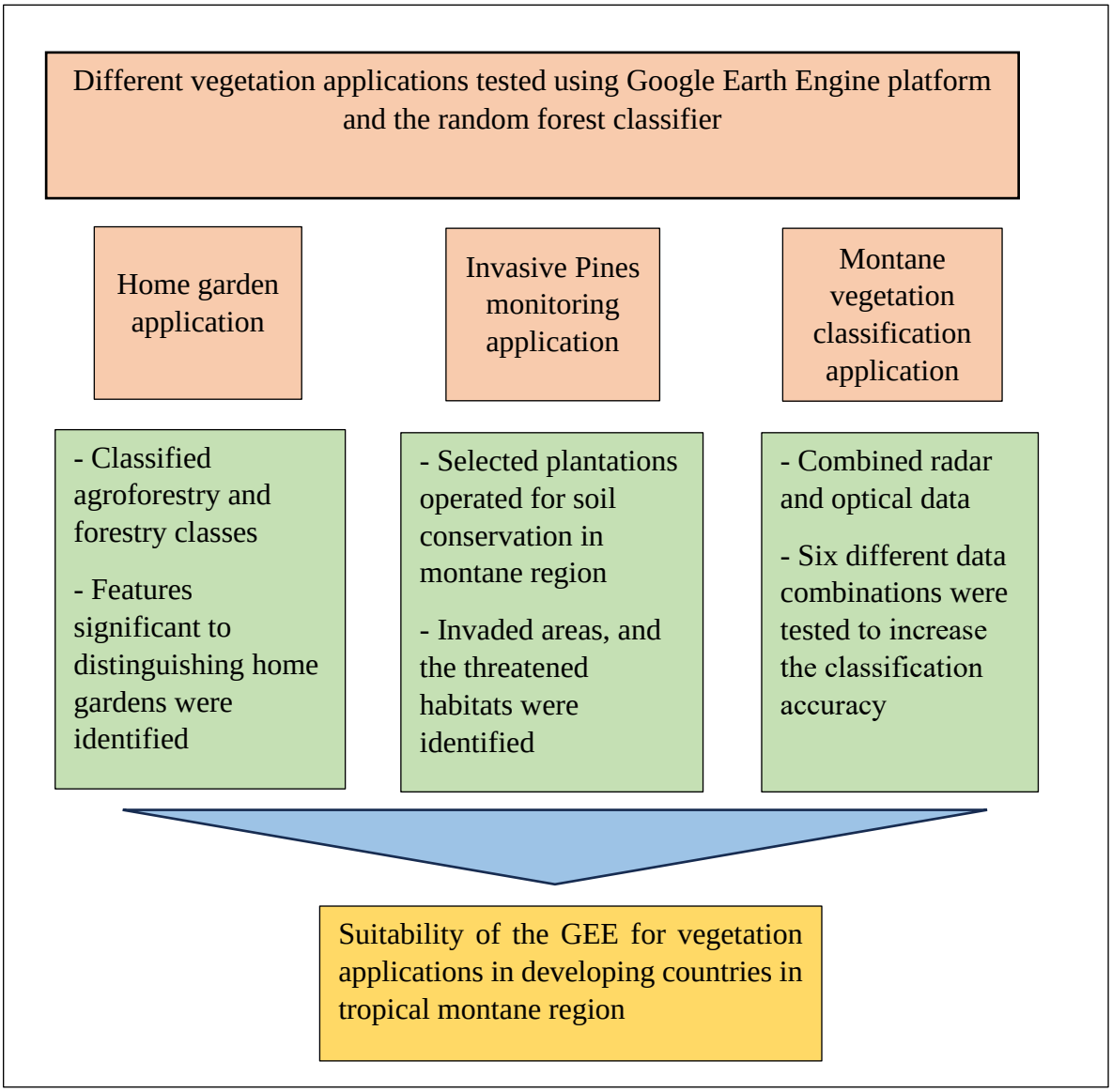

Figure 6.1 Thesis integration

As stated in the introduction, the main objective of this research was to derive robust and accurate information through satellite images, using solutions that are affordable to Sri Lanka, where resources are limited. This included assessing the best combination of data sources and image analysis techniques. Four key questions resulting from this objective were provided in Chapter 1. Following section describes how each of these questions has been answered.

Q1: Is the Google Earth Engine (GEE) platform suitable for mapping vegetation in developing countries?

Our research has demonstrated the dependability and versatility of the GEE platform in mapping vegetation in Sri Lanka. We utilized various applications, including forestry and agroforestry studies, to showcase its capabilities. With a comprehensive archive of historical

satellite imagery from Landsat, GEE facilitated change analysis spanning over two decades. Moreover, high-resolution images from Sentinel-2 can detect land use at the habitat level, while the different data sources of radar provide the advantage of acquiring information in a cloudy tropical region. As an interactive platform, GEE supports integrating auxiliary data, such as elevation data, into remote sensing analysis. Further, the GEE cloud-based platform and its large-scale analysis enable efficient processing and mosaicking of numerous satellite images to create a continuous, gap-free image.

This research confirmed that the GEE platform and its extensive range of analysis functions and free processing power is suitable for countries with limited financial resources to map vegetation change over time, including in tropical areas with frequent cloud cover.

Q2: What features are required to distinguish the home garden class from the other classes?

In order to answer this question, the research in Chapter 3 initially differentiated between forest and agroforestry classes in the study area. As the home garden structure and composition differs slightly from other forestry classes, it was necessary to investigate the variables to distinguish the home garden from other agroforestry classes. The random forest algorithm in GEE utilized the Gini method to determine feature importance, concluding that elevation, SWIR bands, and red textural metrics are significant in distinguishing the home garden.

Q3: Can invasive pines be monitored in a complex landscape used for conservation?

This question was answered in Chapter 4. The study presented in Chapter 4 was able to identify the pine plantations and the range of escape of pines to the other natural habitats by comparing images between the years 2000 and 2021. Pine plantations are typically maintained for the purpose of harvesting timber once they have matured. In this study area, pines have conservation values rather than just commercial benefits, and have been preserved for soil conservation purposes. Consequently, the pines have gradually spread into the natural forests. We detect the spread of invasive *Pinus caribaea,* using a combination of spectral, textural, and topographical bands. This research was further able to recognize the impact of invasive species on native forests, and grasslands.

Q4: Does the combination of radar and spectral data from different satellites improve the accuracy of vegetation mapping in cloudy tropical regions?

As Sri Lanka is a tropical moist country and the study area is situated in a mountainous area, cloudiness is a huge problem in remote sensing analysis. This problem can be overcome using radar data, as it can penetrate through the clouds. The research findings demonstrated that combining radar and spectral data improved vegetation classification, with an overall accuracy of 90%. It also confirmed the need to use radar data to improve vegetation analysis classification. In addition, feature importance analysis showed that radar data significantly contribute to classification, because six of the ten most important variables were radar data. However, this research showed that radar data by itself produces poor classification accuracy. Therefore, in tropical mountainous regions with high levels of cloud cover, combining radar data with optical data for vegetation classification improves accuracy.

6.2 Limitations

The use of mid-low-resolution images, such as those provided by Landsat and Sentinel, limit the spatial detail of the features that can be extracted. Currently, these are the main satellite data sources available for free, and the use of these freely available data was a constraint of this research, set by the research objectives.

In the near future, we can expect to see an increase in the accessibility of data, particularly LiDAR, for developing countries. These data are crucial for accurately identifying vegetation based on its height. The availability of higher resolution LiDAR data would significantly enhance vegetation classification. Currently, this type of data is freely and publicly available for research purposes in developed countries, but researchers in developing countries have to purchase it to cover the cost of data acquisition. By making geospatial data freely available, it would empower spatial researchers in developing countries to produce more accurate vegetation maps.

Originally, this research aimed to gather ground truth data of the study area. However, due to COVID-19 travel restrictions and border closures, collecting data in person was not possible. High-resolution satellite imagery from Google Earth was used to collect reference data to overcome this obstacle. This is found to be a viable reference data acquisition process, especially when access to ground truth data is restricted, or in situ data is insufficient. This

process involves utilizing my extensive local knowledge of the study area, which I have gained over 17 years. Although Google Earth images have a high resolution and can identify vegetation classes, the results would be more dependable if ground truth data were collected.

Researchers can perform massive geospatial computations in GEE, a powerful analytical platform that has access to a 40-year data archive. However, creating final maps can be challenging, due to GEE's lack of user-friendly features. To overcome this hurdle, this research employed the use of ArcGIS Pro - a costly software by ESRI which offers cheap deals for developing nations. It is also widely used in academic research, as it is graphic-friendly. Another viable option for such countries is the use of open-source GIS software like QGIS and GRASS GIS, which are also quite popular.

This thesis examined a tropical mountainous region in Sri Lanka and used various methods to classify the vegetation types. Sri Lankan montane forests are difficult to classify because of the variable terrain and cloudy atmospheric conditions. Therefore, the methods demonstrated in this thesis have been tested under challenging environments. They should therefore work in less challenging environments, such as lowland tropical and temperate regions. An exception may be the identification of the home garden class, as this class will vary considerably across countries. Therefore, it is necessary to adjust the parameters such as spectral signature, textural properties, and input variables to fit the specific research region.

6.3 Implications for mapping vegetation and future research

This research has focused on the Random Forest classifier because it works well and outperforms the other machine learning classifiers, as proven by many researchers when comparing different classification algorithms. However, research needs to be constantly evaluating the use of new classifiers, such as Deep Neural Network (DNN), Convolutional Neural Network (CNN) and Recurrent Neural Networks (RNN) to improve the accuracy of vegetation classification (Hanson et al., 2022). Additionally, the multi-classifiers – a classifier ensemble that combines individual classifiers for each vegetation class – have great potential to improve the accuracy and reliability of remote sensing image classification.

Data availability was a huge problem in the past. Although satellite data were available publicly, they were not accessible to developing countries due to the cost. However, with the open data source policy, Landsat, MODIS, Sentinel, and PALSAR data are currently freely available. As

we move toward the future, it is probable that many expensive commercial satellite data sets will become cheaper or even free. This may provide opportunities for future researchers to combine data from different sources and extract more reliable classifications.

As new data availability continues to grow, in the near future, remote sensing information is expected to be a key factor in shaping new developments in vegetation analysis. Likewise, researchers can expand their studies to include biomass analysis and vegetation structure, thanks to the diverse range of new data sets available such as NISAR, GEDI, RADARSAT Constellation Mission, MOLI, or future active sensors like BIOMASS (Crowley & Cardille, 2020). Additionally, researchers can utilize Unmanned Aerial Vehicles (UAV) observations, such as drone imagery, to map vegetation on a micro-level. Drones offer a higher resolution, allowing for more detailed and focused observations of regions. Although they can be costly and difficult for developing nations to access, the open data policy has made it possible for nontraditional datasets to be openly available. For example, the GeoNadir platform now offers an open repository of global drone data (GeoNadir, 2023).

In addition to the improvements in remote sensing data, there have also been advancements in technology and computing power, including various cloud-based platforms that are now available for geospatial analysis. This means that researchers are not limited to just using GEE. Microsoft has introduced Microsoft Planetary Computer (MPC) as an alternative cloud computing platform that provides petabytes of environmental monitoring data (Microsoft, 2023). Some other cloud-based hardware can also be used for free, although there are limitations compared to the GEE. Sentinel Hub is an engine for processing large amounts of Sentinel satellite data, and it can be integrated with other applications. The Digital Earth Australia (DEA) Sandbox and The Digital Africa (DE) Africa Sandbox are two additional cloud-based computational platforms that provide limited but free computing resources for technical users and data scientists to explore these continental data and products.

Another implication of this research is the importance of recognizing the nuance of classes of landuse cover in different countries. Chapter 3 focused on home gardens, but there are also other nuance classes that are overshadowed by global classifications. Shifting cultivation, which is commonly practised in tropical regions and known as ‘Chena’ in Sri Lanka, has distinct features that should be identified in order to understand how human activity impacts forest degradation in Sri Lanka. Moreover, wet and dry Pathana are two different grassland types in Sri Lanka that differ from Savannas and play a crucial role in soil conservation and

watershed management. It is recommended that researchers utilize remote sensing to accurately identify and map these unique vegetation classes in Sri Lanka.

With technological advancement and data availability, vegetation classification is becoming increasingly powerful, easier to implement, and widely tested in different regions and scenarios. However, it is crucial to check and validate these classifications and models thoroughly using error modelling. Frequently, global error statistics, such as Total Error and Kappa are used to validate a classification, which hides specific accuracy of each class. It is important that accuracy statistics on specific classes are provided, because as these classes may be important to users. Global statistics include classes that are easy to classify, such as water, resulting in misrepresenting the accuracy of classes that are difficult to classify. Accuracy assessment is also dependant on the sampling methods used for collecting ground truth data. It is important that this is systematically collected, to ensure each vegetation class is well-represented.

6.4 Overall conclusion

Google Earth Engine is a revolutionary step in geospatial analysis history. Previously, researchers who utilized remotely sensed data were limited to downloading satellite images and conducting analysis on their own computer systems. GEE, with its open and freely available high-capacity analysis platform, has greatly altered the potential for accessing and analysing images and combining data from different remote sensing sources to better understand the surface of the earth. This has empowered researchers in developing nations to do massive scale analyses cost-effectively.

Not only has hardware advanced, but access to various types of geospatial data has greatly changed the approach to remote sensing that has been used for many years. By combining not just spectral and radar data but also topographical and GIS data, classification accuracy can be improved. Moreover, machine learning classifiers outperform traditional classifications in handling large amounts of data and have evolved from single classifiers to multiple classifiers and deep learning algorithms.

This research has shown that developing countries, like Sri Lanka, can now advance remote sensing analysis using freely available data sources and cloud platforms, which can be used for different vegetation monitoring applications.

6.5 References

Crowley, M. A., & Cardille, J. A. (2020). Remote Sensing's Recent and Future Contributions to Landscape Ecology. *Current Landscape Ecology Reports*, *5*(3), 45-57. https://doi.org/10.1007/s40823-020-00054-9

GeoNadir. (2023). *The global home of drone mapping data*. Retrieved 10th of May from https://geonadir.com/

Hanson, C. C., Brabyn, L., & Gurung, S. B. (2022). Diversity-accuracy assessment of multiple classifier systems for the land cover classification of the Khumbu region in the Himalayas. *Journal of Mountain Science*, *19*(2), 365-387. https://doi.org/10.1007/s11629-021-7130-7

Microsoft. (2023). *A Planetary Computer for a Sustainable Future*. Retrieved 12th of May from https://planetarycomputer.microsoft.com/A Planetary Computer for a Sustainable Future

Reference

Abebe, T., Sterck, F. J., Wiersum, K. F., & Bongers, F. (2013). Diversity, composition and density of trees and shrubs in agroforestry homegardens in Southern Ethiopia [Article]. *Agroforestry systems*, *87*(6), 1283-1293. https://doi.org/10.1007/s10457-013-9637-6

Addabbo, P., Focareta, M., Marcuccio, S., Votto, C., & Ullo, S. (2016). Contribution of Sentinel-2 data for applications in vegetation monitoring. *ACTA IMEKO*, *5*, 44. https://doi.org/10.21014/acta_imeko.v5i2.352

Afrin, S., Sharmin, S., & Mowla, Q. A. (2010). The Environmental Impact of Alien Invasive Plant Species in Bangladesh. International Conference on Environmental Aspects of Bangladesh (ICEAB10), Japan.

Agapiou, A. (2020). Estimating Proportion of Vegetation Cover at the Vicinity of Archaeological Sites Using Sentinel-1 and -2 Data, Supplemented by Crowdsourced OpenStreetMap Geodata. *Applied Sciences*, *10*(14), 4764. https://www.mdpi.com/2076-3417/10/14/4764

Albinet, C., Whitehurst, A. S., Jewell, L. A., Bugbee, K., Laur, H., Murphy, K. J., Frommknecht, B., Scipal, K., Costa, G., Jai, B., Ramachandran, R., Lavalle, M., & Duncanson, L. (2019). A Joint ESA-NASA Multi-mission Algorithm and Analysis Platform (MAAP) for Biomass, NISAR, and GEDI. *Surveys in Geophysics*, *40*(4), 1017-1027. https://doi.org/10.1007/s10712-019-09541-z

Amaral, C. H., Roberts, D. A., Almeida, T. I. R., & Souza Filho, C. R. (2015). Mapping invasive species and spectral mixture relationships with neotropical woody formations in southeastern Brazil. *ISPRS Journal of Photogrammetry and Remote Sensing*, *108*, 80-93. https://doi.org/https://doi.org/10.1016/j.isprsjprs.2015.06.009

Andrew, M. E., & Ustin, S. L. (2008). The role of environmental context in mapping invasive plants with hyperspectral image data. *Remote Sensing of Environment*, *112*(12), 4301-4317. https://doi.org/https://doi.org/10.1016/j.rse.2008.07.016

April, S., E., Sarr, D. A., Van Kirk, R. W., & Jules, E. S. (2015). Quantifying habitat loss: Assessing tree encroachment into a serpentine savanna using dendroecology and remote sensing. *Forest Ecology and Management*, *340*, 9-21. https://doi.org/https://doi.org/10.1016/j.foreco.2014.12.019

Ayala, L., Perevolotsky, A., Kigel, J., & Noy-Meir, I. (2005). Invasion of Pinus halepensis from Plantations into Adjacent Natural Habitats. *Applied Vegetation Science*, *8*(1), 85-92. http://www.jstor.org/stable/4620435

Bajpai, K., & Soni, R. (2017). Analysis of Image Enhancement Techniques Used in Remote Sensing Satellite Imagery. *International Journal of Computer Applications*, *169*(10).

Balasubramanian, K. I. (2017). *Identifying the most important spectral and textural feature features to map specific crops with very high resolution images* University of Twente].

Bhattacharjee, R., Choubey, A., Das, N., Ohri, A., & Gaur, S. (2021). Detecting the Carotenoid Pigmentation due to Haloarchaea Microbes in the Lonar Lake, Maharashtra, India Using Sentinel-2 Images. *Journal of the Indian Society of Remote Sensing*, *49*(2), 305-316. https://doi.org/10.1007/s12524-020-01219-z

Bhunia, G. S., Shit, P. K., & Sengupta, D. (2021). Free-Open Access Geospatial Data and Tools for Forest Resources Management. In P. K. Shit, H. R. Pourghasemi, P. Das, & G. S. Bhunia (Eds.), *Spatial Modeling in Forest Resources Management : Rural Livelihood and Sustainable Development* (pp. 651-675). Springer International Publishing. https://doi.org/10.1007/978-3-030-56542-8_28

Biswas, S., Huang, Q., Anand, A., Mon, M. S., Arnold, F.-E., & Leimgruber, P. (2020). A Multi Sensor Approach to Forest Type Mapping for Advancing Monitoring of Sustainable Development Goals (SDG) in Myanmar. *Remote Sensing*, *12*(19), 3220. https://www.mdpi.com/2072-4292/12/19/3220

Bjerreskov, K. S., Nord-Larsen, T., & Fensholt, R. (2021). Classification of Nemoral Forests with Fusion of Multi-Temporal Sentinel-1 and 2 Data. *Remote Sensing*, *13*(5). https://doi.org/10.3390/rs13050950

Bourgine, B., & Baghdadi, N. (2005). Assessment of C-band SRTM DEM in a dense equatorial forest zone. *Comptes Rendus Geoscience*, *337*(14), 1225-1234. https://doi.org/https://doi.org/10.1016/j.crte.2005.06.006

Bouvet, A., Mermoz, S., Ballère, M., Koleck, T., & Le Toan, T. (2018). Use of the SAR Shadowing Effect for Deforestation Detection with Sentinel-1 Time Series. *Remote Sensing*, *10*(8).

Bouvet, A., Mermoz, S., Le Toan, T., Villard, L., Mathieu, R., Naidoo, L., & Asner, G. P. (2018). An above-ground biomass map of African savannahs and woodlands at 25m resolution derived from ALOS PALSAR. *Remote Sensing of Environment*, *206*, 156-173. https://doi.org/https://doi.org/10.1016/j.rse.2017.12.030

Boyd, D. S., & Danson, F. M. (2005). Satellite remote sensing of forest resources: three decades of research development. *Progress in Physical Geography: Earth and Environment*, *29*(1), 1-26. https://doi.org/10.1191/0309133305pp432ra

Bradley, B. A. (2014). Remote detection of invasive plants: a review of spectral, textural and phenological approaches. *Biological Invasions*, *16*(7), 1411-1425. https://doi.org/10.1007/s10530-013-0578-9

Breiman, L. (2001). Random Forests. *Machine Learning*, *45*(1), 5-32. https://doi.org/10.1023/A:1010933404324

Broich, M., Hansen, M. C., Potapov, P., Adusei, B., Lindquist, E., & Stehman, S. V. (2011). Time-series analysis of multi-resolution optical imagery for quantifying forest cover loss in Sumatra and Kalimantan, Indonesia. *International Journal of Applied Earth Observation and Geoinformation*, *13*(2), 277-291. https://doi.org/https://doi.org/10.1016/j.jag.2010.11.004

Burley, J., & Barnes, R. D. (2004). Tropical Ecosystems | Tropical Pine Ecosystems and Genetic Resources. In J. Burley (Ed.), *Encyclopedia of Forest Sciences* (pp. 1728-1740). Elsevier. https://doi.org/https://doi.org/10.1016/B0-12-145160-7/00089-2

Camargo, F. F., Sano, E. E., Almeida, C. M., Mura, J. C., & Almeida, T. (2019). A Comparative Assessment of Machine-Learning Techniques for Land Use and Land Cover Classification of the Brazilian Tropical Savanna Using ALOS-2/PALSAR-2 Polarimetric Images. *Remote Sensing*, *11*(13). https://mdpi-

res.com/d_attachment/remotesensing/remotesensing-11-01600/article_deploy/remotesensing-11-01600.pdf?version=1562324911

Camarretta, N., Harrison, P. A., Bailey, T., Potts, B., Lucieer, A., Davidson, N., & Hunt, M. (2020). Monitoring forest structure to guide adaptive management of forest restoration: a review of remote sensing approaches. *New Forests*, *51*(4), 573-596. https://doi.org/10.1007/s11056-019-09754-5

Campbell, J. B., & Wynne., R. H. (2011). *Introduction to Remote Sensing* (5th Edition ed.). The Guilford Press.

Cannell, M. G. R. (1988). Agroforestry - A Decade of Development. Edited by H. A. Steppler and P. K. R. Nair. Nairobi: International Council for Research in Agroforestry (1987). *Experimental Agriculture*, *24*(3), 393-393. https://doi.org/10.1017/S0014479700016252

Carrasco, L., O'Neil, A. W., Morton, R. D., & Rowland, C. S. (2019). Evaluating Combinations of Temporally Aggregated Sentinel-1, Sentinel-2 and Landsat 8 for Land Cover Mapping with Google Earth Engine. *Remote Sensing*, *11*(3), 288. https://www.mdpi.com/2072-4292/11/3/288

Cheng, K., & Wang, J. (2019). Forest Type Classification Based on Integrated Spectral-Spatial-Temporal Features and Random Forest Algorithm—A Case Study in the Qinling Mountains. *Forests*, *10*(7), 559. https://www.mdpi.com/1999-4907/10/7/559

Chuvieco, E. (2016). *Fundamentals of Satellite Remote Sensing: An Environmental Approach*. Taylor & Francis Group.

Congalton, R. G. (2001). Accuracy assessment and validation of remotely sensed and other spatial information. *International Journal of Wildland Fire*, *10*(4), 321-328.

Coppin, P. R., & Bauer, M. E. (1996). Digital change detection in forest ecosystems with remote sensing imagery. *Remote Sensing Reviews*, *13*(3-4), 207-234. https://doi.org/10.1080/02757259609532305

Costa, J. D., Liesenberg, V., Schimalski, M. B., Sousa, R. V., Biffi, L. J., Gomes, A. R., Neto, S. L., Mitishita, E., & Bispo, P. D. (2021). Benefits of Combining ALOS/PALSAR-2 and Sentinel-2A Data in the Classification of Land Cover Classes in the Santa Catarina Southern Plateau. *Remote Sensing*, *13*(2). https://mdpi-res.com/d_attachment/remotesensing/remotesensing-13-00229/article_deploy/remotesensing-13-00229-v3.pdf?version=1611214927

Crowley, M. A., & Cardille, J. A. (2020). Remote Sensing's Recent and Future Contributions to Landscape Ecology. *Current Landscape Ecology Reports*, *5*(3), 45-57. https://doi.org/10.1007/s40823-020-00054-9

Das, T., & Das, A. K. (2014). Mapping and Identification of Homegardens as a Component of the Trees Outside Forests Using Remote Sensing and Geographic Information System [Article]. *Journal of the Indian Society of Remote Sensing*, *42*(1), 233-242. https://doi.org/10.1007/s12524-013-0310-3

Dash, J. P. (2020). *On the Detection and Monitoring of Invasive Exotic Conifers in New Zealand Using Remote Sensing.* University of Canterbury. https://ir.canterbury.ac.nz/bitstream/handle/10092/101329/Dash%2C%20Jonathan_Final%20PhD%20Thesis.pdf?sequence=1&isAllowed=y

Dash, J. P., Watt, M. S., Paul, T. S. H., Morgenroth, J., & Pearse, G. D. (2019). Early Detection of Invasive Exotic Trees Using UAV and Manned Aircraft Multispectral and LiDAR Data. *Remote Sensing*, *11*(15). https://doi.org/10.3390/rs11151812

De Luca, G., M. N. Silva, J., Di Fazio, S., & Modica, G. (2022). Integrated use of Sentinel-1 and Sentinel-2 data and open-source machine learning algorithms for land cover mapping in a Mediterranean region. *European Journal of Remote Sensing*, *55*(1), 52-70. https://doi.org/10.1080/22797254.2021.2018667

De Souza Mendes, F., Baron, D., Gerold, G., Liesenberg, V., & Erasmi, S. (2019). Optical and SAR Remote Sensing Synergism for Mapping Vegetation Types in the Endangered Cerrado/Amazon Ecotone of Nova Mutum—Mato Grosso. *Remote Sensing*, *11*(10). https://mdpi-res.com/d_attachment/remotesensing/remotesensing-11-01161/article_deploy/remotesensing-11-01161.pdf?version=1557913881

Defries, R. S., & Hansen, M. C. (2010). ISLSCP II University of Maryland Global Land Cover Classifications, 1992-1993. In: ORNL Distributed Active Archive Center.

Deng, X., Guo, S., Sun, L., & Chen, J. (2020). Identification of Short-Rotation Eucalyptus Plantation at Large Scale Using Multi-Satellite Imageries and Cloud Computing Platform. *Remote Sensing*, *12*(13). https://doi.org/10.3390/rs12132153

Deng, X. P., Guo, S. X., Sun, L. Y., & Chen, J. S. (2020). Identification of Short-Rotation Eucalyptus Plantation at Large Scale Using Multi-Satellite Imageries and Cloud Computing Platform [Article]. *Remote Sensing*, *12*(13), 18, Article 2153. https://doi.org/10.3390/rs12132153

Dong, J. W., Xiao, X. M., Menarguez, M. A., Zhang, G. L., Qin, Y. W., Thau, D., Biradar, C., & Moore, B. (2016). Mapping paddy rice planting area in northeastern Asia with Landsat 8 images, phenology-based algorithm and Google Earth Engine [Article]. *Remote Sensing of Environment*, *185*, 142-154. https://doi.org/10.1016/j.rse.2016.02.016

Dupuis, C., Lejeune, P., Michez, A., & Fayolle, A. (2020). How Can Remote Sensing Help Monitor Tropical Moist Forest Degradation?—A Systematic Review. *Remote Sensing*, *12*(7). https://doi.org/10.3390/rs12071087

Earth Resources Observation And Science (EROS) Center. (2017). *Global Land Cover Characterization (GLCC)* U.S. Geological Survey. https://doi.org/10.5066/F7GB230D

Edirisinghe, N. (2017). *Enrichment of Pine Plantations of Sri Lanka with native species* https://www.apfnet.cn/uploads/file/20170425/1493111411376528.pdf

Elmes, A., Alemohammad, H., Avery, R., Caylor, K., Eastman, J. R., Fishgold, L., Friedl, M. A., Jain, M., Kohli, D., Laso Bayas, J. C., Lunga, D., McCarty, J. L., Pontius, R. G., Reinmann, A. B., Rogan, J., Song, L., Stoynova, H., Ye, S., Yi, Z.-F., & Estes, L. (2020). Accounting for Training Data Error in Machine Learning Applied to Earth Observations. *Remote Sensing*, *12*(6), 1034. https://www.mdpi.com/2072-4292/12/6/1034

Erasmi, S., Kappas, M., Twele, A., & Ardiansyah, M. (2007). From global to regional scale: Remote sensing-based concepts and methods for mapping land-cover and land-cover change in tropical regions. In T. Tscharntke, C. Leuschner, M. Zeller, E. Guhardja, & A. Bidin (Eds.), *Stability of Tropical Rainforest Margins: Linking Ecological,*

Economic and Social Constraints of Land Use and Conservation (pp. 435-460). Springer https://doi.org/10.1007/978-3-540-30290-2_21

European Space Agency. *Overview*. Retrieved November 6 from http://www.esa.int/Applications/Observing_the_Earth/Copernicus/Overview4.

Evans, T. L., & Costa, M. (2013). Landcover classification of the Lower Nhecolândia subregion of the Brazilian Pantanal Wetlands using ALOS/PALSAR, RADARSAT-2 and ENVISAT/ASAR imagery. *Remote Sensing of Environment*, *128*, 118-137. https://doi.org/https://doi.org/10.1016/j.rse.2012.09.022

Farr, T. G., Rosen, P. A., Caro, E., Crippen, R., Duren, R., Hensley, S., Kobrick, M., Paller, M., Rodriguez, E., Roth, L., Seal, D., Shaffer, S., Shimada, J., Umland, J., Werner, M., Oskin, M., Burbank, D., & Alsdorf, D. . (2007). The Shuttle Radar Topography Mission. *Reviews of Geophysics*, *45*(2). https://doi.org/10.1029/2005rg000183

Feng, Q., Liu, J., & Gong, J. (2015). UAV Remote Sensing for Urban Vegetation Mapping Using Random Forest and Texture Analysis. *Remote Sensing*, *7*(1), 1074-1094. https://www.mdpi.com/2072-4292/7/1/1074

Foody, G. M. (2002). Status of land cover classification accuracy assessment. *Remote Sensing of Environment*, *80*(1), 185-201. https://doi.org/https://doi.org/10.1016/S0034-4257(01)00295-4

Foody, G. M. (2003). Remote sensing of tropical forest environments: Towards the monitoring of environmental resources for sustainable development. *International Journal of Remote Sensing*, *24*(20), 4035-4046. https://doi.org/10.1080/0143116031000103853

Foody, G. M. (2020). Explaining the unsuitability of the kappa coefficient in the assessment and comparison of the accuracy of thematic maps obtained by image classification. *Remote Sensing of Environment*, *239*, 111630. https://doi.org/https://doi.org/10.1016/j.rse.2019.111630

Forkuor, G., Dimobe, K., Serme, I., & Tondoh, J. E. (2018). Landsat-8 vs. Sentinel-2: examining the added value of sentinel-2's red-edge bands to land-use and land-cover mapping in Burkina Faso. *Giscience & Remote Sensing*, *55*(3), 331-354. https://doi.org/10.1080/15481603.2017.1370169

Förster, M., Gränzig geb. Schmidt, T., Wolf, R., Kleinschmit, B., Fassnacht, F., Cabezas Peña, J., & Kattenborn, T. (2017). *Detecting the spread of invasive species in central Chile with a Sentinel-2 time-series* 9th International Workshop on the Analysis of Multitemporal Remote Sensing Images (MultiTemp), Brugge, Belgium. https://ieeexplore.ieee.org/document/8035216

Franklin, S. E. (2001). *Remote Sensing for Sustainable Forest Management* (1st ed.). Lewis Publishers.

Friedl, M., & Sulla-Menashe, D. (2019). *MCD12Q1 MODIS/Terra+Aqua Land Cover Type Yearly L3 Global 500m SIN Grid V006*. https://doi.org/10.5067/MODIS/MCD12Q1.006

Gavier-Pizarro, G. I., Kuemmerle, T., Hoyos, L. E., Stewart, S. I., Huebner, C. D., Keuler, N. S., & Radeloff, V. C. (2012). Monitoring the invasion of an exotic tree (Ligustrum lucidum) from 1983 to 2006 with Landsat TM/ETM+ satellite data and Support Vector

Machines in Córdoba, Argentina. *Remote Sensing of Environment*, *122*, 134-145. https://doi.org/https://doi.org/10.1016/j.rse.2011.09.023

GeoNadir. (2023). *The global home of drone mapping data*. Retrieved 10th of May from https://geonadir.com/

Gómez, C., Wulder, M. A., White, J. C., Montes, F., & Delgado, J. A. (2012). Characterizing 25 years of change in the area, distribution, and carbon stock of Mediterranean pines in Central Spain. *International Journal of Remote Sensing*, *33*(17), 5546-5573. https://doi.org/10.1080/01431161.2012.663115

Goncalves, V. P., Ribeiro, E. A., & Imai, N. N. (2022). Mapping Areas Invaded by Pinus sp. from Geographic Object-Based Image Analysis (GEOBIA) Applied on RPAS (Drone) Color Images. *Remote Sensing*, *14*(12). https://doi.org/10.3390/rs14122805

Gong, P., Yu, L., Li, C., Wang, J., Liang, L., Li, X., Ji, L., Bai, Y., Cheng, Y., & Zhu, Z. (2016). A new research paradigm for global land cover mapping. *Annals of GIS*, *22*(2), 87-102. https://doi.org/10.1080/19475683.2016.1164247

Gorelick, N., Hancher, M., Dixon, M., Ilyushchenko, S., Thau, D., & Moore, R. (2017). Google Earth Engine: Planetary-scale geospatial analysis for everyone. *Remote Sensing of Environment*, *202*, 18-27. https://doi.org/https://doi.org/10.1016/j.rse.2017.06.031

Green, K. (2017). *Imagery and GIS : best practices for extracting information from imagery*. Esri Press.

Hall-Beyer, M. (2017). Practical guidelines for choosing GLCM textures to use in landscape classification tasks over a range of moderate spatial scales. *International Journal of Remote Sensing*, *38*(5), 1312-1338. https://doi.org/10.1080/01431161.2016.1278314

Hansen, M. C., Potapov, P. V., Moore, R., Hancher, M., Turubanova, S. A., Tyukavina, A., Thau, D., Stehman, S. V., Goetz, S. J., Loveland, T. R., Kommareddy, A., Egorov, A., Chini, L., Justice, C. O., & Townshend, J. R. G. (2013). High-Resolution Global Maps of 21st-Century Forest Cover Change. *Science*, *342*(6160), 850. https://doi.org/10.1126/science.1244693

Hanson, C. C., Brabyn, L., & Gurung, S. B. (2022). Diversity-accuracy assessment of multiple classifier systems for the land cover classification of the Khumbu region in the Himalayas. *Journal of Mountain Science*, *19*(2), 365-387. https://doi.org/10.1007/s11629-021-7130-7

Haralick, R. M., Shanmugam, K., & Dinstein, I. (1973). Textural Features for Image Classification. *IEEE Transactions on Systems, Man, and Cybernetics*, *SMC-3*(6), 610-621. https://doi.org/10.1109/TSMC.1973.4309314

Haregeweyn, N., Tsunekawa, A., Tsubo, M., Meshesha, D., & Melkie, A. (2013). Analysis of the invasion rate, impacts and control measures of Prosopis juliflora: a case study of Amibara District, Eastern Ethiopia. *Environmental Monitoring and Assessment*, *185*(9), 7527-7542. https://doi.org/10.1007/s10661-013-3117-3

Higgins, S. I., & Richardson, D. M. (1998). Pine Invasions in the Southern Hemisphere: Modelling Interactions between Organism, Environment and Disturbance. *Plant Ecology*, *135*(1), 79-93. http://www.jstor.org/stable/20050598

Holtgrave, A.-K., Röder, N., Ackermann, A., Erasmi, S., & Kleinschmit, B. (2020). Comparing Sentinel-1 and -2 Data and Indices for Agricultural Land Use Monitoring. *Remote Sensing*, *12*, 2919. https://doi.org/10.3390/rs12182919

Huang, X., Ziniti, B., Torbick, N., & Ducey, M. (2018). Assessment of Forest above Ground Biomass Estimation Using Multi-Temporal C-band Sentinel-1 and Polarimetric L-band PALSAR-2 Data. *Remote Sensing*, *10*, 1424. https://doi.org/10.3390/rs10091424

Immitzer, M., Neuwirth, M., Böck, S., Brenner, H., Vuolo, F., & Atzberger, C. (2019). Optimal Input Features for Tree Species Classification in Central Europe Based on Multi-Temporal Sentinel-2 Data. *Remote Sensing*, *11*(22), 2599. https://www.mdpi.com/2072-4292/11/22/2599

Immitzer, M., Vuolo, F., & Atzberger, C. (2016). First Experience with Sentinel-2 Data for Crop and Tree Species Classifications in Central Europe. *Remote Sensing*, *8*(3), 166. https://www.mdpi.com/2072-4292/8/3/166

Ingram, J. C., Dawson, T. P., & Whittaker, R. J. (2005). Mapping tropical forest structure in southeastern Madagascar using remote sensing and artificial neural networks. *Remote Sensing of Environment*, *94*(4), 491-507. https://doi.org/https://doi.org/10.1016/j.rse.2004.12.001

Jahromi, M. N., Jahromi, M. N., Zolghadr-Asli, B., Pourghasemi, H. R., & Alavipanah, S. K. (2020). Google Earth Engine and Its Application in Forest Sciences. In (pp. 629-649). Cham: Springer International Publishing.

Janssen, L. L. F., & van der Wel, F. (1994). Accuracy assessment of satellite derived land-cover data: A review. *Photogramm. Eng. Remote Sensing 60 (1994) 419-426.*, *60*.

Jayawardane, S. S. B. D. G., & Weerasena, L. A. (2000). Crop Diversification in Sri Lanka. Crop Diversification in the Asia-Pacific Region., Bangkok.

Jayawardhane, J., & Gunaratne, A. (2020). Restoration Success Evaluation of a Thinned and Enriched Pine Plantation in Sri Lanka. *Journal of Tropical Forest Science*, *32*(4), 402-413. https://www.jstor.org/stable/26940730

Jensen, J. R. (2016). *Introductory digital image processing: a remote sensing perspective*. Pearson education.

Jiao, X., McNairn, H., Yekkehkhany, B., Dingle Robertson, L., & Ihuoma, S. (2022). Integrating Sentinel-1 SAR and Sentinel-2 optical imagery with a crop structure dynamics model to track crop condition. *International Journal of Remote Sensing*, *43*(17), 6509-6537. https://doi.org/10.1080/01431161.2022.2142077

Johansen, K., Phinn, S., & Taylor, M. F. J. (2015). Mapping woody vegetation clearing in Queensland, Australia from Landsat imagery using the Google Earth Engine. *Remote Sensing Applications: Society and Environment*, *1*, 36-49.

Jucker, T., Caspersen, J., Chave, J., Antin, C., Barbier, N., Bongers, F., Dalponte, M., van Ewijk, K. Y., Forrester, D. I., Haeni, M., Higgins, S. I., Holdaway, R. J., Iida, Y., Lorimer, C., Marshall, P. L., Momo, S., Moncrieff, G. R., Ploton, P., Poorter, L., Rahman, K. A., Schlund, M., Sonké, B., Sterck, F. J., Trugman, A. T., Usoltsev, V. A., Vanderwel, M. C., Waldner, P., Wedeux, B. M. M., Wirth, C., Wöll, H., Woods, M., Xiang, W., Zimmermann, N. E., & Coomes, D. A. (2017). Allometric equations for

integrating remote sensing imagery into forest monitoring programmes. *Global Change Biology*, *23*(1), 177-190. https://doi.org/https://doi.org/10.1111/gcb.13388

Kamga, M. A., Nguemhe Fils, S. C., Ayodele, M. O., Olatubara, C. O., Nzali, S., Adenikinju, A., & Khalifa, M. (2020). Evaluation of land use/land cover changes due to gold mining activities from 1987 to 2017 using landsat imagery, East Cameroon. *GeoJournal*, *85*(4), 1097-1114. https://doi.org/10.1007/s10708-019-10002-8

Kaplan, G. (2021). Broad-Leaved and Coniferous Forest Classification in Google Earth Engine Using Sentinel Imagery. *Environmental Sciences Proceedings*, *3*(1), 64. https://www.mdpi.com/2673-4931/3/1/64

Kauth, R. J., & Thomas, G. S. P. (1976). The Tasselled Cap -- A Graphic Description of the Spectral-Temporal Development of Agricultural Crops as Seen by Landsat. Symposium on Machine Processing of Remotely Sensed Data, West Lafayette, Indiana.

Kehlenbeck, K., & Maass, B. L. (2004). Crop diversity and classification of homegardens in Central Sulawesi, Indonesia. *Agroforestry systems*, *63*(1), 53-62. https://doi.org/10.1023/B:AGFO.0000049433.95038.25

Khare, S., Latifi, H., & Ghosh, S. K. (2018). Multi-scale assessment of invasive plant species diversity using Pléiades 1A, RapidEye and Landsat-8 data. *Geocarto International*, *33*(7), 681-698. https://doi.org/10.1080/10106049.2017.1289562

Kim, Y., & Zyl, J. J. v. (2009). A Time-Series Approach to Estimate Soil Moisture Using Polarimetric Radar Data. *IEEE Transactions on Geoscience and Remote Sensing*, *47*(8), 2519-2527. https://doi.org/10.1109/TGRS.2009.2014944

Kumar, B. M., & Nair, P. K. R. (2006). Introduction. In B. M. Kumar & P. K. R. Nair (Eds.), *Tropical Homegardens: A Time-Tested Example of Sustainable Agroforestry* (pp. 1-10). Springer Netherlands. https://doi.org/10.1007/978-1-4020-4948-4_1

Kumar, L., & Mutanga, O. (2018). Google Earth Engine Applications Since Inception: Usage, Trends, and Potential. *Remote Sensing*, *10*(10), 1509. https://www.mdpi.com/2072-4292/10/10/1509

Kumar, S. D., Sitiraju, S., & Sharma, J. (2013). *Radar Vegetation Index as an Alternative to NDVI for Monitoring of Soyabean and Cotton* XXXIII INCA International Congress, Jodhpur.

Kumar, V., Sharma, A., Bhardwaj, R., & Thukral, A. K. (2018). Comparison of different reflectance indices for vegetation analysis using Landsat-TM data. *Remote Sensing Applications: Society and Environment*, *12*, 70-77. https://doi.org/https://doi.org/10.1016/j.rsase.2018.10.013

Kumara, C. (2010). *Effectiveness of Establishing Forest Buffer Zones as a Community Forest Management Approach a Case Study from the Sripada Tropical Peak Wilderness Sanctuary in Sri Lanka.* University of Agder.

Kuplich, T. M., Curran, P. J., & Atkinson, P. M. (2005). Relating SAR image texture to the biomass of regenerating tropical forests. *International Journal of Remote Sensing*, *26*(21), 4829-4854. https://doi.org/10.1080/01431160500239107

Labonté, J., Drolet, G., Sylvain, J.-D., Thiffault, N., Hébert, F., & Girard, F. (2020). Phenology-Based Mapping of an Alien Invasive Species Using Time Series of Multispectral

Satellite Data: A Case-Study with Glossy Buckthorn in Québec, Canada. *Remote Sensing*, *12*(6), 922. https://www.mdpi.com/2072-4292/12/6/922

Lafortezza, R., Chen, J., Crow, T. R., & Sanesi, G. (2008). *Patterns and Processes in Forest Landscapes: Multiple Use and Sustainable Management* (1. Aufl. ed.). Springer Netherlands.

Land Use Policy Planning Department. (2020). *Data and Information of Home Gardens in ratnapura District*. (Annex 24). Ministry of Lands and Land Development

Lapini, A., Pettinato, S., Santi, E., Paloscia, S., Fontanelli, G., & Garzelli, A. (2020). Comparison of Machine Learning Methods Applied to SAR Images for Forest Classification in Mediterranean Areas. *Remote Sensing*, *12*(3). https://mdpi-res.com/d_attachment/remotesensing/remotesensing-12-00369/article_deploy/remotesensing-12-00369-v2.pdf?version=1580641917

Lechner, A., Foody, G., & Boyd, D. (2020). Applications in Remote Sensing to Forest Ecology and Management. *One Earth*, *2*, 405-412. https://doi.org/10.1016/j.oneear.2020.05.001

Lee, J., Cardille, J. A., & Coe, M. T. (2018). BULC-U: Sharpening Resolution and Improving Accuracy of Land-Use/Land-Cover Classifications in Google Earth Engine. *Remote Sensing*, *10*(9). https://doi.org/10.3390/rs10091455

Lehmler, S., Förster, M., & Frick, A. (2022). *Modelling green volume using Sentinel-1, -2, PALSAR-2 satellite data and machine learning for urban and semi-urban areas in Germany*. Research Square Platform LLC. https://dx.doi.org/10.21203/rs.3.rs-2349291/v1

Li, G., Lu, D., Moran, E., Dutra, L., & Batistella, M. (2012). A comparative analysis of ALOS PALSAR L-band and RADARSAT-2 C-band data for land-cover classification in a tropical moist region. *ISPRS Journal of Photogrammetry and Remote Sensing*, *70*, 26-38. https://doi.org/https://doi.org/10.1016/j.isprsjprs.2012.03.010

Lien, P. T. H. (2018). *Mapping Vegetation With Remote Sensing And Gis Data Using Object-Based Analysis And Machine Learning Algorithms*. University of Waikato.

Lim, K., Treitz, P., Wulder, M., St-Onge, B., & Flood, M. (2003). LiDAR remote sensing of forest structure. *Progress in Physical Geography: Earth and Environment*, *27*(1), 88-106. https://doi.org/10.1191/0309133303pp360ra

Lindström, S., Mattsson, E., & Nissanka, S. P. (2012). Forest cover change in Sri Lanka: The role of small scale farmers. *Applied Geography*, *34*, 680-692. https://doi.org/https://doi.org/10.1016/j.apgeog.2012.04.011

Ling, F., Li, Z., Chen, E., & Wang, Q. (2009, October 26-30). Comparison of ALOS PALSAR RVI and Landsat TM NDVI for forest area mapping. 2009 2nd Asian-Pacific Conference on Synthetic Aperture Radar, Xi'an, China.

Liu, L., Guo, Y., Li, Y., Zhang, Q., Li, Z., Chen, E., Yang, L., & Mu, X. (2022). Comparison of Machine Learning Methods Applied on Multi-Source Medium-Resolution Satellite Images for Chinese Pine (Pinus tabulaeformis) Extraction on Google Earth Engine. *Forests*, *13*(5). https://doi.org/10.3390/f13050677

Liu, Y., Gong, W., Hu, X., & Gong, J. (2018). Forest Type Identification with Random Forest Using Sentinel-1A, Sentinel-2A, Multi-Temporal Landsat-8 and DEM Data. *Remote Sensing*, *10*(6), 946. https://www.mdpi.com/2072-4292/10/6/946

Lopes, M., Frison, P.-L., Crowson, M., Warren-Thomas, E., Hariyadi, B., Kartika, W. D., Agus, F., Hamer, K. C., Stringer, L., Hill, J. K., & Pettorelli, N. (2020). Improving the accuracy of land cover classification in cloud persistent areas using optical and radar satellite image time series [https://doi.org/10.1111/2041-210X.13359]. *Methods in Ecology and Evolution*, *11*(4), 532-541. https://doi.org/https://doi.org/10.1111/2041-210X.13359

Lukeš, P., Stenberg, P., Rautiainen, M., Mõttus, M., & Vanhatalo, K. M. (2013). Optical properties of leaves and needles for boreal tree species in Europe. *Remote Sensing Letters*, *4*(7), 667-676. https://doi.org/10.1080/2150704X.2013.782112

Marcel, B., Bruno, S., Luc, B., Bert, D. R., Myroslava, L., Nandin-Erdene, T., Martin, H., & Steffen, F. (2020). *Copernicus Global Land Service: Land Cover 100m: collection 3: epoch 2019: Globe*. https://doi.org/10.5281/zenodo.3939050

Martin, M., Geiger, K., Singhakumara, B. M. P., & Ashton, M. S. (2019). Quantitatively characterizing the floristics and structure of a traditional homegarden in a village landscape, Sri Lanka. *Agroforestry systems*, *93*(4), 1439-1454. https://doi.org/10.1007/s10457-018-0254-2

Mathieu, R., Freeman, C., & Aryal, J. (2007). Mapping private gardens in urban areas using object-oriented techniques and very high-resolution satellite imagery. *Landscape and Urban Planning*, *81*(3), 179-192. https://doi.org/https://doi.org/10.1016/j.landurbplan.2006.11.009

Mattsson, E., Ostwald, M., Nissanka, S. P., & Marambe, B. (2013). Homegardens as a Multi-functional Land-Use Strategy in Sri Lanka with Focus on Carbon Sequestration. *Ambio*, *42*(7), 892-902. https://doi.org/10.1007/s13280-013-0390-x

McEwan, A., Marchi, E., Spinelli, R., & Brink, M. (2020). Past, present and future of industrial plantation forestry and implication on future timber harvesting technology. *Journal of Forestry Research*, *31*(2), 339-351. https://doi.org/10.1007/s11676-019-01019-3

Medawatte, W., Tennakoon, K., Hulme, P., Gunatilleke, C., & Gunatilleke, I. (2010). Is Caribbean pine invading grasslands in the Knuckles range. *Invasive alien species–strengthening capacity to control introduction and spread in Sri Lanka*, 131-140.

Mensah, A. A., Akoto Sarfo, D., & Partey, S. T. (2019). Assessment of vegetation dynamics using remote sensing and GIS: A case of Bosomtwe Range Forest Reserve, Ghana. *The Egyptian Journal of Remote Sensing and Space Science*, *22*(2), 145-154. https://doi.org/https://doi.org/10.1016/j.ejrs.2018.04.004

Mertes, C. M., Schneider, A., Sulla-Menashe, D., Tatem, A. J., & Tan, B. (2015). Detecting change in urban areas at continental scales with MODIS data. *Remote Sensing of Environment*, *158*, 331-347. https://doi.org/10.1016/j.rse.2014.09.023

Metrikaityte, G., Suziedelyte Visockiene, J., & Papsys, K. (2022). Digital Mapping of Land Cover Changes Using the Fusion of SAR and MSI Satellite Data. *Land*, *11*(7).

Microsoft. (2023). *A Planetary Computer for a Sustainable Future*. Retrieved 12th of May from https://planetarycomputer.microsoft.com/A Planetary Computer for a Sustainable Future

Miettinen, J., Stibig, H.-J., & Achard, F. (2014). Remote sensing of forest degradation in Southeast Asia—Aiming for a regional view through 5–30 m satellite data. *Global*

Ecology and Conservation, *2*, 24-36. https://doi.org/https://doi.org/10.1016/j.gecco.2014.07.007

Mishra, S., Shrivastava, P., & Dhurvey, P. (2017). Change detection techniques in remote sensing: A review. *International Journal of Wireless and Mobile communication for Industrial systems*, *4*(1), 1-8.

Mitchell, A. L., Rosenqvist, A., & Mora, B. (2017). Current remote sensing approaches to monitoring forest degradation in support of countries measurement, reporting and verification (MRV) systems for REDD+. *Carbon Balance and Management*, *12*(1), 9. https://doi.org/10.1186/s13021-017-0078-9

Mngadi, M., Odindi, J., Peerbhay, K., & Mutanga, O. (2021). Examining the effectiveness of Sentinel-1 and 2 imagery for commercial forest species mapping. *Geocarto International*, *36*(1), 1-12. https://doi.org/10.1080/10106049.2019.1585483

Mohamed, S. A., & El-Raey, M. E. (2019). Land cover classification and change detection analysis of Qaroun and Wadi El-Rayyan lakes using multi-temporal remotely sensed imagery. *Environmental Monitoring and Assessment*, *191*(4), 229. https://doi.org/10.1007/s10661-019-7339-x

Mondal, P., McDermid, S. S., & Qadir, A. (2020). A reporting framework for Sustainable Development Goal 15: Multi-scale monitoring of forest degradation using MODIS, Landsat and Sentinel data. *Remote Sensing of Environment*, *237*, 111592. https://doi.org/https://doi.org/10.1016/j.rse.2019.111592

Morin, D., Planells, M., Guyon, D., Villard, L., Mermoz, S., Bouvet, A., Thevenon, H., Dejoux, J.-F., Le Toan, T., & Dedieu, G. (2019). Estimation and Mapping of Forest Structure Parameters from Open Access Satellite Images: Development of a Generic Method with a Study Case on Coniferous Plantation. *Remote Sensing*, *11*(11). https://mdpi-res.com/d_attachment/remotesensing/remotesensing-11-01275/article_deploy/remotesensing-11-01275.pdf?version=1559124264

Muchoney, D. M., & Haack, B. N. (1994). Change detection for monitoring forest defoliation. *Photogrammetric engineering and remote sensing*, *60*(10), 1243-1252.

Müller, H., Rufin, P., Griffiths, P., Barros Siqueira, A. J., & Hostert, P. (2015). Mining dense Landsat time series for separating cropland and pasture in a heterogeneous Brazilian savanna landscape. *Remote Sensing of Environment*, *156*, 490-499. https://doi.org/https://doi.org/10.1016/j.rse.2014.10.014

Nandasena, W. D. K. V., Brabyn, L., & Serrao-Neumann, S. (2020). Using Remote Sensing for Sustainable Forest Management in Developing Countries. In *The Palgrave Handbook of Global Sustainability* (pp. 1-22). Springer International Publishing. https://doi.org/10.1007/978-3-030-38948-2_35-1

Nasirzadehdizaji, R., Balik Sanli, F., Abdikan, S., Cakir, Z., Sekertekin, A., & Ustuner, M. (2019). Sensitivity Analysis of Multi-Temporal Sentinel-1 SAR Parameters to Crop Height and Canopy Coverage. *Applied Sciences*, *9*(4). https://mdpi-res.com/d_attachment/applsci/applsci-09-00655/article_deploy/applsci-09-00655.pdf?version=1550208973

Nissanka, S. P., Mohotti, K., & Wijetunga, A. (2005). Alleopathic influences of Pinus caribea on vegetation regeneration and soil biodiversity. Fourth World Congress on Allelopathy, Wagga Wagga, NSW, Australia.

Nordin, S. A., Abd Latif, Z., & Omar, H. (2019). Individual tree crown segmentation in tropical peat swamp forest using airborne hyperspectral data. *Geocarto International*, *34*(11), 1218-1236. https://doi.org/10.1080/10106049.2018.1475511

Office of the Cabinet of Ministers-Sri Lanka (2017). *Conversion of the Pinus Plantation in Sri Lanka into a Plantation of indigenous plant species*. Office of the Cabinet of Ministers-Sri Lanka Retrieved from http://www.cabinetoffice.gov.lk/cab/index.php?option=com_content&view=article&id=16&Itemid=49&lang=en&dID=8386

Omar, H., Misman, M. A., & Kassim, A. R. (2017). Synergetic of PALSAR-2 and Sentinel-1A SAR Polarimetry for Retrieving Aboveground Biomass in Dipterocarp Forest of Malaysia. *Applied Sciences*, *7*(7). https://mdpi-res.com/d_attachment/applsci/applsci-07-00675/article_deploy/applsci-07-00675.pdf?version=1498827928

Ouma, Y. O., Tetuko, J., & Tateishi, R. (2008). Analysis of co-occurrence and discrete wavelet transform textures for differentiation of forest and non-forest vegetation in very-high-resolution optical-sensor imagery. *International Journal of Remote Sensing*, *29*(12), 3417-3456. https://doi.org/10.1080/01431160701601782

Palo, M., & Mery, G. (1996). Transition from deforestation to sustainable forestry -a distant dream? In M. Palo & G. Mery (Eds.), *Sustainable Forestry Challenges for Developing Countries* (Vol. 10, pp. 1-13). Kluwer Academic Publishers.

Pauchard, A., Escudero, A., García, R. A., de la Cruz, M., Langdon, B., Cavieres, L. A., & Esquivel, J. (2016). Pine invasions in treeless environments: dispersal overruns microsite heterogeneity. *Ecology and Evolution*, *6*(2), 447-459. https://doi.org/10.1002/ece3.1877

Pauchard, A., García, R., Zalba, S., Sarasola, M., Zenni, R., Ziller, S., & Nuñez, M. A. (2016). Pine Invasions in South America: Reducing Their Ecological Impacts Through Active Management. In J. Canning-Clode (Ed.), *Biological Invasions in Changing Ecosystems: Vectors, Ecological Impacts, Management and Predictions* (pp. 318-342). De Gruyter Open Poland. https://doi.org/10.1515/9783110438666-020

Perera, A. (2001). Perera, G.A.D. 2001. Secondary forest situation in Sri Lanka: a review. Journal of Tropical Forest Science, 13(4): 768-785. *Journal of Tropical Forest Science*, *13*, 768-785.

Perera, A. H., & Rajapakse, R. M. N. (1991). A baseline study of Kandyan Forest Gardens of Sri Lanka: Structure, composition and utilization. *Forest Ecology and Management*, *45*(1), 269-280. https://doi.org/https://doi.org/10.1016/0378-1127(91)90222-H

Perera, K., Herath, S., Apan, A., & Tateishi, R. (2012). Application of Modis Data to Assess the Latest Forest Cover Changes of Sri Lanka. *ISPRS Ann. Photogramm. Remote Sens. Spatial Inf. Sci.*, *I-7*, 165-170. https://doi.org/10.5194/isprsannals-I-7-165-2012

Perera, K., & Tsuchiya, K. (2009). Experiment for mapping land cover and it's change in southeastern Sri Lanka utilizing 250m resolution MODIS imageries. *Advances in Space Research*, *43*(9), 1349-1355. https://doi.org/https://doi.org/10.1016/j.asr.2008.12.016

Pérez-Hoyos, A., Rembold, F., Kerdiles, H., & Gallego, J. (2017). Comparison of Global Land Cover Datasets for Cropland Monitoring. *Remote Sensing*, *9*(11). https://doi.org/10.3390/rs9111118

Perry, D. A. (1994). *Forest Ecosystems*. Johns Hopkins University Press.

Petersen, R., Goldman, E. D., Harris, N. L., Sargent, S. N., Aksenov, D., Manisha, A., Esipova, E., Shevade, V. S., Loboda, T. V., Kuksina, N., & Kurakina, I. (2016). Mapping Tree Plantations with Multispectral Imagery: Preliminary Results for Seven Tropical Countries.

Peterson, E. B. (2005). Estimating cover of an invasive grass (Bromus tectorum) using tobit regression and phenology derived from two dates of Landsat ETM+ data. *International Journal of Remote Sensing*, *26*(12), 2491-2507. https://doi.org/10.1080/01431160500127815

Pham, L. H., Pham, L. T. H., Dang, T. D., Tran, D. D., & Dinh, T. Q. (2022). Application of Sentinel-1 data in mapping land-use and land cover in a complex seasonal landscape: a case study in coastal area of Vietnamese Mekong Delta. *Geocarto International*, *37*(13), 3743-3760. https://doi.org/10.1080/10106049.2020.1869329

Pham, T. D., Yokoya, N., Xia, J., Ha, N. T., Le, N. N., Nguyen, T. T., Dao, T. H., Vu, T. T., Pham, T. D., & Takeuchi, W. (2020). Comparison of Machine Learning Methods for Estimating Mangrove Above-Ground Biomass Using Multiple Source Remote Sensing Data in the Red River Delta Biosphere Reserve, Vietnam. *Remote Sensing*, *12*(8). https://mdpi-res.com/d_attachment/remotesensing/remotesensing-12-01334/article_deploy/remotesensing-12-01334.pdf?version=1587650177

Piiroinen, R., Fassnacht, F. E., Heiskanen, J., Maeda, E., Mack, B., & Pellikka, P. (2018). Invasive tree species detection in the Eastern Arc Mountains biodiversity hotspot using one class classification. *Remote Sensing of Environment*, *218*, 119-131. https://doi.org/https://doi.org/10.1016/j.rse.2018.09.018

Poortinga, A., Tenneson, K., Shapiro, A., Nquyen, Q., San Aung, K., Chishtie, F., & Saah, D. (2019). Mapping Plantations in Myanmar by Fusing Landsat-8, Sentinel-2 and Sentinel-1 Data along with Systematic Error Quantification. *Remote Sensing*, *11*(7), 831. https://www.mdpi.com/2072-4292/11/7/831

Potapov, P., Li, X., Hernandez-Serna, A., Tyukavina, A., Hansen, M. C., Kommareddy, A., Pickens, A., Turubanova, S., Tang, H., Silva, C. E., Armston, J., Dubayah, R., Blair, J. B., & Hofton, M. (2021). Mapping global forest canopy height through integration of GEDI and Landsat data. *Remote Sensing of Environment*, *253*, 112165. https://doi.org/https://doi.org/10.1016/j.rse.2020.112165

Premakantha, K. T., Puspakumara, D. K. N. G., & Dayawansa, N. (2009). Identification of Tree Resources Outside Forest in up country of Sri Lanka using medium resolution satellite imagery. *Tropical agricultural research*, *20*, 354-365.

Pu, R., Gong, P., Tian, Y., Miao, X., Carruthers, R. I., & Anderson, G. L. (2008). Invasive species change detection using artificial neural networks and CASI hyperspectral imagery. *Environmental Monitoring and Assessment*, *140*(1), 15-32. https://doi.org/10.1007/s10661-007-9843-7

Puetz, A., & Olsen, R. (2006). *Haralick texture features expanded into the spectral domain* (Vol. 6233). SPIE. https://doi.org/10.1117/12.665699

Punyawardena, B. V. R. (2020). Climate. In R. B. Mapa (Ed.), *The Soils of Sri Lanka* (pp. 13-22). Springer International Publishing. https://doi.org/10.1007/978-3-030-44144-9_2

Pushpakumara, D., Marambe, B., Gllp, S., Weerahewa, J., & Bvr, P. (2012). A review research on homegardens in Sri Lanka: the status, importance and future perspective. *Tropical Agriculturist*, *160*, 55-125.

Qin, Y., Xiao, X., Dong, J., Zhang, G., Shimada, M., Liu, J., Li, C., Kou, W., & Moore, B. (2015). Forest cover maps of China in 2010 from multiple approaches and data sources: PALSAR, Landsat, MODIS, FRA, and NFI. *ISPRS Journal of Photogrammetry and Remote Sensing*, *109*, 1-16. https://doi.org/https://doi.org/10.1016/j.isprsjprs.2015.08.010

Ranagalage, M., Gunarathna, M. H. J. P., Surasinghe, T. D., Dissanayake, D., Simwanda, M., Murayama, Y., Morimoto, T., Phiri, D., Nyirenda, V. R., Premakantha, K. T., & Sathurusinghe, A. (2020). Multi-Decadal Forest-Cover Dynamics in the Tropical Realm: Past Trends and Policy Insights for Forest Conservation in Dry Zone of Sri Lanka. *Forests*, *11*(8), 836. https://www.mdpi.com/1999-4907/11/8/836

Rathnayake, C. W., Jones, S., & Soto-Berelov, M. (2020). Mapping Land Cover Change over a 25-Year Period (1993–2018) in Sri Lanka Using Landsat Time-Series. *Land*, *9*(1), 27. https://www.mdpi.com/2073-445X/9/1/27

Rees, W. G. (2013). *Physical Principles of Remote Sensing*. Cambridge University Press.

Rejmánek, M. (2014). Invasive trees and shrubs: where do they come from and what we should expect in the future? *Biological Invasions*, *16*(3), 483-498. https://doi.org/10.1007/s10530-013-0603-z

Rejmánek, M., & Richardson, D. M. (2013). Trees and shrubs as invasive alien species – 2013 update of the global database. *Diversity and Distributions*, *19*(8), 1093-1094. https://doi.org/https://doi.org/10.1111/ddi.12075

Reusing, M. (2000). Change detection of natural high forests in Ethiopia using remote sensing and GIS techniques. *International archives of photogrammetry and remote sensing*, *33*(B7/3; PART 7), 1253-1258.

Richardson, D., Rundel, P., Jackson, S., Teskey, R., Aronson, J., Bytnerowicz, A., Wingfield, M., & Procheş, Ş. (2007). Human Impacts in Pine Forests: Past, Present, and Future. *Annual Review of Ecology, Evolution and Systematics*, *38*, 275-97297. https://doi.org/10.1146/annurev.ecolsys.38.091206.095650

Roberts, D. A., Ustin, S. L., Ogunjemiyo, S., Greenberg, J., Dobrowski, S. Z., Chen, J., & Hinckley, T. M. (2004). Spectral and Structural Measures of Northwest Forest Vegetation at Leaf to Landscape Scales. *Ecosystems*, *7*(5), 545-562. https://doi.org/10.1007/s10021-004-0144-5

Rocchini, D., Petras, V., Petrasova, A., Horning, N., Furtkevicova, L., Neteler, M., Leutner, B., & Wegmann, M. (2017). Open data and open source for remote sensing training in ecology. *Ecological Informatics*, *40*, 57-61. https://doi.org/https://doi.org/10.1016/j.ecoinf.2017.05.004

Sá, N. C. d., Carvalho, S., Castro, P., Marchante, E., & Marchante, H. (2017). Using Landsat Time Series to Understand How Management and Disturbances Influence the Expansion of an Invasive Tree. *IEEE Journal of Selected Topics in Applied Earth Observations and Remote Sensing*, *10*(7), 3243-3253. https://doi.org/10.1109/JSTARS.2017.2673761

Sangakkara, U. R., & Frossard, E. (2016). Characteristics of South Asian rural households and associated home gardens - A case study from Sri Lanka [Article]. *Tropical Ecology*, *57*(4), 765-777. <Go to ISI>://WOS:000397193000014

Sano, E. E., Ferreira, L. G., & Huete, A. R. (2005). Synthetic Aperture Radar (L band) and Optical Vegetation Indices for Discriminating the Brazilian Savanna Physiognomies: A Comparative Analysis. *Earth Interactions*, *9*(15), 1-15. https://doi.org/10.1175/ei117.1

Senanayake, S., Pradhan, B., Huete, A., & Brennan, J. (2020). Assessing Soil Erosion Hazards Using Land-Use Change and Landslide Frequency Ratio Method: A Case Study of Sabaragamuwa Province, Sri Lanka. *Remote sensing (Basel, Switzerland)*, *12*(9), 1483. https://doi.org/10.3390/rs12091483

Senf, C., Pflugmacher, D., Van Der Linden, S., & Hostert, P. (2013). Mapping Rubber Plantations and Natural Forests in Xishuangbanna (Southwest China) Using Multi-Spectral Phenological Metrics from MODIS Time Series. *Remote Sensing*, *5*(6), 2795-2812. https://doi.org/10.3390/rs5062795

Setiani, P., Devianto, L. A., & Ramdani, F. (2021). Rapid estimation of CO2 emissions from forest fire events using cloud-based computation of google earth engine. *Environmental Monitoring and Assessment*, *193*(10), 669. https://doi.org/10.1007/s10661-021-09460-w

Shahfahad, Talukdar, S., Ali, R., Nguyen, K.-A., Naikoo, M. W., Liou, Y.-A., Islam, A. R. M. T., Mallick, J., & Rahman, A. (2022). Monitoring drought pattern for pre- and post-monsoon seasons in a semi-arid region of western part of India. *Environmental Monitoring and Assessment*, *194*(6), 396. https://doi.org/10.1007/s10661-022-10028-5

Shimada, M., Itoh, T., Motooka, T., Watanabe, M., Shiraishi, T., Thapa, R., & Lucas, R. (2014). New global forest/non-forest maps from ALOS PALSAR data (2007–2010). *Remote Sensing of Environment*, *155*, 13-31. https://doi.org/https://doi.org/10.1016/j.rse.2014.04.014

Shimizu, K., Ota, T., & Mizoue, N. (2019). Detecting Forest Changes Using Dense Landsat 8 and Sentinel-1 Time Series Data in Tropical Seasonal Forests. *Remote Sensing*, *11*(16). https://doi.org/10.3390/rs11161899

Signori, L., & Ducati, J. (2019). Spatio-Temporal Mapping of the Invasive Alien Species Pinus Sp in the Northern Area of the Lagoa Do Peixe National Park-Rs. *Revista Árvore*, *43*. https://doi.org/10.1590/1806-90882019000100007

Singh, S. P., Inderjit, Singh, J. S., Majumdar, S., Moyano, J., Nuñez, M. A., & Richardson, D. M. (2018). Insights on the persistence of pines (Pinus species) in the Late Cretaceous and their increasing dominance in the Anthropocene. *Ecology and Evolution*, *8*(20), 10345-10359. https://doi.org/10.1002/ece3.4499

Sothe, C., Almeida, C. M. d., Liesenberg, V., & Schimalski, M. B. (2017). Evaluating Sentinel-2 and Landsat-8 Data to Map Sucessional Forest Stages in a Subtropical Forest in Southern Brazil. *Remote Sensing*, *9*(8), 838. https://www.mdpi.com/2072-4292/9/8/838

Spracklen, B., & Spracklen, D. V. (2021). Synergistic Use of Sentinel-1 and Sentinel-2 to Map Natural Forest and Acacia Plantation and Stand Ages in North-Central Vietnam. *Remote Sensing*, *13*(2). https://mdpi-res.com/d_attachment/remotesensing/remotesensing-13-00185/article_deploy/remotesensing-13-00185-v2.pdf?version=1610241527

Srinet, R., Nandy, S., Padalia, H., Ghosh, S., Watham, T., R, P., & Chauhan, P. (2020). Mapping plant functional types in Northwest Himalayan foothills of India using random forest algorithm in Google Earth Engine. *International Journal of Remote Sensing*, *41*, 1-14. https://doi.org/10.1080/01431161.2020.1766147

Starkloff, R. (1998, Nov. 4-6). *Social and environmental aspects of watershed vulnerability in the Sri Lankan hill country* National Water Conference, Colombo Sri Lanka.

Steiniger, S., & Hay, G. J. (2009). Free and open source geographic information tools for landscape ecology. *Ecological Informatics*, *4*(4), 183-195. https://doi.org/https://doi.org/10.1016/j.ecoinf.2009.07.004

Stibig, H. J., Belward, A. S., Roy, P. S., Rosalina-Wasrin, U., Agrawal, S., Joshi, P. K., Beuchle, R., Fritz, S., Mubareka, S., & Giri, C. (2007). A land-cover map for South and Southeast Asia derived from SPOT-VEGETATION data. *Journal of Biogeography*, *34*(4), 625-637. https://doi.org/10.1111/j.1365-2699.2006.01637.x

Subasinghe, K., Sumanapala, A. P., & Weerawardhena, S. R. (2014). The impact of forest conversion on bird communities in the northern flank of the Knuckles Mountain Forest Range, Sri Lanka. *Journal of Asia-Pacific Biodiversity*, *7*(4), 367-373. https://doi.org/https://doi.org/10.1016/j.japb.2014.07.004

Subasinghe, S. (2007). *Plantation forestry in Sri Lanka challenges and constraints* Annual Sessions of the Institute of Biology, Sri Lanka.

Taufik, A., Ahmad, S. S. S., & Ahmad, A. (2016). Classification of Landsat 8 Satellite Data Using NDVI Tresholds. *Journal of Telecommunication, Electronic and Computer Engineering*, *8*, 37-40.

Torbick, N., Chowdhury, D., Salas, W., & Qi, J. (2017). Monitoring Rice Agriculture across Myanmar Using Time Series Sentinel-1 Assisted by Landsat-8 and PALSAR-2. *Remote Sensing*, *9*(2). https://mdpi-res.com/d_attachment/remotesensing/remotesensing-09-00119/article_deploy/remotesensing-09-00119-v2.pdf?version=1487336211

Tsai, Y. H., Stow, D., Chen, H. L., Lewison, R., An, L., & Shi, L. (2018). Mapping Vegetation and Land Use Types in Fanjingshan National Nature Reserve Using Google Earth Engine. *Remote Sensing*, *10*(6), 927. https://www.mdpi.com/2072-4292/10/6/927

UNBigData. (2019, 27 September 2019). *Planet and Google are ready to help the United Nations in the data work behind the 2030 Agenda for Sustainable Development*. Retrieved 1st of August from https://unstats.un.org/bigdata/blog/2019/planet-google.cshtml

United Nations. (2015). *Transforming our world : the 2030 Agenda for Sustainable Development*. https://sustainabledevelopment.un.org/content/documents/21252030%20Agenda%20for%20Sustainable%20Development%20web.pdf

USGS. (2018). *NDVI, the Foundation for Remote Sensing Phenology*. Retrieved 13th of November from https://www.usgs.gov/core-science-systems/eros/phenology/science/ndvi-foundation-remote-sensing-phenology?qt-science_center_objects=0#qt-science_center_objects

Vafaei, S., Soosani, J., Adeli, K., Fadaei, H., Naghavi, H., Pham, T. D., & Tien Bui, D. (2018). Improving Accuracy Estimation of Forest Aboveground Biomass Based on Incorporation of ALOS-2 PALSAR-2 and Sentinel-2A Imagery and Machine Learning: A Case Study of the Hyrcanian Forest Area (Iran). *Remote Sensing*, *10*(2). https://mdpi-res.com/d_attachment/remotesensing/remotesensing-10-00172/article_deploy/remotesensing-10-00172.pdf?version=1516898085

Van Tricht, K., Gobin, A., Gilliams, S., & Piccard, I. (2018). Synergistic Use of Radar Sentinel-1 and Optical Sentinel-2 Imagery for Crop Mapping: A Case Study for Belgium. *Remote Sensing*, *10*(10). https://mdpi-res.com/d_attachment/remotesensing/remotesensing-10-01642/article_deploy/remotesensing-10-01642.pdf?version=1539685241

Verbyla, D. L. (1995). *Satellite Remote Sensing of Natural Resources*. Lewis Publishers.

Vick, T. (2008). Comparing Pixel- and Object-Based Classification Methods for Determining Land-Cover in the Gee Creek Watershed, Washington. *Geography Masters Research Papers.*, *22*. https://doi.org/10.15760/geogmaster.22

Wang, G., & Weng, Q. (2013). *Remote Sensing of Natural Resources*. Taylor & Francis Group. http://ebookcentral.proquest.com/lib/waikato/detail.action?docID=1316400

Wang, L., Zhang, X., Luo, Y., Shi, J., & Huang, H. (2006, 31 July-4 August). A Study on the Changes of Pinus Massoniana Spatial Pattern by Pine Wood Nematode Invasion Based on Remote Sensing and GIS. 2006 IEEE International Symposium on Geoscience and Remote Sensing, Denver, USA.

Wang, T., Zhang, H., Lin, H., & Fang, C. (2016). Textural–Spectral Feature-Based Species Classification of Mangroves in Mai Po Nature Reserve from Worldview-3 Imagery. *Remote Sensing*, *8*(1), 24. https://www.mdpi.com/2072-4292/8/1/24

Weisberg, P. J., Lingua, E., & Pillai, R. B. (2007). Spatial Patterns of Pinyon-Juniper Woodland Expansion in Central Nevada. In (Vol. 60, pp. 115-124): Society for Range Management.

Weng, Q. (2018). *Remote sensing time series image processing*. CRC Press, Taylor & Francis Group.

Wessel, M., Brandmeier, M., & Tiede, D. (2018). Evaluation of Different Machine Learning Algorithms for Scalable Classification of Tree Types and Tree Species Based on Sentinel-2 Data. *Remote Sensing*, *10*(9), 1419. https://www.mdpi.com/2072-4292/10/9/1419

Wijerathna, N., Hettiarachchi, C., & Wickramagamage, P. (2016). Effect of Pinus Caribaea Plantation on Vegetation Diversity and Distribution by Reforestation in Lower Hantana.

International Conference on the Humanities and the Social Sciences (ICHSS) 2016, Peradeniya, Sri Lanka.

Wijesundera, S. (2008, 11th November). Major invasive plant species in different climatic zones of Sri Lanka. Proceedings of the National Symposium on Invasive Alien Species (IAS 2008), Sri Lanka Foundation Institute.

Williams, D. L. (1991). A comparison of spectral reflectance properties at the needle, branch, and canopy level for selected Conifer species. *Remote Sensing of Environment*, *35*(2), 79-93. https://doi.org/https://doi.org/10.1016/0034-4257(91)90002-N

Wu, W. J., Zhao, X. J., Gong, C., Li, X. W., & Ieee. (2018). Obtain The Patterns Of Global Forest Npp And Its Influence Factors With Google Earth Engine. In *Igarss 2018 - 2018 Ieee International Geoscience and Remote Sensing Symposium* (pp. 2898-2901). Ieee. <Go to ISI>://WOS:000451039802244

Xie, Y., Sha, Z., & Yu, M. (2008). Remote sensing imagery in vegetation mapping: a review. *Journal of Plant Ecology*, *1*(1), 9-23. https://doi.org/10.1093/jpe/rtm005

Xu, D., Chen, B., Yan, Y., Sun, X., & Xin, X. (2018). Spatial-temporal dynamic monitoring of Mongolian pine (Pinus sylvestris var. mongolica) based on remote sensing data. *Remote Sensing Letters*, *9*(11), 1079-1088. https://doi.org/10.1080/2150704X.2018.1508908

Ye, S., Rogan, J., Zhu, Z., Hawbaker, T. J., Hart, S. J., Andrus, R. A., Meddens, A. J. H., Hicke, J. A., Eastman, J. R., & Kulakowski, D. (2021). Detecting subtle change from dense Landsat time series: Case studies of mountain pine beetle and spruce beetle disturbance. *Remote Sensing of Environment*, *263*, 112560. https://doi.org/https://doi.org/10.1016/j.rse.2021.112560

Yu, X., Lu, D., Jiang, X., Li, G., Chen, Y., Li, D., & Chen, E. (2020). Examining the Roles of Spectral, Spatial, and Topographic Features in Improving Land-Cover and Forest Classifications in a Subtropical Region. *Remote Sensing*, *12*(18). https://doi.org/10.3390/rs12182907

Zhang, M. N., Gong, P., Qi, S. H., Liu, C., & Xiong, T. W. (2019). Mapping bamboo with regional phenological characteristics derived from dense Landsat time series using Google Earth Engine [Article; Proceedings Paper]. *International Journal of Remote Sensing*, *40*(24), 9541-9555. https://doi.org/10.1080/01431161.2019.1633702

Zheng, B., Ciais, P., Chevallier, F., Chuvieco, E., Chen, Y., & Yang, H. (2021). Increasing forest fire emissions despite the decline in global burned area. *Science Advances*, *7*, eabh2646. https://doi.org/10.1126/sciadv.abh2646

Zhou, W. (2019). *High-resolution Remote Sensing to Identify Tree Plantations from Natural Forests and Agriculture in Southern India* [master's thesis, University of Michigan].

Zhou, X., Li, L., Chen, L., Liu, Y., Cui, Y., Zhang, Y., & Zhang, T. (2019). Discriminating Urban Forest Types from Sentinel-2A Image Data through Linear Spectral Mixture Analysis: A Case Study of Xuzhou, East China. *Forests*, *10*(6), 478. https://www.mdpi.com/1999-4907/10/6/478

Zhu, X., & Liu, D. (2014). Accurate mapping of forest types using dense seasonal Landsat time-series. *ISPRS Journal of Photogrammetry and Remote Sensing*, *96*, 1-11. https://doi.org/https://doi.org/10.1016/j.isprsjprs.2014.06.012

Zhu, Z., & Woodcock, C. E. (2014). Continuous change detection and classification of land cover using all available Landsat data. *Remote Sensing of Environment*, *144*, 152-171. https://doi.org/https://doi.org/10.1016/j.rse.2014.01.011

Zhu, Z., Wulder, M. A., Roy, D. P., Woodcock, C. E., Hansen, M. C., Radeloff, V. C., Healey, S. P., Schaaf, C., Hostert, P., Strobl, P., Pekel, J.-F., Lymburner, L., Pahlevan, N., & Scambos, T. A. (2019). Benefits of the free and open Landsat data policy. *Remote Sensing of Environment*, *224*, 382-385. https://doi.org/https://doi.org/10.1016/j.rse.2019.02.016

Zurqani, H. A., Post, C. J., Mikhailova, E. A., Schlautman, M. A., & Sharp, J. L. (2018). Geospatial analysis of land use change in the Savannah River Basin using Google Earth Engine. *International Journal of Applied Earth Observation and Geoinformation*, *69*, 175-185. https://doi.org/https://doi.org/10.1016/j.jag.2017.12.006

Appendices

Appendix I-Supplementary Material -Chapter 3

3.SM.1 Confusion matrix of k fold analysis

Table 3.SM1 shows the confusion matrix of the K fold analysis

Table 3.SM1 Confusion Matrix of 5 folds

	fold 1						fold 2						fold 3						fold 4						fold 5					
	Forestry classes				Agroforestry Classes		Forestry classes				Agroforestry Classes		Forestry classes				Agroforestry Classes		Forestry classes				Agroforestry Classes		Forestry classes				Agroforestry Classes	
Land Cover	Pine	Natural	Grassland	Shrub	HG	Cultivation	Pine	Natural	Grassland	Shrub	HG	Cultivation	Pine	Natural	Grassland	Shrub	HG	Cultivation	Pine	Natural	Grassland	Shrub	HG	Cultivation	Pine	Natural	Grassland	Shrub	HG	Cultivation
Pine	16	0	0	0	0	0	17	0	0	0	0	0	11	0	0	0	0	0	9	1	0	0	0	0	21	0	0	0	0	0
Natural	0	9	0	0	0	3	0	14	0	0	0	1	0	19	0	0	0	1	0	14	0	0	0	1	0	20	0	0	0	1
Grassland	0	0	10	3	0	3	0	0	12	1	0	0	0	0	2	2	0	0	0	0	7	1	0	0	0	0	5	0	0	0
Shrub	1	0	1	7	0	0	0	0	1	7	0	0	0	0	10	10	0	0	0	0	0	11	0	0	0	1	0	6	0	0
HG	0	0	0	0	43	0	0	0	0	1	46	1	0	0	0	0	57	0	0	0	1	0	90	0	0	0	0	0	57	1
Cultivation	0	0	0	0	0	5			0	0	2	4	0	0	0	0	2	4	0	1	0	1	3	8	0	0	0	0	1	4
producer accuarcy	0.94	1.00	0.91	0.70	1.00	0.45	1.00	1.00	0.92	0.78	0.96	0.67	1.00	1.00	0.82	0.83	0.97	0.80	1.00	0.88	0.88	0.85	0.97	0.89	1.00	0.95	1.00	1.00	0.98	0.67
Consumer accuracy	1.00	0.75	0.63	0.78	1.00	1.00	1.00	0.93	0.92	0.88	0.96	0.67	1.00	0.95	0.82	0.83	1.00	0.67	0.90	0.93	0.88	1.00	0.99	0.62	1.00	0.95	1.00	0.86	0.98	0.80
OA	0.89						0.93						0.94						0.98						0.97					
kappa	0.85						0.91						0.91						0.90						0.95					

3.SM.2 GEE code of chapter 3

3.SM2 shows the java script code use for the home garden analysis using the GEE code layout

```
//Navigate to area of interest
Map.centerObject(study_area)
// define the Elelvation data or import the elevation data
var dem=DEM.clip(study_area)
 Map.addLayer (dem, {min:300, max:2500},'Dem');
print (dem,'DEM');
// extracting terrain features from the DEM
// selecting the elevation
var elevation = dem.select('elevation');
Map.addLayer(elevation, {min: 300, max: 2500}, 'elevation');
//select the slope
var slope = ee.Terrain.slope(elevation);
Map.addLayer(slope, {min: 0.3, max: 80}, 'slope');
print (slope);
// selct the aspect
var aspect=ee.Terrain.aspect(dem)
// Importing the S2 satellite collection and select a cloud free image through different filtering
//and selcting  the most cloud free image in the date range
    var shape = ee.Image(sent2
// filter date
    .filterDate("2020-01-01", "2020-07-01")
// filter boundary
    .filterBounds(study_area)
// filter by clouds coverage
    .sort("CLOUD_COVERAGE_ASSESSMENT")
  // least cloud coverga image
    .first()
.clip(study_area));
```

```
  print("A Sentinel-2 scene:", shape);


// var shape= image.clip(campus);
// Define visualization parameters in a JavaScript dictionary for true colour rendering. Bands 4,3 and 2 needed for RGB.
   var trueColour = {
      bands: ["B4", "B3", "B2"],
      min: 500,
      max: 3500,
      gamma: 1.3
      };
Map.addLayer(shape,trueColour,'shape')
// Compute the Normalized Difference Vegetation Index (NDVI).
var nir = shape.select('B8');
var red = shape.select('B4');
var ndvi = nir.subtract(red).divide(nir.add(red)).rename('NDVI');
print (ndvi,'ndvi')
// Display the result.
var ndviParams = {min: -1, max: 1, palette: ['blue', 'white', 'green']};
Map.addLayer(ndvi, ndviParams, 'NDVI image');
//Use ndvi thershold to remove non vegetaive areas
var newndvi=ndvi.select('NDVI').gte(0.35).rename('NDVI').selfMask();
Map.addLayer(newndvi, ndviParams , 'NDVI THRESHOLD',false);
//upsample to 10m
function resample10m(img) {
  var b2 = shape.select('B8A')
  var image10m = shape.resample('bicubic').reproject({crs:b2.projection().crs(), scale:10})
  return image10m
}
var upsampled_newshape= resample10m(shape.addBands(shape.select(['B8A'])))
print(upsampled_newshape,'upsampled_pc ')
// // //add NDVI index to the analysis
```

```
var newshape=upsampled_newshape.addBands(newndvi)
print(newshape,'newshape')
// to select the vegatative area for further analysis
//1.  convert vegetative area to vectors  for assist clip

var vector=newndvi.reduceToVectors({
  reducer:ee.Reducer.countEvery(),
  geometry:study_area,
  scale:10,
  bestEffort:true,
})
Map.addLayer(vector,{},'vector',false)
// clipping the main satellite image with masked.
var vegetative_area=newshape.clip(vector)
print(vegetative_area,'vegetative_area')
Map.addLayer(vegetative_area,trueColour,'vegetative_area')
// creating different vegeation indexes//////////////////////****
//1./EVI- Enhance vegation index
var EVI = vegetative_area.expression('(2.5 * float(NIR - RED)) / (NIR + (2.4 * RED) + 10000)',
//(https://gis.stackexchange.com/questions/226325/calculating-2-bands-evi-from-sentinel-2?rq=1)
{
     'NIR': vegetative_area.select('B8'),
     'RED': vegetative_area.select('B4'),
     'BLUE': vegetative_area.select('B2')
}).rename('EVI');
// //creating Green Chlorophlly index
//2.///GCI = (NIR) / (Green) – 1
var GCI = vegetative_area.expression ('float (((NIR) / (GREEN)) - 1)', {
   'NIR': vegetative_area.select ('B8'),
   'GREEN': vegetative_area.select ('B3')}).rename('GCI');
Map.addLayer(GCI , {min: 0, max: 5 ,palette:['Green','yellow','white']},'GCI ');
```

```
//  Red Edge Chlorophyll Index
//3.///RGCI-(B7)(/B5)-1
var RGCI = vegetative_area.expression ('float (((REDEdge3) / (REDEdge1)) - 1)', {
   'REDEdge3': vegetative_area.select ('B7'),
   'REDEdge1': vegetative_area.select ('B5')}).rename('RGCI');
//4.///// GLI (Green Leaf Index)
var GLI = vegetative_area.expression ('float (((GREEN - RED) + (GREEN - BLUE)) / ((2 * GREEN) + RED + BLUE))', {
   'GREEN': vegetative_area.select ('B3'),
   'RED': vegetative_area.select ('B4'),
   'BLUE': vegetative_area.select ('B2')}).rename('GLI');
//5.////// SAVI (Soil Adjusted Vegetation Index)
var SAVI = vegetative_area.expression ('float (((NIR - RED) / (NIR + RED + L))* (1+L))',{
   'L': 0.5, // Cobertura vegetacion 0-1
   'NIR': vegetative_area.select ('B8'),
   'RED': vegetative_area.select ('B4')}).rename('SAVI');
// //6.//// NBRI (Normalized Burned Ratio Index)
var NBRI = vegetative_area.expression ('float (NIR - SWIR2) / float (NIR + SWIR2)', {
   'NIR': vegetative_area.select ('B8'),
   'SWIR2': vegetative_area.select ('B12')}).rename('NBRI');
//  //7. NDMI-Normalized difference moisture index
/// //(NIR-SWIR)/(NIR+SWIR)
var NDMI = vegetative_area.expression ('float (NIR - SWIR1) / float (NIR + SWIR1)', {
   'NIR': vegetative_area.select ('B8'),
   'SWIR1': vegetative_area.select ('B11')}).rename('NDMI');
//////dimesion reduction//////////////
//use PCA for dimension reduction
// // // Set some information about the input to be used later.
var scale = 10;
var newband=vegetative_area.select(['B2', 'B3', 'B4', 'B5', 'B6', 'B7', 'B8', 'B8A','B11', 'B12']);
var bandNames = newband.bandNames();
```

```
// Mean center the data to enable a faster covariance reducer and an SD stretch of the principal components.
var meanDict = newband.reduceRegion({
    reducer: ee.Reducer.mean(),
    geometry: study_area,
    scale: scale,
    maxPixels: 1e9
});
var means = ee.Image.constant(meanDict.values(bandNames));
var centered = newband.subtract(means);
// This helper function returns a list of new band names.
var getNewBandNames = function(prefix) {
  var seq = ee.List.sequence(1, bandNames.length());
  return seq.map(function(b) {
    return ee.String(prefix).cat(ee.Number(b).int());
  });
};
// This function accepts mean centered imagery, a scale and a region in which to perform the analysis.  //It returns the // Principal Components (PC) in the region as a new image.
var getPrincipalComponents = function(centered, scale, campus) {
  // Collapse the bands of the image into a 1D array per pixel.
  var arrays = centered.toArray();
  // Compute the covariance of the bands within the region.
  var covar = arrays.reduceRegion({
    reducer: ee.Reducer.centeredCovariance(),
    geometry: campus,
    scale: scale,
    maxPixels: 1e9
  });
  // Get the 'array' covariance result and cast to an array.  This represents the band-to-band covariance within the region.
  var covarArray = ee.Array(covar.get('array'));
  // Perform an eigen analysis and slice apart the values and vectors.
```

```
  var eigens = covarArray.eigen();
  // This is a P-length vector of Eigenvalues.
  var eigenValues = eigens.slice(1, 0, 1);
  //print(eigenValues,'eigenValues')
  // This is a PxP matrix with eigenvectors in rows.
  var eigenVectors = eigens.slice(1, 1);
//print (eigenVectors,'eigenVectors')
 // Convert the array image to 2D arrays for matrix computations.
  var arrayImage = arrays.toArray(1);

  // Left multiply the image array by the matrix of eigenvectors.
  var principalComponents = ee.Image(eigenVectors).matrixMultiply(arrayImage);
  // Turn the square roots of the Eigenvalues into a P-band image.
  var sdImage = ee.Image(eigenValues.sqrt())
    .arrayProject([0]).arrayFlatten([getNewBandNames('sd')]);
  // Turn the PCs into a P-band image, normalized by SD.
  return principalComponents
    // Throw out an an unneeded dimension, [[]] -> [].
    .arrayProject([0])
    // Make the one band array image a multi-band image, [] -> image.
    .arrayFlatten([getNewBandNames('pc')])
    // Normalize the PCs by their SDs.
    .divide(sdImage);
};
// Get the PCs at the specified scale and in the specified region
var pcImage = getPrincipalComponents(centered, scale, study_area);
// Plot each PC as a new layer
for (var i = 0; i < bandNames.length().getInfo(); i++) {
  var band = pcImage.bandNames().get(i).getInfo();
  //Map.addLayer(pcImage.select([band]), {min: -2, max: 2}, band);
}
print (pcImage,'pc no');
```

```
 Map.addLayer(pcImage, {min: -2, max: 2}, 'band');
  // Select second PCA
  var texture_pc=pcImage.select('pc2').rename('PC2')
  print(texture_pc,'pc_texture')
//Add PC as a band to the satellite image
var vegetativearea_PC=newshape.addBands(texture_pc)
print(vegetativearea_PC,'vegetativearea_PC')
// ////  ////////////////////////////GLCM//////////////////////////////
// convert the PCA-2 into 32 bit interger
  var byte_pc=pcImage.select(['pc2']).int32()
  // convert PCA to grey level texture with a window size 8*8
  var texture_GLCM= byte_pc.glcmTexture(5)
  print(texture_GLCM,'texture_GLCM')
// // //add PCA-2 texture as a band indexes to the image
var shape1=vegetativearea_PC.addBands(texture_GLCM)
print(shape1,'vegetativearea')
// selct spectral bands for texture
var B2= shape1.select('B2')
var B3=shape1.select('B3')
var B4=shape1.select('B4')
var B8=shape1.select('B8')
var B8A=shape1.select('B8A')
var B12=shape1.select('B12')
var NDVI=shape1.select('NDVI')
var B5=shape1.select('B5')
var B6=shape1.select('B6')
var B7=shape1.select('B7')
var B11=shape1.select('B11')
//converting spectral bands to texture
var b2_texture=B2.glcmTexture()
var b3_texture=B3.glcmTexture()
var b4_texture=B4.glcmTexture()
```

```
var b8_texture=B8.glcmTexture()

var b8A_texture=B8A.glcmTexture()

var b12_texture=B12.glcmTexture()

var NDVI_texture=NDVI.glcmTexture()

var b5_texture=B5.glcmTexture()

var b6_texture=B6.glcmTexture()

var b7_texture=B7.glcmTexture()

var b11_texture=B11.glcmTexture()

//add topographical data, vegatation indices and  textural bands to the analysis

var
vegetativearea=shape1.addBands(elevation).addBands(slope).addBands(aspect).addBands(G
CI ).addBands(GLI).addBands(NDMI)

.addBands(RGCI).addBands(EVI).addBands(SAVI).addBands(NBRI).addBands(b2_texture).
addBands(b3_texture).addBands(b4_texture).addBands(b8_texture).addBands(b8A_texture).
addBands(b12_texture).addBands(NDVI_texture).addBands(b5_texture).addBands(b6_textur
e).addBands( b7_texture).addBands(b11_texture)

print(vegetativearea,'vegetativearea')

// // ////////////////////// Adding Train data and propertites only for home garden and planation
/////////////

var Train_HG = HomeGarden.map(function(x) {

  return x.set('use1', 4)

})

var Train_cultivation = tea.map(function(x) {

  return x.set('use1', 5)

})

// // // // // // Creating Classes for training data

var                                    classNames                                    =
pines_plantation.merge(natural_vegetation).merge(Grassland).merge(shrub).merge(Train_H
G).merge(Train_cultivation) ;

print (classNames,'classnames');

//all the features considered for the classification

var                                    bands                                    =
['GLI','NDMI','NBRI','SAVI','EVI','RGCI','GCI','elevation','slope','aspect','PC2','pc2_asm','pc
2_contrast','pc2_corr','pc2_var',
```

```
'pc2_idm','pc2_savg','pc2_svar','pc2_sent','pc2_dvar','pc2_dent','pc2_imcorr2','pc2_diss','pc2_
inertia','pc2_prom','B2_var','B2_asm','B2_idm','B2_savg','B2_svar','B2_sent','B2_dvar','B2_d
ent','B2_imcorr2','B2_diss','B2_inertia','B2_prom','B2',

'B3',
'B3_asm','B3_idm','B3_savg','B3_svar','B3_sent','B3_dvar','B3_dent','B3_imcorr2','B3_diss','
B3_inertia','B3_prom','B4','B4_var','B4_asm','B4_idm','B4_savg','B4_svar','B4_sent','B4_dva
r','B4_dent','B4_imcorr2','B4_diss','B4_inertia','B4_prom','B8',
'B8_var','B8_asm','B8_idm','B8_savg','B8_svar','B8_sent','B8_dvar','B8_dent','B8_imcorr2','B
8_diss','B8_inertia','B8_prom',

'B5_var','B5_asm','B5_idm','B5_savg','B5_svar','B5_sent','B5_dvar','B5_dent','B5_imcorr2','B
5_diss','B5_inertia','B5_prom','B5', 'B6',
'B7','B8A','B8A_asm','B8A_idm','B8A_savg','B8A_svar','B8A_sent','B8A_dvar','B8A_dent','
B8A_imcorr2','B8A_diss','B8A_inertia','B8A_prom',
'B12','B12_var','B12_asm','B12_idm','B12_savg','B12_svar','B12_sent','B12_dvar','B12_dent',
'B12_imcorr2','B12_diss','B12_inertia','B12_prom','B2_contrast','B11','B11_corr','B11_contra
st','B11_var','B11_asm','B11_idm','B11_savg','B11_svar','B11_sent','B11_dvar','B11_dent','B
11_imcorr2','B11_diss','B11_inertia','B11_prom','B2_corr','B3_contrast','B3_corr','B8_contras
t','B8_corr','B4_contrast','B4_corr','B12_contrast','B12_corr','B8A_contrast','B8A_corr',

'B5_contrast','B5_corr','B6_contrast','B6_corr','B7_contrast','B7_corr'];

// ////////////////////////////

//K-fold analysis//////////////


// Create a feature collection of classes

var exampleFC = ee.FeatureCollection(classNames).randomColumn('PoI');

Map.addLayer(exampleFC, {}, 'Example Samples');

// Input the explicit parameters for the k-fold function

var inputtedFeatureCollection = exampleFC;

var imageToClassify = vegetativearea;

var k = 5;

var classifierOfChoice = ee.Classifier.smileRandomForest(350, null, 1, 0.5, null,
0).setOutputMode('CLASSIFICATION');//'REGRESSION'

 var propertyToPredictAsString = 'use1';

 var scaleToSample = 10;

// Adopted from devin.routh

// var kFoldCrossValidation = function(inputtedFeatureCollection, imageToClassify, k,
classifierOfChoice, propertyToPredictAsString, scaleToSample) {

//         /*

//         Arguments:
```

```
//          inputtedFeatureCollection: an ee.FeatureCollection() of sample points object with a property of interest imageToClassify: the image used to classify/regress the point samples
// //       k: the number of folds
//          classifierOfChoice: the classifier/regressor of choice
//          propertyToPredictAsString: the name of the property to predict as a string object
//          scaleToSample: the scale at which to sample the image
//          */
// The sections below are the function's code, beginning with preparation of the inputted feature collection of sample points
          var collLength = inputtedFeatureCollection.size();
           print('Number of Sample Points',collLength);
          var sampleSeq = ee.List.sequence(1, collLength);
          print('Sample Sequence',sampleSeq);
          var inputtedFCWithRand = inputtedFeatureCollection.randomColumn('Rand_Num', 42).sort('Rand_Num').toList(collLength);
           print('Total FC with Random Column',inputtedFCWithRand);
          // Prep the feature collection with random fold assignment numbers
          var preppedListOfFeats = sampleSeq.map(function(numberToSet) {
                    return ee.Feature(inputtedFCWithRand.get(ee.Number(numberToSet).subtract(1))).set('Fold_ID', ee.Number(numberToSet));
          });
           print('Prepped FC', preppedListOfFeats);
          // This section divides the feature collection into the k folds
          var averageFoldSize = collLength.divide(k).floor();
           print('Average Fold Size',averageFoldSize);
          var remainingSampleSize = collLength.mod(k);
           print('Remaining Sample Size', remainingSampleSize);
          var foldSequenceWithoutRemainder = ee.List.sequence(0, k - 1).map(function(fold) {
                    var foldStart = ee.Number(fold).multiply(averageFoldSize).add(1);
                    var foldEnd = ee.Number(foldStart).add(averageFoldSize.subtract(1));
                    var foldNumbers = ee.List.sequence(foldStart, foldEnd);
                    return ee.List(foldNumbers);
          });
```

```
print('Fold Sequence Without Remaining Samples',foldSequenceWithoutRemainder);

var remainingFoldSequence = ee.List.sequence(ee.Number(ee.List(foldSequenceWithoutRemainder.get(foldSequenceWithoutRemainder.length().subtract(1))).get(averageFoldSize.subtract(1))),

ee.Number(ee.List(foldSequenceWithoutRemainder.get(foldSequenceWithoutRemainder.length().subtract(1))).get(averageFoldSize.subtract(1))).add(ee.Number(remainingSampleSize).subtract(1)));

print('Remaining Fold Sequence',remainingFoldSequence);

// This is a list of lists describing which features will go into each fold

var listsWithRemaindersAdded = foldSequenceWithoutRemainder.zip(remainingFoldSequence).map(function(list) {

return ee.List(list).flatten();

});

print('Lists with Remainders Added',listsWithRemaindersAdded);

var finalFoldLists = listsWithRemaindersAdded.cat(foldSequenceWithoutRemainder.slice(listsWithRemaindersAdded.length()));

print('Final Fold Lists Formatted',finalFoldLists);

var mainFoldList = ee.List.sequence(0, k - 1);

print('Main Fold List',mainFoldList);


// Compute the collected training data

var trainingData = mainFoldList.map(function(foldNumber) {

var listWithoutFold = finalFoldLists.get(foldNumber);

var foldListOfLists = ee.FeatureCollection(preppedListOfFeats).filter(ee.Filter.inList('Fold_ID', listWithoutFold).not()).toList(collLength);

return foldListOfLists;

});

print('Training Data Folds', trainingData);

//        // Compute the validation folds

var val_pine = pine.map(function(x) {

  return x.set('use', 0)

})

var val_natural = tree.map(function(x) {
```

```
  return x.set('use', 1)
})
var val_grassland = tgrassland.map(function(x) {
  return x.set('use', 2)
})
var val_shrub = tshurb.map(function(x) {
  return x.set('use', 3)
})
var val_HG = vHG.map(function(x) {
  return x.set('use', 4)
})
var val_tea = vTEA.map(function(x) {
  return x.set('use', 5)
})
var fullValidationDataSet = val_pine.merge(val_natural).merge(val_grassland).merge(val_shrub).merge(val_HG).merge(val_tea)
print(fullValidationDataSet,'fullValidationDataSet')
// Input the explicit parameters for the validation function
//var inputtedFeatureCollection = exampleFC;
var imageToClassify = vegetativearea;

var k = 5;

var classifierOfChoice = ee.Classifier.smileRandomForest(350, null, 1, 0.5, null, 0).setOutputMode('CLASSIFICATION');//'REGRESSION'
var propertyToPredictAsString1 = 'use';
var scaleToSample = 10;
var kFoldCrossValidation = function(fullValidationDataSet, imageToClassify, k, classifierOfChoice, propertyToPredictAsString1, scaleToSample) {
        var collLength1 = fullValidationDataSet.size();
         print('Number of Sample Points',collLength1);
        var sampleSeq1 = ee.List.sequence(1, collLength1);
```

```
print('Sample Sequence',sampleSeq1);


var inputtedFCWithRand1 = fullValidationDataSet.randomColumn('Rand_Num', 42).sort('Rand_Num').toList(collLength1);

 print('Total FC with Random Column',inputtedFCWithRand1);

// Prep the feature collection with random fold assignment numbers

var preppedListOfFeats1 = sampleSeq1.map(function(numberToSet) {

        return ee.Feature(inputtedFCWithRand1.get(ee.Number(numberToSet).subtract(1))).set('Fold_ID', ee.Number(numberToSet));

});

 print('Prepped FC', preppedListOfFeats1);

var averageFoldSize = collLength1.divide(k).floor();

 print('Average Fold Size',averageFoldSize);

var remainingSampleSize = collLength1.mod(k);

 print('Remaining Sample Size', remainingSampleSize);

var foldSequenceWithoutRemainder = ee.List.sequence(0, k - 1).map(function(fold) {

        var foldStart = ee.Number(fold).multiply(averageFoldSize).add(1);

        var foldEnd = ee.Number(foldStart).add(averageFoldSize.subtract(1));

        var foldNumbers = ee.List.sequence(foldStart, foldEnd);

        return ee.List(foldNumbers);

});

 print('Fold Sequence Without Remaining Samples',foldSequenceWithoutRemainder);

var remainingFoldSequence = ee.List.sequence(ee.Number(ee.List(foldSequenceWithoutRemainder.get(foldSequenceWithoutRemainder.length().subtract(1))).get(averageFoldSize.subtract(1))),


ee.Number(ee.List(foldSequenceWithoutRemainder.get(foldSequenceWithoutRemainder.length().subtract(1))).get(averageFoldSize.subtract(1))).add(ee.Number(remainingSampleSize).subtract(1)));

print('Remaining Fold Sequence',remainingFoldSequence);


// This is a list of lists describing which features will go into each fold

var listsWithRemaindersAdded = foldSequenceWithoutRemainder.zip(remainingFoldSequence).map(function(list) {
```

```
        return ee.List(list).flatten();
    });
     print('Lists with Remainders Added',listsWithRemaindersAdded);
    var finalFoldLists = listsWithRemaindersAdded.cat(foldSequenceWithoutRemainder.slice(listsWithRemaindersAdded.length()));
    print('Final Fold Lists Formatted',finalFoldLists);
    var mainFoldList = ee.List.sequence(0, k - 1);
    print('Main Fold List',mainFoldList);
// Compute the validation folds
    var validationData = mainFoldList.map(function(foldNumber) {
        var listWithoutFold = finalFoldLists.get(foldNumber);
        var foldListOfLists = ee.FeatureCollection(preppedListOfFeats1).filter(ee.Filter.inList('Fold_ID', listWithoutFold)).toList(collLength1);
        return foldListOfLists;
    });
    print('Validation Data Folds', validationData);
    // Train the data and retrieve the values at the sample points
    // Classify the images based on the training folds
    var classifiedImages = mainFoldList.map(function(foldNumber) {
        var trainingFold = imageToClassify.sampleRegions(ee.FeatureCollection(ee.List(trainingData.get(foldNumber))));
        var trainedClassifier = classifierOfChoice.train(trainingFold, propertyToPredictAsString);
        var classifiedImages = imageToClassify.classify(trainedClassifier).rename(ee.String(propertyToPredictAsString).cat('_Classification'));
        return classifiedImages;
    });
     print('Classified Images', classifiedImages);
    // Retrieve the validation data from the validation folds
    var validationResults = mainFoldList.map(function(foldNumber) {
        var imageToSample = ee.Image(classifiedImages.get(foldNumber));
```

```
            var validationFoldSamples = ee.List(validationData.get(foldNumber)).map(function(feat) {
                return ee.Feature(feat).set('Fold_Number', foldNumber);
            });
            var validationResults = imageToSample.sampleRegions({
                collection: ee.FeatureCollection(validationFoldSamples).select([propertyToPredictAsString1, 'Fold_Number', 'Fold_ID', 'Sample_Num']),
                scale: scaleToSample
            }).toList(collLength1);
            return validationResults;
        });
         print('Validation Results',validationResults);
        var validationResultsFlattened = ee.FeatureCollection(ee.List(validationResults.flatten()));
         print('Validation Results Flattened and Formatted',validationResultsFlattened);
        return validationResultsFlattened;
};
var kFoldCVResults = kFoldCrossValidation(fullValidationDataSet, imageToClassify, k, classifierOfChoice, propertyToPredictAsString1, scaleToSample);
print('k-Fold Cross Validation Results', kFoldCVResults);
// // Export the results
Export.table.toDrive(kFoldCVResults);
//////////////Find the accuracy for each fold//////////
var testAccuracyRT=validation0.errorMatrix('use', 'use1_Classification');
// var testAccuracyRT = kFoldCVResults.select(ee.List('Fold_Number'))
print (testAccuracyRT,'testAccuracyRT')
```

Appendix II-Supplementary Material -Chapter 4

4.SM.1 Confusion matrix of the year 2000

4.SM1 shows the confusion matrix of the year 2000

Table 4.SM1 Confusion matrix for the year 2000

	Classification						
	Land cover	Pine plantation	Broadleaf forest	Grassland	Bare land	Settlement	Total
Reference	Pine plantation	90	14	12	4	0	120
	Broadleaf forest	0	96	24	0	0	120
	Grassland	13	3	87	17	0	120
	Bare land	6	5	30	79	0	120
	Settlement	0	4	4	8	4	20
	Total	109	122	157	108	4	500
	User Accuracy (%)	82	79	58	73	100	
	Producer Accuracy (%)	75	84	72	66	20	
	Overall accuracy (%)			72			

4.SM.2 Confusion matrix for the year 2021

4.SM2 shows the confusion matrix of the year 2021

Table 4.SM2 Confusion matrix for the year 2021

	Classification						
	Land cover	Pine plantation	Broadleaf forest	Grassland	Bare land	Settlement	Total
Reference	Pine plantation	116	4	0	0	0	120
	Broadleaf forest	0	120	0	0	0	120
	Grassland	0	4	104	12	0	120
	Bare land	0	0	30	84	6	120
	Settlement	0	18	18	18	66	120
	Total	116	146	152	114	72	600
	User Accuracy (%)	100	82	68	74	92	
	Producer Accuracy (%)	96	100	86	70	55	
	Overall accuracy (%)			81			

4.SM.3 GEE code of the chapter 4

4.SM3 shows the code use for the to recognize the invasive pines during 21 years

```
//Navigate to area of interest////

Map.centerObject(study_area,15)

// define the Elelvation data or import the elevation data
var dem=DEM.clip(study_area)
 Map.addLayer (dem, {min:300, max:2500},'Dem',false);
print (dem,'DEM');
// extracting terrain features from the DEM
// selecting the elevation
var elevation = dem.select('elevation');
Map.addLayer(elevation, {min: 300, max: 2500}, 'elevation',false);
//select the slope
var slope = ee.Terrain.slope(elevation);

Map.addLayer(slope, {min: 0.3, max: 80, palette:[ 'red','green','yellow','black']},'slope');
print (slope);
// selct the aspect
var aspect=ee.Terrain.aspect(dem)
//////----------------------------cloud mask functions---------------------------------

// Use this function to mask clouds in Landsat 8 imagery.
var maskClouds = function(image) {
  var quality = image.select('pixel_qa');
  var cloud01 = quality.eq(61440);
  var cloud02 = quality.eq(53248);
  var cloud03 = quality.eq(28672);
  var mask = cloud01.or(cloud02).or(cloud03).not();
  return image.updateMask(mask);
};

//cloud masking_Fmask
 function fmask(img) {
  var cloudShadowBitMask = 1 << 8;
  var cloudsBitMask = 1 << 4;
  var qa = img.select('pixel_qa');
  var mask = qa.bitwiseAnd(cloudShadowBitMask)
                .eq(0)
                .and(qa.bitwiseAnd(cloudsBitMask).eq(0));
  return img.updateMask(mask);
}

// ////////////////////Earth engine data catalogue code/////////////////////////////////////////
function maskL8sr(imagecollection) {
```

```
  // Bits 3 and 5 are cloud shadow and cloud, respectively.
var cloudShadowBitMask = (1 << 3);
var cloudsBitMask = (1 << 5);
  // Get the pixel QA band.
var qa = imagecollection.select('pixel_qa');
  // Both flags should be set to zero, indicating clear conditions.

  var mask = qa.bitwiseAnd(cloudShadowBitMask).eq(0)
                 .and(qa.bitwiseAnd(cloudsBitMask).eq(0));
  return imagecollection.updateMask(mask);
}

///////////////----------------------clipping function and setting year--------------------

//Set year

 var setyear= function(a)
 {return a.set('year',ee.Image(a).date().get('year'))}
 ;

//clip
var study=function clip2 (img){return img.clip(study_area)}

// visual parameters //
var visParams = {
  bands: ['B4', 'B3', 'B2'],
  min: 0,
max: 3000,
gamma: 1.4,
};

// ///////////////-----------------------------------creating different vegetation indexes-functions----
----------
//// //creating Green Chlorophyll index
//1.///GCI = (NIR) / (Green) – 1

function GCI (image) {
var GCI = image.expression ('float (((nir) / (green)) - 1)', {
    'nir': image.select ('nir'),
    'green': image.select ('green')}).rename('GCI');
 return image.addBands(GCI);


  }

//2.////1./EVI- Enhance vegation index //
//calculate EVI over each image in the collection

  function  EVI (image) {
    var EVI = image.expression(
```

```
      '2.5 * (nir - red) / (nir + 6 * red - 7.5 * blue + 1)',
        {
          red: image.select('red'),    // 620-670nm, RED
          nir: image.select('nir'),    // 841-876nm, NIR
          blue: image.select('blue')    // 459-479nm, BLUE
        }).rename('EVI');
    return image.addBands(EVI);
  };


//3. /////// GLI (Green Leaf Index)

   function GLI(image) {
     var GLI = image.expression ('float (((green - red) + (green- blue)) / ((2 * green) + red +
blue))', {
    'green': image.select ('green'),
    'red': image.select ('red'),
    'blue': image.select ('blue')}).rename('GLI');

  return image.addBands(GLI);
};
//4. // function NDVI (image)
  function NDVI (image) {
  var NDVI = image.normalizedDifference(['nir','red']).rename('NDVI');
  return image.addBands(NDVI)
}

// //6.//// NBRI (Normalized Burned Ratio Index)
function NBRI (image) {
var NBRI = image.expression ('float (NIR - SWIR2) / float (NIR + SWIR2)', {
    'NIR': image.select ('nir'),
    'SWIR2': image.select ('swir2')}).rename('NBRI');
return image.addBands(NBRI);
}

//  //7. NDMI-Normalized difference moisture index
/// //(NIR-SWIR)/(NIR+SWIR)
function NDMI (image) {
var NDMI = image.expression ('float (NIR - SWIR1) / float (NIR + SWIR1)', {
    'NIR': image.select ('nir'),
    'SWIR1': image.select ('swir1')}).rename('NDMI');
return image.addBands(NDMI);
}

//////----------------------------------function_tassled cap------------------

var calculateTasseledCap = function (image){
   var b = image.select([0,1,2,3,4,5]);
  //var b = image.select('blue', 'green', 'red', 'nir', 'swir1', 'swir2');//'blue', 'green', 'red', 'nir',
'swir1', 'swir2')
```

```
  var brightness_= ee.Image([0.3561, 0.3972, 0.3904, 0.6966, 0.2286, 0.1596]);
  var greenness_= ee.Image([-0.3344, -0.3544, -0.4556, 0.6966, -0.0242, -0.2630]);
  var wetness_= ee.Image([0.2626, 0.2141, 0.0926, 0.0656, -0.7629, -0.5388]);
  var fourth_= ee.Image([0.0805, -0.0498, 0.1950, -0.1327, 0.5752, -0.7775]);
  var fifth_= ee.Image([-0.7252, -0.0202, 0.6683, 0.0631, -0.1494, -0.0274]);
  var sixth_= ee.Image([0.4000, -0.8172, 0.3832, 0.0602, -0.1095, 0.0985]);
  var sum = ee.call("Reducer.sum");

  var brightness = b.multiply(brightness_).reduce(sum);
  var greenness = b.multiply(greenness_).reduce(sum);
  var wetness = b.multiply(wetness_).reduce(sum);
  var fourth = b.multiply(fourth_).reduce(sum);
  var fifth = b.multiply(fifth_).reduce(sum);
  var sixth = b.multiply(sixth_).reduce(sum);

var tct=ee.Image(brightness).addBands(greenness)
                        .addBands(wetness)
                        .addBands(fourth)
                        .addBands(fifth)
                        .addBands(sixth);
  var                                                   tct                                                =
tct.select([0,1,2,3,4,5],["Brightness","Greenness","Wetness","Fourth","Fifth","Sixth"])

  return image.addBands(tct);
};


///////////////Landsat 8 collection ////////////////////////////////////////////
var l8 = ee.ImageCollection('LANDSAT/LC08/C01/T1_SR')
   .merge(ee.ImageCollection('LANDSAT/LC08/C01/T2_SR'))
      .filterBounds(study_area)///Filter a collection by intersection with geometry(aoi),,
  .filterDate('2021-01-01', '2022-12-31')
  .filter(ee.Filter.lt('CLOUD_COVER', 30))
  .map(setyear)
  .map(study)
  .map(maskL8sr)

  .select(
      ['B2', 'B3', 'B4', 'B5', 'B6', 'B7', 'pixel_qa'],
      ['blue', 'green', 'red', 'nir', 'swir1', 'swir2', 'pixel_qa']
  )

.map(GLI).map(NBRI).map(NDMI).map(EVI).map(NDVI).map(GCI).map(NDVI).map(calc
ulateTasseledCap)
    .median()

// Add elevation bands
var l8=l8.addBands(elevation).addBands(slope).addBands(aspect)
```

```
////////////////----------------------classifiaction L8-2021----------------------/////////////////////////

  //____________________-Assign class name

 var                                                    classNames                                                    =
largly_pine.merge(forest2021).merge(grass_2021).merge(bareland2021).merge(urban2021)
print (classNames,'classnames');

//creating training data
var collection=ee.Image().byte().paint(classNames,'class').rename('class')
var trainingSample = collection.stratifiedSample({
    numPoints: 1500,
    classBand:'class',
    region: study_area,
    scale:10,
    classValues:[0,1,2,3,4],
    classPoints:[500,500,500,500,500],
    //tileScale:8,
    seed:1,
    geometries:true
});
print(trainingSample, 'trainingSample_new');
// // features considered for the classification

var bands = ['blue', 'green', 'red', 'nir', 'swir1', 'swir2', //spectral
'Brightness','Greenness','Wetness','Fourth','Fifth', //tesslescup bands
'elevation','slope','aspect', // topography
'NDVI','NDMI','NBRI','EVI','GCI']; // vegataion indicies

// // training the classes
var training = l8.select(bands).sampleRegions({
  collection: trainingSample,
  properties: ['class'],
  scale: 30
});
print(training,'training');
// // // // // // /////// random forest Calssification/////

var classifierforest = ee.Classifier.smileRandomForest(500, null, 1, 0.5, null, 0).train({
  features: training,
  classProperty: 'class',
  inputProperties: bands
});
// //Run the classification
var classifiedforest = l8.select(bands).classify(classifierforest);
print(classifiedforest,'random forest');
print(classifiedforest.bandNames())

Map.addLayer(classifiedforest, {min: 0, max: 3, palette: [ 'red','green','yellow','black','blue']},
'classification_RF_2021',false);
```

```
// // //Assign classes to validation data.
var val_pine2021 = Vpine2021.map(function(x) {
  return x.set('use', 0)
})
var val_natural2021 = Vforest2021.map(function(x) {
  return x.set('use', 1)
})

var val_grass2021 = Vgrass2021.map(function(x) {
  return x.set('use', 2)
})
var val_bare2021 = Vbare2021.map(function(x) {
  return x.set('use', 3)
})

var val_urban2021 = Vurban2021.map(function(x) {
  return x.set('use', 4)
})

var fullValidationDataSet = val_pine2021.merge(val_natural2021).merge(val_grass2021).merge(val_bare2021).merge(val_urban2021)
// Sample your classification results to your new validation areas
var validationRT = classifiedforest.sampleRegions({
  collection: fullValidationDataSet,
  properties: ['use'],
  scale: 30,
});
print(validationRT, 'Validation-RT');
// // //// // //Compare the landcover of your validation data against the classification result-RANDOM TREE (landsat8)
var testAccuracyRT = validationRT.errorMatrix('use', 'classification');
//Print the error matrix to the console
print('Validation error matrix_RT*****: ', testAccuracyRT);
//Print the overoll accuracy to the console
print('Validation accuracy() *****: ', testAccuracyRT.accuracy());
//Print the consumer  accuracy to the console
print('Validation consumersAccuracy() *****: ', testAccuracyRT.consumersAccuracy());
//Print the producer accuracy to the console
print('Validation producerAccuracy() *****: ', testAccuracyRT.producersAccuracy());
//Print the kappa to the console
print('Validation  kappa() *****: ', testAccuracyRT.kappa());
 ///////////////Landsat 7 collection ////////////////////////////////////////////
  var l7 = ee.ImageCollection('LANDSAT/LE07/C01/T1_SR')
    .merge(ee.ImageCollection('LANDSAT/LE07/C01/T2_SR'))
    .filterBounds(study_area)///Filter a collection by intersection with geometry(aoi),
  .filterDate('2000-01-01', '2000-12-31')
  .filter(ee.Filter.lt('CLOUD_COVER', 20))
  .map(setyear)
```

```
.map(maskL8sr)
  .map(study)
  .select(
     ['B1', 'B2', 'B3', 'B4', 'B5', 'B7', 'pixel_qa'],
     ['blue', 'green', 'red', 'nir', 'swir1', 'swir2', 'pixel_qa']
    )

.map(GLI).map(NBRI).map(NDMI).map(EVI).map(NDVI).map(GCI).map(calculateTasseledCap)
    .median()
    Map.addLayer (l7,{min:0.0, max:3000.0, bands: ['swir2', 'swir1', 'red']},'Urban') //urban identifaction//

    Map.addLayer (l7,{min:0.0, max:3000.0,  bands: ['red','green', 'blue']},'landsat7_2000')

print (l7,'l7')
//add bands//

var l7=l7.addBands(elevation).addBands(slope).addBands(aspect)
print(l7,'elevation bands')

////////////////----------classifiaction L7-2000----------/////////////////////////

  //_____-Assign class name

var classNames2000 = pine_2000.merge(forest_2000).merge(grassland2000).merge(bare2000).merge(urban2000)
print (classNames2000,'classnames');

//Ref: video https://www.youtube.com/watch?v=auTVoKs-Uz8----------
var collection_2000=ee.Image().byte().paint(classNames2000,'class').rename('class')
var trainingSample_2000 = collection_2000.stratifiedSample({
    numPoints: 1500,
    classBand:'class',
    region: study_area,
    scale:30,
    classValues:[0,1,2,3,4],
    classPoints:[500,500,500,500,500],
    //tileScale:8,
    seed:1,
    geometries:true
});
print(trainingSample_2000, 'trainingSample_2000')

// // features considered for the classiafication

var bands = ['blue', 'green', 'red', 'nir', 'swir1', 'swir2', //spectral
'Brightness','Greenness','Wetness','Fourth','Fifth','Sixth', //tesslescup bands
'elevation','slope','aspect', // topography
'GLI','NDVI','NDMI','NBRI','EVI','GCI']; // vegataion indicies
```

```
// // training the classes
var training_2000 = l7.select(bands).sampleRegions({
  collection: trainingSample_2000,
  properties: ['class'],
  scale: 30
});
print(training_2000,'training');

// // // // // /////// random forest Calssification/////
var classifierforest_7 = ee.Classifier.smileRandomForest(500, null, 1, 0.5, null, 0).train({
  features: training_2000,
  classProperty: 'class',
  inputProperties: bands
});

// //Run the classification
var classifiedforest_7 = l7.select(bands).classify(classifierforest_7);
print(classifiedforest_7,'random forest_7');
print(classifiedforest_7.bandNames())

Map.addLayer(classifiedforest_7, {min: 0, max: 3, palette: [
'red','green','yellow','black','blue']},
'classification_RF_2000', false);

Export.image.toDrive({//image, description, folder, fileNamePrefix, dimensions, region, scale,
crs, crsTransform, maxPixels, shardSize, fileDimensions, skipEmptyTiles, fileFormat,
formatOptions
  image:classifiedforest_7,
  description:'classifiaction_2000',
  fileNamePrefix:'classifiaction_2000',
  region:study_area,
  scale: 30
})


// // //Display validation.
var val_pine = Vpine2000.map(function(x) {
  return x.set('use', 0)
})
var val_natural = Vforest2000.map(function(x) {
  return x.set('use', 1)
})

var val_grassland = Vgrassland2000.map(function(x) {
  return x.set('use', 2)
})

var val_bareland = Vbareland2000.map(function(x) {
  return x.set('use', 3)
```

```
})

var val_urban = Vurban_points2000.map(function(x) {
  return x.set('use', 4)
})
var fullValidationDataSet07 = val_pine.merge(val_natural).merge(val_grassland).merge(val_bareland).merge(val_urban)

// Sample your classification results to your new validation areas
var validationRT_7 = classifiedforest_7.sampleRegions({
  collection: fullValidationDataSet07,
  properties: ['use'],
  scale: 30,
});
print(validationRT, 'Validation-RT');
var testAccuracyRT_7 = validationRT_7.errorMatrix('use', 'classification');
//Print the error matrix to the console
print('Validation error matrix_RT*****: ', testAccuracyRT_7);
//Print the overoll accuracy to the console
print('Validation accuracy() *****: ', testAccuracyRT_7.accuracy());
//Print the consumer  accuracy to the console
print('Validation consumersAccuracy() *****: ', testAccuracyRT_7.consumersAccuracy());
//Print the producer accuracy to the console
print('Validation producerAccuracy() *****: ', testAccuracyRT_7.producersAccuracy());
//Print the kappa to the console
print('Validation  kappa() *****: ', testAccuracyRT_7.kappa());
```

Appendix III-Supplementary Material -Chapter 5

5.SM.1 GEE code of the chapter 5

5.SM1 shows the code used to test six different scenarios of combing data

```
//Navigate to area of interest////
Map.centerObject(study_area,12)

/* clip function used for all the image collections
*/
var study=function clip2 (img){return img.clip(study_area)}

///////Sentinel-2/////////////////
// Function to mask clouds using the Sentinel-2 QA band.
function maskS2clouds(image) {
  var qa = image.select('QA60')

  // Bits 10 and 11 are clouds and cirrus, respectively.
  var cloudBitMask = 1 << 10;
  var cirrusBitMask = 1 << 11;

  // Both flags should be set to zero, indicating clear conditions.
  var mask = qa.bitwiseAnd(cloudBitMask).eq(0).and(
             qa.bitwiseAnd(cirrusBitMask).eq(0))

  // Return the masked and scaled data, without the QA bands.
  return image.updateMask(mask).divide(10000)
      .select("B.*")
      .copyProperties(image, ["system:time_start"])
}
```

```
//----------------Sentinel_2 only //-----------------
var S2 = ee.ImageCollection('COPERNICUS/S2_SR_HARMONIZED')
.filterBounds(study_area)///Filter a collection by intersection with geometry(aoi),
    .filterDate('2020-01-31', '2021-12-31')///filter to given date
    // Pre-filter to get less cloudy granules.
    .filter(ee.Filter.lt('CLOUDY_PIXEL_PERCENTAGE', 5))///Filter to metadata less than the given value
   .map(maskS2clouds);///mapping over image collection
 var se2_image = S2.median();
    print (se2_image,'se2_image')
var trueColour = {
        bands: ["B4", "B3", "B2"],
        min: 500,
        max: 3500,
        gamma: 1.3
        };


// Compute the Normalized Difference Vegetation Index (NDVI).
var nir = se2_image.select('B8');
var red = se2_image.select('B4');
var ndvi = nir.subtract(red).divide(nir.add(red)).rename('NDVI');
print (ndvi,'ndvi')
// Display the result.
var ndviParams = {min: -1, max: 1, palette: ['blue', 'white', 'green']};
Map.addLayer(ndvi, ndviParams, 'NDVI image');
//Use ndvi threshold to remove non vegetative areas
var newndvi=ndvi.select('NDVI').gte(0.03).rename('NDVI').selfMask();
Map.addLayer(newndvi.clip(study_area), ndviParams , 'NDVI THRESHOLD',false);
// to select the vegetative area for further analysis
//1.  convert the vegetative area to vectors  for assist clip
```

```
var vector=newndvi.reduceToVectors({
  reducer:ee.Reducer.countEvery(),
  geometry:study_area,
  scale:10,
  //geometryType, eightConnected, labelProperty, crs, crsTransform, maxPixels, tileScale, geometryInNativeProjection)
  bestEffort:true,
})
Map.addLayer(vector,{},'vector',false)

// clipping the main satellite image with masked.
var vegetative_area=se2_image.clip(vector)

print(vegetative_area,'vegetative_area')
Map.addLayer(vegetative_area,trueColour,'vegetative_area')

var classification = vegetative_area.select('B2','B3','B4','B5','B6','B7','B8','B8A','B11','B12');
print(classification,'classifaction')
// training

var Train_HG = HG.map(function(x) {
  return x.set('use1', 4)
})
var gt1 = forest2021.merge(largly_pine).merge(poly_grassland).merge(shrub).merge(homegarden).merge(poly_cultivation);
//////////////////----------------------------
//creating training data
var collection=ee.Image().byte().paint( gt1,'use1').rename('class')
var trainingSample = collection.stratifiedSample({
```

```
    numPoints: 3000,
    classBand:'class',
    region: study_area,
    scale:10,
    classValues:[0,1,2,3,4,5],
    classPoints:[500,500,500,500,500,500],
    //tileScale:8,
    seed:1,
    geometries:true
});
print(trainingSample, 'trainingSample_new');

var training_S2 = classification.sampleRegions({
  collection:  trainingSample,
  properties: ['class'],
  scale: 10
});

print(training_S2,'training_combination')
////////////////////////////----------------------------
// Make a Random Forest classifier and train it.
var classifier_S2 = ee.Classifier.smileRandomForest(300)
    .train({
      features: training_S2,
      classProperty: 'class',
    });
var classified_S2 = classification.classify(classifier_S2);

var classifed_mapS2 = classified_S2.updateMask(classified_S2.lt(6));
```

```
Map.addLayer(classifed_mapS2,
            {min: 1, max:5 , palette: ['yellow','red','green']},
            'classification_S2');


// // // // // // // validation
var val_pine = pine.map(function(x) {
  return x.set('use', 0)
})
var val_natural = tree.map(function(x) {
  return x.set('use', 1)
})

var val_grassland = tgrassland.map(function(x) {
  return x.set('use', 2)
})

var val_shrub = tshurb.map(function(x) {
  return x.set('use', 3)
})

var val_HG = vHG.map(function(x) {
  return x.set('use', 4)
})

var val_tea = vTEA.map(function(x) {
  return x.set('use', 5)
})
```

```
var fullValidationDataSet = val_pine.merge(val_natural).merge(val_grassland).merge(val_shrub).merge(val_HG).merge(val_tea)
print(fullValidationDataSet,'fullValidationDataSet')
// Sample the classification results to new validation areas
var validation_S2 = classification.sampleRegions({
  collection: fullValidationDataSet,
  properties: ['use'],
  scale: 10
});
// Classify the validation data.
var validated_S2 = validation_S2.classify(classifier_S2);
// Get a confusion matrix representing expected accuracy.
var testAccuracy_S2= validated_S2.errorMatrix('use', 'classification');
print('Validation error matrix: ', testAccuracy_S2);
print('Validation OA_Sentinel2: ', testAccuracy_S2.accuracy());
 print('Validation consumersAccuracy(Sentinel2) *****: ', testAccuracy_S2.consumersAccuracy());
print('Validation producerAccuracy(Sentinel2) *****: ', testAccuracy_S2.producersAccuracy());
//Print the kappa to the console
print('Validation  kappa(Sentine2) *****: ', testAccuracy_S2.kappa())
/**
* Get collection of Sentinel-1 radar data.
*/
var start = '2020-01-01'
var finish = '2021-12-31'

var SAR = ee.ImageCollection('COPERNICUS/S1_GRD')
  .filterBounds(study_area)
  .filterMetadata('transmitterReceiverPolarisation','equals',["VV", "VH"])
  .filterMetadata('instrumentMode','equals','IW')
```

```
  .filterDate(start, finish)

var s = SAR.aggregate_histogram('transmitterReceiverPolarisation')
print(s)
print(SAR.size())

print (SAR,'SAR')
// stop
Map.addLayer(SAR.first().select('VV').clip(study_area), {min: -25, max: 0}, 'VV', false)
Map.addLayer(SAR.first().select('VH').clip(study_area), {min: -25, max: -10}, 'VH', false)
// https://stackoverflow.com/questions/73952483/rgee-radar-vegetation-index)

var RVI = SAR.map(function (image){

  var rvi = image.expression('4*vh/(vv+vh)',
    {'vv': image.select('VV'),
    'vh': image.select('VH')
    }

    ).rename ('RVI');

    return rvi;
  });

var imageVisParam = {"opacity":1,
                     "bands":["VV"],
                     "min":0.01548,
                     "max":0.46221,
                     "gamma":1};
```

```
RVI= RVI.reduce(ee.Reducer.median()).rename(RVI.first().bandNames())

print (RVI,'RVI')


/**

* Make a mosaic by selecting the first clear observation at each pixel.

*/

var mosaique = SAR.mosaic()

var palette = ['#8c510a','#bf812d','#dfc27d','#f6e8c3','#f5f5f5','#c7eae5','#80cdc1','#35978f','#01665e'].reverse()

Map.addLayer(mosaique.select('VV'), {min: -25, max: 0, palette: palette}, 'VV Mosaique', false)

Map.addLayer(mosaique.select('VH'), {min: -25, max: -10, palette: palette}, 'VH Mosaique', false)

/**

* The median value for each pixel.

*/

var median = SAR.reduce(ee.Reducer.median()).rename(SAR.first().bandNames())

var rapportDeLaMedian = median.select('VV').subtract(median.select('VH')).rename('rapport')

median = median.addBands(rapportDeLaMedian).addBands(RVI)

print (median,'median')

Map.addLayer(median.select(['VV', 'VH', 'rapport']).clip(study_area), {min:[-18, -25, 1], max:[0, -5, 12]}, 'Mediane RGB', false);


Map.addLayer(median.select('VV').clip(study_area), {min: -25, max: 0, palette: palette}, 'VV Mosaique', false)

Map.addLayer(median.select('VH').clip(study_area), {min: -25, max: -10, palette: palette}, 'VH Mosaique', false)


/**7. Apply filter to reduce speckle

*/

var SMOOTHING_RADIUS = 50;
```

```
var SAR_filtered = median.focal_mean(SMOOTHING_RADIUS, 'circle', 'meters');
print(SAR_filtered, 'SAR_filtered');

var SAR_filtered=SAR_filtered.clip(vector)

Map.addLayer(SAR_filtered.select('VV').clip(study_area), {min:-27,max:9}, 'SAR VH Filtered',0);
Map.addLayer(SAR_filtered.select('VH').clip(study_area), {min:-27,max:-2}, 'SAR VH Filtered',0);

//----------------------------------------PALSAR-----------------------------//

var palsar=  ee.ImageCollection("JAXA/ALOS/PALSAR/YEARLY/SAR_EPOCH")
 .filter(ee.Filter.date('2020-01-01', '2021-12-31'))
  //.filterBounds(study_area)
  .map(study)
  .mean();

  print (palsar,'palsar')

  /**7. Apply filter to reduce speckle
 */

var SMOOTHING_RADIUS = 50;
var palsar_filtered = palsar.focal_mean(SMOOTHING_RADIUS, 'circle', 'meters');
print(palsar_filtered, 'palsar_filtered');

// var upsampled_newshape= resample10m(palsar.addBands(shape.select(['B8A'])))
// print(upsampled_newshape,'upsampled_pc ')

var thirdcollection=palsar_filtered.select ('HH','HV')
```

```
var thirdcollection=thirdcollection.clip(vector)
var classifaction2= vegetative_area.select('B2','B3','B4','B5','B6','B7','B8','B8A','B11','B12').addBands(mer,['VV', 'VH','rapport','RVI'],classifaction2);
//---------------------only radar-------------------------------------//


  var mer=SAR_filtered.select ('VV','VH','rapport','RVI')
   print (mer,'mer')


var RADAR= mer.addBands(thirdcollection,['HH','HV'],RADAR);
print(RADAR,'RADAR')


// training
var training_RADAR = RADAR.sampleRegions({
  collection: trainingSample,
  properties: ['class'],
  scale: 10
});


print(training_RADAR,'training_RADAR')


// Make a Random Forest classifier and train it.
var classifier_RADAR = ee.Classifier.smileRandomForest(300)
    .train({
      features: training_RADAR,
      classProperty: 'class',


    });
var classified_RADAR = RADAR.classify(classifier_RADAR);
```

```
var masked_RADAR = classified_RADAR.updateMask(classified_RADAR.lt(6));

Map.addLayer(masked_RADAR,
        {min: 1, max:5 , palette: ['yellow','red','green']},
        'classification_RADAR');

// Sample the classification results to new validation areas
var validation_RADAR = RADAR.sampleRegions({
  collection: fullValidationDataSet,
  properties: ['use'],
  scale: 10
});

// Classify the validation data.
var validated_RADAR = validation_RADAR.classify(classifier_RADAR);

// Get a confusion matrix representing expected accuracy.
var testAccuracy_RADAR = validated_RADAR.errorMatrix('use', 'classification');
print('Validation error matrix_RADAR: ', testAccuracy_RADAR);
print('Validation OA_RADAR: ', testAccuracy_RADAR.accuracy());
 print('Validation consumersAccuracy(RADAR) *****: ',
testAccuracy_RADAR.consumersAccuracy());
print('Validation producerAccuracy(RADAR) *****: ',
testAccuracy_RADAR.producersAccuracy());
//Print the kappa to the console
print('Validation  kappa(RADAR) *****: ', testAccuracy_RADAR.kappa())

//--------------------RADAR and OPTICAL data_____________________

var classifactionall_dataset= classifaction2.addBands(thirdcollection);
print(classifactionall_dataset,'classifactionall_dataset')
```

```
var classifactionall_dataset= classifactionall_dataset.clip(vector)
var training_all_dataset = classifactionall_dataset.sampleRegions({
  collection: trainingSample,
  properties: ['class'],
  scale: 10
});

print(training_all_dataset,'training_combination')

// Make a Random Forest classifier and train it.
var classifier_all_dataset = ee.Classifier.smileRandomForest(300)
    .train({
      features: training_all_dataset,
      classProperty: 'class',

    });
var classified_all_dataset = classifactionall_dataset.classify(classifier_all_dataset);

var masked_all_dataset = classified_all_dataset.updateMask(classified_all_dataset.lt(6));
// // // // // // // validation

var fullValidationDataSet = val_pine.merge(val_natural).merge(val_grassland).merge(val_shrub).merge(val_HG).merge(val_tea)
print(fullValidationDataSet,'fullValidationDataSet')

// Sample the input with a different random seed to get validation data.
var validation_all_dataset = classifactionall_dataset.sampleRegions({
  collection: fullValidationDataSet,
  properties: ['use'],
  scale: 10
```

```
});


// Classify the validation data.
var validated_all_dataset = validation_all_dataset.classify(classifier_all_dataset);
// Get a confusion matrix representing expected accuracy.
var testAccuracy_all_dataset = validated_all_dataset.errorMatrix('use', 'classification');
print('Validation error matrix: ', testAccuracy_all_dataset);
print('Valida_OA_all data source: ', testAccuracy_all_dataset.accuracy());
 print('Validation consumersAccuracy_all data source *****: ', testAccuracy_all_dataset.consumersAccuracy());
print('Validation producerAccuracy_all data source *****: ', testAccuracy_all_dataset.producersAccuracy());
//Print the kappa to the console
print('Validation  kappa(all data source) *****: ', testAccuracy_all_dataset.kappa())


//_____--DEM_____
Map.addLayer(DEM.clip(study_area), {
  min: 3,
  max: 281,
  palette: ['blue', 'green', 'yellow', 'white']
},'elevation');
print(DEM, 'DEM');


//slope, aspect----------
function radians(image) {return image.toFloat().multiply(Math.PI).divide(180);
}
function hillshade(az, ze, slope, aspect) {
  // Convert angles to radians.
  var azimuth = radians(ee.Image(az));
  var zenith = radians(ee.Image(ze));
  // Note that methods on images are needed to do the computation.
```

```
  // i.e. JavaScript operators (e.g. +, -, /, *) do not work on images.
  // The following implements:
  // Hillshade = cos(Azimuth - Aspect) * sin(Slope) * sin(Zenith) +
  //     cos(Zenith) * cos(Slope)
  return azimuth.subtract(aspect).cos()
    .multiply(slope.sin())
    .multiply(zenith.sin())
    .add(
      zenith.cos().multiply(slope.cos()));
}
// Compute terrain measures
var terrain = ee.Algorithms.Terrain(DEM);
// print(terrain, 'terrain');
var slope = radians(terrain.select('slope'));
var slope_D = ee.Terrain.slope(DEM);
var azimuth = radians(terrain.select('azimuth'));
var zenith = radians(terrain.select('zenith'));
var aspect = radians(terrain.select('aspect'));

//Calculate topographic position index (TPI)
        //TPI = Eo - En
        //Eo = elevation in meters at a given location (or cell)
        //En = mean elevation of all cells within a neighborhood

var tpi_10 = DEM.subtract(DEM.clip(study_area).focal_mean(10));
// Map.addLayer(tpi_10, {
//   min:-60,
//   max:90,
//   palette: ['blue', 'yellow', 'red']
// }, 'tpi_10');
```

```
print (tpi_10,'tpi_10')

//300-m circular TPI - fixed across scales

var tpi_300m = DEM.subtract(DEM.focal_mean({radius: 450, units: 'meters'}).clip(study_area));

// Weiss et al. (http://www.jennessent.com/downloads/tpi-poster-tnc_18x22.pdf)

var kernel = ee.Kernel.circle(300, 'meters', false)

  .add(ee.Kernel.circle(150, 'meters', false, -1));

var tpi_300m = DEM.subtract(DEM.focal_mean({kernel: kernel}).clip(study_area)).rename('tpi300');

var withelevation_data=classifactionall_dataset.addBands(slope_D).addBands(aspect).addBands(tpi_10)

//.addBands(zenith).addBands(azimuth)

print ( withelevation_data,'elevation_data')


var training_withelevation =  withelevation_data.sampleRegions({

  collection: trainingSample,

  properties: ['class'],

  scale: 10

});


print(training_withelevation,'training_combination')


// Make a Random Forest classifier and train it..

var classifier_withelevation = ee.Classifier.smileRandomForest(300)

    .train({

      features: training_withelevation,

      classProperty: 'class',


    });

var classified_withelevation =  withelevation_data.classify(classifier_withelevation);
```

```
Map.addLayer(classified_withelevation,
        {min: 1, max:5 , palette: ['yellow','red','green']}, 'classification_with elevation');

// // // // // // // validation
var trainAccuracy_withelevation = classifier_withelevation.confusionMatrix();
print('Resubstitution error matrix: ', trainAccuracy_withelevation);
print('Training overall accuracy_withelevation: ', trainAccuracy_withelevation.accuracy());

// Sample the classification results to validation areas
var validation_withelevation =  withelevation_data.sampleRegions({
  collection: fullValidationDataSet,
  properties: ['use'],
  scale: 10
});

// Classify the validation data.
var validated_withelevation = validation_withelevation.classify(classifier_withelevation);

// Get a confusion matrix representing expected accuracy.
var testAccuracy_withelevation = validated_withelevation.errorMatrix('use', 'classification');
print('Validation error matrix: ', testAccuracy_withelevation);
print('Validation_OA: ', testAccuracy_withelevation.accuracy());
 print('Validation consumersAccuracy_n *****: ',
testAccuracy_withelevation.consumersAccuracy());
print('Validation producerAccuracy *****: ',
testAccuracy_withelevation.producersAccuracy());
//Print the kappa to the console
print('Validation  kappa *****: ', testAccuracy_withelevation.kappa())

//_____vegeation incies_____
```

```
// creating different vegeation indexes//////////////////////****

//1./EVI

var EVI = vegetative_area.expression('(2.5 * float(NIR - RED)) / (NIR + (2.4 * RED) + 10000)',      //(https://gis.stackexchange.com/questions/226325/calculating-2-bands-evi-from-sentinel-2?rq=1)

{

    'NIR': vegetative_area.select('B8'),

    'RED': vegetative_area.select('B4'),

    'BLUE': vegetative_area.select('B2')

}).rename('EVI');


// Map.addLayer(EVI, {min: -0, max: 0.6,palette:['Orange','Black','white']},'EVI_2band');


// //creating Green Chlorophlly index

//2.///GCI = (NIR) / (Green) – 1

var GCI = vegetative_area.expression ('float (((NIR) / (GREEN)) - 1)', {

   'NIR': vegetative_area.select ('B8'),

   'GREEN': vegetative_area.select ('B3')}).rename('GCI');

Map.addLayer(GCI , {min: 0, max: 5 ,palette:['Green','yellow','white']},'GCI ');


//  Red Edge Chlorophyll Index

//3.///RGCI-(B7)(/B5)-1

var RGCI = vegetative_area.expression ('float (((REDEdge3) / (REDEdge1)) - 1)', {

   'REDEdge3': vegetative_area.select ('B7'),

   'REDEdge1': vegetative_area.select ('B5')}).rename('RGCI');

// Map.addLayer(RGCI , {min: 0, max: 4.2 ,palette:['Red','Blue','Yellow']},'RGCI ');


//4./////  GLI (Green Leaf Index)

var GLI = vegetative_area.expression ('float (((GREEN - RED) + (GREEN - BLUE)) / ((2 * GREEN) + RED + BLUE))', {

   'GREEN': vegetative_area.select ('B3'),
```

```
    'RED': vegetative_area.select ('B4'),
    'BLUE': vegetative_area.select ('B2')}).rename('GLI');

Map.addLayer(GLI , {min: -0, max: 0.3 ,palette:['yellow','blue','black']},'Green Leaf Index ');

//5.////// SAVI (Soil Adjusted Vegetation Index)
var SAVI = vegetative_area.expression ('float (((NIR - RED) / (NIR + RED + L))* (1+L))',{
    'L': 0.5, // Cobertura vegetacion 0-1
    'NIR': vegetative_area.select ('B8'),
    'RED': vegetative_area.select ('B4')}).rename('SAVI');

// Map.addLayer(SAVI , {min:-0, max: 1.5 ,palette:['Green','Yellow','Brown']},'Soil Adjusted Vegetation Index ')
// //6.//// NBRI (Normalized Burned Ratio Index)
var NBRI = vegetative_area.expression ('float (NIR - SWIR2) / float (NIR + SWIR2)', {
    'NIR': vegetative_area.select ('B8'),
    'SWIR2': vegetative_area.select ('B12')}).rename('NBRI');

// Map.addLayer(NBRI , {min: -0, max: 0.9,palette:['Blue','Brown','Black']},'Normalized Burned Ratio Index ');

//  //7. NDMI-Normalized difference moisture index
/// //(NIR-SWIR)/(NIR+SWIR)

var NDMI = vegetative_area.expression ('float (NIR - SWIR1) / float (NIR + SWIR1)', {
    'NIR': vegetative_area.select ('B8'),
    'SWIR1': vegetative_area.select ('B11')}).rename('NDMI');

Map.addLayer(NDMI , {min: -0.24, max: 0.6,palette:['Blue','Brown','Black']},'Normalized difference moisture index')
```

```
//8. Bare Soil Index (BSI)----------------------------------------------------------------
  var bsi = vegetative_area.expression ('float ((RED + SWIR) - (NIR + BLUE)) / ((RED + SWIR) + (NIR + BLUE)) ',{
    'RED': vegetative_area.select('B4'),
    'BLUE': vegetative_area.select('B2'),
    'NIR': vegetative_area.select('B8'),
    'SWIR': vegetative_area.select ('B11')}).rename('BSI');
var final_VI=withelevation_data.addBands(bsi).addBands(NDMI).addBands(NBRI).addBands(SAVI).addBands(GLI).addBands(RGCI).addBands(GCI).addBands(EVI)
print (final_VI,'final')

var training_VI = final_VI.sampleRegions({
  collection: trainingSample,
  properties: ['class'],
  scale: 10
});

print(training_VI,'training_combination')

// // Make a Random Forest classifier and train it.
var classifier_VI = ee.Classifier.smileRandomForest(300)
    .train({
      features: training_VI,
      classProperty: 'class',

    });
var classified_VI = final_VI.classify(classifier_VI);

Map.addLayer(classified_VI,
            {min: 1, max:5 , palette: ['yellow','red','green']},
```

```
            'classification_VI');
// // // // // // // // validation
var validation_VI = final_VI.sampleRegions({
  collection: fullValidationDataSet,
  properties: ['use'],
  scale: 10
});
var validated_VI = validation_VI.classify(classifier_VI);
var testAccuracy_VI = validated_VI.errorMatrix('use', 'classification');
print('Validation error matrix: ', testAccuracy_VI);
print('Valida_OA_final: ', testAccuracy_VI.accuracy());
 print('Validation consumersAccuracy_final *****: ', testAccuracy_VI.consumersAccuracy());
print('Validation producerAccuracy_final *****: ', testAccuracy_VI.producersAccuracy());
//Print the kappa to the console
print('Validation  kappa(final) *****: ', testAccuracy_VI.kappa())

///----------------------Feature imporatnce check----------------------------//
var importance=classifier_VI.explain()
print(importance,'importance')

var variable_importance = ee.Feature(null, ee.Dictionary(importance).get('importance'));

var chart =
  ui.Chart.feature.byProperty(variable_importance)
    .setChartType('ColumnChart')
    .setOptions({
      title: 'Random Forest Variable Importance',
      legend: {position: 'none'},
      hAxis: {title: 'Bands'},
      vAxis: {title: 'Importance'}
```

```
    });


print(chart);


// trying to export the feature importance
// Cast into a ee.Feature and a ee.FeatureCollection for exporting the importance as CSV
var variable_importance = ee.Feature(null, ee.Dictionary(importance).get('importance'));
var variable_importance01 = ee.FeatureCollection(variable_importance);


 ///_____exclude radar _____//


  var optical = vegetative_area.select('B2','B3','B4','B5','B6','B7','B8','B8A','B11','B12').addBands(bsi).addBands(NDMI).addBands(NBRI).addBands(SAVI).addBands(GLI).addBands(RGCI).addBands(GCI).addBands(EVI).addBands(slope_D).addBands(aspect).addBands(tpi_10);
print(optical ,'optical ')
  var bands= vegetative_area.select('B2','B3','B4','B5','B6','B7','B8','B8A','B11','B12')
var training_all_optical = optical .sampleRegions({
  collection: trainingSample,
  properties: ['class'],
  scale: 10
});


print(training_all_optical,'training_all_optical')
// Make a Random Forest classifier and train it.
var classifier_all_optical  = ee.Classifier.smileRandomForest(300)
    .train({
      features: training_all_optical ,
      classProperty:'class',
```

```
    });
var classified_optical =optical .classify(classifier_all_optical);
// // // // // // // validation
var validation_all_optical = optical .sampleRegions({
  collection: fullValidationDataSet,
  properties: ['use'],
  scale: 10
});

// Classify the validation data.
var validated_all_optical  = validation_all_optical .classify(classifier_all_optical );
var testAccuracy_all_optical  = validated_all_optical .errorMatrix('use', 'classification');
print('Validation error matrix: ', testAccuracy_all_optical);
print('Valida_OA_all_opticale: ', testAccuracy_all_optical.accuracy());
print ('Validation consumersAccuracy_all_optical *****: ', testAccuracy_all_optical.consumersAccuracy());
print ('Validation producerAccuracy_all_optical *****: ', testAccuracy_all_optical.producersAccuracy());
//Print the kappa to the console
print('Validation  kappa(all_optical) *****: ', testAccuracy_all_optical.kappa())
```

Appendix IV-Co-Authorship Forms

THE UNIVERSITY OF WAIKATO
Te Whare Wānanga o Waikato

Co-Authorship Form

Postgraduate Studies Office
Student and Academic Services Division
Wahanga Ratonga Matauranga Akonga
The University of Waikato
Private Bag 3105
Hamilton 3240, New Zealand
Phone +64 7 838 4439
Website: http://www.waikato.ac.nz/sasd/postgraduate/

This form is to accompany the submission of any PhD that contains research reported in published or unpublished co-authored work. **Please include one copy of this form for each co-authored work**. Completed forms should be included in your appendices for all the copies of your thesis submitted for examination and library deposit (including digital deposit).

Please indicate the chapter/section/pages of this thesis that are extracted from a co-authored work and give the title and publication details or details of submission of the co-authored work.

Chapter 2 | Using remote sensing for sustainable forest management in developing countries | Published in The Palgrave Handbook of Global Sustainability (2020) pp. 1-22 | Springer International Publishing | https://doi.org/10.1007/978-3-030-38948-2_35-1

Nature of contribution by PhD candidate	Principal author: Conceptual design, literature review, and book chapter writing
Extent of contribution by PhD candidate (%)	90

CO-AUTHORS

Name	Nature of Contribution
Lars Brabyn	Second author: Conceptual design, reviewed draft versions, and book chapter editing
Silvia Serrao_Neumann	Third author: Conceptual design, reviewed draft versions, and book chapter editing

Certification by Co-Authors

The undersigned hereby certify that:

- the above statement correctly reflects the nature and extent of the PhD candidate's contribution to this work, and the nature of the contribution of each of the co-authors; and

Name	Signature	Date
Lars Brabyn	Lars Brabyn	27/06/2023
Silvia Serrao-Neumann	S Neumann	28/06/2023

July 2015

THE UNIVERSITY OF WAIKATO
Te Whare Wānanga o Waikato

Co-Authorship Form

Postgraduate Studies Office
Student and Academic Services Division
Wahanga Ratonga Matauranga Akonga
The University of Waikato
Private Bag 3105
Hamilton 3240, New Zealand
Phone +64 7 838 4439
Website: http://www.waikato.ac.nz/sasd/postgraduate/

This form is to accompany the submission of any PhD that contains research reported in published or unpublished co-authored work. **Please include one copy of this form for each co-authored work.** Completed forms should be included in your appendices for all the copies of your thesis submitted for examination and library deposit (including digital deposit).

Please indicate the chapter/section/pages of this thesis that are extracted from a co-authored work and give the title and publication details or details of submission of the co-authored work.

Chapter 3 | Using Google Earth Engine to classify unique forest and agroforest classes using a mix of Sentinel 2a spectral data and topographical features: a Sri Lanka case study | Published in Geocarto International Journal (2022) 37, NO. 25, 9544–9559 | https://doi.org/10.1080/10106049.2021.2022010

Nature of contribution by PhD candidate	Principal author: Conceptual design, data collection, analysis, and manuscript writing
Extent of contribution by PhD candidate (%)	90

CO-AUTHORS

Name	Nature of Contribution
Lars Brabyn	Second author: Conceptual design, reviewed draft versions, and manuscript editing
Silvia Serrao_Neumann	Third author: Conceptual design, reviewed draft versions, and manuscript editing

Certification by Co-Authors

The undersigned hereby certify that:

- the above statement correctly reflects the nature and extent of the PhD candidate's contribution to this work, and the nature of the contribution of each of the co-authors; and

Name	Signature	Date
Lars Brabyn	Lars Brabyn	27/6/2023
Silvia Serrao-Neumann	S Neumann	28/06/2023

July 2015

THE UNIVERSITY OF WAIKATO
Te Whare Wānanga o Waikato

Co-Authorship Form

Postgraduate Studies Office
Student and Academic Services Division
Wahanga Ratonga Matauranga Akonga
The University of Waikato
Private Bag 3105
Hamilton 3240, New Zealand
Phone +64 7 838 4439
Website: http://www.waikato.ac.nz/sasd/postgraduate/

This form is to accompany the submission of any PhD that contains research reported in published or unpublished co-authored work. **Please include one copy of this form for each co-authored work**. Completed forms should be included in your appendices for all the copies of your thesis submitted for examination and library deposit (including digital deposit).

Please indicate the chapter/section/pages of this thesis that are extracted from a co-authored work and give the title and publication details or details of submission of the co-authored work.

Chapter 4 |Monitoring invasive pines using remote sensing: A case study from Sri Lanka | Published in Environmental Monitoring Assessment 195, 347 (2023) | https://doi.org/10.1007/s10661-023-10919-1

Nature of contribution by PhD candidate	Principal author: Conceptual design, data preparation and analysis, and manuscript writing
Extent of contribution by PhD candidate (%)	90

CO-AUTHORS

Name	Nature of Contribution
Lars Brabyn	Second author: Conceptual design, reviewed draft versions, and manuscript editing
Silvia Serrao_Neumann	Third author: Conceptual design, and manuscript editing

Certification by Co-Authors

The undersigned hereby certify that:

- the above statement correctly reflects the nature and extent of the PhD candidate's contribution to this work, and the nature of the contribution of each of the co-authors; and

Name	Signature	Date
Lars Brabyn	Lars Brabyn	27/6/2023
Silvia Serrao-Neumann	S Neumann	28/06/2023

July 2015

THE UNIVERSITY OF WAIKATO
Te Whare Wānanga o Waikato

Co-Authorship Form

Postgraduate Studies Office
Student and Academic Services Division
Wahanga Ratonga Matauranga Akonga
The University of Waikato
Private Bag 3105
Hamilton 3240, New Zealand
Phone +64 7 838 4439
Website: http://www.waikato.ac.nz/sasd/postgraduate/

This form is to accompany the submission of any PhD that contains research reported in published or unpublished co-authored work. **Please include one copy of this form for each co-authored work.** Completed forms should be included in your appendices for all the copies of your thesis submitted for examination and library deposit (including digital deposit).

Please indicate the chapter/section/pages of this thesis that are extracted from a co-authored work and give the title and publication details or details of submission of the co-authored work.

Chapter 5 | Evaluating the addition of radar with optical data for vegetation mapping in a tropical montane region: a case study in Sri Lanka | submitted to Journal of Mountain Science (2023)

Nature of contribution by PhD candidate	Principal author: Conceptual design, data preparation, analysis, and manuscript writing
Extent of contribution by PhD candidate (%)	90

CO-AUTHORS

Name	Nature of Contribution
Lars Brabyn	Second author: Conceptual design, reviewed draft versions, and manuscript editing
Silvia Serrao_Neumann	Third author: Conceptual design, manuscript editing

Certification by Co-Authors

The undersigned hereby certify that:

- the above statement correctly reflects the nature and extent of the PhD candidate's contribution to this work, and the nature of the contribution of each of the co-authors; and

Name	Signature	Date
Lars Brabyn	Lars Brabyn	27/6/2023
Silvia Serrao-Neumann	S Neumann	28/06/2023

July 2015